



HAL
open science

Analysis and diagnosis of faults in the PMSM drivetrains for series hybrid electrical vehicles (SHEVs)

Seyed Saeid Moosavi Anchehpoli

► **To cite this version:**

Seyed Saeid Moosavi Anchehpoli. Analysis and diagnosis of faults in the PMSM drivetrains for series hybrid electrical vehicles (SHEVs). Electric power. Université de Technologie de Belfort-Montbéliard, 2013. English. NNT: 2013BELF0224 . tel-01501498

HAL Id: tel-01501498

<https://theses.hal.science/tel-01501498v1>

Submitted on 4 Apr 2017

HAL is a multi-disciplinary open access archive for the deposit and dissemination of scientific research documents, whether they are published or not. The documents may come from teaching and research institutions in France or abroad, or from public or private research centers.

L'archive ouverte pluridisciplinaire **HAL**, est destinée au dépôt et à la diffusion de documents scientifiques de niveau recherche, publiés ou non, émanant des établissements d'enseignement et de recherche français ou étrangers, des laboratoires publics ou privés.

SPIM

Thèse de Doctorat



école doctorale sciences pour l'ingénieur et microtechniques
UNIVERSITÉ DE TECHNOLOGIE BELFORT-MONTBÉLIARD

Analysis and diagnosis of faults in
the PMSM drivetrains for series
hybrid electrical vehicles (SHEVs)



Seyed Saeid MOOSAVI

SPIM

Thèse de Doctorat



école doctorale sciences pour l'ingénieur et microtechniques
UNIVERSITÉ DE TECHNOLOGIE BELFORT-MONTBÉLIARD

PhD thesis in Electrical Engineering

Analysis and diagnosis of faults in the PMSM drivetrains for series hybrid electrical vehicles

Presented on December 11, 2013 by,

MOOSAVI-ANCHEHPOLI Sayed-Saeid

to the jury :

Reviewers:

BEN AMMAR Faouzi, Full professor, LMMA, INSAT, Tunis - Tunisia
HECQUET Michel, Full professor, L2EP, ECL, Lille – France

Examiners:

KRISHNAMURTHY Mahesh , Associate professor, IIT, Chicogo-USA
PIETRZAK-DAVID Maria, Full professor, LAPLACE, ENSEEIHT, Toulouse - France
ROGER Daniel, Full professor, LSEE, FSA, Bethune – France

Supervisors:

DJERDIR Abdesslem, Associate professor, IRTES-SET, UTBM, Belfort- France
AIT-AMIRAT Youcef, Associate professor, FEMTO-ST, UFC, Belfort- France
DAVOOD Arab Khaburi, Associate professor, ERC, IUST, Tehran-Iran

To my parents and all my family

ACKNOWLEDGEMENT

Foremost, I wish to express my sincere gratitude to my advisor Dr. Abdesslem Djerdir for the continuous support of my Ph.D study and research, for his patience, motivation, enthusiasm, and immense knowledge. His guidance helped me in all the time of research and writing of this thesis.

My sincere thanks also go to Dr. Davood Arab Khaburi and Dr. Youcef Ait Amirat for their support, guidance, encouragement, and the interesting discussions we had together.

I would like to thank Professor Faouzi Ammar and Professor Michel Hecquet for being committee members of my thesis reviewer. They provided me many insightful comments and constructive suggestions in the review of my research proposal and dissertation. My special thanks go to Professor Mahesh Krishnamurthy, Professor Maria Pietrzak-David and Professor Daniel Roger as well for being examiner committee member and their invaluable advice and questions.

I am also grateful to Dr. Abdoul. N-Diaye for his kindly help during my experimental data collection.

My thanks are extended to my fellow colleagues majoring in electrical engineering, who built an academic and friendly research environment that made my study at University of technology Belfort Montbeliard most enjoyable. I cherish the friendship with them since my first arrival at this continent and meeting with: Eric Sugny, Abdelmajid Naimi, Djelali Larrioumlil, Karine Diez, and Prof. Yusien Ruichek.

Last but not least, I am always indebted to all my family members, especially my parents and my wife, for their endless support and love. I greatly appreciate the sacrifices and understanding of my mother and father during my struggling years, without which the completion of my study would not have been possible.

Seyed Saeid MOOSAVI

Table of Contents

GENERAL INTRODUCTION	15
----------------------	----

Chapter I

1. Introduction	19
2. Global CO2 Regulations	19
3. How is HEV helping to reach these goals?	21
3.1. Why hybrid electric vehicle? Efficiency perspective:	21
3.2. Why hybrid electric vehicle? Technology enablers:	22
4. Different architectures of HEV	22
5. Hybrid Electric vehicle propulsion system design: supervisory and control perspective,	25
5.1. Batteries	26
5.1.1 HEV battery requirements:	27
5.1.2 Challenges in HEV battery:	28
5.2. Electric motor drive selection issues for HEV propulsion systems:	28
5.2.1 HEVs electric propulsion requirements:	29
5.2.2 Variety in usage of different types of electric machine in HEV application:	30
5.2.3 Challenges in HEV electric propulsion:	31
5.3. Power electronic requirements	31
5.3.1 Types of semiconductor switches	32
5.3.2 Power Converter Control Methods	32
5.3.3 Power converter requirements:	33
5.3.4 Electromagnetic Compatibility	33
5.3.5 Challenges in HEV power converters:	34
6. Thesis objective	34
7. Conclusion	35
8. References of chapter I	36

Chapter II

1. Introduction	41
------------------------	-----------

2. Requirements of fault diagnosis	41
3. Fault specification of drive-train of SHEV	44
3.1. Stator winding faults:	44
3.2. Stator core-related faults	45
3.3. Open phase, phase to ground, line to line, line to line to ground faults	46
3.4. Unbalanced voltage fault.....	47
3.5. Demagnetization fault	48
3.6. Eccentricity fault	52
3.7. Bearing fault.....	53
3.8. Power converter	55
4. Diagnosis methods, a deep investigation and comparison on drivetrain faults	57
4.1. Investigations based on simulation – analytical or finite element methods	58
4.1.1 Frequency domain analysis.....	59
4.1.2 Time-Frequency (TF) domain analysis.....	63
4.1.3 Analytical model based analysis.....	67
4.1.4 Modeling method design based analysis.....	68
4.1.5 Investigations based on design changes - practical design	71
4.1.6 Parameter estimation:.....	72
4.1.7 Fuzzy logic.....	72
4.1.8 Artificial Neural network.....	72
4.1.9 Synthesis study	74
4.1.10 Conclusion	74
5. References of chapter II	76

Chapter III

1. Introduction	85
2. Short circuit fault.....	86
2.1. Short circuit fault sensitive modeling of PMSM: analytical approach.....	86
2.1.1Analytical modeling of PMSM under inter turn short circuit fault.	87
2.1.2Limits of analytical modeling approach.....	91
2.2. Experimental approach: faults characterization of PMSM associated to its controller.....	96
2.2.1 Set up description.....	96
2.2.2 Software program of the PMSM vector control.....	99
2.2.3 Healthy mode: constant speed - unloaded motor.....	102
2.2.4 Healthy mode: constant speed – loaded motor.....	103
2.2.5Faulty mode: Influence of the short circuit fault on motor currents	104

2.2.6 ..Motor behaviors under different inter-turn short circuits faults: variable speed operating	109
2.3. Diagnosis algorithm of PMSM short circuit faults.....	111
3. Demagnetization fault	111
3.1. Theoretical approach	111
3.2. FEM fault simulation with FLUX-2D software.....	113
3.2.1	FEM simulation results: health and demagnetized PMSM113
3.2.2	Comparison study between analytical and FEM models118
3.3. Diagnosis algorithm of PMSM demagnetization fault.....	119
4. Eccentricity & bearing fault	119
4.1. Eccentricity & bearing sensitive modeling	120
4.2. Diagnosis algorithm of PMSM eccentricity &bearing	120
5. Conclusion	121
6. References of Chapter III	122

Chapter IV

1. Introduction	125
2. Power converters behaviors in healthy and faulty operation mode	126
2.1. AC-DC converter fault modeling: theoretical and experimental investigation.....	126
2.2. Experimental setup	Erreur ! Signet non défini.
2.3. Best data identification for acquisition by aim of successful signal processing	127
2.3.1 Simulation result validation of AC-DC converter fault detection of SHEV	128
2.3.2 Experimental results.....	131
2.4. Pattern identification	134
2.4.1 Fault detection strategy and algorithm for the experimental setup.....	134
2.4.2 Influence of the DC-Bus capacitor on fault signatures	137
2.4.3 Influence of the load changes on fault signatures.....	137
2.4.4 Influence of the speed changes on fault signatures	138
2.5. Fault detection investigation thyristor base AC-DC converter operation.....	139
2.5.1 Pattern identification.....	139
2.6. Fault sensitive modeling DC/AC inverter	141
3. Conclusion.....	145
4. References of chapter IV	146

Chapter V

- 1. Introduction..... 149**
- 2. Global strategy of supervision and diagnosis of drive-trains of SHEVs 149**
 - 2.1. Level 0..... 150
 - 2.2. Level 1..... 150
 - 2.3. Level 2..... 151
 - 2.4. Level 3..... 151
- 3. Global algorithm of drive-trains fault diagnosis and classification 152**
- 4. ANN Based Fault Diagnosis of Stator Winding Inter-Turn short circuit 154**
 - 4.1. Justification of ANN for Using Inter-Turn Fault Diagnosis..... 154
 - 4.2. ANN training..... 156
 - 4.3. Implementation of short circuit fault diagnosis by using ANN..... 158
- 5.ANN Based Fault Diagnosis of switch open circuit of AC-DC Power Converter160**
 - 5.1. Justification of ANN for using AC-DC fault diagnosis 160
 - 5.2. ANN training..... 161
 - 5.3. Implementation of open phase fault diagnosis in AC/DC converter by Using ANN..... 163
- 6. ANN based fault diagnosis of switch open circuit of DC-AC power converter 165**
- 7. Conclusion 167**
- 8. References of chapter V 169**
- GENERAL CONCLUSION 171**
- Appendix 3A 173**
- Appendix 3B 181**
- Appendix 3C 187**
- Appendix 3D 195**
- Appendix 3E 201**
- Appendix 5A 209**

List of Figures

Fig. 1.1: Example of HEV architecture (Audi Q5)	23
Fig. 1.2 : Series HEV (SHEV)	23
Fig. 1.3 : Parallel HEV (PHEV)	23
Fig. 1.4 : Power Split HEV (PSHEV)	24
Fig. 1.5 : Hybrid electric vehicle control network	25
Fig. 1.6 : A generic supervisory control perspective of SHEV	26
Fig. 1.7 : Typical cell characteristics.....	28
Fig. 1.8 : A sample PMSM efficiency characteristic	30
Fig. 1.9 : Sources of PMSMs machine faults	31
Fig. 1.10 : A comparison of power ability and switching frequency of power converters.....	32
Fig. 2.1 : Different types of fault acting on a system	43
Fig. 2.2: Medium motors derating factor due to unbalanced voltage	48
Fig. 2.3 : Effect of increasing temperature on the operating point.....	49
Fig. 2.4 : Demagnetization curve of magnetic materials.....	50
Fig. 2.5 : Maximum operating temperature of different magnet materials	51
Fig. 2.6 : Different types of eccentricity fault.....	53
Fig. 2.7 : Principle construction of a ball bearing with the required geometrical variables.....	55
Fig. 2.8 : The scope of power train fault investigation	58
Fig. 2.9 : A classification of TF method.....	64
Fig. 2.10 : Modeling method design-based analysis subsections flowcharts.....	68
Fig. 2.11 : Main concept of proposed technique for PMSM rotor fault detection; stator ac and dc field excitation in the d -axis is used for extraction of L'_d	70
Fig. 2.12 : Different shapes of magnet due to optimizing process against demagnetization fault [31] (Finally, the author Introduces the shape model 1 as a robust permanent magnet type of outer rotor PMSM for HEV)	71
Fig. 3.1 : Different PMSM structures : (a) Surface permanent magnet synchronous machine (SPMSM) without pole saliency, (b) inset SPMSM with pole saliency (mounted Magnet), (c) interior permanent magnet (IPM) with one layer of permanent magnet (V-shaped internal magnet), (d) (IPM) with one layer permanent magnet and squirrel cage for starting.....	86
Fig. 3.2 : Model of identification and diagnosis of abnormal behaviors of PMSMs	87
Fig. 3.3 : Model of identification and diagnosis of inter turn short circuit fault of PMSMs	88
Fig. 3.4 : Winding the PMSM with a short circuit between turns of the phase 'a' and 'b', dq stator reference.....	89
Fig. 3.5 : (a) - FFT analysis of stator current in healthy mode; (b) - Harmonic analysis of stator current in faulty mode	93
Fig. 3.6 : Cross section of the studied machine with one teeth having double width.....	94
Fig. 3.7 : Geometry of machine drawn in Flux2D	95
Fig. 3.8 : FFT analysis of stator currents simulated in healthy mode	95
Fig. 3.9 : FFT - analysis of stator currents in case of single phase circuit in phase 'a' with 15% turns short circuited at a speed of 1000 rpm.....	96

Fig. 3.10 : Modified geometry of the studied PMSM machine “symmetric magnetic circuit”	96
Fig. 3.11 : FFT- analysis of stator currents in healthy mode “symmetric magnetic circuit”	97
Fig. 3.12 : The general plan of test bench.....	97
Fig. 3.13 : PMSM motor structure, load situation and stator winding distribution by aiming different short circuit test.....	98
Fig. 3.14 : Angular position measurement.....	99
Fig. 3.15 : Inverter and its drivers	100
Fig. 3.16 : DSPASE 1104.....	100
Fig. 3.17 : Model of identification and diagnosis of inter turn fault of the vector controlled PMSM	101
Fig. 3.18 : Computer interface for managing the experimental tests.....	102
Fig. 3.19 : Motor speed under health operation.....	103
Fig. 3.20 : The measured speed changes based on reference speed changes by helping vector control regulation of 1000 rpm to 900 rpm	103
Fig. 3.21 : Motor 3 phase currents under healthy operation.....	104
Fig. 3.22 : FFT analysis of motor 3 phases currents under healthy operation.	104
Fig. 3.23 : FFT analysis of motor 3 phases currents under half load health operation... ..	105
Fig. 3.24 : (a)- Three PMSM stator currents in healthy and short circuit fault conditions (25% short circuit fault on phase A); (b)-Zoom on the same three PMSM stator currents	106
Fig. 3.25 : FFT analysis of motor 3 phases currents under 25% short circuit fault operation in phase B.	107
Fig. 3.26 : FFT analysis of motor 3 phases currents under 25% short circuit fault operation in phase B by speed fixed in 1000rpm. (b)-Zoom on the same three PMSM stator currents	108
Fig. 3.27 : Currents I_d and I_q under faulty operation.	108
Fig. 3.28 : FFT analysis under healthy and faulty operation (a)- Motor I_d currents; (b)- Motor I_q current.....	109
Fig. 3.29 : Fault diagnosis strategy of PMSM inter turn short circuits for SHEV application	112
Fig. 3.30 : Geometry of the electromagnetic problem.....	113
Fig. 3.31 : Cross section of the simulated PMSM geometry and the corresponding field distribution	114
Fig. 3.32 : (a) Magnetic flux density (B) FFT analysis of flux density in health case of PMSM	115
Fig. 3.33 : (a) Symmetric magnet failure and magnetic field distribution; (b) Flux density characteristic; (c) FFT analysis of the flux density	116
Fig. 3.34 : (a) Complete asymmetric for one magnet failure and magnetic field distribution; (b) Flux distribution; (c) FFT analysis of the flux.....	117
Fig. 3.35 : (a) Partial asymmetric for one magnet failure and magnetic field distribution; (b) Flux distribution; (c) FFT analysis of the flux density	118
Fig. 3.36 : Back EMF under healthy motor operation.....	119
Fig. 3.37 : Back EMF under Faulty motor operation (in this case one segment of 25 segments is demagnetized).....	119
Fig. 3.38 : Fault diagnosis strategy of PMSM demagnetization for SHEV application ..	120
Fig. 3.39 : Model of identification and diagnosis of eccentricity and bearing fault of PMSM for electric vehicles	121

Fig. 3.40 : Fault diagnosis strategy of PMSM eccentricity for SHEV application 122

Fig. 4.1 : Schematic diagram of a generator (G), 3-phase full bridge rectifier, 3-phase full bridge inverter and 3-phase induction motor by application in SHEV 126

Fig. 4.2 : Experimental setup 128

Fig. 4.3 : MATLAB/SIMULINK Simulation of a sample of SHEV 129

Fig. 4.4 : DC-BUS voltage under healthy mode operation of system (a- Simulation result; b- Experimental result) 130

Fig. 4.5 : DC-BUS current under healthy mode operation of system (a- Simulation results; b-Experimental result) 130

Fig. 4.6 : FFT analysis on DC-Bus current, a- healthy mode simulation and experimental result; b- Faulty mode simulation and experimental result (switch S2 is opened)..... 131

Fig. 4.7 : Zoom view of experimental and simulation FFT analysis results under faulty mode operation of motor (switch S2 is opened) 131

Fig. 4.8 : FFT analysis Comparison between motor current phase A under healthy mode operation, faulty mode by open phasing in switch S2 and also under open phasing fault by opening S1S3S2'S1' of Fig. (4.1)..... 132

Fig. 4.9 : FFT analysis comparison between DC-BUS voltage under normal mode operation, under open phase fault by opening S2 and under open phase fault by opening S1S2'1' of Fig. (1.4)..... 133

Fig. 4.10 : FFT analysis Comparison between DC-BUS current under normal mode operation, under open phase fault by opening S2 and under open phase fault by opening S1S2'1' of Fig (1.4)..... 133

Fig. 4.11 : Pattern identification and fault detection strategy..... 134

Fig. 4.12 : Fault Detection and implementation algorithm 135

Fig. 4.13 : Comparison between DC-BUS current under health state operation and under open phase fault by opening S2 of group 2 in table (4.1)..... 136

Fig. 4.14 : Consideration of capacitor influence on pattern identified under healthy and faulty operation of AC-DC converter (switch S2 is opened)..... 137

Fig. 4.15 : Consideration of load variations influence on pattern identified under faulty operation of AC-DC converter (switch S2 is opened)..... 138

Fig. 4.16 : Consideration of speed variations influence on pattern identified under faulty operation of AC-DC converter (switch S2 is opened)..... 138

Fig. 4.17 : FFT analysis under health and all faulty states operation (G2 – G5) with thyristor fire angle of ($\alpha=15^\circ$) 140

Fig. 4.18 : FFT analysis under health and all faulty states operation (G2 – G5) with thyristor fire angle of ($\alpha=30^\circ$) 140

Fig. 4.19 : FFT analysis under health and all faulty states operation (G2 – G5) with thyristor fire angle of ($\alpha=45^\circ$) 141

Fig. 4.20 : Model of identification and diagnosis of power converter fault in electric vehicles 141

Fig. 4.21 : Model of identification and diagnosis of open phasing fault of DC/AC power converter for electric vehicles 143

Fig. 4.22 : 3 phase motor voltage in healthy operation in 1000 rpm 143

Fig. 4.23 : 3 phase motor voltage in faulty operation in 1000 rpm and no load (13% UV) 143

Fig. 4.24 : 3 phase motor current in faulty operation in 1000 rpm and no load (22% UC) 144

Fig. 4.25 : 3 phase motor voltage in faulty operation in 800 rpm and no load (15% UV)	144
Fig. 4.26 : 3 phase motor current in faulty operation in 800 rpm	144
Fig. 5.1: Global strategy of supervision and diagnosis on drive trains of SHEV	150
Fig. 5.2 : Illustration of the “Level 0” of the vehicle diagnosis	150
Fig. 5.3 : Illustration of the “Level 1” of the vehicle diagnosis	151
Fig. 5.4 : Illustration of the “Level 0” of the vehicle diagnosis	151
Fig. 5.5: Illustration of the “Level 3” of the vehicle diagnosis	152
Fig. 5.6 : Implementation algorithm of drive-train fault diagnosis of SHEV	153
Fig. 5.7 : Different position of overlap between ANN training data,	155
Fig. 5.8 : ANN training results for 6 iterations	156
Fig. 5.9 : ANN based inter turn short circuit fault diagnosis test results for 6 iterations	157
Fig. 5.10 : ANN based inter turn short circuit fault diagnosis implementation	158
Fig. 5.11 : Different position of overlap between training data to ANN	161
Fig. 5.12 : ANN training results for 6 iterations	162
Fig. 5.13 : ANN result for fault diagnosis of AC-DC converter for 6 time repetition	163
Fig. 5.14 : AC/DC power converter fault diagnosis implementation	164
Fig. 5.15 : DC/AC power converter fault diagnosis implementation	166

List of Tables

Table 1.1: The advantage and disadvantage of HEVs [1], and [17]	24
Table 1.2 : EVs important parameters of battery	27
Table 1.3 : Electric propulsion adopted in the automotive industry	30
Table 1.4 : Characteristic of different propulsion system	30
Table 2.1 : comparison of different condition monitoring techniques	57
Table 2.2: A compression of different fault detection methods	58
Table 2.3 : Number of required search coils for different fault case	70
Table 3.1 : Possibility of experimental short circuit faults efforts according introduced connection in figure (3.13).	109
Table 3.2 : 3 phase motor current FFT analysis under different severity of short circuit fault noted in table (3.1).	109
Table 3.3: 3 phase motor current FFT analyses in different speeds under short circuit fault a2-N case.	110
Table 4.1 : Different fault structures in 3-phase full bridge ac/dc converter investigated by application in SHEV.....	127
Table 4.2 : Different thyristor angle fire in investigated 3-phase full bridge ac/dc converter.....	127
Table 4.3 : Main parts of experimental setup presented in figure (4.2).....	128
Table 4.4 : Rated characteristic of the used three-phase motor	128
Table 5.1 : Possibility of experimental short circuit faults efforts according introduced connection in chapter 3-figure (3.13).	154
Table 5.2 : ANN output results under different level of short circuit in SHEV application	159
Table 5.3 : ANN output results under different level of AC/DC switches open circuit in SHEV application (for 10 sample test)	165
Table 5.4 : Possibility of experimental unbalanced voltage faults efforts in terms of open phasing fault.....	167
Table 5.5 : ANN output results under different level of DC/AC switches open circuit in SHEV application (for 5 sample test)	167

General introduction

Since several years the orientation of the laboratory IRTES-SET⁽¹⁾ program was focused on transportation problems notably in collaboration with FEMTO-ST⁽²⁾ within the topic of electrical and hybrid vehicles (EV and HEV). The latter aim at zero emission is one of the challenges of the scientific researchers. Over the last years many thesis have treated the problems of electrical vehicles simulation, the drivetrains design, integration and control. These works led to a building of several prototypes of EV, HEV and Fuel cell electrical vehicle (FCEV). This experience accordingly to the literature highlighted the problem of availability of the electrical drives regarding to the classical ICE. So, to be competitive the electrical drive has to be more robust.

This thesis has been done in the frame work of the availability of the SHEV propelled by a PMSM. Indeed, the permanent magnet synchronous machines (PMSM) are increasingly integrated into various hybrid electrical vehicles as a traction motor or for ensuring an auxiliary function as the steering assistance. This success was confirmed during the last ten years, due to many advantages offered by these machines namely, a high power density, high efficiency and a very good reliability. In this context the PMSM will evolve to meet the socioeconomic constraints. Indeed, the wide public use of the HEV exposes the PMSM to the problems of materials cost (permanent magnets, copper, iron, etc.) which push to design optimization such as minimization of masses, the volumes and the cost. Such design will lead to PMSM more fragile than it is known until now. Furthermore, the transportation application requires a high degree of availability (continuity of service) despite the very severe operating conditions. To meet this societal demand, a good knowledge of the behavior of these machines in extreme environment conditions (vibrations, wide speed ranges and temperatures, repetitive starts and stops, etc.) is more essential than ever.

The work of this thesis will focus on the problem of availability of SHEV drivetrains based on PMSM. This device is generally composed of the primary power source (ICE) associated with an electric power generator, AC/DC and DC/AC power converters, the PMSM and the associated automatic control. The sensitive modeling by using the analytical and the experimental approaches is the potential contribution of our electrical and engineering research. Such models should provide a compromise between accuracy and computational speed. Also, they must be able to assess the severity of defects detected so as to define with the greatest possible accuracy the performances of the drivetrain in a faulty state. This allows doing a better management of the degraded modes of the drive train.

This report is composed of five chapters organized as following:

Chapter 1 summarizes the reasons of usage of HEV, investigates the different structures of HEV and presents the main performance, requirement and challenges in each electrical part of SHEV's drive-trains.

In chapter 2, a literature review of state of the art on power converter and electrical machines faults has been done. Because of our objective in this work, we more focused

⁽¹⁾IRTES-SET : Laboratoire SET (Systems et Transports) de l'IRTES (Institut de Recherche sur les Transport, l'Energie et la Société)

⁽²⁾FEMTO-ST : Franche-Comté Electronique Mécanique Thermique et Optique - Sciences et Technologies

on PMSMs. Different types of faults in power train of HEV as open circuit, short circuit and the problem of semi-conductors have been studied. In PMSMs, short circuit fault in stator winding, eccentricity, bearing, open phasing and etc. have been studied and different diagnosis methods have been considered. An analysis of advantages and drawbacks of each method lead to select the best method according to objective of this work.

In chapter 3, a deep study on diagnosis on short circuit fault in order to EVs and SHEVs applications have been done. The main steps required for artificial neural network (ANN) training by aim short circuit fault diagnosis in different speeds and loads of motor operation is investigated by help experimental data. Furthermore, the problem of demagnetization in an inset surface permanent magnet synchronous motor (ISPMSM) has been studied. One analytical model and one simulation model has been developed for characterizing the demagnetization faults of this kind of machines. This allows larger diagnosis knowledge about the PMSMs. Also, a study on the PMSM eccentricity and bearing fault has been performed and briefly explained.

Chapter 4 firstly presents a study on AC/DC power converter as an electric power bridge crossing for supplying PMSM. A deep theoretical and experimental investigation on fault modeling on this system has been done. The open phase fault effects on AC/DC converter have been studied. Two new patterns have been identified for this type of fault and the results validate by experimental test in different states of HEV application. Also a brief study on DC/AC converter has been presented while research is ongoing over inverter faults too.

In chapter 5, a Multilayer Perception (MLP) feed-forward neural network has been employed to classify the PMSM drive-trains faults. Different kinds of inter turn short circuit fault in stator winding of PMSM, different groups of switch breakout of AC/DC power converter and open circuit in DC/AC inverter faults have been detected by three dedicated ANN: 13 different classes of inter turn short circuit, 6 different classes of open phase fault in AC/DC converter and 13 different classes of unbalanced voltage caused by open circuit in DC/AC inverter have been detected, classified, and introduced as contribution of this ANN diagnosis model. In this regard, the sensitive models developed in chapters 3 and 4 are employed to train ANN to reach the said goals.

Chapter I

Problem of faults in the drivetrains of series hybrid electric vehicles (SHEV)

1. Introduction	19
2. Global CO2 Regulations	19
3. How is HEV helping to reach these goals?	21
3.1. Why hybrid electric vehicle? Efficiency perspective:.....	21
3.2. Why hybrid electric vehicle? Technology enablers:	22
4. Different architectures of HEV.....	22
5. Hybrid Electric vehicle propulsion system design: supervisory and control perspective,	25
5.1. Batteries	26
5.1.1 HEV battery requirements:.....	27
5.1.2 Challenges in HEV battery:	28
5.2. Electric motor drive selection issues for HEV propulsion systems:.....	28
5.2.1 HEV's electric propulsion requirements:.....	29
5.2.2 Variety in usage of different types of electric machine in HEV application:	30
5.2.3 Challenges in HEV electric propulsion:.....	31
5.3. Power electronic requirements.....	31
5.3.1 Types of semiconductor switches	32
5.3.2 Power Converter Control Methods.....	32
5.3.3 Power converter requirements:	33
5.3.4 Electromagnetic Compatibility.....	34
5.3.5 Challenges in HEV power converters:.....	34
6. Thesis objective.....	34
7. Conclusion.....	35
8. References of chapter I	36

1. Introduction

According to the last adopted regulation concerning the CO₂ emission limitations over the world (Europe, USA, china, Japan,...) the HEVs are more and more presented as a transient solution to a zero emission vehicle. However, the complexity of the HEVs drive-trains makes them fragile in terms of availability. So, in order to be competitive on the market where certain classical ICE vehicles are guaranteed by their manufacturers for seven years, the reliability of the electrical drive-train is considered by the searchers as one of the most important obstacles against a large public use of the HEVs [1]. This has led to the increasing importance of this topic in the last decade. It can be briefly expressed [2], and [3] as follow:

Transportation sector is a big user of fossil fuel

- For example: Transportation consumed 28% of 2008 USA energy output of 99.3 quadrillion BTU

Transportation sector is a major contributor in CO₂ emission

- For example: Transportation produced 33% of 2008 USA CO₂ emission total of 5814 MMT

Personal transportation is important

- Important mobility solution
- Big contributor to petroleum consumption (60% by automobile and light truck)

Automotive industry has been working on:

- Improving ICE based power-train efficiency
 - Electrification
- Improving power-train overall efficiency
 - Link to renewable energy supply
 - Alternative fuels
- Reducing petroleum consumption and CO₂ emission
- Reducing vehicle energy demand on per mile per person basis

Regulations, consumers, and infrastructure are integral to the endeavor

In this chapter, the global CO₂ regulations and the reasons of usage of HEV are investigated. Thus, different structures of HEV are shown with a focus on the main performances, requirements and challenges of the drivetrain of SHEVs. Finally, the principal problematic considered by our thesis is explained.

2. Global CO₂ Regulations

• United States [4]:

– In April 2010, the U.S. Environmental Protection Agency (EPA) and U.S. Department of Transportation (DOT) finalized a joint regulation for greenhouse gas (GHG) emissions and fuel economy for light duty vehicles for model years 2012-2016.

– The proposed fleet-average targets are 250g CO₂ /mile or 34.1 miles per gallon – The standards are based on vehicle footprint and separate car and light-truck standards have been formulated.

– The US released a Notice of Intent on September 30th, which lays out initial scenarios of potential stringency of fleet-wide GHG/fuel economy targets for cars and light trucks during the 2017-2025 timeframe.

– The scenarios represent 3 to 6 percent annual decrease in GHG levels from the MY¹2016 fleet.

– average of 250g CO₂ e/mile and translate into a range of fleet-wide targets from 190 to 143 gCO₂ /mile.

• **The European Union:**

– In 2009, the European Parliament and the Council adopted a Regulation (EC) N° 443/2009 setting CO₂ emission performance standards for new passenger cars. The fleet average to be achieved by all new passenger cars registered in the EU is 130 grams CO₂ per kilometer (gCO₂/km) by 2015. This target will be phased in from 2012, when 65% of each manufacturer's lowest emitting cars newly registered in that year must comply. This will rise to 75% in 2013, 80% in 2014, and 100% from 2015 onwards.

– A so-called limit value curve implies that heavier cars are allowed higher emissions than lighter cars while preserving the overall fleet average.

– The target of 95g CO₂/km is specified for the year 2020. Details on how this target will be reached will have to be defined in a review to be completed early 2013. Further legislative measures to reduce CO₂ emissions include mandatory fitting of tyre pressure monitoring system (by 2015), low rolling resistance tyres (by 2018) and gear shift indicators (by 2015) on all new passenger cars. In early 2011, the European Parliament and the Council approved the first CO₂ emission standard of 175 g/km in 2017 for light-commercial vehicles.

– A long-term target for CO₂ emissions of light commercial vehicles in 2020 (147g CO₂/km) has been included as well. Similar to the passenger vehicles, the details of the long-term target will be defined.

• **China:**

– In December 2009 the China Ministry of Industry and Information Technology (MIIT) issued its proposed Phase III fuel consumption regulation for passenger cars, aimed at reducing the fuel consumption of new passenger vehicles to 7l/100km (167 g CO₂/km) by 2015.

– The China Automotive Technology and Research Center (CATARC) is now developing a detailed implementation and enforcement plan because of shift from a per-vehicle standard to a corporate average standard.

• **Japan:**

– Introduced in 2007, the current fuel efficiency regulation set weight-based binned corporate average standards for model year 2015.

¹ MY : Model Year

– When the 2015 targets are met, the fleet average fuel economy is expected to be 16.8 km/L under the new Japanese JC08 driving test cycle, a 23.5% increase over 2004 performance of 13.6 km/L.

– Japan is now in the process of determining a standard for passenger car fuel economy for 2020, and a formal proposal is expected by the third quarter of 2011.

Regulation is leading the game:

- New Corporate Average Fuel Economy (CAFE) regulations are set, calling for 50% reduction in fuel consumption on per mile basis.
- EPA and ARB are also focusing on GHG emissions which depend on both fuel carbon content and fuel economy.
- Increased concern over oil imports has resulted in push for alternative fuels and electricity.
- Fuel economy is become more important in customer's purchasing decision
- Fuel economy improvement has become an integral part of product plans

3. How is HEV helping to reach these goals?

- CO₂ reduction of about 88.495 g CO₂/km, 33% reduction averagely
- Reducing less efficient engine operations such as engine idling and low load engine operation
 - Recovering kinetic energy by regenerative braking
 - Downsizing engine enabled by available battery power
 - Optimizing engine operations (more efficient) by:
 - EVT: electrically variable transmission
 - Using battery power and energy buffer for transient
 - Displacing fuel by depleting on-board energy storage that can be charged from the grid (PHEV) [2], [3], and [8].

3.1. Why hybrid electric vehicle? Efficiency perspective:

- 1- Higher overall vehicle power-train efficiency enabled by:
 - Dual energy converters
 - ICE: converting fuel chemical energy to mechanical energy
 - EM: conversion between electric energy and mechanical energy
 - Various configurations to enable blending of two powers for vehicle operations
 - Series HEV
 - Parallel HEV
 - Power split HEV: 1-mode, 2-mode
 - And more
 - Operating strategies optimized for applications

- 2- Lower vehicle accessory energy consumption enabled by:
 - Electrifying accessories such as
 - Electric power steering
 - Electric water pump
 - Electric AC compressor
 - Better accessory load management [2], [3], and [8].

3.2. Why hybrid electric vehicle? Technology enablers:

- Battery power density and energy density are more practical
 - For example: 2010 Prius NiMH pack: 44kg / 35L / 201.6V/6.5Ah
- Practical battery operating temperature range
 - For example: NiMH can operate between -30 °C to 52 °C
- Improved battery cycle life and calendar life
 - 15% SOC window, 300,000 shallow cycles (20-50wh)
- Electric machines and power electronics are more efficient and compact
 - 60kW motor /40kg / 15L, about 1.5 kW/kg, 96% peak efficiency
 - 50kW inverter /7kg / 7L, about 7 kW/kg, 98% peak efficiency
- Cost of battery and power electronics are becoming more manageable
 - Battery: \$1000/kWh or \$30/kW
 - Motor/Inverter: \$25/kW
- integrated vehicle controls to deal system complexities in:
 - Fuel Economy
 - Emission
 - Drivability
 - Safety
 - Durability [2], [3], [5] and [10].

4. Different architectures of HEV

The figure (1.1) shows a realistic representation of the integration of the main components of the drivetrain of an example of HEV architecture. Also general structures of hybrid electric vehicle include SHEV, PHEV and PS-HEV found in literature and used by industrial and academic researchers (but are not only limited to those) can be summarized by the synoptic diagram shown in figure (1.2), (1.3) and (1.4). The advantage and disadvantage of the major group of HEV include series, parallel and power split for a good comparison of their parameters are presented in table (1.1) in summary [2], [3], [8], [10], [14], and [15].

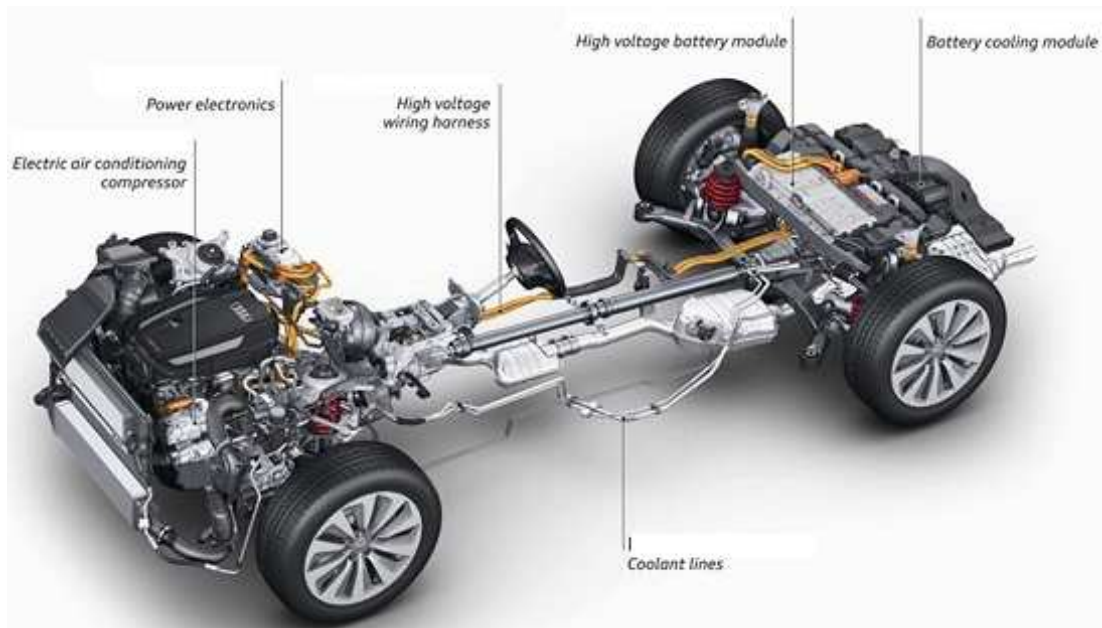


Fig. 1.1: Example of HEV architecture (Audi Q5)

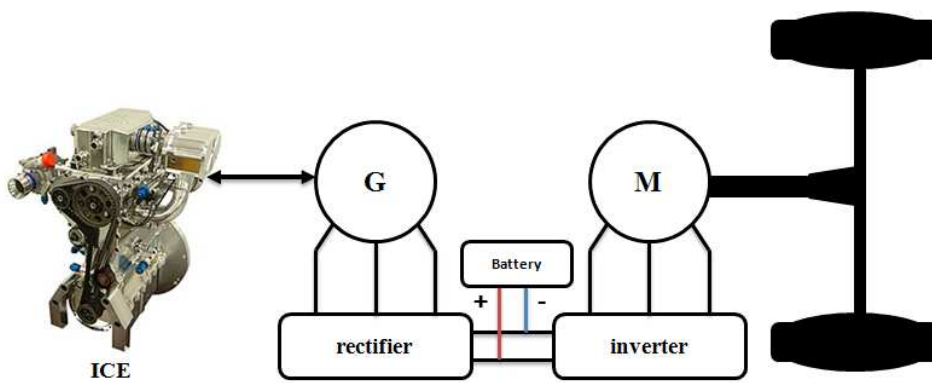


Fig. 1.2 : Series HEV (SHEV)

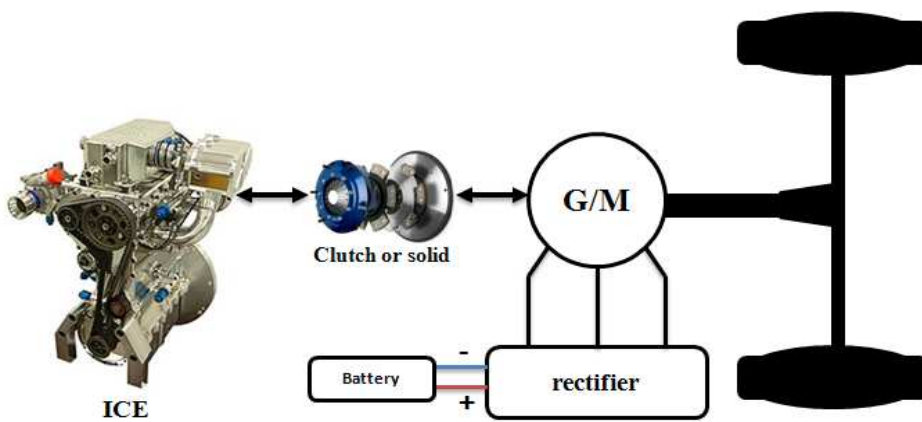


Fig. 1.3 : Parallel HEV (PHEV)

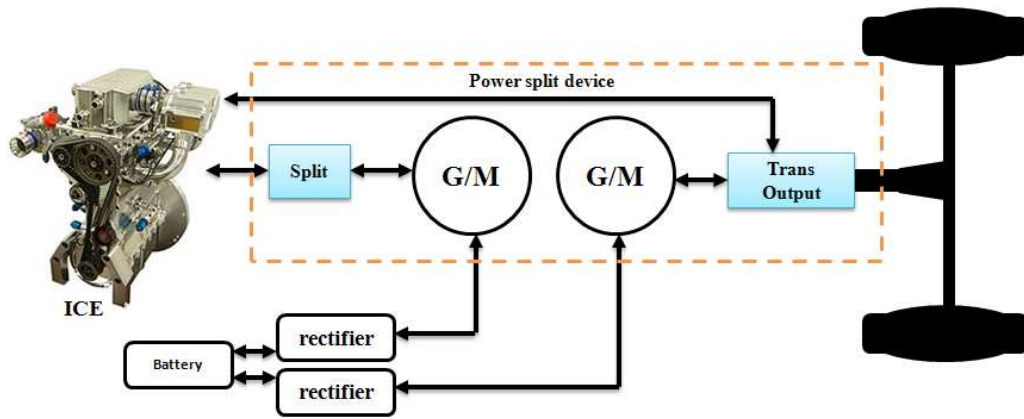


Fig. 1.4 : Power Split HEV (PSHEV)

Table 1.1: The advantage and disadvantage of HEVs [1], and [17]

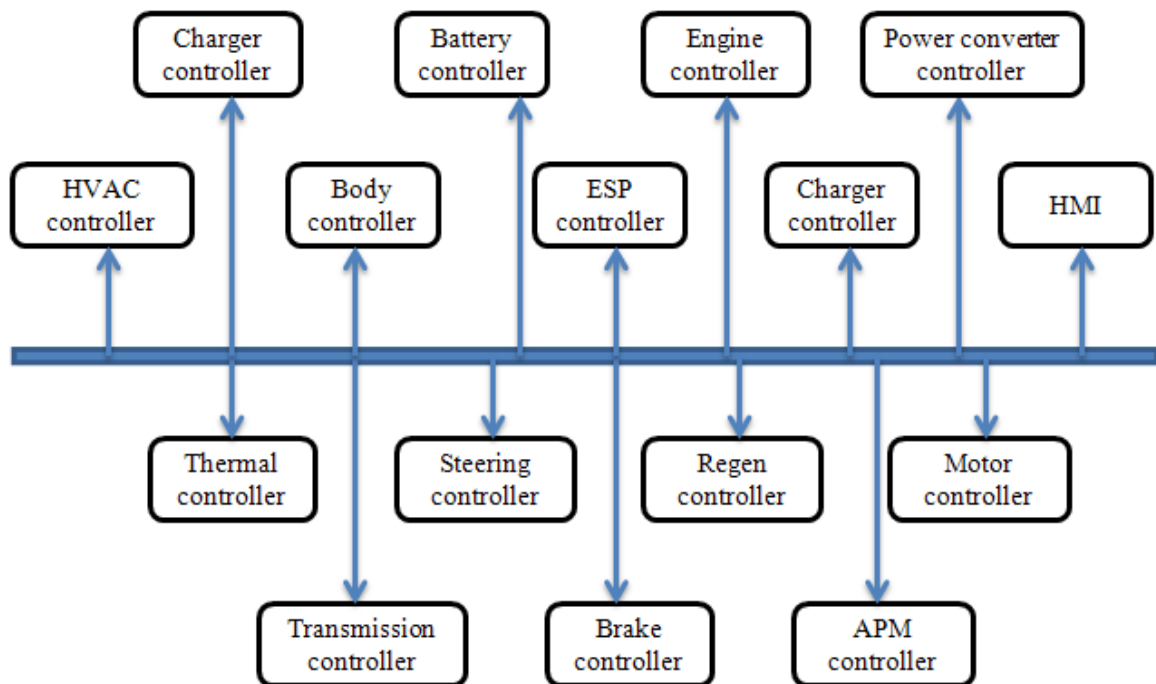
Different Types of HEV	Advantages	Disadvantages
Series HEV (S-HEV)	<ul style="list-style-type: none"> • Engine is decoupled from driven train, better for: <ul style="list-style-type: none"> - Engine efficiency, emission and controls optimization - Generator design optimization - E-drive capability and start-stop control • No special transmission integrated with EMs • Better transient efficiency because of more powerful traction system • The ICE is running mostly at its optimal combination of speed and torque 	<ul style="list-style-type: none"> • Need size traction motor and battery for peak traction requirement • Need size engine and generator for continuous traction requirement • Higher requirement for motor/generator efficiency
Parallel HEV (PHEV)	<ul style="list-style-type: none"> • Single motor/inverter • Lower electric power and efficiency requirements because of: <ul style="list-style-type: none"> - Direct ICE torque path • Less disturbance to vehicle architecture because of: <ul style="list-style-type: none"> - Nominal transmission integrated with a motor 	<ul style="list-style-type: none"> • Restricted E-drive <ul style="list-style-type: none"> - Limited space for more powerful EM - Reserve for Start control
Power Split HEV (PSHEV)	<ul style="list-style-type: none"> • EVT: electrically continuous variable transmission without clutches <ul style="list-style-type: none"> - Better engine operations - Better engine start-stop control • Recirculation power may be reduced with proper mechanical point • Highly integrated trans-axle • Production proven (Prius, Fusion etc.) 	<ul style="list-style-type: none"> • Motor loss due to recirculation power is still significant • E-drive capability may be restricted by kinematics • Less efficiency for aggressive driving

5. Hybrid Electric vehicle propulsion system design: supervisory and control perspective,

In general, the most common drive train of series hybrid electric vehicle (SHEV) consists of a three-phase AC generator coupled to a rectifier bridge, an inverter and the traction motor, as it is shown in figure (1.2). The internal combustion engine (ICE) mechanical output is first converted into electricity by the AC generator. Then, the three-phase bridge rectifier converts the AC voltage to DC with a ripple component, which is generally filtered by using a capacitor to reduce harmonics applied to the motor. Finally, the inverter converts DC to AC with the harmonic content limited by the choice of switching strategy [2], [3], and [14].

Control and monitoring of SHEV don't limit to electrical elements shown in figure (1.2) only. A more detail components of SHEV can be introduced as shown in figure (1.5) and (1.6) by control and supervisory perspective.

As is specified on figure (1.6), this work has a focus on AC/DC power converter and electric machine fault diagnosis by this aim that the extracted results can be used for control chains shown in figure (1.6).



(HVAC: Heating, Ventilation, and Air Condition), (ESP: Electronic Stability Program), (HMI: Human Machine Interface), (Regen: REGENERATION), (APM: AutoPilot Mega)

Fig. 1.5 : Hybrid electric vehicle control network

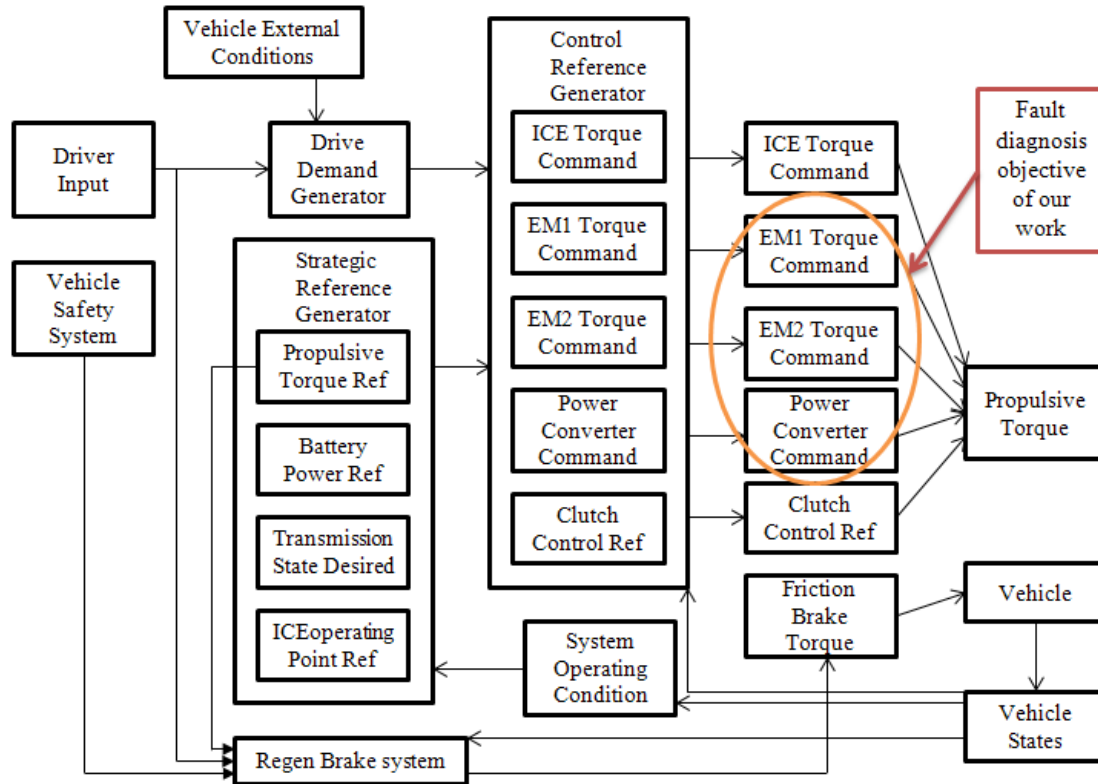


Fig. 1.6 : A generic supervisory control perspective of SHEV

Because of energy storage and propulsion systems are heart of HEV, in continue an investigation on specification of each electric parts have been presented briefly. Of course, because of objective of this work, it is more focused on electric machine and power converter.

5.1. Batteries

Actually are being used advanced batteries, how the battery valve regulated lead-acid (VRLA), the battery Nickel metal hidrure (Ni-MH), the Lithium-Ion battery (Li-Ion) among others, fuel cells and ultracapacitores to improve the source power of EVs. Nevertheless the battery is the part more important of an electric vehicle. The following is a list of the criteria for the selection of a battery for an electric vehicle according to [6], [9], [10], [11], and [13]:

- Voltage.
- Ampere-hour rating.
- Discharge rated.
- Watt-hour rating.
- Energy density.
- Cycle life.

Some of the most important parameters, as they are:

Specific energy, energy density, specific power, cycle life and costs of the batteries more used in EVs are in table (1.2).

Table 1.2 : EVs important parameters of battery

	Specific Energy (Wh/Kg)	Energy Density (Wh/l)	Specific Power (W/kg)	Cycle Life (cycles)	Cost (US\$/KWh)
VRLA	30-45	60-90	200-230	400-600	150
Ni-Cd	40-60	80-110	150-350		300
Ni-Zn	60-65	120-130	150-300	300	100-300
Ni-MH	60-70	130-170	150-300	600-1200	200-350
Li-Ion	90-130	140-200	250-450	800-1200	>200

According to table (1.2), batteries of low cost exist like the battery VRLA, nevertheless the energy density is low. The batteries have high energy density as the Ni-Zn battery, but their cycle life is reduced.

The Ni-MH battery presents better characteristics as high energy density, a great cycle life and great specific power, although the only disadvantage is its high cost. Nevertheless according to the Ni-MH battery has better benefits.

5.1.1 HEV battery requirements:

- 1- Battery charge/discharge power capability
 - Depends on battery temperature and SOC
 - Need to cover temperature range of -30 to 60° C
 - Typical full HEV: +/- 30 kW in nominal temperature and SOC range
- 2- Only need a limited energy window for HEV driving cycles
 - Typical < 300 wh
- 3- Light and compact
 - 70 wh/kg is quite satisfactory
- 4- Good cycle life for specified HEV shallow cycles
 - Approximately 300,000 cycle, 5% SOC
- 5- Safety
 - Sealed
 - Structurally sound
 - No thermal runaway
- 6- Uniformity across the pack
 - Balanced cells, Adequate cooling
- 7- Robust BMS performance

Typical cell characteristics are shown in figure (1.7). Cell behavior can be modeled as a resistor/capacitor network

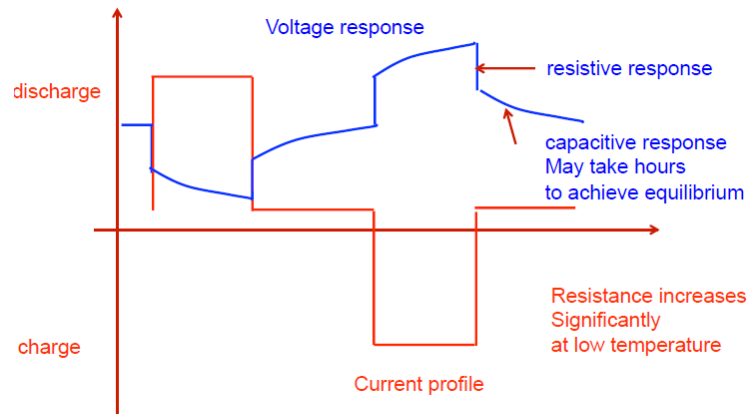


Fig. 1.7 : Typical cell characteristics

5.1.2 Challenges in HEV battery:

Challenges in HEV battery are:

- Precise battery power control to avoid over voltage / under voltage at low battery temperature.
- Accurate and robust SOC estimation:
 - SOC may drift away if it solely relies on current integration.
- To maintain cell uniformities across the whole pack:
 - Weak cells tend to be stressed more.
- Aging process is not well understood, therefore aging related monitoring and adjustment are difficult.

5.2. Electric motor drive selection issues for HEV propulsion systems:

Selection of traction motors for hybrid propulsion systems is a very important step that requires special attention. In fact, the automotive industry is still seeking for the most appropriate electric propulsion system for HEVs and even for electric vehicles. In this case, key features are efficiency, reliability and cost. The process of selecting the appropriate electric propulsion systems is however difficult and should be carried out at the system level. In fact, the choice of electric propulsion systems for HEVs mainly depends on three factors: driver expectation, vehicle constraint, and energy source. With these considerations, it is obvious that the overall motor operating point is not tightly defined. Therefore, selecting the most appropriate electric propulsion system for a HEV is a challenging task. [2], [3], [6], [8], [9], [10], [14], and [16].

In an industrial point of view, the major types of electric motors adopted or under serious consideration for HEVs and also for electric vehicles include the dc motor, the induction motor, the permanent magnet synchronous motor, and the switched reluctance motor. Moreover, according to an exhaustive review of the state of the art related to electric propulsion systems, it is observed that investigations on cage induction motors

and the permanent magnet motors are highly dominant, whereas those on dc motors are dropping while those on switching reluctance motors are gaining much interest.

5.2.1 HEVs electric propulsion requirements:

The major requirements of HEVs electric propulsion, as mentioned in past literature, are summarized as follows:

- High instant power and high power density.
- High torque at low speeds for starting and climbing, as well as high power at high speed for cruising.
- Very wide speed range including constant-torque and constant-power regions.
- Fast torque response.
- High efficiency over wide speed and torque ranges.
- High efficiency for regenerative braking.
- High reliability and robustness for various vehicle-operating conditions.
- Reasonable cost.

Moreover, in the event of faulty operation, the electric propulsion should be fault-tolerant. Finally, in an industrial point of view, an additional selection criterion is the market acceptance degree of each motor type, which is closely associated with the comparative availability and cost of its associated power converter technology.

Figure (1.8) illustrates the standard characteristics of an electric motor used in EVs or HEVs. This characteristic corresponds to the profile of the tractive effort versus speed on the driven wheels. It should be noted that these characteristics depend on the Hybridization Factor (HF) shown by (1.1).

$$HF = \frac{P_{EM}}{P_{EM} + P_{ICE}} = \frac{P_{EM}}{P_{HEV}} \quad (1.1)$$

Where P_{HEV} is the maximum total traction power to propel the HEV? It has been demonstrated that hybridization improves HEV fuel economy and dynamic performances up to a critical optimum point ($HF = 0.3$ to 0.5). After this point, increasing the electric propulsion system capacity will not improve the HEV performances against fuel consuming.

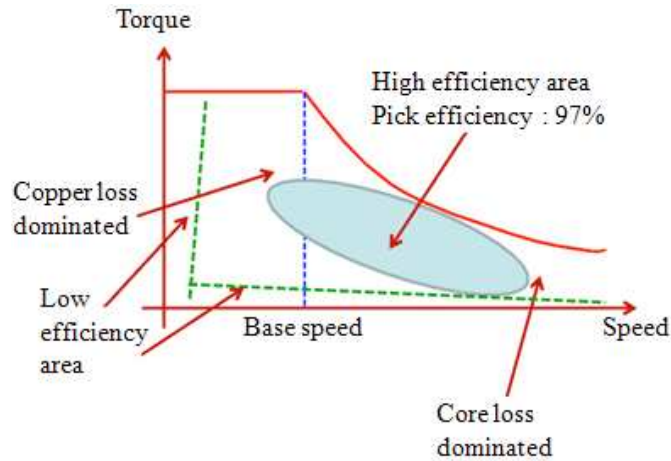


Fig. 1.8 : A sample PMSM efficiency characteristic

5.2.2 Variety in usage of different types of electric machine in HEV application:

Table (1.3) briefly reviews the electric propulsion adopted in the automotive industry. The induction motor seems to be the most adapted candidate for the electric propulsion of urban HEVs. In fact, this solution is a consensual one as illustrated by the evaluation summarized in table (1.4) and based on the main characteristics of the HEV electric propulsion, each of them is graded from 1 to 5 points, where 5 points means the best. Indeed, this evaluation is an update of the one done.

Table 1.3 : Electric propulsion adopted in the automotive industry

HEV Model	Propulsion System
<i>PSA Peugeot-Citroën / Berlingo (France)</i>	<i>DC Motor</i>
<i>Holden /ECOMmodore (Australia)</i>	<i>Switched Reluctance Motor</i>
<i>Nissan/Tino (Japan)</i> <i>Honda/Insight (Japan)</i> <i>Toyota/Prius (Japan)</i>	<i>PMSM</i>
<i>Renault/Kangoo (France)</i> <i>Chevrolet/Silverado (USA)</i> <i>DaimlerChrysler/Durango (Germany/USA)</i> <i>BMW/X5 (Germany)</i>	<i>IM</i>

Table 1.4 : Characteristic of different propulsion system

Propulsion system	DC	IM	PM	SRM
Characteristics				
<i>Power density</i>	2.5	3.5	5	3.5
<i>Efficiency</i>	2.5	3.5	5	3.5
<i>Controllability</i>	5	4	4	3
<i>Reliability</i>	3	5	4	5
<i>Technological maturity</i>	5	5	4	4
<i>cost</i>	4	5	3	4
Total	22	26	25	23

5.2.3 Challenges in HEV electric propulsion:

However electric machines are used in electric vehicles has high reliability but under conditions of continuous operation and under continuous load and speed changes are incurred some damages. As a summary of the sources of faults and their types can include [18] and [19] as shown in figure (1.9).

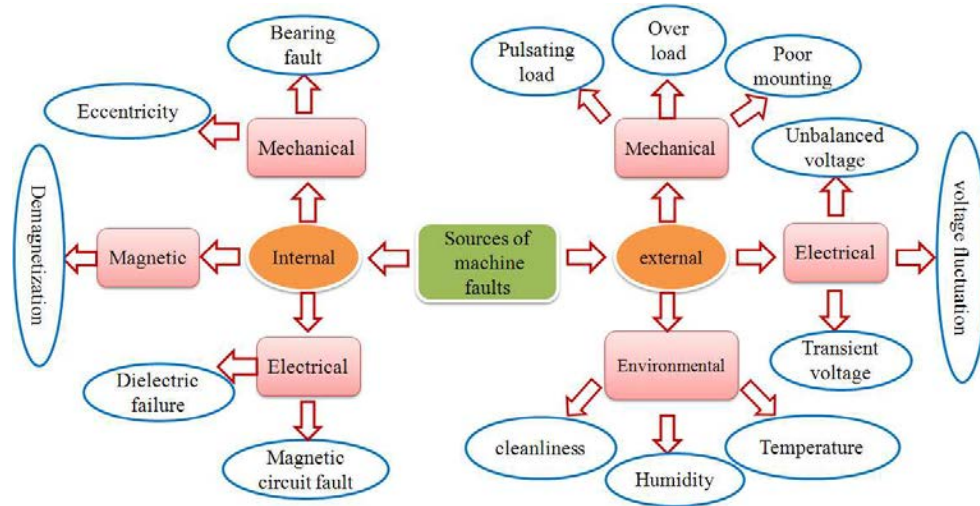


Fig. 1.9 : Sources of PMSMs machine faults

A study on the major component failure of powerhouse motors has been conducted by IEEE-IGA and EPRI (Electric Power Research Institute). According to these studies, stator faults (ground insulation, turn insulation, bracing, wedges, core and etc.) and bearing faults (sleeve bearings, anti friction bearings, seals, trust bearings and etc.) have been allocated highest percentage of failure in electrical machines. The study is carried out on the basis of opinion as reported by the motor manufacturer [20], and [21].

5.3. Power electronic requirements

The power switching devices, electric motors, and associated control systems and components play a key role in bringing hybrid and fuel-cell vehicles to market with reliability and affordability. The power electronic system should be efficient to improve the range of the electric vehicles and fuel economy in hybrid vehicles. The selection of power semiconductor devices, converters/inverters, control and switching strategies, the packaging of the individual units, and the system integration are very crucial to the development of efficient and high-performance vehicles. In addition to power devices and controllers, there are several other components such as capacitors, inductors, bus bars, thermal systems, etc., that form a major portion of a power electronic unit. The packaging of all these units as one system has significant challenges [5], [6], [7], [12], and [14].

5.3.1 Types of semiconductor switches

Uncontrollable: Devices turn on and off depending upon circuit operation, Ex: Diode. Turn on controllable: Devices turn on when a gate signal is applied, they turn off when the circuit turns them off, Ex: Silicon Controlled Rectifier (SCR)

Fully controllable: Devices turn on when a gate signal is applied, and they turn off when the gate signal is removed, Ex: MOSFET, IGBT.

We often assume “ideal switches”: Zero current thru them when “off” (open circuit), Zero voltage across them when “on” (short circuit)

A comparison of different silicon power switches has been shown in figure (1.10). Majority carrier devices (e.g. MOSFET) have very high switching frequencies, but relatively low power capability. Minority carrier devices (e.g. IGBT) have moderate switching frequencies, and medium-high power ratings. Latching devices (e.g. IGCT or Thyristor) have low switching frequencies but very high power ratings.

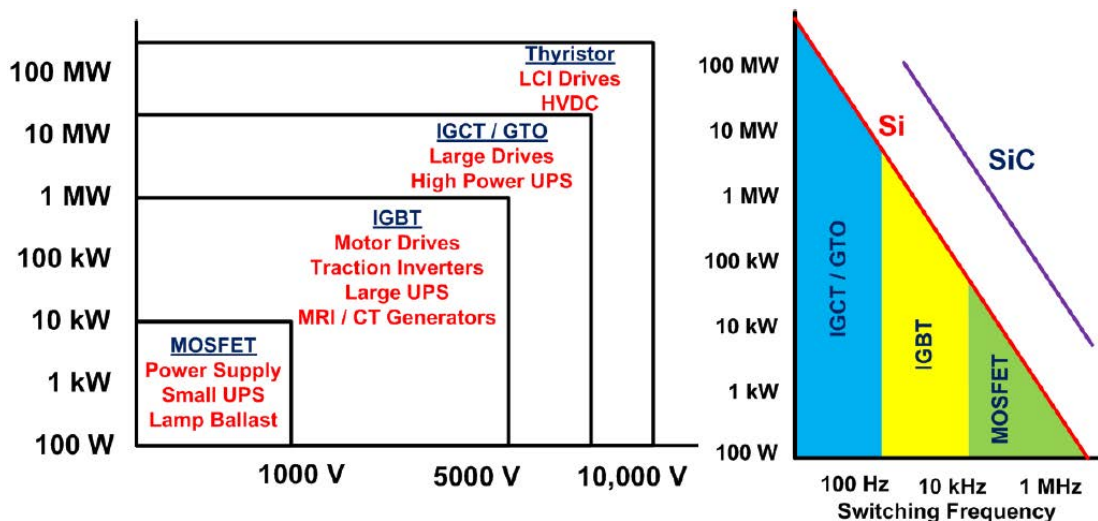


Fig. 1.10 : A comparison of power ability and switching frequency of power converters

5.3.2 Power Converter Control Methods

There are many control methods used to regulate the output voltage of a switching power supply. The two most common methods are voltage mode control (VMC) and current mode control (CMC).

These both adjust the converter duty cycle to provide regulation, generally it is to keep the output voltage fixed. The perturbations that need to be adjusted for are changes in the input voltage, load current, and other parameters.

VMC: the output voltage of the converter is processed, usually by an operational amplifier, as the signal in to the PWM ramp comparator.

CMC: the PWM ramp comparator has its input as the inductor current, sometimes with a small additional ramp. The other comparator input is a control reference voltage.

This creates an inner control loop, and simplifies the control characteristics. An additional current sensor is required.

5.3.3 Power converter requirements:

In the power electronics, by decades the pulse wide modulation (PWM) in converters DC-AC has been used mainly, due to its circuit simplicity. But because of switching losses, the switching frequency of PWM converters is usually around a few kilohertz when the power rating is tens of kilowatts. However, power density and circuit performance are improved with higher switching frequency. Higher switching frequencies in PWM converters are limited by the following aspects given by [15]:

- 1) Because of high voltage and current peaks, switching stresses on the power devices are very higher during the turn-on and turn-off transients, which result in over-sizing the Safe Operation Area (SOA).
- 2) Turn-on and turn-off switching losses.
- 3) When the voltage rise and fall, the capacitance coupling current in turn oscillates with the line inductance, resulting in severe di/dt and dv/dt , which produce electromagnetic interference (EMI).

There are some power electronics performance specifications for propulsion system of EV such as,

- 1) Efficiency: >98 % peak
- 2) Cost: <\$10/kW
- 3) Power density: >1000 kW/ft³
- 4) dv/dt <1000 μ s
- 5) Switching frequency: >20 kHz
- 6) Reliability: failure before the end of the vehicle life.
- 7) zero emissions and no interference
- 8) Robustness

Several converters soft switching using switching zero voltage (ZVS) or switching zero current (ZCS) has been proposed in the literature, and the idea is to improve the operation in high frequency with the reduction of losses in switching and EMI. Some converters soft switching proposed in [16] were compared with a converter DC/AC in hard switching, the proposed converters were:

- Inverter with 6 switches with transition zero current (ZCT).
- Inverter with exchanged pole resonant aid (ARCP) and transition zero voltage (ZVT).
- Inverter ZCT with 3 switches of low cost.

The comparison of efficiency indicates that the inverter soft switching evaluated doesn't show improvements on the inverter in switching hard, besides which its cost is more elevated due to the circuit's aids and also involves a greater space.

5.3.4 Electromagnetic Compatibility

Electromagnetic compatibility refers to the ability of a system to create un-intentional high frequency energy, either conducted or radiated. This is due to the high " dv/dt " and " di/dt " associated with the power semiconductor switching.

There are regulatory limits that constrain how much electrical energy can exit the system. In the United States, the regulatory agency is the Federal Communications Commission (FCC).

The regulations are specified over a defined frequency band, usually 150 kHz to 30 MHz for conducted emissions, and above 30 MHz for radiated missions. There is a controlled set of operating conditions (RBW, quasi-peak, average, etc) for the tests. A specified "limit line" sets a maximum value for a product to be compliant. Thus, at all frequencies the product must be below the limit line value, or else it fails.

5.3.5 Challenges in HEV power converters:

Despite a clear change in their electrical and thermal performance in recent years, semiconductors and power modules components remain among the most fragile conversion components in the drivetrains of HEV. They are the first victims of any excessive stress and possible problems that may occur during the life of the equipment (eg thermal runaway or transient overvoltage breakdown of a driver, short – circuits, the load loss insulation to ground, or defect of control signal transmissions). The failure of a power chip is usually a highly critical event as the risk of the housing explosion, power interconnections and the failure propagation within the system itself resulting interruption of service [22].

This issue is a major problem for HEVs, where providing redundancy is not easy regarding to the limited spaces on board of the vehicle. Consequently, the reliability of power converters request the use of close monitoring and protection to ensure the device safety but also the continuity of its mission even in the presence of an internal failure.

The solution generally proposed for this problem is to design and evaluate new structures of power converters inherently secured thanks to their ability of internal reconfiguration and fault tolerance properties. These new systems as well as the classical ones require a high degree of monitoring and diagnosis. The latter may be performed through the detection, the location and the severity evaluation of internal faults of these systems before any control reconfiguration.

6. Thesis objective

Since several years the orientation of Laboratory IRTES-SET program was focused on transportation problems by adopting a systemic approach. The electro-

mobility aiming at zero emission is one of the challenges of the scientific researchers developed by IRTES-SET teams. Over the last years many thesis have treated the problems of electrical vehicles simulation, the drivetrains design, integration and control. These works led to a building of several prototypes of EV, HEV and Fuel cell electrical vehicle (FCEV). This experience accordingly to the literature highlighted the problem of availability of the electrical drives regarding to the classical ICE. So, to be competitive the electrical drive has to be more robust.

The thesis presented in this report has been done in the frame work of the availability of the SHEV propelled by a PMSM. Indeed, the permanent magnet synchronous machines (PMSM) are increasingly integrated into various hybrid electrical vehicles as a traction motor or for ensuring an auxiliary function as the steering assistance. This success was confirmed during the last ten years, due to many advantages offered by these machines namely, a high power density, high efficiency and a very good reliability. In this context the PMSM will evolve to meet the socioeconomic constraints. Indeed, the wide public use of the HEV exposes the PMSM to the problems of materials cost (permanent magnets, copper, iron, etc.) which push to optimization design such as minimization of masses, the volumes and the cost. Such design will lead to PMSM more fragile than it is known until now. Furthermore, the transportation application requires a high degree of availability (continuity of service) despite the very severe operating conditions. To meet this societal demand, a good knowledge of the behavior of these machines in extreme environment conditions (vibrations, wide speed ranges and temperatures, repetitive starts and stops, etc.) is more essential than ever.

The work of this thesis will focus on the problem of availability of SHEV drivetrains based on PMSM. This device is generally composed of the primary power source (ICE) associated with an electric power generator, AC/DC and DC/AC power converters, the PMSM and the associated automatic control. The sensitive modeling by using the analytical and the experimental approaches is the potential contribution of our electrical and engineering research. Such models should provide a compromise between accuracy and computational speed. Also, they must be able to assess the severity of defects detected so as to define with the greatest possible accuracy the performances of the drivetrain in a faulty state. This allows doing a better management of the degraded modes of the drive train.

7. Conclusion

In this chapter, we presented a state of the art on HEV by a focus on SHEV drivetrain. Then we give information about their main components (batteries, PMSM, AC-DC and CD-AC power converters) in terms of characteristics and limits of operating against their competitiveness regarding to the classical ICE vehicles. Much of this chapter was devoted to the problem of availability of the SHEV drivetrains as one of the most important challenges of this technology to have a place on the automotive market. This topic has been defined as the principal objective of the thesis work presented in this report. Indeed, to study and implement fault diagnosis systems in these vehicles is necessary to enable them to be more reliable and safe enhancing its sustainability.

In Chapter 2, more details will be given on how the diagnosis problem has been treated in the electrical engineering area. The goal is to select the best methods to carry out the objectives of this thesis.

8. References of chapter I

- [1] Seyed saeid Moosavi, A. N'Diaye, A. DjerdirY. Aït. Amirat, D. A. Khaburi, "Pattern Identification For Fault Detection In The Power Supply Of A Series Hybrid Electric Vehicle (SHEV)", 4th IEEE International Conference on Power Electronics, Drive System & Technologies (PEDSTC 13), 13-14 Feb 2013.
- [2] C. C. CHAN, "The State of the Art of Electric and Hybrid Vehicles", Proceedings of the IEEE, Vol. 90, No. 2, February 2002.
- [3] C. C. CHAN, "The State of the Art of Electric, Hybrid, and Fuel Cell Vehicles", Proceedings of the IEEE | Vol. 95, No. 4, April 2007.
- [4] http://ec.europa.eu/clima/policies/transport/vehicles/index_en.htm
- [5] Harvey J. Schwartz, "A Summary of HEV Propulsion Technology", IEEE Transactions on Vehicular Technology. Vol. VT-32. NO. 1, February 1983.
- [6] Alcalá, A. Claudio, G. V. Guerrero, "Analysis of Propulsion Systems in Electric Vehicles", 2nd International Conference on Electrical and Electronics Engineering (ICEEE) and XI Conference on Electrical Engineering (CIE 2005) Mexico City, Mexico. September 7-9, 2005.
- [7] Fabien Meinguet, Paul Sandulescu, Xavier Kestelyn, and Eric Semail, "A Method for Fault Detection and Isolation Based on the Processing of Multiple Diagnostic Indices: Application to Inverter Faults in AC Drives", IEEE Transactions On Vehicular Technology, Vol. 62, No. 3, March 2013.
- [8] Mehrdad Ehsani, Khwaja M. Rahman, , and Hamid A. Toliyat, "Propulsion System Design of Electric and Hybrid Vehicles", IEEE Transactions On Industrial Electronics, Vol. 44, No. 1, February 1997.
- [9] Yimin Gao and Mehrdad Ehsani John M. Miller, "Hybrid Electric Vehicle: Overview and State of the Art", IEEE ISIE 2005, June 20-23, 2005, Dubrovnik, Croatia.
- [10] Chunbo ZHU, "Emerging Transportation Markets in China", ITEC 2012.
- [11] Alireza Khaligh, and Zhihao Li, "Battery, Ultracapacitor, Fuel Cell, and Hybrid Energy Storage Systems for Electric, Hybrid Electric, Fuel Cell, and Plug-In Hybrid Electric Vehicles: State of the Art", IEEE Transactions On Vehicular Technology, Vol. 59, No. 6, July 2010.
- [12] M. Abul Masrur, ZhiHang Chen, and Yi Lu Murphey, "Intelligent Diagnosis of Open and Short Circuit Faults in Electric Drive Inverters For Real-Time Applications", IET-Power Electronics (Journal), 03 MAR 2009.
- [13] Eckhard Karden, Serv'e Ploumen, Birger Fricke, Ted Miller b, Kent Snyder, "Energy storage devices for future hybrid electric vehicles", Journal of Power Sources 168 (2007).
- [14] Ali Emadi, Young Joo Lee, and K. Rajashekara, "Power Electronics and Motor Drives in Electric, Hybrid Electric, and Plug-In Hybrid Electric Vehicles"; IEEE Transactions On Industrial Electronics, Vol. 55, No. 6, June 2008.
- [15] Ali Emadi, Kaushik Rajashekara, Sheldon S.Williamson, and Srdjan M. Lukic, "Topological Overview of Hybrid Electric and Fuel Cell Vehicular Power System Architectures and Configurations", IEEE Transactions On Vehicular Technology, Vol. 54, No. 3, May 2005.
- [16] M. Zeraoulia1, M.E.H. Benbouzid1, and D. Diallo2, "Electric Motor Drive Selection Issues for HEV Propulsion Systems: A Comparative Study", 2005 IEEE Conference on Vehicle Power and Propulsion, VPPC2005.
- [17] Seyed saeid Moosavi, D. A. Khaburi, Y. Aït. Amirat, A. Djerdir, "Fault Detection Investigation In A Full Bridge Thyristor Base AC-DC Converter", 39th Annual Conference of the IEEE Industrial Electronics Society, IECON 2013, 10-13 November, Vienna.
- [18] Rosero. J, Romeral. L, Cusido. J, Ortega. J. A, "Fault detection by means of wavelet transform in a PMSMW under demagnetization", Industrial Electronics Society, 2007. IECON 2007. 33rd Annual Conference of the IEEE , Publication Year: 2007 , Page(s): 1149 – 1154.

- [19] “Report of Large Motor Reliability Survey of Industrial and Commercial Installations, Part I,” Industry Applications, IEEE Transactions on, vol. 21, no. 4, pp. 853-864, 1985.
- [20] Rotating Electrical Machines, Part 4: Methods for Determining Synchronous Machine Quantities from Tests, IEC Standard 60034-4, 2008.
- [21] Sanada, M.; Inoue, Y.; Morimoto, S, “Rotor structure for reducing demagnetization of magnet in a PMASynRM with ferrite permanent magnet and its characteristics” Energy Conversion Congress and Exposition (ECCE), 2011 IEEE Digital Object Identifier: 10.1109/ECCE.2011.6064340 Publication Year: 2011 , Page(s): 4189 – 4194.
- [22] www.seedsresearch.eu, “Rapport prospectives 2012-2013 du GdR-SEEDS, France 2013.

Chapter II

**A review of state of the art
on drivetrains faults of
SHEV**

1. Introduction	41
2. Requirements of fault diagnosis	41
3. Fault specification of drive-train of SHEV	44
3.1. Stator winding faults:	44
3.2. Stator core-related faults	45
3.3. Open phase, phase to ground, line to line, line to line to ground faults.....	46
3.4. Unbalanced voltage fault.....	47
3.5. Demagnetization fault	48
3.6. Eccentricity fault	52
3.7. Bearing fault.....	53
3.8. Power converter	55
4. Diagnosis methods, a deep investigation and comparison on drivetrain faults	57
4.1. Investigations based on simulation – analytical or finite element methods	58
4.1.1 Frequency domain analysis	59
4.1.2 Time-Frequency (TF) domain analysis.....	63
4.1.3 Analytical model based analysis.....	67
4.1.4 Modeling method design based analysis	68
4.1.5 Investigations based on design changes - practical design	71
4.1.6 Parameter estimation:	72
4.1.7 Fuzzy logic.....	72
4.1.8 Artificial Neural network.....	72
4.1.9 Synthesis study	74
4.1.10 Conclusion	74
5. References of chapter II.....	76

1. Introduction

The most important steps in fault diagnosis are fault recognition (to identify the specification of faults and their effects on system), select of a suitable data for acquisition (current, voltage, torque, flux, vibration, modeling and etc.), signal processing and data analysis method (FFT, TF, ANN and etc.) aiming to reach proper pattern identification.

In this chapter, after a quick study on fault diagnosis requirements, a literature review of state of the art on electrical machines (EM) and power converter faults has been done in regard to said objective.

2. Requirements of fault diagnosis

In general, monitoring and diagnosis require the detection and analysis of signals containing specific information (symptoms or signatures) that characterizes the degradation of the machine [1], and [2].

In order to carry out an online fault diagnosis scheme, it is highly desirable to use an easy-to-calculate fault severity index with low computational burden [3].

Condition monitoring of electric systems problems is essential to guarantee high performance, efficiency, and reliability [4].

Different names are used to distinguish the diagnosis steps according to their depth [4]:

- 1- Fault detection: distinction that a fault has occurred or no. This step determines the time at which the system is subject to some fault.
- 2- Fault isolation: find in which component a fault has occurred. This step determines the location of the fault.
- 3- Fault identification and fault estimation: identify the fault and estimate its magnitude. This step determines the kind of fault and its severity.

Faults also can be categorized into additive and multiplicative faults, in terms of how the faults influence the system variables. Additive faults influence the variables additively, such as offsets of sensor; while multiplicative faults usually affect the system parameters by a product factor. Another way of categorizing faults is time-based, namely abrupt and incipient faults. An abrupt fault represents an undesired and sudden change, while an incipient fault is a fault that causes undesirable drifts away from healthy values and gradually grows with time. There are many ways to categorize the different diagnosis schemes described in literature, but here we divided them into two groups, Model-free and Model-based methods. In the Model-free methods, the fault detection and isolation methods do not use a model of the plant and they range from physical redundancy and special sensors through limit-checking and spectrum analysis to logical reasoning.

The general idea of fault diagnosis model based methods is to compare the available measurements of the monitored system with their corresponding predictions obtained using an analytic or qualitative model. If they differ significantly, then it may be concluded that a fault has occurred. Nonetheless, the problem with this approach is that

a precise description of a system that takes the effects of faults. Different kinds of simplified models are used in fault detection and isolation. When classifying models applied to the diagnostics of processes (systems), it is possible to distinguish models of systems applied to fault detection and models used for fault isolation. Models used for fault detection describe relationships existing within the system between the input signals (u) and output signals (y), and allow detecting changes (fault signals φ) caused by faults. Models used for fault isolation define the existing relationship between fault signals φ and faults f , which will be represented by $\varphi \rightarrow f$.

If you choose any method, it is clear that rapid diagnosis and correction of a failure in an electrical vehicle ensures optimum reliability, maximum safety, maintenance on time prevention and rescue of electric vehicle applications. Many methods have been developed during the last 15 years to detect faults in the different parts of electrical vehicle as EM. General monitoring systems consist of three major targets of safety, economy and technical follow. Each of these targets is to include a few key points [5] and [6] that are follows:

❖ **Safety objectives,**

- Increasing safety, reduce stress and worry in staff (in industrial zone) or passengers (in EV and Traction application),
- Reducing the risks and environmental damage in the timely identification of defects,

❖ **Economic objectives,**

- Reducing operating costs by accurate and regular monitoring,
- Reducing the number of care staff,
- Reducing costs out of Circuit with a better plan to cut out of the circuit for care of it,
- Proper planning for replacement of a new element to identify the elements status on the network,

❖ **Technical objectives**

- Increased reliability and network element
- To obtain technical information with a conscious action to prevent the fault
- Optimization of system and element performance and the identification of the element available loading on element and network.
- Obtaining quantitative information about how to change and behavior of measurable quantities.
- Identifying dependencies between measurable quantities and time Distances of the measurement.

The fault acting upon a system can be divided into three types of faults, see figure (2.1).

- Sensor (Instrument) faults. Fault acting on the sensors.
- Actuator faults. Fault acting on the actuators.

- Component (system) faults. Fault acting upon the system or the process we wish to diagnose.

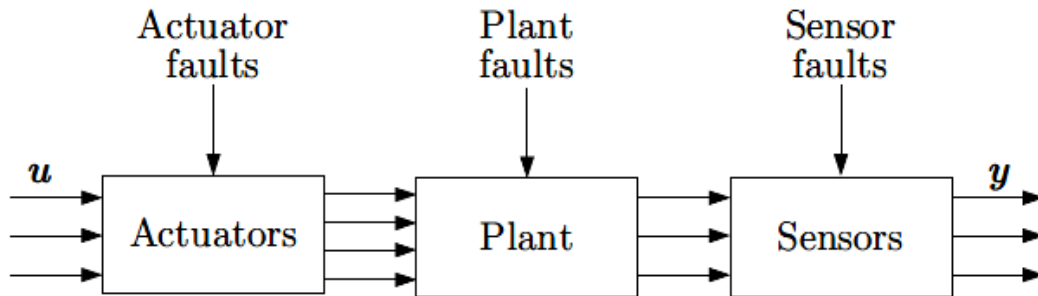


Fig. 2.1 : Different types of fault acting on a system

Based on figure (2.1), the most important factors for diagnosis [6] and [7] are listed in below:

- 1- What type of instrumentation is required to monitor some of the most popular parts used in EV fault detection?
- 2- The degree of accuracy of fault indication that may be obtained when relying on a specific parameter,
- 3- The level of expertise an operator needs in order to interpret the recorded data,
- 4- How a dedicated sensor for each fault indicator would be invasive?
- 5- Possible means of analysis (signal processing techniques)

The most important points for sensors that are used for fault detection are listed below too [7],

- 1- The sensor should be non-invasive,
- 2- The sensor and instrumentation system must be reliable,
- 3- The diagnosis must be reliable,
- 4- The severity of the problem should be quantified,
- 5- Ideally, an estimation of the remaining run-life should be given,
- 6- Ideally, a prediction of the fundamental cause(s) of the fault should be provided via on-line information from sensors etc.

The large amount of previous work carried out in the area of fault diagnosis and condition monitoring shows that there have been many challenges and opportunities for engineers and researchers to focus on this issue. Various recommendations and solutions concerning condition monitoring technologies have been given in this area, mainly depending on the machine type, size, operating conditions (loading), available instrumentation, cost constraints, etc.

In order to allow analysts to correlate different aspects of each technology to troubleshoot symptoms and determine a course of action to avert failures, several fields of science and technology, such as electrical, mechanical, thermal, and sometimes chemical engineering should be closely considered and combined whenever possible. In some articles, the control methods are based on data acquisition and analysis of these

data and the design of a control algorithm. In contrast, some methods use additional equipment on the primary system to control the system [8], [9] and [10]. Complete analysis of these methods for fault diagnosis and the effects of faults in the SHEV applications are discussed in this work subsequently.

3. Fault specification of drive-train of SHEV

3.1. Stator winding faults:

The stator winding fault due to short-circuited turns is known as the most common electrical fault in electrical machine. The majority of winding fault are caused by the breakdown of turn-to-turn insulation as a result of the voltage, current, or thermal stress acted on the stator winding. The process of insulation breakdown is a complex one. Beginning with partial discharge and very localized heating and progressing to a low resistance short circuit capable of carrying considerable current.

Consider a motor by the rated current 20.3 A. If a turn to turn short circuit occurs within a motor winding containing “ n ” turns, so as to form a shorted coil of “ m ” turns, then the portion of the back EMF seen by the shorted turns will drive a current of “ n/m ” times terminal short circuit current (neglecting resistance).

Clearly the most severe case is a single shorted turn. Since for this machine that contains 50 turns per phase and has a terminal short circuit current of 20.3 A, a single shorted turn will try to carry 1015 A. In contrast to a phase short circuit where the reactance dominates, the resistance often plays an important part in limiting the current in a single shorted turn. Even at rated speed when the electrical frequency and hence reactance are at a maximum, resistance makes a significant contribution to the impedance of a shorted turn. Thus the current in the shorted turn is limited to a certain amount (in this reference to 673 A, which is 33.2 times rated current). Also this large current will cause the temperature of the shorted turn to rise at a rate of $1545^{\circ}\text{C}\cdot\text{S}^{-1}$.

Consideration of current in the shorted turn does not flow through the power electronics. Clearly fault progress and continued operation under this type of fault must be avoided, the fault must be detected and action must be taken in an appropriate time. The action required to enable continued operation of the faulty phases of the machine will vary according to the machine type [11]. The detection system should be easier to implement in larger machines. Note that whilst the method should be applicable to all kinds of synchronous machines, the overall system is considerably more complex due to mutual coupling between phases. Also an early detection during operation is quite important to avoid subsequent damage to adjacent turns and stator core and to reduce machine downtime for unscheduled maintenance [12-16].

Some of the most frequent causes of stator winding failures [17] are:

- High stator core or winding temperatures,
- Slack core lamination, slot wedges, and joints,
- Loose bracing for end winding,
- Contamination caused by oil, moisture, and dirt,
- Short circuits,

- Starting stresses,
- Electrical discharges,
- Leakages in the cooling systems.

It is believed that phase-to-ground or phase-to-phase and coil to coil faults start as undetected turn-to-turn faults that finally grow and culminate into major ones [18], [19], and [20]. Although short-circuit current is limited to a rated value by designing the machine with a high phase inductance, short circuit between turns is the most critical fault in the machine and is quite difficult to detect and almost impossible to remove.

In the case of a short circuit in a PMSM, there is a risk of irreversibly demagnetization of the permanent magnets of the motor due to the strong opposing magnetic field from the short-circuit current. The high torque at a short circuit can also lead to mechanical failures of the machine, the shaft coupling, or the load [21].

3.2. Stator core-related faults

Stator core problems are rare (1% of all faults) compared to stator winding problems and such problems are not usually a major concern for small machines. However, the repair/rebuild process is more costly in the case of a stator core failure, since it usually requires the entire core to be replaced. Also, the adverse impact on reputation and its subsequent fallout on future business cannot be neglected [22].

Excessive heating caused by turn-to-turn short circuits is the reason why motors in this condition will almost always fail in a matter of minutes, if not seconds. A basic rule of thumb to consider is that every additional 10°C causes the winding to deteriorate twice as fast as when the operation takes place in the allowable temperature range. Failure of the insulation between the winding and ground can cause a large ground current, which would result in irreversible damage to the core of the machine. This fault may be so severe that the machine might even have to be removed from service. If the fault is detected at an early stage, the machine can be put back into service by just re-winding the stator, while, on the other hand, replacing the whole motor means increased downtime [23].

The stator cores of electrical machines are built from thin insulated steel laminations with the purpose of minimizing the eddy current losses for higher operational efficiency. In the case of medium/large machines, the core is compressed after the core laminations are stacked in order to prevent the individual lamination sheets from vibrating and to maximize the thermal conductance in the core. The main causes of stator core failure are [23], and [24]:

- Core end-region heating resulting from axial flux in the end-winding region,
- Core melting caused by ground fault currents,
- Lamination vibration resulting from core clamping relaxation,
- loosening of core-tightening at the core end resulting from vibration during operation,
- Relaxation of lamination material resulting from the compression of insulation material with time and temperature,
- Manufacturing defects in laminations

- Non-uniform thickness within lamination sheets causes cumulative non-uniform pressure distribution,
- Inter-laminar insulation failure,
- mechanical damage to the inner surface of the stator during assembly, inspection, re-wind, and re-wedge,
- Heat, chemicals, or mechanical force applied when stripping the winding during rewind,
- Stator-rotor rubs during assembly and operation,
- arcing from winding failure,
- Foreign particles introduced during assembly, inspection, or repairing,

If laminations are shorted together for one of the reasons above, a circulating eddy current larger than that found in normal operation is induced in the fault loop. The circulating fault current causes additional power loss in the core and results in localized heating, which may grow in severity and eventually cause the laminations to burn or melt. As a result, the stator insulation and windings can also be damaged, causing ground current through the stator core, which may potentially cause machine failure [22] and [25].

Inter-laminar core faults are very difficult to monitor online based on terminal measurements unless the fault has progressed to a severe stage, since the fault causes localized flux redistribution and heating in a very small region. Therefore, the core of large EMs is inspected offline whenever possible or anytime core damage is suspected, to ensure efficient and reliable machine operation [22].

The primary requirement for core testing is the sensitivity and reliability of fault detection. Since the test cannot be performed online, opportunities for core fault testing are limited. Therefore, it is critical to detect incipient faults when they start to develop to prevent core failure. Minimizing the noise level in the measurement increases the chances of detecting faults that are smaller and located deeper in the core. The noise in the signal can be caused by the irregularities of the core surface and by the measurement itself. Therefore, a method that is insensitive to mechanical irregularities and has improved signal-to-noise ratio in the measurement is desired for detection of this type of fault [22].

3.3. Open phase, phase to ground, line to line, line to line to ground faults

An important fault class for an IPM machine is considered in which one of the phases becomes open-circuited. This type of fault can be caused by mechanical failure of a machine terminal connector, an internal winding rupture, or by an electrical failure in one of the inverter phase legs [26].

The open-phase fault produces electromagnetic torque oscillations which cause abnormal rotor vibrations and give abnormalities in the drive's operation [20]. The amplitude of current increases by approximately 60 %, and the two phases currents are shifted 2π , thus the risk of destruction of stator winding.

3.4. Unbalanced voltage fault

Unbalanced voltage is one of the most frequent interferences in electrical systems. Large single phase loads, unbalance loads, system faults, etc. are some of the causes of unbalanced voltage. Most of the standards only specify the percentage of unbalanced voltage without indicating the unbalanced condition. In fact, there are many unbalanced voltage cases which have the same unbalanced voltage factor but have different effects on loads. Unbalanced Voltage causes the performance of motor to deviate from desirable condition as shown in [27], [28], [29], and [30].

In electrical motors, at normal operating speed, the stator currents under unbalanced voltage state will be approximately “6 to 10” times its normal quantity (without faulty condition) which is a great difference. This can cause malfunction in motor protection system. The locked-rotor torque and breakdown torque are decreased when the voltage is unbalanced. If the unbalanced voltage was extremely severe, the torque might not be adequate for the application although the full-load speed is reduced slightly when the motor operates with unbalanced voltages [30].

It must be consider that operation of motor under high percentages unbalanced voltage tests, it doesn't take a long time because, the temperature rises more than that of the motor operating under the same condition with balanced voltages.

For a 3-phase system, there are two different definitions of the unbalanced voltage: IEC standard definition and NEMA standard definition. The IEC standard definition defines the unbalanced voltage as the ratio between the amplitude of the negative sequence component, V_2 , to that of the positive sequence component, V_1 , as in (2.1):

$$\text{Percent Voltage Unbalance} = \frac{V_2}{V_1} \times 100 \quad (2.1)$$

While the NEMA standard defines the voltage unbalance as the ratio between the maximum deviation from the mean value of 3 line voltage magnitudes, V_{ab} , V_{bc} and V_{ca} , to the mean value of these 3 line voltages, The voltage unbalance percentage may be defined as in (3):

$$\text{Percent Voltage Unbalance} = \frac{v_{\max} - v_{\text{average}}}{v_{\text{average}}} \times 100 \quad (2.2)$$

If the voltages are unbalanced, the rated horsepower of the motor should be multiplied by the factor shown in figure (2.2) to reduce the possibility of damage in the motor. Operation of the motor above a 5% voltage unbalance condition is not recommended. When the derating curve of figure (2.2) is applied for operation on unbalanced voltages, the selection and setting of the overload device should take into account the combination of the derating factor applied to the motor and the increase in current resulting from the unbalanced voltages.

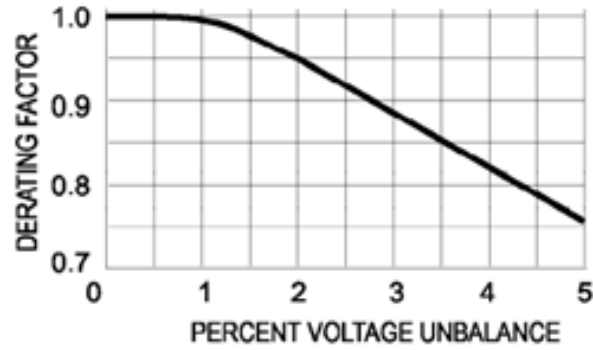


Fig. 2.2: Medium motors derating factor due to unbalanced voltage

3.5. Demagnetization fault

Magnet faults include microscopic fissures, chips, disintegration due to corrosion, complete or even partial demagnetization. Among these, demagnetization fault play a more important role in magnet failure as claimed in [31-36].

Demagnetization can be complete, that is, all over the pole, or partial, on a certain region of the pole. Depending on the severity of fault, demagnetization can be reversible or irreversible. However it has been verified that irreversible demagnetization does not arise in the PMs under the steady states. Instead, it arises under transient states [3], [39], [37], and [31-36].

The demagnetization phenomenon can be due to the armature reaction, especially under conditions of operation requiring strong torque for example at high loads or during sharp transients or even high temperature [38], [37], and [36].

In high performance applications, the rotor magnets are usually made of sintered rare earth materials such as samarium cobalt and neodymium-boron iron (NdFeB). Such materials are easy to crack, brittle and easy to erode owing to high humidity or dew. During installation the permanent magnets are exposed to mechanical pressure which may cause small cracks which may lead to disintegration at high speed [3]. In addition, metallurgical changes in the magnet material at high temperatures and/or due to corrosion/oxidation can result in irreversible demagnetization too.

A direct impact on the motor may also damage the magnets, leading to partial demagnetization. Additionally, under certain circumstances, the magnets may be exposed to different types of contaminants, including dust pollution, salt and cooling lubricants and aging of magnet among others, which also may lead to disintegration [3], [37], and [39].

Normally the thickness of the magnets is designed to tolerate the current due to maximum rated torque or to the short circuit torque [40] according to (2.3):

$$l_m > \frac{3}{2} \left(\left| \frac{N\sqrt{2}I}{2p} \right| + B_r \frac{g}{\mu_0} \right) \frac{1}{H_{ci}} - g \quad (2.3)$$

Where l_m is the magnet thickness, N is the number of the conductors in series per phase, p is the pole pairs number, B_r is the residual flux density and H_{ci} is the intrinsic coercive force of the magnetic material employed, g is the air-gap, and I is the RMS of the maximum current among the maximum torque current and the short circuit current. However even if the magnet thickness is well designed, the magneto motive force due to high current in the stator can lead to a demagnetization on magnet trailing edges when the rotor is overheated [39].

Influence of temperature on the magnetic remanence is approximately linear below Curie temperature expressed in (2.4),

$$B_r(T) = B_r(T_0) [1 + \Delta_B (T - T_0)] \quad (2.4)$$

Where T is magnet's operation temperature, T_0 is the preferred temperature, $B_r(T_0)$ is the remanence at T_0 , and Δ_B is the reversible temperature coefficient, which is a negative number. The moving of operating point due to increasing temperature is illustrated in figure (2.3).

Magnet's permeance coefficient P_c is a function of magnet length, air gap length, and armature current. It is usually greater than one to keep the operation point far away from the knee point because operation around the knee area will cause irreversible demagnetization too. However temperature change along with demagnetization fault lead to displacement of operation point. If the failure causes the operating point to "fall off" the lower end of recoil line, there will be an irreversible flux loss [41], [38], and [42].

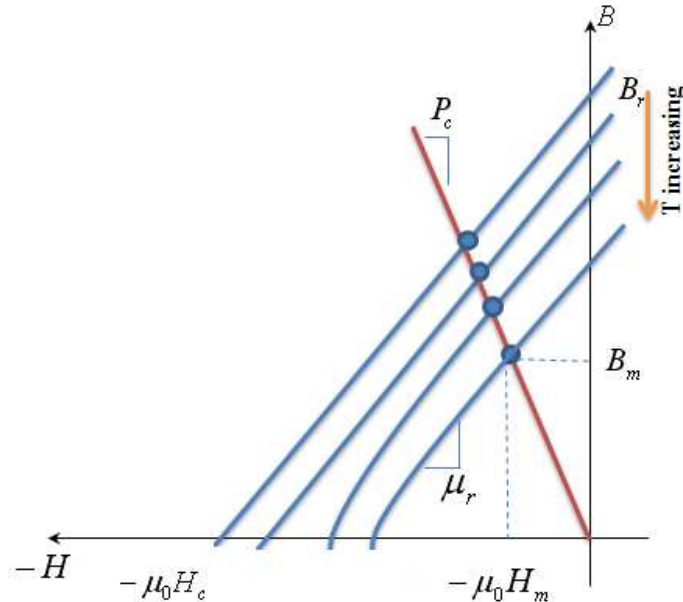


Fig. 2.3 : Effect of increasing temperature on the operating point

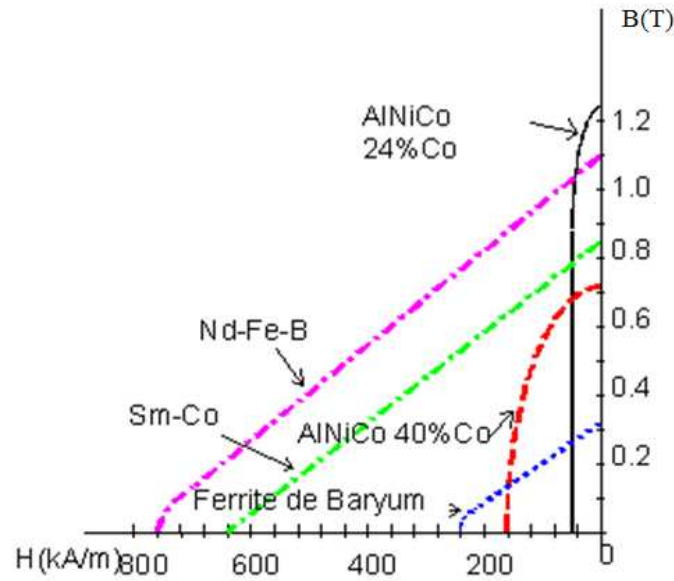


Fig. 2.4 : Demagnetization curve of magnetic materials

According to the demagnetization characteristics, permanent magnets can be divided into several groups, the three main ones are as follows:

- 1- Alinco (Alinco5, Alinco5-7, Alinco9 and etc.)
- 2- Ferrites (Barium ferrite, strontium ferrite and etc.)
- 3- Rare Earths (Samarium cobalt (SmCo), Neodymium-iron-boron (Nd-Fe-B))

The demagnetization curves of these materials are presented in figure (2.4). It is clear from this figure that the Alinco have the highest residual induction, a very small coercive field and a nonlinear curve. The Alinco can be magnetized and demagnetized easily. They were widely used in DC motors with permanent magnets until the ferrite magnets have become commercially available.

Ferrites are better than the Alinco, in terms of the coercive field but their residual induction is lower. The ferrite permanent magnets are the cheapest on the market. They are commonly used for machines with low power PM. Rare earth materials like Samarium Cobalt (SmCo) and Neodymium Iron Boron (Nd-Fe-B) have almost a linear demagnetization curve. They have a remanent flux density and a high coercivity. However, the cost of SmCo is much higher than other PMs. Although the cost of Nd-Fe-B is higher than that of ferrites, it is more appropriate for machines with high performance AP, because of superior magnetic properties. The disadvantage of Nd-Fe-B lies in their low corrosion resistance [43].

The approximate maximum operation temperature of some commercial magnets is illustrated [4] in figure (2.5).

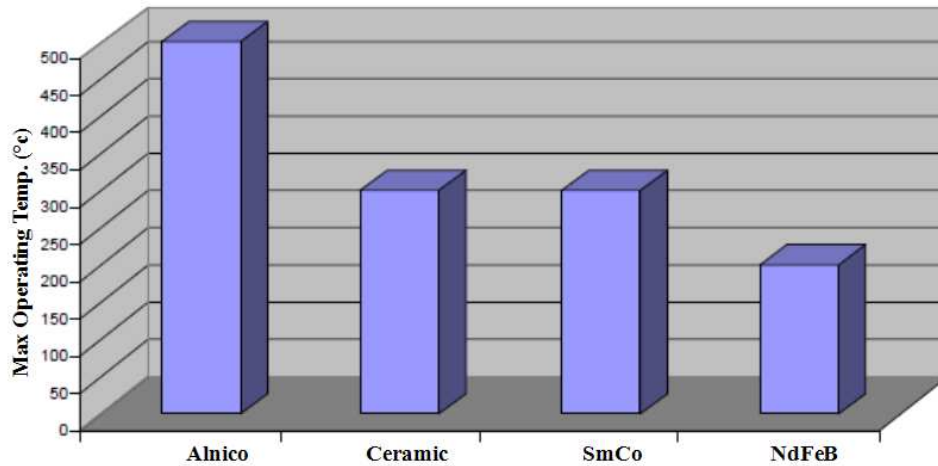


Fig. 2.5 : Maximum operating temperature of different magnet materials

During the normal operation of the PMSM, the electrical current of the stator winding produces an inverse magnetic field that opposes the remnant induction of the permanent magnets. This repeated phenomenon can cause demagnetization in the permanent magnets too. In addition, a major fault condition of permanent-magnet machines is the stator fault in the opening or shorting of one or more of stator phase windings [44 - 47].

Normally the synchronous machines should be proof against the sudden short-circuit current after the rated load condition. It should be considered in inter turn short circuit faults when a small number of turns are shorted, the additional flux is not enough to demagnetize the PM. In opposite, when a large number of turns are involved in a stator turn fault, the additional flux resulting from the turn fault can demagnetize the PMs, and consequently, can result in an irreversible damage to the motor too [45]. Two-phase short circuit is more common and at the same time more dangerous from the demagnetization of permanent magnets point of view than three-phase and one-phase short circuits. Such condition will drastically increase the demagnetizing effect of the external magnetic field, enlarging the magnetic loop response of the permanent magnets.

These effects can bring the permanent operating point below the knee region on the magnetic characteristic, i.e. out of linear region. Linear assumption of magnet behavior seems to be very simplified regarding the real material behavior in the EM operation. In such applications, the permanent magnets have the undesirable quality of potential demagnetization. The demagnetization states associated with the macroscopic behavior of permanent magnets are strongly dependent on the external magnetic field. It is necessary to consider both linear and nonlinear behavior of magnet to the author that wants to do a FEM simulation or analytical analysis for demagnetization fault diagnosis to reach to a suitable model for accurate representation of reversible and irreversible magnetic processes [31], and [34].

In addition to being irreversible flux losses from demagnetization fault which worsen the motor efficiency, it can lead to the magnetic force harmonics that can also provoke noise, vibration, increase of copper losses, power factor changes, air-gap magnetic flux distribution deterioration and reduction of the mechanical torque in the machine [1], [44], [38], [45], [34], [36], [49-52].

3.6. Eccentricity fault

Almost 50 % of all motor failures are related to mechanical faults, and they lead to a noise and vibrations, and even to the total damage of the machine and the mechanics coupled to it if the failure is not detected and isolated [53], and [44].

Due to tolerance in manufacture and assembly, where the inherent level of eccentricity is expected to be within 5%–10% of the air gap, every machine possesses a certain degree of eccentricity entailing a non-uniform air gap thickness and magnetic field [3], and [54 - 56].

When eccentricity becomes large, the resulting unbalanced radial forces (also known as unbalanced magnetic pull or UMP) can cause stator to rotor rub, which result in a serious damage to stator core and windings [31].

There are two types of air-gap eccentricity: the static air-gap eccentricity (SE) and the dynamic air gap eccentricity (DE) as shown in figure (2.6). In the case of the static air-gap eccentricity, the position of the minimal radial air-gap length is fixed in space. In this case, the air gap length is fixed in space. Static eccentricity ratio is defined as (2.5),

$$\bar{e}_s = \frac{\bar{\epsilon}_s}{g} \quad (2.5)$$

Where ϵ_s is the radial distance between rotor axis and stator axis, and g is the uniform air-gap length. If the rotor-shaft assembly is sufficiently stiff, the level of static eccentricity is not significant. In case of dynamic eccentricity, the center of the rotor is not at the center of the rotation and the position of minimum air-gap rotates with the rotor.

$$\bar{e}_d = \frac{\bar{\epsilon}_d}{g} = \frac{|\bar{\epsilon}_d| \angle \omega t}{g} \quad (2.6)$$

Where ϵ_d is the radical distance between rotor's axis and stator's axis. This misalignment may be caused due to several factors such as a bent rotor shaft, bearing wear or misalignment, mechanical resonance at critical speed, etc. Combination of both static and dynamic eccentricities is called mixed eccentricity [3], [4], [31], [32], and [53]. The equation of the mixed eccentricity is completely explained in [57].

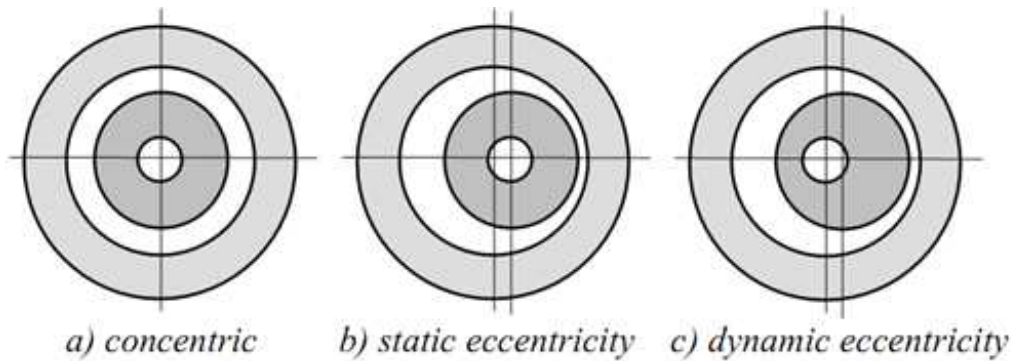


Fig. 2.6 : Different types of eccentricity fault

Static eccentricity may be caused by the ovality of the stator core or by the incorrect positioning of the rotor or stator at the commissioning stage. Assuming that the rotor-shaft assembly is sufficiently stiff, the level of static eccentricity does not change. The dynamic eccentricity may be caused by several factors, such as manufacturing tolerances, wear of bearings, or misalignment, mechanical resonance at critical speed, and incorrect manufacture of the machine components. Rotor “whirl” near a critical speed is another source of dynamic eccentricity and is an important consideration in larger, flexible-shaft machines.

Static eccentricity causes a steady UMP (unbalanced magnetic pull) in one direction and with usage this may lead to a bent rotor shaft, bearing wear and tear, etc., resulting in some degree of dynamic eccentricity. Unless detected early, the eccentricity becomes large enough to develop high unbalanced radial Forces that may cause stator-to-rotor rub, leading to a major breakdown of the machine [3], [58], and [59].

3.7. Bearing fault

Bearing is a mechanical component which consists of two rings and a set of balls rolling between them and it has been recorded as one of the dominant causes for EM failure. Since bearing fault manifest itself as a vibration of rotor and unbalance air gap length, it is sometimes also classified in the eccentricity category. However, it has its own frequency signatures related to its number of balls, ball diameter and ball pitch, which is not the same as eccentricity. This is a common issue to all machines with similar effects on performance.

Bearing faults may account for 40%-45% of all motor failures. Motor bearings may cost between 3 and 10% of the actual cost of the motor, but the hidden costs involved in downtime and lost production combine to make bearing failure a rather expensive abnormality [53].

List of reasons and mechanisms that usually cause bearing failures are presented as following [4], and [51]:

- Thermal overloading,
- Misalignment of the shaft,
- Excessive loading (both static and/or dynamic), (axial/radial combined),
- Mechanical overload,

- Excessive shock and vibration,
- Inappropriate shaft fit,
- Machining defects,
- Bad handling and/or mounting,
- Improper application,
- Improper installation,
- Heavy radial and axial stresses caused by shaft deflection,
- Lifetime load profile,
- Environmental/external problems,
- Contamination and corrosion caused by pitting and the sanding action of hard and abrasive particles or corrosive action of water, acid, etc.
- Improper lubrication, including both over- and under-lubrication, causing heating and abrasion
- Bearing currents,
- Shear stress.

Even under normal operating conditions with balanced load and good alignment, fatigue failures may take place. Flaking or spalling of bearings might occur when fatigue causes small pieces to break loose from the bearing.

It can be concluded that bearing damage causing an eccentricity in the rotor movement. Different stresses acting upon a bearing may lead to excessive audible noise, uneven running, reduced working accuracy, and the development of mechanical vibrations and, as a result, increased wear. As long as these stresses are kept within the design capabilities of the bearing, premature failure should not occur. However, if any combination of them exceeds the capacity of the bearing, then the lifetime may be drastically diminished and a catastrophic failure could occur.

It should be noted that specific information concerning the bearing construction is required to calculate the exact characteristic frequencies. In [80] authors deal with mechanical fault detection in the PMSM, especially broken bearings, by using MCSA (Motor Current Signature Analysis) method applied to composed stator currents in the frame dq0.

It is well known that damaged ball in the internal ring produces specific fault mechanical frequencies given by (2.7):

$$f_{ORF_B} = \frac{D_i}{D_o + D_i} N_b f_r \quad (2.7)$$

Where: D_i : inner diameter, D_o : outer diameter, N_b : number of rolling elements, and f_r : rotor frequency. Ref [52] deals with the diagnosis of rolling bearing faults based on frequency response analysis. The frequency response, which can be considered as a nonparametric model of the system, is obtained by processing two measured signals. Principle construction of a ball bearing with the required geometrical variables is shown in figure (2.7). The characteristic fault frequencies produced by the bearings that can be seen in the frequency response can be given as (2.8) and (2.9): (outer and Inner-Race Bearing Faults)

$$f_{ORF} = \frac{Z}{2} f_n \left(1 - \frac{d_b}{d_c} \cos(\theta) \right) \quad (2.8)$$

$$f_{IRF} = \frac{Z}{2} f_n \left(1 - \frac{d_b}{d_c} \cos(\theta) \right) \quad (2.9)$$

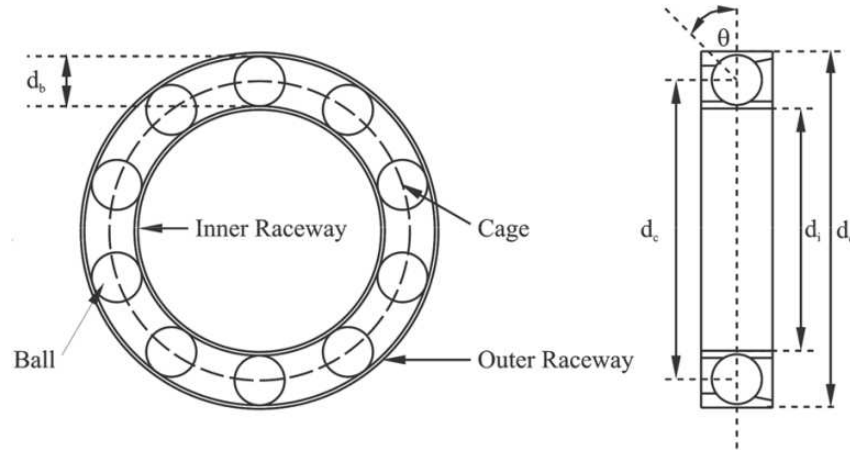


Fig. 2.7 : Principle construction of a ball bearing with the required geometrical variables

Where d_b is ball diameter, d_c is pitch diameter that is equal to $(d_i + d_o)/2$, θ is ball contact angle; Z is number of rolling elements. The bearing damages produce a periodic disturbance torque as well as a disturbance in the velocity signal. These disturbances lead to changes in the frequency response of the mechanical system at the frequencies f_{S_ORF} and f_{S_IRF} respectively. For calculating the frequency response of the mechanics in the closed loop speed control, the torque generating component of the stator current $I_q(t)$ and the speed of the motor $n_m(t)$ are utilized. For that reason the frequency response analysis yields more reliable results than the frequently used one channel FFT analysis.

3.8. Power converter

Factors such as electrical loading, mechanical vibration, and environmental condition, all exert stresses on a power electronics system. For example, the electrical traction drive for an urban tram may experience $10^6 - 10^8$ power cycles, with temperature swings up to 80°C , during its lifetime. These power cycles critically affect the reliability and lifetime of the power device packaging. This has been a key driver in improving the reliability of power devices [60].

Based on 500 000 IHM/IHV (insulated gate bipolar transistor (IGBT) high power and high voltage) modules, the failure rate dropped from 1000 failures in time (FITs) in 1995 to 20 FITs in 2000 [5], and to only a few FITs nowadays, where $1 \text{ FIT} = 1 \times 10^{-9}$ failures per device-hour. Furthermore, for safety-critical applications, such as aeroplanes, the zero-defect concept has been proposed to meet stricter reliability requirements [60].

Semiconductor and soldering failures in device modules totals 34% of converter system failures, according to a survey based on over 200 products from 80 companies. According to another survey, around 38% of the faults in variable-speed ac drives are due to failures of power devices. Typically demanding applications for converters are in traction, especially metro rail traction and urban driving for automotive electric traction, and for renewable wind turbines. The results of a recent questionnaire for industrial power electronics also showed that only 50% of respondents were satisfied with reliability monitoring methods, showing that research effort is needed in health management [60], [61].

Reliability modeling gives a tool of achieving a specified lifetime expectation as the converter design proceeds. This may reduce converter failure rate, but cannot prevent a catastrophic failure from happening. In order to guarantee converter reliability during operation, a condition monitoring scheme can be implemented and the aforementioned modeling work can also be applied to inform the development of such a scheme. This allows warning to be issued of device deterioration. In this sense, condition monitoring serves as an aid in scheduling maintenance to extend the lifetime of the converter system. Like for rotating electrical machines and transformers, this is to capture weak signatures hidden in large signals during normal operation. Another challenge of condition monitoring power electronics is that the high-power density of a semiconductor device means that it will be difficult to embed sensors inside the device; it is more favorable to capture signatures in external measurements that are already used for converter control and protection.

Furthermore, the operating condition of a converter is likely to vary, accompanied by loss and temperature excursions. Most failure mechanisms have a thermal aspect, so the masking effect of normal load variation must be addressed. To develop a condition monitoring scheme, the effects of semiconductor device degradation on its terminal characteristic and converter performance should be understood. In principle, condition monitoring can be implemented through the following three ways, though they may be combined, to capture and interpret the corresponding signatures:

1) Device parameters indicative of the degradation. For an IGBT, these include ON-state voltage or resistance $V_{CE,sat}$ or R_{ON} , threshold gate voltage $V_{GE,th}$ and internal thermal resistance R_{th} . These parameters, which are difficult to measure in practice, may in turn cause changes in the operational characteristics at a device or converter system level. The latter may be more practical to capture for the purpose of condition monitoring.

2) Dedicated sensors embedded in the device can be used to directly monitor the occurrence and the level of physical degradation, for example, in situ mechanical stress monitoring using strain gauges and bonding wire lift off detection through localized electrical resistance measurement within a device or module.

3) Model-based condition monitoring is particularly attractive to converter systems working under variable load and ambient conditions, such as in electric vehicles and renewable energy systems. It is expected that the response of the converter system to the stimulus—applied externally or available internally during normal operation—is dependent on the device condition, and degradation can be detected by comparing the measured response to that predicted by a healthy model.

All of the possibilities have not been fully explored as condition monitoring of power electronics is still in the infant stage of development. This paper reviews the techniques experimented so far and comments on their characteristics and the need of further development. It has been attempted to capture the change of device ON-state voltage (V_{ON}) (measured through $V_{CE,sat}$ or R_{ON}) to detect bond wire liftoff. It has also been attempted to capture the change of device internal thermal resistance R_{th} to indicate solder cracking; the temperature rise for a given set of power loss and ambient conditions can be used to extract R_{th} indirectly.

These are the techniques currently under intensive development, while dedicated sensor-based and dynamic model-based techniques are also being actively studied. A summary of advantage and disadvantage of each introduced method for fault detection and condition monitoring on power converters are presented in table (2.1):

Table 2.1 : comparison of different condition monitoring techniques

Methods	Advantages and disadvantages
$V_{CE,sat}$ R_{ON}	Adv: highly related to degradation Dis-adv: difficult to measure small variations
R_{th}	Adv: solder degradation detectable Dis-adv: difficult to measure T_j
Gate signal	Adv: electrical fault detectable Dis-adv: high real time requirement
Switch time	Adv: gate drive failure detectable Dis-adv: short switch time measurement needed
Sensor based	Adv: reliable and accurate Dis-adv: direct-bonded copper (DBC) layout modification
System identification	Adv: no additional hardware modification Dis-adv: difficult correlation & complicated algorithm

4. Diagnosis methods, a deep investigation and comparison on drivetrain faults

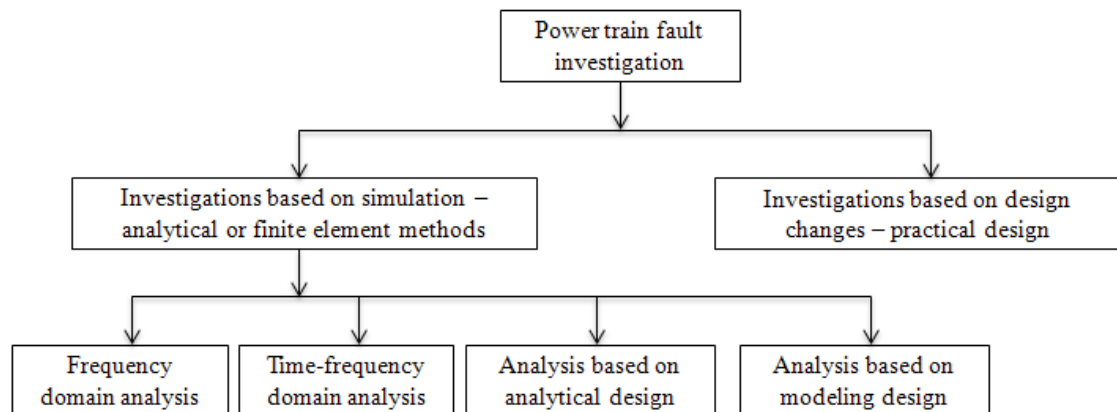
In order to carry out an online and offline fault diagnosis scheme, it is highly desirable to use an easy-to-calculate fault severity index with low computational burden [2]. Condition monitoring of electrical machines problems is essential for guaranteeing high motor performance, efficiency, and reliability [4].

So far several reviews have been presented on different methods of fault detection and diagnosis, especially, on induction motors (however many of these methods are common for other types of electrical machines too). A summary of these works is presented in table (2.2).

Table 2.2: A compression of different fault detection methods

Parameter	Measurement device	Potential information richness	Intrusive to electrical machine	On/off line	Operator skill required	Measurement frequency	Measured as part of control strategy	References
Current	Hall effect transducer	Average	No	On	High	Continuous	Yes	[32], [36],[37],[55]
Voltage	DVM	Average	No	On	High	Continuous	Yes	[32],[37]
Flux	Search coil	Very High	Yes and No	On	High	Hourly	No	[13], [32], [36],[37],[57]
	Hall effect device							
Force	Dynamometer	Very High	No	On	High	Continuous	No	[32],[37]
Vibration	Accelerometer	High	Yes and No	On	Expert	Hourly	No	[32],[37]
Acoustics	Microphone	High	No	On	Expert	Hourly	No	[32],[37]
Temperature	Hand-held probe	Low	Yes and No	Off	Low	Monthly or on suspected deterioration	No	[32],[37]
	Thermal paint		Yes					
	Thermocouple	Average	Yes	On	Average	Continuous	Yes	
	Infra-red camera	High	No		Expert	Monthly or on suspected deterioration	No	
Instantaneous angular speed	Encoder	Average	No	On	High	Continuous	Yes	[37]
Torque	Torque sensors (magneto elastic, piezo electric, strain gauge)	High	No	On	Expert	Continuous	Yes and no	[32],[36],[74]

Power train fault investigation can be divided to two main parts. Investigation based on simulation-Analytical or Finite Element- methods and also second part; investigation based on design changes as mentioned in figure (2.8). Details of each part have been explained in continue.

**Fig. 2.8 :** The scope of power train fault investigation

4.1. Investigations based on simulation – analytical or finite element methods

Today MATLAB SIMULINK/M-FILE and Finite Elements Methods (FEM) has become to a powerful and reliable method for comparison between theoretical methods and own experimental results. Regardless of the method used for design of motor under power train fault, there are different methods for fault data analysis and fault diagnosis. In this part, 4 types of most popular related methods are investigated as following:

4.1.1 Frequency domain analysis

Any observed signals, as acquired from measuring sensors in raw form, are in the time-domain. Historically, Fourier spectral analysis has provided a general method for examining the global energy-frequency distributions and has been used for damage detection.

In [11], The PWM current ripple is used for detecting a single shorted turn in a machine by monitoring. Today, Fast Fourier Transform (FFT) is known as a conventional method in electrical machine fault detection, especially in stationary operation state. The main disadvantage of FFT is the restricted application to stationary signals, i.e. signals without a variation in time. Unfortunately, the faults in the machine could be time-variable; therefore the symptoms are non-stationary signals. In the analysis of non-stationary signals the time frequency can be used [48], [38], [4], [62], and [63].

A simulation work confirmed through experimental work in [14] used a simple and practical on-line fault detecting scheme of short circuit fault based on monitoring only the second-order harmonic components in the q-axis current. To this end, an indication of fault is defined as follows:

$$I_F = h_{q2} / h_{2n} \quad (2.10)$$

In which that, h_{q2} is second-order harmonic current q-axis and h_{2n} represents the amplitude of the second order harmonic current contained in the q-axis at the same speed and operating current below normal- without fault- condition.

In [64] the inset permanent magnet (IPM) and surface permanent-magnet (SPM) motors under short-circuit fault has been simulated by magnetic equivalent circuit (MEC). It has been demonstrated that the peak of short-circuit current in the IPM motors is smaller than that of the SPM motors. Two analysis methods applied to turn to turn fault diagnosis:

- frequency analysis of air gap magnetic flux density
In this case, Magnetic field contains full information about the stator, rotor, and mechanical parts of the motor. For turn short circuit, raises the amplitude of sideband components as shown in (2.11) can be used as applicable criterion for short-circuit fault recognition. Where K_{sa} is constant coefficient.

$$f_{sc-field} = (1 \pm [(2k_{sa}) / p]) f_s \quad (2.11)$$

- frequency analysis of line current
It is seen that 1 turn short circuit raises the amplitude of sideband components at frequencies shown in (2.12).

$$f_{sc-current} = (1 \pm [(2k_{sa}) / p]) f_s \quad (2.12)$$

The amplitude of the sideband components at the mentioned frequencies for different number of short-circuit turns and load levels exposes that albeit the introduced criterion does not change perceptibly due to the load variations, it rises considerably due to short-circuit fault and increases of short-circuit turns.

In [17], an equivalent circuit for short circuit condition of a surface mounted permanent magnet is shown. According to this reference, the new equation for calculation of short circuit current has been presented.

A mathematical machine model that allows studying the effects of stator windings inter-turn faults under stationary and non-stationary conditions has been developed in [65]. As a novelty [65], destroying in 5th and 7th harmonics show an inter turn short circuit condition.

In [20] and [64], frequency components and their amplitudes are used to a suitable signature for open phase fault detection. The spectrum is obtained using a Fast Fourier Transform (FFT) that is performed on the stator current. Based on this paper, an open phase fault will have a significant effect in frequencies of $2f_s, 3f_s, 4f_s, 5f_s, \dots$ for completion of fault diagnosis, the detection of these faults can be implemented by using the phase angle.

In [66] a study based on analyzing the harmonics obtained using the Fast Fourier Transform (FFT) of stator and zero sequence currents is presented. The fault frequencies due to rotor demagnetization can be localized as (2.13) [3], [41], [2], [37], [34] and [56 - 59]:

$$f_f = f_e \left(1 \pm \frac{k}{p} \right) \quad (2.13)$$

Where f_f is the fault frequency, f_e is the electrical fundamental frequency, k is an integer, and p is the number of pole pairs. The results clearly show that odd harmonics (1/3, 5/3 among others) appear when dealing with a 3-pole-pair PMSM with a partially demagnetized pair of poles.

It is very essential to note that in some PMSMs by using the specific stator windings configuration like the sample mentioned in [3], the fault harmonics predicted by (2.13) are not presented in the current spectrum.

Since it is the asymmetry in the flux pattern that induces the current component in (2.13), uniform demagnetization cannot be detected with motor current signature analysis (MCSA).

Uniform demagnetization is a very common type of PM defect that can occur in service, when the motor is operated at elevated temperature.

Another critical limitation of the MCSA is that the oscillating load torque (e.g., reciprocating compressors) produces sidebands at the same frequency component as (2.13), which are larger in magnitude than that due to the fault, and there is no practical means for separating them [3], and [58].

Similar to current frequency, indications of several faults are also found to be hidden in other spectrums, such as noise, vibration and torque, etc. However, due to the high cost of accelerometer or torque meter, they are usually implemented in relatively larger machines.

The limitations of these frequency analysis based algorithms are relatively time consuming to some certain extent, and it is too hard to determine the source of specific harmonics, so it cannot discriminate faults that have the same signature frequencies, like partial demagnetization, dynamic eccentricity and unbalanced load [67], and [68].

Authors in [7] proposed a new non-invasive method for magnet faults detection that includes local and uniform demagnetization by means of a Fourier transform of the space vector of back-EMF. The proposed approach is then validated for three permanent magnet synchronous motors with different winding configurations (as mentioned before, different winding configurations may lead to canceling of some harmonic ranges that is used for fault detection, see [52], [2], and [69]). The results show how the chains of frequency are univocally related to the considered winding configuration for a local detect on the rotor, making the fault easier to detect. On the other hand, for uniform demagnetization only the variation of harmonics (in respect to fundamental) that are already presented in the spectrum of back-EMF can be used in signature analysis approach.

In [32], two different stator winding configurations are considered in the analysis, series and parallel connected windings. From this analysis, a fault detection strategy based on the information contained in winding-current spectrum and electromagnetic torque is proposed.

According to this investigation, the results show that in series winding connection, current harmonic analysis has not any valuable effect for fault detection.

Regarding the analysis of the spectrum for the electromagnetic torque, it is possible to observe a reduction in the frequency component amplitudes due to fault though. No new components appear associated to fault in series or in parallel, which makes fault diagnosis and detection difficult. Also, it is mentioned that, if load is of resistive type, such reduction appears in the current too. So it is not possible to observe the frequency components associated to the fault at this point, but only a reduction of the total flux linked by the windings observed.

References [52], [2], and [69] presented a method based on the measure of the zero-sequence voltage component (ZSVC). In this work it is proved that in this type of motor, partial demagnetization faults generate harmonics in the spectrum of the back-EMF of a single slot because the flux linking the stator windings is not symmetrical. In this paper a valuable notice is presented so that the back-EMF spectrum of the partially demagnetized SPMSM does not contain fractional harmonics. Thus, in summary, although the back-EMF in a single pole of a phase winding contains fractional

harmonics, they do not appear when considering an entire phase winding. This means that for the analyzed SPMSM, it is not feasible to diagnose this particular demagnetization by analyzing the fractional harmonics in the back-EMF voltage or in the stator currents spectrum. Although FFT allows detecting demagnetization faults by analyzing the amplitude of harmonics in stationary signals (Compliance with limitations expressed), it fails when dealing with non-stationary signals. Thus, when dealing with signals that contain changes of speed and torque, FFT is not well-suited for detecting motor faults [41], [38], [4], [43], and [53].

Motor current signature analysis (MCSA) is the most actively researched detection method considered for PMSM rotor faults too, as it provides sensor-less, continuous, and online monitoring independent of motor parameters and temperature [3], and [31]. The rotor rotational speed frequency component, shown in (2.14), is suggested as an indicator for rotor problems that include partial PM demagnetization, SE, DE, misalignment, or rotor/load unbalance:

$$f_f = f_e \left(1 \pm \frac{k}{p} \right) \quad (2.14)$$

Where f_f is the fault frequency, f_e is the electrical fundamental frequency, K is an integer, and P is the number of pole pairs.

Instead of using stator current spectrum, harmonic decomposition of zero component current in dq0 frame is proposed in [53] to detect eccentricity harmonics in the faulty motor, despite its low amplitude. As zero components current collects the sum of the effects of thirds components, it is assumed that harmonics 3, 6, 9, 12, 15, 18 ... of this i_0 current component could show better than harmonics of the phase current the eccentricity fault.

Rotor eccentricities affect the permeance which in turn affects the motor inductances resulting in unique harmonic components in the current [31]. As shown in (2.15), this theory can be applied to detect rotor eccentricities in synchronous machines. The frequencies that can be used to detect dynamic eccentricity in BLDC motors are given by:

$$f_{de} = n_{ws} f_e + k \frac{2}{p} f_e \quad (2.15)$$

Where f_{de} is the dynamic eccentricity frequency, f_e is the fundamental frequency, is the slip, and k is any integer, n_{ws} is any integer. The dynamic eccentricity sidebands around the fundamental $n_{ws} = 1$ are usually the most significant and are given by (2.16):

$$f_{de} = f_e + k \frac{2}{p} f_e \quad (2.16)$$

This paper also has been investigated the effect of a pulsating load torque similar to the one encountered in applications such as reciprocating compressors and also misalignments effects are investigated.

In [70] FFT has been used for open circuit fault detection of an uncontrolled AC/DC power converter. Harmonic amplitude changes are used for classification of different types of faults.

4.1.2 Time-Frequency (TF) domain analysis

The need for more effective signal analysis approaches for fault detection of time variable signals becomes clear only when it comes to many real-life time-variable signals with non-stationary nature whose frequency content changes over time and Fourier Transform is unable to reveal it.

TF not only show what frequencies (notes) are present in a signal, just like Fourier Transform does, but also show where in time that they appear in the signal and for how long they last. That is what “time localization of frequency” implies.

Linear TFs are those which follow the linearity superposition principle and a TF quadratic, it should follow the quadratic superposition principle. Let $x(t)$ be the sum of two signals $x_1(t)$ and $x_2(t)$ as (2.17):

$$x(t) = x_1(t) + x_2(t) \quad (2.17)$$

A linear TF, $T_x^L(t, f)$ of the original signal $x(t)$ has the form (2.18):

$$T_x^L = T_{x1}^L + T_{x2}^L \quad (2.18)$$

And a quadratic TF, $T_x^Q(t, f)$ of the original signal $x(t)$ has the form (2.19):

$$T_x^Q = T_{x1}^Q + T_{x2}^Q + 2\Re\{T_{x1x2}^Q\} \quad (2.19)$$

Where T_{x1x2}^Q is the cross term and \Re denotes the real part. Regardless of what exactly a “cross term” is, there is an important fact to mention about it: the fact that a quadratic TF does not follow the linear superposition principle, i.e. a quadratic TF of sum of two signals is not equal to the sum of the same quadratic TF of the individual signals. As a result, due to the presence of $2\Re\{T_{x1x2}^Q\}$ term, or the cross term, any quadratic TF present interference terms. In general “cross terms” have been considered as the main disadvantage of quadratic TFs.

According to aim of this work by focus on drive-train fault detection, it is found five TF methods include Wavelet Transform (WT), Short-Time Fourier Transform (STFT), Wigner Ville Distribution (WVD), Hilbert Huang Transform (HHT) and Choi-Williams Distribution (CWD) that these are mentioned in this work. We did a deep investigation on all existence TFs as shown in figure (2.9) [41], [38], [43], [58], [71] and [72].

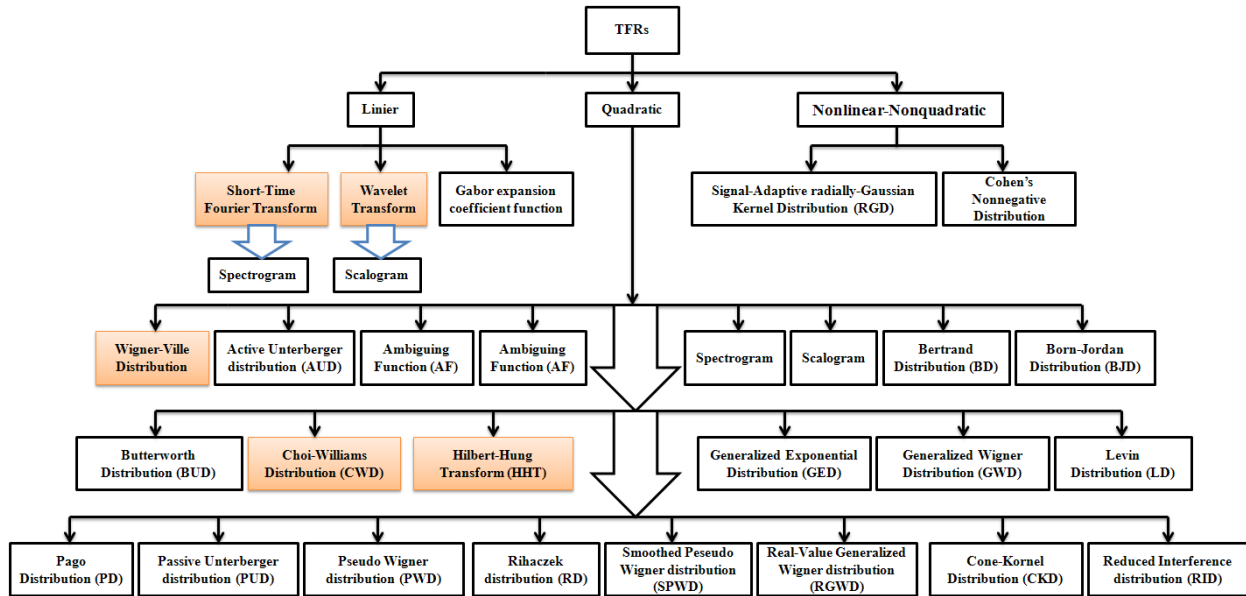


Fig. 2.9 : A classification of TF method

However TFs have a lot of advantage that make them useful for usage, but also attention to drawback of these methods can led to a correct selection for reach to goal. In general “cross terms” have been considered as the main disadvantage of quadratic TFs, as it mentioned before, in part of electrical faults, but also it is tried to explain about each method as much as possible.

TFR methods are actually mathematical maps of a raw signal (input) to an analyzed and transformed signal (output). Lack of a single time-frequency representation that is "best" for all applications has resulted in a proliferation of TFRs, each corresponding to a different, fixed mapping from signals to the time-frequency plane. A major drawback of all fixed mapping is that, for each mapping the resulting TFR is satisfactory only for a limited class of signals.

Some of these TFRs have the ability to alter the method they use for mapping based on the specific signal characteristics. It means, for example, if the raw signal is too coarse, they perform the mapping in a way that the coarse components are more visible and clear to distinguish. These types of TFRs are called "adaptive" methods. As another example consider a signal with linearly increasing frequency: linear chirp. As an adaptive TFR, Wavelet Packet Transform, first performs the mapping. But in this first step the linearity of the frequency increase might not be clear enough. Therefore, using some methods, it can alter the mapping by changing some parameters so that the linear pattern becomes visible. On the other hand TFRs whose methods leave no way for alternation based on the input signal are too solid to adapt to the characteristics of the signal, are called non-adaptive methods such as STFT and WT.

In fact, adaptive TFRs were proposed to adapt to the signal time-frequency changes. In particular, an adaptive TFR can be obtained by estimating some relevant parameters of a signal-dependent function at different time intervals. Such TFRs provide highly localized representations without suffering from quadratic TFR Cross Terms. The trade-off is that these TFRs may not satisfy some desirable properties such as energy preservation.

Considering different properties of the TFRs introduced in this part, this can be realized there is no optimal TFR for every application. Different methods provide different advantages and have their own drawbacks. However, for a wise choice of method among different TFRs one should be familiar with the basics of each method. The following subsections summarize almost all necessary information needed for making a first choice with regard to a specific application.

1- Frequency Transform (FT)

- Analyzing function: sinus and cosines, which oscillate indefinitely
- Variable: frequency
- Accessible information: the frequencies that make up the signal
- Suited for: stationary signals (predictable: obeying constant laws)
- Notes: With the fast Fourier Transform (FFT) it takes $[n \log(n)]$ computations to compute the Fourier transform of a signal with n points
- Basis: a priori
- Frequency: convolution: global uncertainty
- Presentation: energy-frequency
- Non-linear: no
- Non-stationary: no
- Feature extraction: no
- Theoretical basis: theory complete
- Strength: precise frequency resolution
- Weakness: no temporal information

2- Short Time Frequency Transform (STFT)

- Kind of decomposition: time-frequency
- Analyzing function: a wave limited in time, multiplied by trigonometric oscillations. The size of the wave or "window" is fixed for each analysis, but the frequency inside the window varies.
- Variables: frequency; position of the window
- Information: the smaller the window, the better time information one has, at the cost of losing information about low frequencies; large windows give better frequency information but less precision about time.
- Suited for: quasi-stationary signals (stationary at the scale of the window)
- Basis: a priori
- Frequency: convolution
- Presentation: atomic decomposition
- Non-linear: no
- Non-stationary: no
- Feature extraction: no
- Theoretical basis: complete
- Strength: easy to implement
- Weakness: piecewise stationary of the data assumption not always justified; time-frequency resolution limited by the Heisenberg principle; non-adaptive nature; feature extraction impossible, non-invertible

3- Wavelet Transform (WT)

- Kind of decomposition: time-scale
- Analyzing function: a wave limited in time, with a fixed number of oscillations; the wavelet is contracted or dilated to change the size of the "window" and thus the scale at which one looks at the signal. Since the number of oscillations does not change, the "frequency" of the wavelet changes as the scale changes.
- Variables: scale; position of the wavelet
- Information: small wavelets provide good time information but poorer frequency information. Large wavelets provide good frequency information but poorer information about time.
- Suited for: Non-stationary signals, such as very brief signals and signals with interesting components at different scales
- Basis: a priori
- Frequency: convolution: regional uncertainty
- Presentation: energy-time-frequency
- Non-linear: no
- Non-stationary: yes
- Feature extraction: discrete: no; continuous: yes
- Theoretical basis: theory complete
- Strength: basis functions obtained by shifting and scaling a particular function; uniform resolution; non-stationary data analysis; feature extraction possible.
- Weakness: uniformly poor resolution; leakage generated by the limited length of the basic wavelet function; non-adaptive nature; cannot resolve intra-wave frequency modulation; high-frequency range observation to define local events; variable window size.

4- Wigner Ville Distribution (WVD)

- Basis: adaptive
- Frequency: convolution: regional uncertainty
- Presentation: energy-time-frequency
- Non-linear: yes; quadratic
- Non-stationary: yes
- Feature extraction: no
- Theoretical basis: complete
- Strength: Perfect localization on linear chirp signals; invertible
- Weakness: can be misleading due the presence of cross terms

5- Hilbert-Hung transform (HHT)

- Basis: adaptive
- Frequency: differentiation: local certainty
- Presentation: energy-time-frequency
- Non-linear: yes
- Non-stationary: yes
- Feature extraction: yes
- Theoretical basis: empirical

- Strength: high time-frequency resolution; generalized Fourier analysis with variable amplitudes and frequencies; the first local and adaptive method in time-frequency analysis; can clearly define both inter-and intra-wave frequency modulations; robust nonlinear and non-stationary data analysis; feature extraction possible.
- Weakness: end effects due to spline fitting and the Hilbert transform; cannot separate signals with very close frequencies; no physical meaning of some IMFs; no mathematical formulation.

The use of TF distributions of the stator current has proved to be suitable for detecting faults in electric motors operating in steady-state and non stationary conditions over the years [72]-[75].

To remove the fundamental and other sub harmonics prior to the applications of the fault detection algorithm, the stator current would have to be filtered. This filtering increases the resolution of TF distributions and makes the calculation of fault metrics easier [21].

In [76] suggests that it is possible to study and identify short circuits in the windings of the PMSM determined by means of higher order spectral analysis (HOSA) as power frequency spectrum density (PSD), Multiple Signal Classification (MUSIC) and bi-spectrum in the whole operation range. The HOSA has been a considerable interest to researchers in the signal processing and this interest has recently been extended to the condition monitoring. HOSA requires no priori data for fault detection and quantification. The disadvantages of HOSA are a high computational overhead, and their complex interpretation. However, the model order and the processing time can be reduced by using filtering and frequency decimating techniques. Bi-spectrum can be used for the analysis of current in a dynamic state of the change in speed or torque. Also, the PSD and the Music can detect the short circuit for all speed range. These methods can be used for preventive maintenance when the test is under controlled conditions and can be made known.

In [41], and [43], time-frequency wavelet-based methods have been successfully applied to detect demagnetization faults in PMSM motors under non-stationary conditions. In [41], two methods based on Continuous wavelet transform (CWT) and Discrete wavelet transform (DWT) to detect demagnetization faults diagnosis in PMSM under non-stationary conditions have been studied by analyzing experimental data.

In [43], [77], [34], and [78] other types of time frequency method that are named Hilbert-Hung transform (HHT) and Choi-williams distribution are used for demagnetization fault diagnosis. This methodology can overcome the FFT drawbacks since it allows analyzing the stator current obtained from experimental data for both steady state and dynamic conditions where speed changes at high, medium, and low velocities.

4.1.3 Analytical model based analysis

The analytical model is based on well-known vector potential formulation by Maxwell's equations for demagnetization fault modeling. A lot of earlier research has already been carried out to model accurately different machine parameters, where the analytical method is a two-dimensional model in polar coordinates and solves the

Laplacian/quasi-Poissonian field equations in the air-gap and magnet regions [1], [36], and [79 - 81].

In [1], and [36] a novel analytical model approach to detect magnet faults such as local demagnetization in brushless permanent-magnet motors has been presented.

What adds in this work is that with the magnet subdivided into elements, equations are written for each element region and a new form of air-gap vector potential equation has been developed which is a function of remanent induction (B_r) of all magnet elements. To reach to this important, in [1] a new form of analytical model that solves the Laplacian/quasi-Poissonian field equations in the machine's air-gap and magnet element regions has been developed. The model verified by using finite-element software in which demagnetization faults were simulated and electromotive force was calculated as a function of rotor position.

An analytical investigation in [64], [12] and [82 - 85], is discussed external faults in electrical machines. He mentioned that the most faults that occur on power systems are unsymmetrical faults, namely, line-to-ground, line-to-line, or double line-to-ground faults. Voltage and current equations change. The current amplitude under L-L fault increase between 8-10 terms in compare to healthy mode operation. However this pick of current will damp with protection switch effect but it will lead to irreparable damage on other equipment in its path as transformations and etc.

4.1.4 Modeling method design based analysis

The modeling method design-based analysis is divided to four main subsections as shown in figure (2.10).

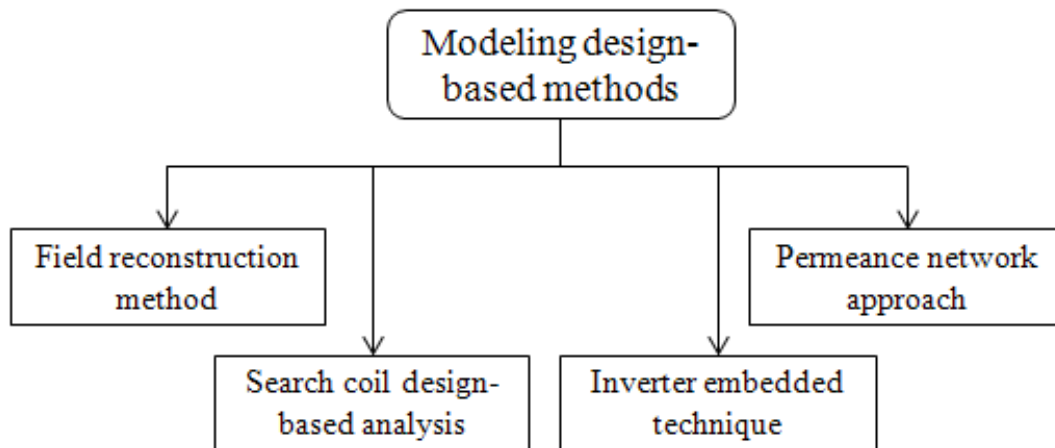


Fig. 2.10 : Modeling method design-based analysis subsections flowcharts.

A. *Field Reconstruction Method (FRM)*

In [44], and [86], because the conventional Finite Element Analysis (FEA) is time consuming, a field reconstruction method has been used to a partial demagnetization fault in PMSM. In this method a comparison of average torque, torque ripple and emitted noise for both healthy and faulty conditions are presented. FRM is known as a new method that improves the computational time used in determining magnetic field distribution within the electromechanical energy converters. Considering the accuracy of

the FRM, the model created in these investigations can substitute the FEA to calculate field and magnetic force (torque) quantities. The difference in computational time is significant. The FRM model can run at about three orders of magnitude faster than FEA while presenting the same level of precision.

Also in [25], a method based on FRM has been applied to open phase fault detection and treatment of PMSM drive. This method uses the field created by a single slot along with the field generated by the permanent magnets on the rotor to find the field distribution and electromagnetic force components. *The advantage of this method is that it reduces the computation time and cost significantly while the accuracy of the results are acceptable.*

In [44], and [86], FRM has been used to an eccentricity fault in PMSM too, The results obtained in the investigation show different values of sound power radiated and vibration analysis for the PMSM under study for each harmonic force. This is due to the different value of the force harmonics acting on the stator teeth. The results presented in [44], claim that, for the targeted PMSM, the eccentricity fault gives the most severe vibration emissions. It has been possible to detect the rotational speed ranges for which a fault is most severe than the other ones.

B. Search coil design by help of FEM and field component analysis

The increase of harmonics can be significant with supply unbalance as well as time harmonics, which can lead to a serious confusion. Hence, in order to unambiguously detect stator inter-turn faults in salient-pole synchronous motors, some of the other frequency components in the field current have been monitored. It was observed that owing to the structural asymmetries of the field winding, a stator inter-turn fault could increase these components in the field current too. (In practice, all the machines are expected to possess internal asymmetries due to manufacturing imperfections and non-homogeneity of iron. The asymmetries can be in the magnetic path, stator winding, air-gap and/or rotor cage/winding). For solve of these problems some of the papers like [87], [5], [88], and [89] chose a different method.

In [87], an alternative multi-faults detection method using search coils is proposed. These invasive coils are wound around armature teeth, so they typically need to be installed during manufacturing. But its immunity to high frequency harmonics makes it suitable for inverter/rectifier fed motors or generators, such as wind turbines and automotive systems. In addition, this method does not require the knowledge of machine parameters. Since the air gap flux is directly measured in this method, it provides much more diagnosis reliability. However in order to verify the validity of the presented scheme, several faults as eccentricity, armature winding short turn, demagnetization running with different torque have been modeled by Finite Element Analysis (EFA) but there isn't experimental validation. The number of required search coils for different fault case is given in table (2.3). To analyze all the given four kinds of fault cases, maximum number of search coils, 12, is chosen.

Table 2.3 : Number of required search coils for different fault case

<i>Fault case</i>	<i>Number of search coils required</i>
<i>Eccentricity</i>	3
<i>Demagnetization</i>	<i>Number of poles</i>
<i>Phase failure</i>	<i>Number of phases</i>
<i>Inter-turn fault</i>	<i>Number of solenoids</i>

Selection of the number of search coils Depends on the precision of work. This means that it may be possible to reduce costs by reducing the number of search coils, but you must consider the loss of detection of some of other faults [5].

The advantages of this method can be needed to only first order harmonic for fault detection usage so that it is immune to the harmonics induced by power electronic devices. Another benefit of this technique is that the load condition does not necessarily need to be specified for accurate fault diagnosis. The drawback of this method is that it is invasive, Moreover, slip rings with brushes will be required to acquire the voltage signal [89], so it might not be very economical for the machines that have already been manufactured, but holds potential for emerging applications.

C. Inverter-embedded technique

In [3], [37], an inverter-embedded technique for automated detection and classification of PMSM rotor faults is proposed as an alternative. The main concept is to use the inverter to perform a test whenever the motor is stopped and to detect rotor faults independent of operating conditions or load torque oscillations as shown in figure (2.11), which is not possible with motor current signature analysis (MCSA). The d-axis is excited with a (direct-current) + (alternating-current) signal, and the variation in the inductance pattern due to the change in the degree of magnetic saturation caused by demagnetization or eccentricity is observed for fault detection.

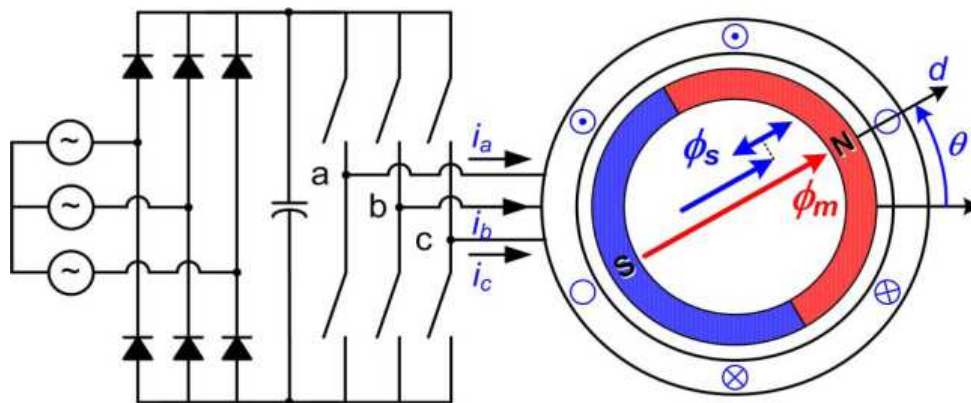


Fig. 2.11 : Main concept of proposed technique for PMSM rotor fault detection; stator ac and dc field excitation in the d -axis is used for extraction of L'_d .

It is well shown that in the presence of demagnetization fault, the rate of X'_d changes and increases by the fault rate.

However a good classification is done between demagnetization and eccentricity faults, the other faults effects on inductance changes must be considered. Willy-nilly, other faults like unbalanced voltage, voltage dips, inter turn and etc, lead to inductance changes in electrical motors [90]. Also complexity of computing inductance changes in on-line diagnosis may be persecutor for designer too.

In [3], as well as mentioned for demagnetization fault detection, this method (inverter-embedded technique) is used for automated detection and classification of PMSM rotor faults too.

It well shown that in presence eccentricity fault, the rate of X'_d changed and by fault rate increase, will be reduced. It is an interested result in compare to inductance change in presence of demagnetization faults wherever the demagnetization faults case to increase of X'_d of its nominal rate.

D. Permeance network approach

In [36] the permeance network approach and superposition theorem have been used to check out the semi-analytical model for demagnetization fault detection. The permeance network is basically a magnetic network analogous to electrical network which is based on machine's geometry. It saves information of geometry within permeances. The connection scheme of permeances can either be in parallel or in series and it is possible to represent a certain part of machine's geometry by one common permeance. The permeance network method has future potential as a research tool, in particular, in the dynamic simulations of an electrical machine. As compared to an accurate finite element method (FEM) analysis, a simple permeance model can solve the problem much more quickly with a little compromise to computational error.

4.1.5 Investigations based on design changes - practical design

In [45], [91], and [15], for minimization of mechanical vibration caused by demagnetization fault, the optimal PM shape is designed. The robust shape model of the permanent magnet for the outer rotor PMSM related to partial demagnetization, cogging torque, load angle curve, and back EMF is suggested. In figure (2.12) a sample of different shapes of magnet due to optimizing process against demagnetization fault, is shown. Also in [91] a structure of high power density PM assisted synchronous reluctance motor employing the ferrite PM, that doesn't cause irreversible demagnetization of PM even in condition of the heavy flux-weakening excitation or inverter's fault is presented.



Fig. 2.12 : Different shapes of magnet due to optimizing process against demagnetization fault [31]
(Finally, the author Introduces the shape model 1 as a robust permanent magnet type of outer rotor PMSM for HEV)

A permanent-magnet-assisted salient-pole synchronous Machine (PMA-SM) under sudden short circuits has been investigated in [35]. Based on this, an additional damper bars is used to reduce the demagnetization in the PMs. As a result, it has been found that making the PM shape a rectangle and adding the damper bars on the outer surfaces of the PMs is effective to reduce the PM demagnetization. Adding the damper bars on the inner surfaces is not effective. Increasing the conventional damper bars is also not effective. Causes of the effectiveness and ineffectiveness of the additional outer and inner damper bars are also shown.

4.1.6 Parameter estimation:

parameter estimation are used in previous years for fault detection and diagnosis of permanent magnet motors [92 - 94], but the newest work in this area is presented in [31] and is related to 2007. In [31] a method based on torque changes is presented to determine magnet strength. The average of the magnet flux linkage derivative terms yields a value that corresponds to twice the mean value of the flat part of the phase back-EMF.

In [94], the estimation of R_d, R_q, L_d, L_q parameters is used for turn to turn fault monitoring in PMSMs.

4.1.7 Fuzzy logic

A fuzzy logic based approach is implemented in [95] to generate a robust detection using the adjusted negative sequence current and negative sequence impedance. The adjusted negative sequence current is obtained by separating the high frequency components caused by the load fluctuation from the total negative sequence current. The adjusted negative sequence current provides a qualitative evaluation on severity of the stator fault. The usage of only negative sequence current under load fluctuation conditions show a significant increase in the high frequency components that can lead to trigger false alarms in conditioning monitoring systems under motor healthy operation.

While the most important point in considering the fault diagnosis and the choice of detection method is to prevent 'false alarm' because of inexact detection of fault [14]. On the contrary, the negative sequence impedance has shown a weak dependency on a load change, but it misses the fault at some time instants. So to compensate for this weakness, combining fuzzy logic with negative sequence analysis, the proposed method conquers the limitations of the negative sequence (current and impedance) based fault detection approaches as mentioned above. In this case, the fault detection technique can not only differentiate between an asymmetry caused by a stator shorted turns and an unbalance due to load variations, but also provide a measure on the fault severity level.

4.1.8 Artificial Neural network

In [95], three types of electrical stator faults have been explored. The first electrical fault is a momentarily opening of one phase between the motor and the inverter. The second and third electrical faults are line-to-ground (L-G) and line to line (L-L) short circuits in the stator windings of the motor. In the proposed hybrid technique, the line currents of different fault conditions and healthy motor are decomposed at the second level of resolution of the packages wavelet transform (WPT). The neural network (NN) was trained using these coefficients based on WPT current line. This method does not

depend on the motor equivalent circuit model parameters. But the comparison with other faults for proving of presented result didn't done! Also the usage of ANN for this type of fault isn't Justifiable!

In [30] and [95], we proposed a neural network based method for detecting unbalanced voltage fault percentage and its load condition in a permanent magnet synchronous motor. Five different load statues considered in motor test condition that it divide to no-load, 25% of nominal load, half load, 75% of nominal load and full load statues, for all presented unbalanced voltage percentages (of 1% - 20%). The Proposed method is independent from load state and fault percentage; it means that the proposed neural network is able to detect fault and load condition without having any assumption of fault level.

A study on monitoring and diagnosis of external faults in a three Phase Induction Motors by getting help from Artificial Neural Network (ANN) is elaborated in [110], such technique apply the results of the RMS measurement of stator voltages, currents and motor speed to train a neural network (NN) to monitor and diagnosis external motor faults. Despite studies on the various faults, unbalanced voltage fault is done only in terms of stationary state and not in dynamic state. An induction Motor Fault Detection and Diagnosis Using Supervised and Unsupervised Neural network is done in [99] too. The supervised NN is only able to detect the faulty machine and it cannot classify the type of fault. Failure identification of induction motors by sensing unbalanced stator currents is done in [96]. Single-phasing, unbalanced voltage, high resistance phase to ground fault, high resistance fault between phases, high resistance ground and phase fault, unbalanced impedance in the rotor has studied by R. Natarajan at 1989. Despite extensive work done well, but in each fault category, classification of fault condition has been remained until now.

In [65], [57], and [12] PMSM with SE, DE, and ME is modeled using time-stepping FEM (TSFEM). In this modeling, the geometrical and physical characteristics of different parts of PMSM, non uniform permeance of air gap due to stator slots, nonlinear characteristics of PM, and stator and rotor cores are considered. Then, stator current, calculated using TSFEM, is chosen as a proper signal for processing and noninvasive fault diagnosis. Fast Fourier transform (FFT) is then used to process the stator current. A three-layer ANN is employed to estimate the eccentricity degree of current profile based on the eccentricity type too.

Thus, a novel pattern frequency is introduced here, which enables one to diagnose the SE, DE, ME as follows:

$$f_{Eccentricity} = \left[1 \pm \left(\frac{2k-1}{p} \right) \right] f_s \quad (2-20)$$

Where k is an integer number 1, 2, 3 and etc. P is the number of pole pairs, and f_s is the supply frequency.

A structured neural network system has been designed, developed and trained to detect and isolate the most common types of faults [97]: single switch open circuit faults, post-short circuits, short circuits, and the unknown faults of an electric drive inverters.

4.1.9 Synthesis study

As it is obvious from existed references, in recent years this kind of fault has been noted by researchers and because of its importance, each year different methods are proposed for detecting it precisely on time. Regarding the vast scope of references that have been studied in this work, besides past methods that were shown in table (2.2) completely, the latest achievements of researchers in recent years were investigated and analyzed. Advantages and disadvantages of each were shortly discussed. It is obvious that there are a lot of other references and methods for fault diagnosis as magnet flux linkage, maximum-likelihood voting (MLV) [98], and etc, but we focused on most commonly used in the literatures. A summary of the newest methods that were proposed is brought below:

- 1) Fast Fourier Transform (FFT) of stator components (zero sequence currents, voltage and current) – [2-4], [31], [48], [52], [65], [41], [38], [43], [66], [67], [14], [17], [20], [64], [53], [62], [63], [32], [58], [68], [69], and [70] – 2006, 07, 08, 09, 10 and 2012.
- 2) Time frequency transform of stator components – [41], [76], [21], [38], [43], [13], [64], [79], [72-75], [82-85], [34], [1], [36], [58], [71], [77], [80], and [81] – 2007, 08, 09, 2010.
- 3) Noise, vibration and torque – [67], [32], [68] - 2006, 08, and 2010.
- 4) Optimization in PM shape and design changes based methods – [45], [91], [15] and [35] – 2006, 10, and 2011.
- 5) Field reconstruction method (sound power radiated) – [44], [25], and [86] – 2010, 11, and 2012.
- 6) Inverter embedded technique – [3], [90], and [37] – 2010 and 2012.
- 7) Parameter estimation based methods – [92], and [93] – 2007.
- 8) Search coils – [5], [87], [89], and [94] – 2010.
- 9) Analytical and Semi-analytical models – [1], [36], [79], [80], and [81] – 2000, 02, 03, 06, and 2008.
- 10) Fuzzy logic based methods – [95], 2008
- 11) Artificial neural network (ANN) based methods– [65], [57], [95], [12], [25], [29], [30], [97], [98], and [99], 2011, 2008, 2009, 2002, 2012, 2007, 2010.

4.1.10 Conclusion

In this chapter, we presented a state of the art of HEV faults by focus on drivetrans. We studied about different probable faults that can be occurred for drivetrains of HEV and also the effects of these faults on their application. Some of these faults can be introduced as : Stator winding short circuit, eccentricity, bearing, unbalanced voltage, open phasing and line to line faults in part of electric motor and also open phasing fault as a prevalent fault in controllable and uncontrollable power converters (AC/DC and DC/AC). A deep investigation on existence data analysis methods has been done in terms of chose a suitable methods aiming to use in fault diagnosis. According to consideration and analysis different diagnosis methods presented by literatures, Fast

Fourier transform (FFT) has been selected as a proper method in stationary state operation.

In chapter 3 and 4, will be given more detail about how usage of selected method for fault diagnosis in electrical machine and power converter. The goal is draw a sensitive model, usable to reach to objective of this work.

5. References of chapter II

- [1] J. A. Farooq, A. Djerdir, and A. Miraoui, "Analytical Modeling Approach to Detect Magnet Defects in Permanent-Magnet Brushless Motors", IEEE TRANSACTIONS ON MAGNETICS, VOL. 44, NO. 12, DECEMBER 2008.
- [2] Urresty, J., Riba Ruiz, J., Romeral, L., "A Back-emf Based Method to Detect Magnet Failures in PMSMs Magnetics" , IEEE TRANSACTIONS, Issue: 99 - Early Access Articles .
- [3] Jongman Hong, Sanguk Park, Doosoo Hyun, Tae-june Kang, Sang Bin Lee, Christian Kral, and Anton Haumer, "Detection and Classification of Rotor Demagnetization and Eccentricity Faults for PM Synchronous Motors", IEEE TRANSACTIONS ON INDUSTRY APPLICATIONS, VOL. 48, NO. 3, MAY/JUNE 2012.
- [4] Yao Da, Xiaodong Shi, Krishnamurthy. M, "Health monitoring, fault diagnosis and failure prognosis techniques for Brushless Permanent Magnet Machines", Vehicle Power and Propulsion Conference (VPPC), 2011 IEEE , Publication Year: 2011 , Page(s): 1 – 7.
- [5] Shah, D.; Nandi, S.; Neti, P., "Stator-Interturn-Fault Detection of Doubly Fed Induction Generators Using Rotor-Current and Search-Coil-Voltage Signature Analysis", IEEE TRANSACTIONS ON INDUSTRY APPLICATIONS Volume: 45 , Issue: 5, Publication Year: 2009 , Page(s): 1831 – 1842.
- [6] Payne, B.S., Husband, S.M., Ball, A.D., 2002, 'Development of condition monitoring techniques for a transverse flux motor', International Conference on Power Electronics, Machines and Drives-PEMD '02 (IEE Conference Publication No. 487), Bath, UK, June 4-7, 2002, pp. 139-144]
- [7] Thomson, W. T., 1999, 'A review of on-line condition monitoring techniques for three-phase squirrel-cage induction motors-past, present and future', 2nd IEEE International Symposium on Diagnostics for Electrical Machines, Power Electronics and Drives-SDEMPED '99, Gijon, Spain, Sept. 1-3, 1999, pp. 3-17.]
- [8] Oskar Wallmark, Lennart Harnefors, and Ola Carlson , "Control Algorithms for a Fault-Tolerant PMSM Drive", IEEE TRANSACTIONS ON INDUSTRIAL ELECTRONICS, VOL. 54, NO. 4, AUGUST 2007.
- [9] N. Bianchi and S. Bolognani, "Fault-tolerant PM motors in automotive applications," in Proc. IEEE Conf. Vehicle Power and Propulsion, 2005, pp. 747-755.
- [10] S. Bolognani, M. Zordan, and M. Zigliotto, "Experimental fault-tolerant control of a PMSM drive," IEEE TRANS. IND. ELECTRON, vol. 47, no. 5, pp. 1134-1141, Oct. 2000.
- [11] Mingzhong Qiao, Xiaofeng Zhang ; Xiuming Ren , "Research of the mathematical model and sudden symmetrical short circuit of the multi-phase permanent-magnet motor", International Conference on Power System Technology, 2002, Page(s): 769 - 773 vol.2.
- [12] B.M. Ebrahimi, J. Faiz, B.N. Araabi, "Pattern identification for eccentricity fault diagnosis in permanent magnet synchronous motors using stator current monitoring", Published in IET Electric Power Applications Received on 23rd June 2009 Revised on 5th November 2009.
- [13] K.-H. Kim, D.-U. Choi, B.-G. Gu, I.-S. Jung, "Fault model and performance evaluation of an inverter-fed permanent magnet synchronous motor under winding shorted turn and inverter switch open", Published in IET Electric Power Applications Received on 25th July 2009 Revised on 23rd September 2009 doi: 10.1049/iet-epa.2009.0183.
- [14] Kyeong-Hwa Kim, "Simple Online Fault Detecting Scheme for Short-Circuited Turn in a PMSM Through Current Harmonic Monitoring", Industrial Electronics, IEEE Transactions on Volume: 58 , Publication Year: 2011 , Page(s): 2565 – 2568.
- [15] Ki-Chan Kim, Seung-Bin Lim, Dae-Hyun Koo, and Ju Lee, "The Shape Design of Permanent Magnet for Permanent Magnet Synchronous Motor Considering Partial Demagnetization", IEEE TRANSACTIONS ON MAGNETICS, VOL. 42, NO. 10, OCTOBER 2006.

-
- [16] S. Saeid. Moosavi, A. Djerdir, Y. Aït-Amirat, D. A. Khaburi, “ Impedance Angle Changes Analysis Applied to Short Circuit Fault Detection ”, IEEE XXth International Conference on Electrical Machines (ICEM'2012), Septembre 2-5-2012, Marseille, France.
- [17] Tavner, P., Penman, J., 1987, ‘Condition Monitoring of Electrical Machines’, Research studies press LTD, 1987. ISSN/ISBN: 0-86380-061-0, 302 p.
- [18] Chris Gerada, Keith Bradley, Mark Sumner, “Winding Turn-to-Turn Faults in Permanent Magnet Synchronous Machine Drives”, Industry Applications Conference, 2005. Fourtieth IAS Annual Meeting, Conference Record of the 2005, Page(s): 1029 - 1036 Vol. 2, Publication Year: 2005.
- [19] Jawad Ahmed Farooq, Tsarafidy Raminosa, Abdesslem Djerdir and Abdellatif Miraoui, “ Modelling and simulation of stator winding inter-turn faults in permanent magnet synchronous motors”, The International Journal for Computation and Mathematics in Electrical and Electronic Engineering (COMPEL), Vol. 27 No. 4, pp. 887-896, 2008.
- [20] A. Khlaief, M. Boussak, M. Gossa, "Open Phase Faults Detection in PMSM Drives Based on Current Signature Analysis", XIX International Conference on Electrical Machines - ICEM 2010, Rome.
- [21] Javier A. Rosero, Luis Romeral, Juan A. Ortega, and Esteban Rosero, “Short-Circuit Detection by Means of Empirical Mode Decomposition and Wigner–Ville Distribution for PMSM Running Under Dynamic Condition”, IEEE TRANSACTIONS ON INDUSTRIAL ELECTRONICS, VOL. 56, NO. 11, NOVEMBER 2009.
- [22] Kliman, G.B., Sang Bin Lee, Shah, M.R., Lusted, R.M., Nair, N.K., 2004, ‘A new method for synchronous generator core quality evaluation’, IEEE Transactions on Energy Conversion, Vol. 19, Issue 3, pp. 576-582.
- [23] Smith A.C., Bertenshaw D, Ho C.W., Chan T, Sasic M, ”Detection of stator core faults in large turbo-generators” IEEE International conference on EMs and Drives Conference, IEMDC '09. Publication Year: 2009 , Page(s): 763 – 770.
- [24] Lee, S.B., Kliman, G.B., Shah, M.R., Nair, N.K., Lusted, R.M., 2005, ‘An iron core probe based inter-laminar core fault detection technique for generator stator cores’, IEEE Transactions on Energy Conversion, Vol. 20 , Issue 2, pp. 344-351.
- [25] Khoobroo. A, Fahimi. B, “A new method of fault detection and treatment in five phase permanent magnet synchronous machine using field reconstruction method”, EMs and Drives Conference, 2009. IEMDC '09. Publication Year: 2009 , Page(s): 682 – 688.
- [26] Brian A. Welchko, Thomas M. Jahns, and Silva Hiti, “IPM Synchronous Machine Drive Response to a Single-Phase Open Circuit Fault”, IEEE TRANSACTIONS ON POWER ELECTRONICS, VOL. 17, NO. 5, SEPTEMBER 2002.
- [27] Ching-Yin Lee, “Effects of Unbalanced Voltage on the Operation Performance of a Three-phase Induction Motor”, IEEE Transactions on Energy Conversion, Vol. 14, No. 2, June 1999.
- [28] Motor and Generators, NEMA Standard Publication No.MG 1- 1998 (Revision 2-2001).
- [29] S. Saeid. Moosavi, A. Djerdir, Y. Aït-Amirat, D. A. Khaburi, “FAULT DETECTION IN 3-PHASE TRACTION MOTOR USING ARTIFICIAL NEURAL NETWORKS”, 2012 IEEE Transportation Electrification Conference and Expo (ITEC 2012)- Michigan, USA.
- [30] S. Saeid. Moosavi, A. Djerdir, Y. Aït-Amirat, D. A. Khaburi, “ARTIFICIAL NEURAL NETWORKS BASED FAULT DETECTION IN 3-PHASE PMSM TRACTION MOTOR ”, IEEE XXth International Conference on Electrical Machines (ICEM'2012), Septembre 2-5-2012, Marseille, France.
- [31] Satish Rajagopalan, Wiehan le Roux, Thomas G. Habetler, and Ronald G. Harley, “Dynamic Eccentricity and Demagnetized Rotor Magnet Detection in Trapezoidal Flux (Brushless DC) Motors Operating Under Different Load Conditions”, IEEE TRANSACTIONS ON POWER ELECTRONICS, VOL. 22, NO. 5, SEPTEMBER 2007.
- [32] Ruschetti. C, Bossio. G, De Angelo. C, Verucchi. C, “Effects of partial rotor demagnetization on permanent magnet synchronous machines”, IEEE International

- Conference on Industrial Technology (ICIT), 2010 Publication Year: 2010 , Page(s): 1233 – 1238.
- [33] W. Le Roux, R. Harley, and T. Habetler, “Rotor fault analysis of a permanent magnet synchronous machine”, International Conference on Electrical Machines (ICEM’02), Brugge, Belgium, 2002.
- [34] Miguel Delgado, Antonio Garcia, Jordi-Roger Riba, César Urresty and Juan Antonio Ortega, “Feature Extraction of Demagnetization Faults in Permanent- Magnet Synchronous Motors Based on Box-Counting Fractal Dimension”, IEEE TRANSACTIONS ON INDUSTRIAL ELECTRONICS, VOL. 58, NO. 5, 2011.
- [35] Tatsuya Hosoi, Hiroya Watanabe, Kazuo Shima, Tadashi Fukami, Ryoichi Hanaoka, Shinzo Takata, “Demagnetization Analysis of Additional Permanent Magnets in Salient-Pole Synchronous Machines With Damper Bars Under Sudden Short Circuits”, IEEE TRANSACTIONS ON INDUSTRIAL ELECTRONICS, VOL. 59, NO. 6, JUNE 2012.
- [36] J. Farooq, S. Srairi, A. Djerdir, and A. Miraoui, “Use of permeance network method in the demagnetization phenomenon modeling in a permanent magnet motor,” IEEE TRANSACTIONS ON MAGNETICS, VOL. 42, NO. 4, PP. 1295–1298, APR. 2006.
- [37] J.Hong, D. Hyun, S. B. Lee, J.Yoo, andK. Lee, “Automated monitoring of magnet quality for permanent magnet synchronous motors at standstill,” IEEE Trans. Ind. Appl., vol. 46, no. 4, pp. 1397–1405, Jul./Aug. 2010.
- [38] Rosero. J, Romeral. L, Cusido. J, Ortega. J. A, “Fault detection by means of wavelet transform in a PMSMW under demagnetization”, Industrial Electronics Society, 2007. IECON 2007. 33rd Annual Conference of the IEEE , Publication Year: 2007 , Page(s): 1149 – 1154.
- [39] S. Ruoho, A. Arkkio, “Partial Demagnetization of Permanent Magnets in Electrical Machines Caused by an Inclined Field”, IEEE TRANSACTIONS ON MAGNETICS, VOLUME 44, ISSUE 7, PART 1, JULY 2008 PAGE(S):1773 – 1778.
- [40] Casadei. D, Filippetti. F, Rossi. C, Stefani. A, “Magnets faults characterization for Permanent Magnet Synchronous Motors” Diagnostics for EMS, Power Electronics and Drives, 2009. SDEMPED 2009. IEEE International Symposium on , Publication Year: 2009 , Page(s): 1 – 6
- [41] Jordi-Roger Riba Ruiz, Javier A. Rosero, Antonio Garcia Espinosa, and Luis Romeral, “Detection of Demagnetization Faults in Permanent-Magnet Synchronous Motors Under Nonstationary Conditions”, IEEE TRANSACTIONS ON MAGNETICS, VOL. 45, NO. 7, JULY 2009.
- [42] J. A Farooq, Study and Detection of demagnetization and Short-Circuit in permanent Magnet Synchronous Machines, PhD Thesis, University of Technology Belfort Montbéliard, France, 2008.
- [43] Antonio Garcia Espinosa, Javier A. Rosero, Jordi Cusid’o, Luis Romeral, and Juan Antonio Ortega, “Fault Detection by Means of Hilbert–Huang Transform of the Stator Current in a PMSM With Demagnetization”, IEEE TRANSACTIONS ON ENERGY CONVERSION, VOL. 25, NO. 2, JUNE 2010.
- [44] Dimitri Torregrossa, Amir Khoobroo, and Babak Fahimi, “Prediction of Acoustic Noise and Torque Pulsation in PM Synchronous Machines With Static Eccentricity and Partial Demagnetization Using Field Reconstruction Method”, IEEE TRANSACTIONS ON INDUSTRIAL ELECTRONICS, VOL. 59, NO. 2, FEBRUARY 2012.
- [45] Hyung-Kyu Kim, Jin-Hur, “Characteristic analysis of IPM type BLDC motor considering the demagnetization of PM by stator turn fault”, Energy Conversion Congress and Exposition (ECCE), 2010 IEEE 12-16 Sept. 2010 Page(s): 3063 - 3070
- [46] G.-H. Kang, Jin Hur, H. Nam, J.-P. Hong and G.-T. Kim “Analysis of Irreversible Magnet Demagnetization in Line-Start Motors Based on the Finite-Element Method”, IEEE TRANSACTIONS ON MAGNETICS, VOL. 39.NO. 4, PP. 1488-1491, MAY 2003.
- [47] S. Ruoho, J. Kolehmainen, J. Ikaheimo, and A. Arkkio, “Interdependence of Demagnetization, Loading, and Temperature Rise in a Permanent- Magnet Synchronous

- Motor,” IEEE TRANSACTIONS ON MAGNETICS, VOL. 46, NO. 3, PP. 949– 953, MAR. 2010.
- [48] Marius Rosu¹, Július Saitz¹, and Antero Arkkio, “Hysteresis Model for Finite-Element Analysis of Permanent- Magnet Demagnetization in a Large Synchronous Motor under a Fault Condition”, IEEE TRANSACTIONS ON MAGNETICS, VOL. 41, NO. 6, JUNE 2005.
- [49] S. Yu and R. Tang, “Electromagnetic and mechanical characterization of noise and vibration in permanent magnet synchronous machines,” IEEE TRANSACTIONS ON MAGNETICS, VOL. 42, NO. 4, PP. 1335–1338, APR. 2006.
- [50] K. C. Kim, S. B. Lim, D. H. Koo, and J. Lee, “The shape optimization of permanent magnet for permanent magnet synchronous motor considering partial demagnetization,” IEEE TRANSACTIONS ON MAGNETICS, VOL. 42, NO. 10, PP. 3485– 3487, OCT. 2006.
- [51] Rosero, J.A.; Cusido, J.; Garcia, A.; Ortega, J.A.; Romeral, L. “Study on the Permanent Magnet Demagnetization Fault in Permanent Magnet Synchronous Machines”, IEEE Industrial Electronics, IECON 2006- ,Publication Year: 2006 , Page(s): 879 – 884.
- [52] Julio-César Urresty, Jordi-Roger Riba, Miguel Delgado, and Luís Romeral, “Detection of Demagnetization Faults in Surface-Mounted Permanent Magnet Synchronous Motors by Means of the Zero-Sequence Voltage Component”, IEEE TRANSACTIONS ON ENERGY CONVERSION, VOL. 27, NO. 1, MARCH 2012.
- [53] J. A. Rosero, J. Cusido, A. Garcia, J.A. Ortega, L. Romeral, “ Broken Bearings and Eccentricity Fault Detection for a Permanent Magnet Synchronous Motor”, IEEE 2006.
- [54] R. Cameron, W. T. Thomson, and A. B. Dow, “Vibration and current monitoring for detecting air gap eccentricity in large induction motors,” Proc. Inst. Elect. Eng., vol. 133, no. 3, pt. B, pp. 155–163, May 1986.
- [55] S. Nandi, S. Ahmed, and H. A. Toliyat, “Detection of rotor slot and other eccentricity related harmonics in a three phase induction motor with different rotor cages,” IEEE Trans. Energy Convers., vol. 16, no. 3, pp. 253–260, Sep. 2001.
- [56] W. le Roux, R. G. Harley, and T. G. Habetler, "Detecting Rotor Faults in Low Power Permanent Magnet Synchronous Machines," IEEE TRANSACTIONS POWER ELECTRON. , VOL. 22, NO. 1, PP. 322-328, JAN. 2007.
- [57] Bashir Mahdi Ebrahimi, Jawad Faiz and Mehrgan Javan Roshtkhari, “Static-, Dynamic-, and Mixed-Eccentricity Fault Diagnoses in Permanent-Magnet Synchronous Motors”, IEEE TRANSACTIONS ON INDUSTRIAL ELECTRONICS, VOL. 56, No. 11, NOVEMBER 2009.
- [58] S. Rajagopalan, J. M. Aller, J. A. Restrepo, T. G. Habetler, and R. G. Harley, “Detection of rotor faults in brushless DC motors operating under non-stationary conditions,” IEEE TRANSACTIONS ON INDUSTRY APPLICATIONS, VOL. 42, NO. 6, PP. 1464–1477, NOV. /DEC. 2006.
- [59] J. Rosero, J. L. Romeral, J. Cusido, J. A. Ortega, and A. Garcia, “Fault detection of eccentricity and bearing damage by means of wavelet transforms decomposition of the stator current”, in Proc. IEEE APEC, 2008, pp. 111–116.
- [60] Shaoyong Yang,, Dawei Xiang, Angus Bryant, Philip Mawby, Li Ran, and Peter Tavner, “Condition Monitoring for Device Reliability in Power Electronic Converters: A Review”, IEEE TRANSACTIONS ON POWER ELECTRONICS, VOL. 25, NO. 11, NOVEMBER 2010
- [61] Fabien Meinguet, Paul Sandulescu, Xavier Kestelyn, and Eric Semail, “A Method for Fault Detection and Isolation Based on the Processing of Multiple Diagnostic Indices: Application to Inverter Faults in AC Drives”, IEEE TRANSACTIONS ON VEHICULAR TECHNOLOGY, VOL. 62, NO. 3, MARCH 2013.
- [62] J. Rosero, A.G. Espinosa. J. Cusido, J. A. Ortega, L. Romeral, “Simulation and Fault Detection of Short Circuit Winding in a Permanent Magnet Synchronous Machine

- (PMSM) by means of Fourier and Wavelet Transform”, Measurement Technology Conference Victoria, Vancouver Island, Canada, May 12-15, 2008.
- [63] F. Auger, P. Flandrin, P. Goncalves, and O. Lemoine, Time-Frequency Toolbox for Use with MATLAB, CNRS (France) and Rice University (USA).
- [64] Bashir Mahdi Ebrahimi and Jawad Faiz, “Feature Extraction for Short Circuit Fault Detection in Permanent-Magnet Synchronous Motors Using Stator-Current Monitoring”, IEEE TRANSACTIONS ON POWER ELECTRONICS, VOL. 25, NO. 10, OCTOBER 2010.
- [65] Romeral, L.; Urresty, J.C.; Riba Ruiz, J.-R.; Garcia Espinosa, A., “Modeling of Surface-Mounted Permanent Magnet Synchronous Motors With Stator Winding Interturn Faults”, Industrial Electronics, IEEE Transactions on Volume: 58 , Issue: 5 Digital Object Identifier: 10.1109/TIE.2010.2062480 Publication Year: 2011 , Page(s): 1576 – 1585.
- [66] Brian A. Welchko, Jackson Wai, Thomas M. Jahns, and Thomas A. Lipo, “Magnet-Flux-Nulling Control of Interior PM Machine Drives for Improved Steady-State Response to Short-Circuit Faults” IEEE TRANSACTIONS ON INDUSTRY APPLICATIONS, VOL. 42, NO. 1, JANUARY/FEBRUARY 2006 113.
- [67] D. Basak, A. Tiwari, and S. Das, “Fault diagnosis and condition monitoring of electrical machines - A Review,” in Industrial Technology, 2006. ICIT 2006. IEEE International Conference on, pp. 3061-3066, 2006.
- [68] Gyu-Hong Kang, Young-Dae Son, and Gyu-Tak Kim, “The Noise and Vibration Analysis of BLDC Motor Due to Asymmetrical Permanent-Magnet Overhang Effects”, IEEE TRANSACTIONS ON INDUSTRY APPLICATIONS, VOL. 44, NO. 5, PP. 1569-1577, 2008.
- [69] Urresty, J, Riba, J, Saavedra, H, Romeral, J, “Analysis of demagnetization faults in surface-mounted permanent magnet synchronous motors with symmetric windings”, IEEE International Symposium on Diagnostics for EMs, Power Electronics & Drives (SDEMPED), Publication Year: 2011 , Page(s): 240 – 245.
- [70] Mehdi Rahiminejad, Chris Diduch, Maryhelen Stevenson, and Liuchen Chang, “Open-Circuit Fault Diagnosis in 3-Phase Uncontrolled Rectifiers”, 3rd IEEE International Symposium on Power Electronics for Distributed Generation Systems (PEDG) 2012.
- [71] R. Carmona, H.L. Hwang, and B. Torresani, Practical Time-Frequency Analysis: Gabor and Wavelet Transforms with and implementation in S, Academic Press, New York, 1998.
- [72] A. Papandreou- Suppappola, Applications In Time-Frequency Signal Processing, CRC Press, Boca Raton, FL, 2003.
- [73] Rosero, J.; Romeral, J.A.O.; Romeral, L.; Rosero, E., “Short circuit fault detection in PMSM by means of empirical mode decomposition (EMD) and wigner ville distribution (WVD)”, Twenty-Third Annual IEEE on Applied Power Electronics Conference and Exposition, APEC 2008, Publication Year: 2008 , Page(s): 98 - 103.
- [74] B. Boashash, Time Frequency Signal Analysis and Processing, Elsevier Ltd., Oxford, 2003.
- [75] A.I. Zemour, The Hilbert-Huang Transform for Damage Detection in Plate Structures, MS thesis at University of Maryland, 2006
- [76] J. Rosero, J. Ortega, J. Urresty, J. Cárdenas, L. Romeral, “Stator Short Circuits Detection in PMSM by means of Higher Order Spectral Analysis (HOSA)”, Applied Power Electronics Conference and Exposition, 2009, Page(s): 964 – 969, Publication Year: 2009.
- [77] Rosero, J.; Garcia, A.; Cusido, J.; Romeral, L.; Ortega, J.A., “Fault detection by means of Hilbert Huang Transform of the stator current in a PMSM with demagnetization Intelligent signal processing”, WISP 2007, Publication Year: 2007, Page(s): 1 – 6.
- [78] Rosero, J.; Romeral, L.; Ortega, J.A.; Urresty, J.C., “Demagnetization fault detection by means of Hilbert Huang transform of the stator current decomposition in PMSM”, IEEE International Symposium on Industrial Electronics, ISIE 2008. Publication Year: 2008 , Page(s): 172 – 177.

- [79] J. A. Rosero, J. Cusido, A. Garcia, J.A. Ortega, L. Romeral, “ Broken Bearings and Eccentricity Fault Detection for a Permanent Magnet Synchronous Motor”, IEEE 2006.
- [80] X. Wang, Q. Li, S. Wang, and Q. Li, “Analytical calculation of air-gap magnetic field distribution and instantaneous characteristics of brushless DC motors,” IEEE TRANSACTIONS ON ENERGY CONVERSION, VOL. 18, NO. 3, PP. 424–432, SEP. 2003.
- [81] A. B. Proca, A. Keyhani, A. El-Antably, W. Lu, and M. Dai, “Analytical model for permanent magnet motors with surface mounted magnets,” IEEE TRANSACTIONS ON ENERGY CONVERSION, VOL. 18, NO. 3, PP. 386–391, SEP. 2003.
- [82] HU.H.HWANG, “Transient Analysis of Unbalanced Short Circuit of Synchronous Machines”, IEEE TRANSACTIONS ON POWER APPARATUS AND SYSTEMS, VOL. PAS-88, NO. 1, JANUARY 1969.
- [83] H. H. Hwang, "Unbalanced operations of ac machines", IEEE Trans. Power Apparatus and Systems, vol. PAS-84, pp. 1054- 1066, November 1965.
- [84] H. H. Hwang, "Mathematical analysis of double line-to-ground short circuit of an alternator", IEEE Trans. Power Apparatus and Systems, vol. PAS-86, pp. 1254-1257, October 1967.
- [85] H. H. HWANG, “Unbalanced Operations of Three-Phase Machines with Damper Circuits”, IEEE TRANSACTIONS ON POWER APPARATUS AND SYSTEMS, VOL. PAS-88, NO. 11, NOVEMBER 1969.
- [86] Kiani, M, Torregrossa, D, Fahimi, B, Peyraut. F, Miraoui. A, “Detection of faults in PMSM using Field Reconstruction Method and Mechanical Impulse Response”, Applied Power Electronics Conference and Exposition (APEC), Twenty-Sixth Annual IEEE, Publication Year: 2011 , Page(s): 1896 – 1901.
- [87] Yao. Da, Krishnamurthy. M, “Novel fault diagnostic technique for permanent Magnet Synchronous Machines using electromagnetic signature analysis”, Vehicle Power and Propulsion Conference (VPPC), 2010 IEEE , Publication Year: 2010 , Page(s): 1 – 6.
- [88] Stoll, R.L.; Hennache, A., “Method of detecting and modelling presence of shorted turns in DC field winding of cylindrical rotor synchronous machines using two airgap search coils” Electric Power Applications, IEE Proceedings B Volume: 135 , Issue: 6 Publication Year: 1988 , Page(s): 281 - 294 IET Journals & Magazines.
- [89] Neti, P.; Nandi, S. ,”Stator Inter turn Fault Detection of Synchronous Machines Using Field Current and Rotor Search-Coil Voltage Signature Analysis Industry Applications”, IEEE Transactions on Volume: 45 , Issue: 3 Publication Year: 2009 , Page(s): 911 – 920.
- [90] D. W. Novotny and T. A. Lipo, “induction machine efficiency improvement by means of voltage control”, lipo.ece.wisc.edu/1980s%20pubs/C11.pdf.
- [91] Sanada, M.; Inoue, Y.; Morimoto, S, “Rotor structure for reducing demagnetization of magnet in a PMASynRM with ferrite permanent magnet and its characteristics” Energy Conversion Congress and Exposition (ECCE), 2011 IEEE Digital Object Identifier: 10.1109/ECCE.2011.6064340 Publication Year: 2011 , Page(s): 4189 – 4194
- [92] Xiang-Qun Liu, Hong-Yue Zhang, Jun Liu, and Jing Yang, “Fault Detection and Diagnosis of Permanent-Magnet DC Motor Based on Parameter Estimation and Neural Network”, IEEE TRANSACTIONS ON INDUSTRIAL ELECTRONICS, VOL. 47, NO. 5, OCTOBER 2000.
- [93] KHOV Makara, REGNIER Jeremi, FAUCHER Jean, “Detection of Turn Short-Circuit Faults in Stator of PMSM by On-Line Parameter Estimation”, International Symposium on Power Electronics, Electrical Drives, Automation and Motion, SPEEDAM 2008.
- [94] Khov, M.; Regnier, J.; Faucher, J, “Monitoring of turn short-circuit faults in stator of PMSM in closed loop by on-line parameter estimation”, Diagnostics for EMs, Power Electronics and Drives, 2009. IEEE International Symposium on SDEMPED 2009. Publication Year: 2009 , Page(s): 1 – 6.
- [95] J. Quiroga, Li Liu, and D. A. Cartes, “Fuzzy Logic based Fault Detection of PMSM Stator Winding Short under Load Fluctuation using Negative Sequence Analysis”, 2008

- American Control Conference, Westin Seattle Hotel, Seattle, Washington, USA June 11-13, 2008.
- [96] M. A. S. K. Khan and M. Azizur Rahman, "Development and Implementation of a Novel Fault Diagnostic and Protection Technique for IPM Motor Drives", IEEE TRANSACTIONS ON INDUSTRIAL ELECTRONICS, VOL. 56, NO. 1, JANUARY 2009.
- [97] E.M. Tag Eldin, H. R. Emara, E.M. Aboul-Zahab, Sh. S. Refaat, "Monitoring and Diagnosis of External Faults in Three Phase Induction Motors Using Artificial Neural Network", IEEE.trans 1- 4244-1298-2007.
- [98] S. Premrudee preechacharn, T. Utthiyuung, K. Kruepengkul, P. Puongkaew, "Induction Motor Fault Detection and Diagnosis Using Supervised and Unsupervised Neural Networks", IEEE ICIT'0Z, bangkok Bangkok, HAILAND,0-7803-7657.91021 - 2002 .
- [99] M. Abul Masrur, ZhiHang Chen and Yi Lu Murphey, "Intelligent diagnosis of open and short circuit faults in electric drive inverters for real-time applications", Power Electronics, IET (Volume:3 , Issue: 2 , Date of Publication: March 2010 , Page(s): 279 - 291 , ISSN : 1755-4535.
- [100] Bekheira Tabbache, Mohamed El Hachemi Benbouzid, "Virtual-Sensor-Based Maximum-Likelihood Voting Approach for Fault-Tolerant Control of Electric Vehicle Powertrains", IEEE TRANSACTIONS ON VEHICULAR TECHNOLOGY, VOL. 62, NO. 3, MARCH 2013.

Chapter III

Faults sensitive modeling of PMSM for diagnosis purpose

1.	Introduction	85
2.	Short circuit fault	86
2.1.	Short circuit fault sensitive modeling of PMSM: analytical approach.....	86
2.1.1	Analytical modeling of PMSM under inter turn short circuit fault	87
2.1.2	Limits of analytical modeling approach.....	91
2.2.	Experimental approach: faults characterization of PMSM associated to its controller	96
2.2.1	Set up description	96
2.2.2	Software program of the PMSM vector control.....	99
2.2.3	Healthy mode: constant speed - unloaded motor.....	102
2.2.4	Healthy mode: constant speed – loaded motor.....	103
2.2.5	Faulty mode: Influence of the short circuit fault on motor currents.....	104
2.2.6	Motor behaviors under different inter-turn short circuits faults: variable speed operating	109
2.3.	Diagnosis algorithm of PMSM short circuit faults	111
3.	Demagnetization fault	111
3.1.	Theoretical approach.....	111
3.2.	FEM fault simulation with FLUX-2D software.....	113
3.2.1	FEM simulation results: health and demagnetized PMSM	113
3.2.2	Comparison study between analytical and FEM models.....	118
3.3.	Diagnosis algorithm of PMSM demagnetization fault	119
4.	Eccentricity & bearing fault	119
4.1.	Eccentricity & bearing sensitive modeling.....	120
4.2.	Diagnosis algorithm of PMSM eccentricity & bearing.....	120
5.	Conclusion	121
6.	References of Chapter III	122

1. Introduction

According to different location of installing of magnets, permanent magnet synchronous machines are divided into three main architectures: surface permanent magnet synchronous machine (SPMSM), insert permanent synchronous machines (IPMSM) and interior permanent magnet (IPM). Within this last category, it is possible to find different structures as v-shaped internal magnets (VI-PMSM) and a rotor with radial arranged internal magnets (RI-PMSM). Figure (3.1) shows some different types of rotor in PMSMs illustrating the structures highlighted above.

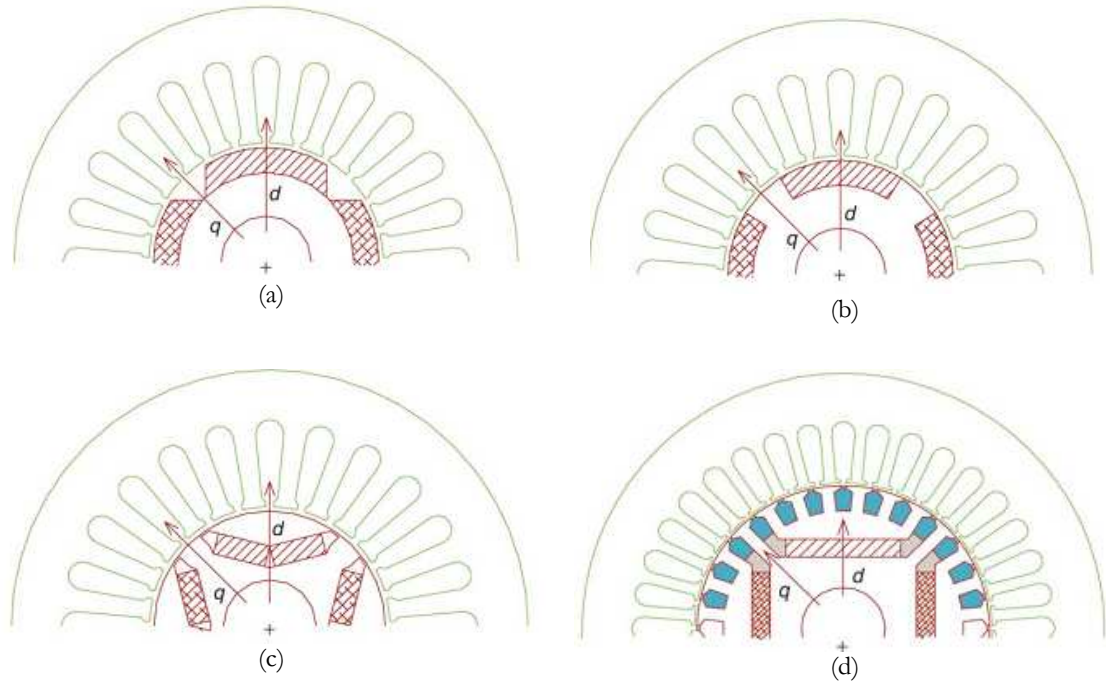


Fig. 3.1 : Different PMSM structures : (a) Surface permanent magnet synchronous machine (SPMSM) without pole saliency, (b) inset SPMSM with pole saliency (mounted Magnet), (c) interior permanent magnet (IPM) with one layer of permanent magnet (V-shaped internal magnet), (d) (IPM) with one layer permanent magnet and squirrel cage for starting

In [1], [2], and [3] has been done a systemically review mathematic models and features of the two major varieties of permanent-magnet synchronous machines, namely interior PM motors and surface-mounted PM motors.

In [4] a development of model under short circuit faults has been presented without addressing the fault detection and diagnosis. In this chapter, is avoided to show and repeating the PMSM simulation results obtained by [4] of PMSM under short circuit faulty state but a deep study on diagnosis on this type of fault in order to EVs and SHEVs applications have been done. Also the main steps required for artificial neural network (ANN) training by aim short circuit fault diagnosis in different speeds and loads of motor operation is investigated by help experimental data.

In second part of this chapter is devoted to the problem of demagnetization in an inset surface permanent magnet synchronous motor (ISPMSM). In fact we used of presented equations in [5], and [4], design for SPMSM and changed them for ISPMSM One analytical model and one simulation model has been developed for characterizing the demagnetization faults of this kind of machines. This allows larger diagnosis

knowledge about the PMSMs. Also, a study on the PMSM eccentricity and bearing fault has been performed and briefly explained.

2. Short circuit fault

Modeling procedure of abnormal behaviors of PMSM in order of fault diagnosis is shown in figure (3.2). In the first step, electromagnetic and vibratory models with current signals (3 phase motor currents and Park's currents "Id and Iq") and vibration signal are even especially developed or taken over from the background of the host laboratory (IRTES-SET). In the second step, pattern identification of experiment of noise of PMSM is done under permanent and transient conditions through FFT or TF analysis. In the third step, patterns identified are used to train artificial neural network as a classification and diagnosis for each kind of faults. The steps 1 and 2 will be treated in this chapter while the 3rd step will be explained in details in chapter 5.

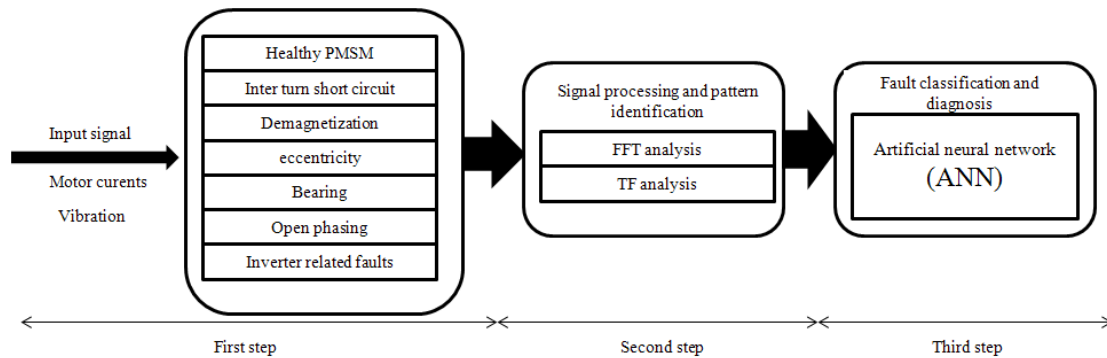


Fig. 3.2 : Model of identification and diagnosis of abnormal behaviors of PMSMs

2.1. Short circuit fault sensitive modeling of PMSM: analytical approach

The main approaches as theoretical, finite element method based and experimental approaches have been introduced by literature in order to inter turn short circuit fault investigation. Figure (3.3) shows the modeling procedure used of inter turn short circuit fault diagnosis of PMSM. In stationary state (as it is the aim of this work), FFT analysis method is used to characterize signatures of different kind and strong of the short-circuit faults.

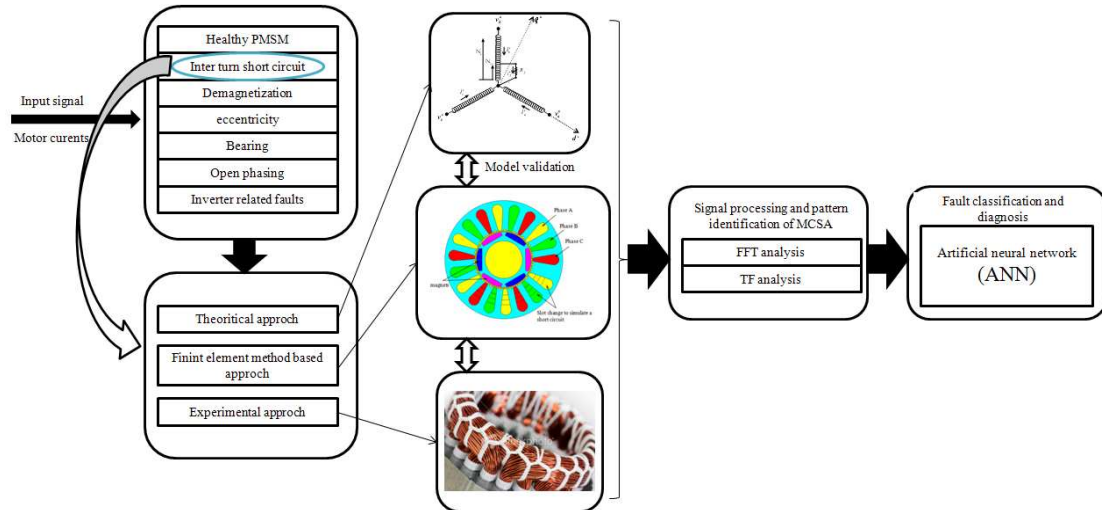


Fig. 3.3 : Model of identification and diagnosis of inter turn short circuit fault of PMSMs

2.1.1 Analytical modeling of PMSM under inter turn short circuit fault

In dynamic models of PMSM, stator (fixed) and the rotor (rotating) are already known. For these models, the rotating frame is generally considered because it concerns the most of PMSMs kind of machines but also due to their simplicity transient and permanent operating regimes [4]. Models in rotating frame (also called dq model) provides convenience important to control the system by the transformation of symmetrical alternative variables continuously in the rotating frame. This advantage can also be used in fault detection for PMSM.

The excitation flux comes from the magnets on or inside of the rotor. Kirchhoff's laws are applied to develop the electrical model of the machine. The model adopts the following assumptions:

- The magnetic permeability of ferromagnetic parts is considered infinite.
- The phenomenon of saturation is neglected.
- The magneto motive force and flux are first considered sinusoidal distributed.

Assume that a short circuit fault occurs between the turns in the phase 'b' of a machine with permanent magnets. Figure (3.4) shows the winding of the machine with an additional branch. Shorted part which forms an additional circuit creates a steady magnetic field. This new magnetic field modifies the main field by adding the fourth part in the magnetic system. The same procedure will be applied if the fault occurs in other phases.

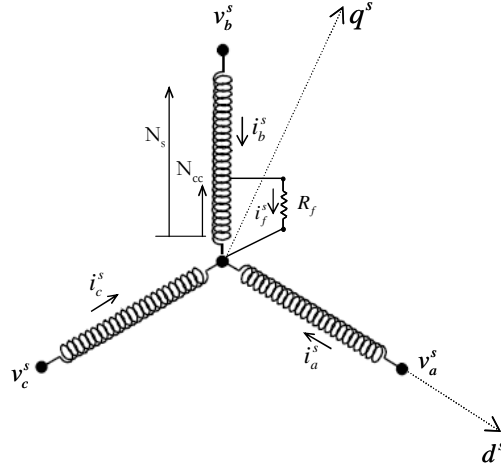


Fig. 3.4 : Winding the PMSM with a short circuit between turns of the phase 'a' and 'b', dq stator reference.

By setting the electrical circuit with the new index 'f', the new equation is reformulated motor voltages as follows:

$$v_{abc}^s = [v_a^s \quad v_{b1}^s \quad v_{b2}^s \quad v_c^s]^T \quad (3.1)$$

Where v_{b1}^s and v_{b2}^s are the voltages across the shorted and healthy coils. Similarly, the current vector becomes:

$$i_{abc}^s = [i_a^s \quad i_b^s \quad (i_b^s - i_f^s) \quad i_c^s]^T \quad (3.2)$$

Where, ' i_f^s ' is the additional current generated by the short circuit. The fundamental problem is how to calculate the new parameters (the new resistors and inductors). Property of proportionality can be used to find new resistance based on the parameter σ , and are calculated as follows:

$$R_{b1}^s = (1 - F_{Shc}) R_b^s, R_{b2}^s = F_{Shc} R_b^s, \text{ With } F_{Shc} = \frac{N_{cc}}{N_s} \quad (3.3)$$

Resistance matrix becomes,

$$R^s = \begin{bmatrix} R_a^s & 0 & 0 & 0 \\ 0 & R_{b1}^s & 0 & 0 \\ 0 & 0 & R_{b2}^s & 0 \\ 0 & 0 & 0 & R_c^s \end{bmatrix} \quad (3.4)$$

The new matrix inductance ' L_s ' is now composed of self and mutual inductances between the short-circuited parts and the healthy parts of the stator windings. The problem of calculating of inductance has already been discussed in several publications [4] and etc. In [4] proposes a method for faults studying in the transformer. This method

offers a good balance between model simplicity and accuracy. The new matrix of the inductance is expressed by:

$$L_s = \begin{bmatrix} L & (1-F_{Shc})M & F_{Shc}M & M \\ (1-F_{Shc})M & (1-F_{Shc})^2L & (1-F_{Shc})F_{Shc}L & (1-F_{Shc})M \\ F_{Shc}M & (1-F_{Shc})F_{Shc}L & F_{Shc}^2L & F_{Shc}M \\ M & (1-F_{Shc})M & F_{Shc}M & L \end{bmatrix} \quad (3.5)$$

Flow through the magnet at the faulty phase can also be divided into two parts which are proportionate to the seriousness of the fault:

$$\Psi_{mabc} = \begin{bmatrix} \Psi_{ma}(\theta_r) \\ \Psi_{mb1}(\theta_r) \\ \Psi_{mb2}(\theta_r) \\ \Psi_{mc}(\theta_r) \end{bmatrix} = \Psi_m \begin{bmatrix} \sin(\theta_r) \\ (1-F_{Shc})\sin\left(\theta_r - \frac{2\pi}{3}\right) \\ F_{Shc}\sin\left(\theta_r - \frac{2\pi}{3}\right) \\ \sin\left(\theta_r + \frac{2\pi}{3}\right) \end{bmatrix} \quad (3.6)$$

A new form of the equation of the machine is obtained.

$$v_{abc}^s = R_s i_{abc}^s + \frac{d\Psi_{abc}^s}{dt} - F_{Shc} R_s i_f^s - F_{Shc} \frac{d\Psi_f^s}{dt} \quad (3.7)$$

Where $R_s = R_a = R_b = R_c$ in healthy mode and:

$$v_{abc}^s = [v_a^s \quad v_b^s \quad v_c^s]^T \quad (3.8)$$

$$i_{abc}^s = [i_a^s \quad i_b^s \quad i_c^s]^T \quad (3.9)$$

Ψ_f is the flow through the short-circuited part of the winding.

$$\Psi_f^s = L_f^s i_f^s \quad (3.10)$$

Where $L_f^s = [M \quad L \quad M]^T$,

Equation (3.7) fully describes the electrical model of a PMSM in the reference abc with defect short circuit between turns in a phase. Following the same approach we can write the equations of the machine in the event of faults in other phases. The voltage across the short-circuited part can be calculated by:

$$v_{b2}^s = F_{Shc} R_s (i_b^s - i_f^s) + \frac{d\Psi_{b2}^s}{dt} = i_f^s R_f \quad (3.11)$$

$$\text{Where } \Psi_{b2}^s = F_{Shc} [L_f]^T i_{abc}^s - F_{Shc}^2 L i_f^s + F_{Shc} \Psi_{mb},$$

In equation (3.11), ' R_f ' is a dummy resistor connected in parallel with the short-circuited part in order to control of short-circuit as shown in figure (3.4). Using this resistance the proposed model is valid for both healthy and degraded mode. This feature eliminates the need to change the model of a healthy functioning operating to a faulty functioning operating.

In case of three short circuits between turns at the phases of the stator, the three parameters σ_a , σ_b and σ_c define the percentages of the turns in short-circuit according to three respective fault. The new equation of voltages reformulated as follows:

$$v_{abc}^s = [v_{a1}^s \quad v_{a2}^s \quad v_{b1}^s \quad v_{b2}^s \quad v_{c1}^s \quad v_{c2}^s]^T \quad (3.12)$$

Where v_{a1}^s and v_{a2}^s are the voltages across the healthy and shorted coils. It is the same for the other phases. The current vector is:

$$i_{abc}^s = [i_a^s \quad (i_a^s - i_{fa}^s) \quad i_b^s \quad (i_b^s - i_{fb}^s) \quad i_c^s \quad (i_c^s - i_{fc}^s)]^T \quad (3.13)$$

Resistance matrix becomes,

$$R^s = \begin{bmatrix} (1-F_{Shca}) \cdot R_a^s & 0 & 0 & 0 & 0 & 0 \\ 0 & F_{Shca} \cdot R_a^s & 0 & 0 & 0 & 0 \\ 0 & 0 & (1-F_{Shcb}) \cdot R_b^s & 0 & 0 & 0 \\ 0 & 0 & 0 & F_{Shcb} \cdot R_b^s & 0 & 0 \\ 0 & 0 & 0 & 0 & (1-F_{Shcc}) \cdot R_c^s & 0 \\ 0 & 0 & 0 & 0 & 0 & F_{Shcc} \cdot R_c^s \end{bmatrix} \quad (3.14)$$

And the inductance matrix can be expressed by,

$$L_s = \begin{bmatrix} (1-F_{Shca})^2 L & (1-F_{Shca})F_{Shca}L & (1-F_{Shca})(1-F_{Shcb})M & (1-F_{Shca})F_{Shcb}M & (1-F_{Shca})(1-F_{Shc})M & (1-F_{Shca})F_{Shc}M \\ (1-F_{Shca})F_{Shca}L & F_{Shca}^2 L & F_{Shca}(1-F_{Shcb})M & F_{Shca}F_{Shcb}M & F_{Shca}(1-F_{Shc})M & F_{Shca}F_{Shc}M \\ (1-F_{Shca})(1-F_{Shcb})M & F_{Shca}(1-F_{Shcb})M & (1-F_{Shcb})^2 L & (1-F_{Shcb})F_{Shcb}L & (1-F_{Shcb})(1-F_{Shc})M & (1-F_{Shcb})F_{Shc}M \\ (1-F_{Shca})F_{Shcb}M & F_{Shca}F_{Shcb}M & (1-F_{Shcb})F_{Shcb}L & F_{Shcb}^2 \cdot L & F_{Shcb}(1-F_{Shc})M & F_{Shcb}F_{Shc}M \\ (1-F_{Shca})(1-F_{Shc})M & F_{Shca}(1-F_{Shc})M & (1-F_{Shcb})(1-F_{Shc})M & F_{Shcb}(1-F_{Shc})M & (1-F_{Shc})^2 \cdot L & (1-F_{Shc})F_{Shc}L \\ (1-F_{Shca})F_{Shc}M & F_{Shca}F_{Shc}M & (1-F_{Shcb})F_{Shc}M & F_{Shcb}F_{Shc}M & (1-F_{Shc})F_{Shc}L & F_{Shc}^2 \cdot L \end{bmatrix} \quad (3.15)$$

The magnet flux through the three phases, that all of them are under faulty state, may also be divided into two parts which are proportionate to the seriousness of the fault:

$$\Psi_{mabc} = \begin{bmatrix} \Psi_{ma1}(\theta_r) \\ \Psi_{ma2}(\theta_r) \\ \Psi_{mb1}(\theta_r) \\ \Psi_{mb2}(\theta_r) \\ \Psi_{mc1}(\theta_r) \\ \Psi_{mc1}(\theta_r) \end{bmatrix} = \Psi_m \begin{bmatrix} (1 - F_{Shc_a}) \sin(\theta_r) \\ F_{Shc_a} \sin(\theta_r) \\ (1 - F_{Shc_b}) \sin\left(\theta_r - \frac{2\pi}{3}\right) \\ F_{Shc_b} \sin\left(\theta_r - \frac{2\pi}{3}\right) \\ (1 - F_{Shc_b}) \sin\left(\theta_r + \frac{2\pi}{3}\right) \\ F_{Shc_b} \sin\left(\theta_r + \frac{2\pi}{3}\right) \end{bmatrix} \quad (3.16)$$

By sum of lines 1 and 2, then 3 and 4 and then 5 and 6 of the equation (3.12), the new equation form of the machine is given by:

$$v_{abc}^s = R_s i_{abc}^s + L_s \frac{di_{abc}^s}{dt} - F_{Shc_{abc}} R_s i_{abc_f}^s - [F_{Shc_{abc}} \cdot L_f]^T \frac{di_{abc_f}^s}{dt} \quad (3.17)$$

$$\text{Where } F_{Shc_{abc}} = \begin{bmatrix} F_{Shc_a} & 0 & 0 \\ 0 & F_{Shc_b} & 0 \\ 0 & 0 & F_{Shc_c} \end{bmatrix}$$

$$\text{With } L_f = L_s = \begin{bmatrix} L & M & M \\ M & L & M \\ M & M & L \end{bmatrix}$$

Equation (3.16) fully describes the electrical model of a PMSM in the reference abc with the inclusion of any short-circuit fault between the turns in the three phases. In this general model, canceling the parameters F_{Shc_a} and F_{Shc_c} and by setting $F_{Shc_b} = F_{Shc}$, we find the model of the fault in phase 'b'.

2.1.2 Limits of analytical modeling approach

The detection of the fault short circuit of a PMSM on the basis of only the analytical model shown above is strongly dependent on the accuracy of the used physical parameters of such model. The latter assumes several hypotheses such as linearity and symmetry of the magnetic circuit of the considered machine. However, one of the most common problems of the PMSM is the non-linearity of its magnetic circuit namely non-symmetry due to manufacturing. So, to be efficient the developed models have to take into account this kind of phenomenon.

In this section a theoretical and experimental study has been achieved to highlight the analytical modeling limitations. A focus is made on one geometrical abnormality through the analysis of some experimental measurements and finite element simulations. Thus, the impact of this kind of abnormalities on the proposed model is highlighted as a limitation for this model using in diagnosis purpose.

In order to check the validity of the proposed model an experimental test has been build, (see section 2.2). This test bench allows notably simulating different type of inter-turn short circuit faults. Measurements of stator currents in healthy mode and faulty mode obtained by applying a 20% partial short-circuit one stator phase of the studied PMSM.

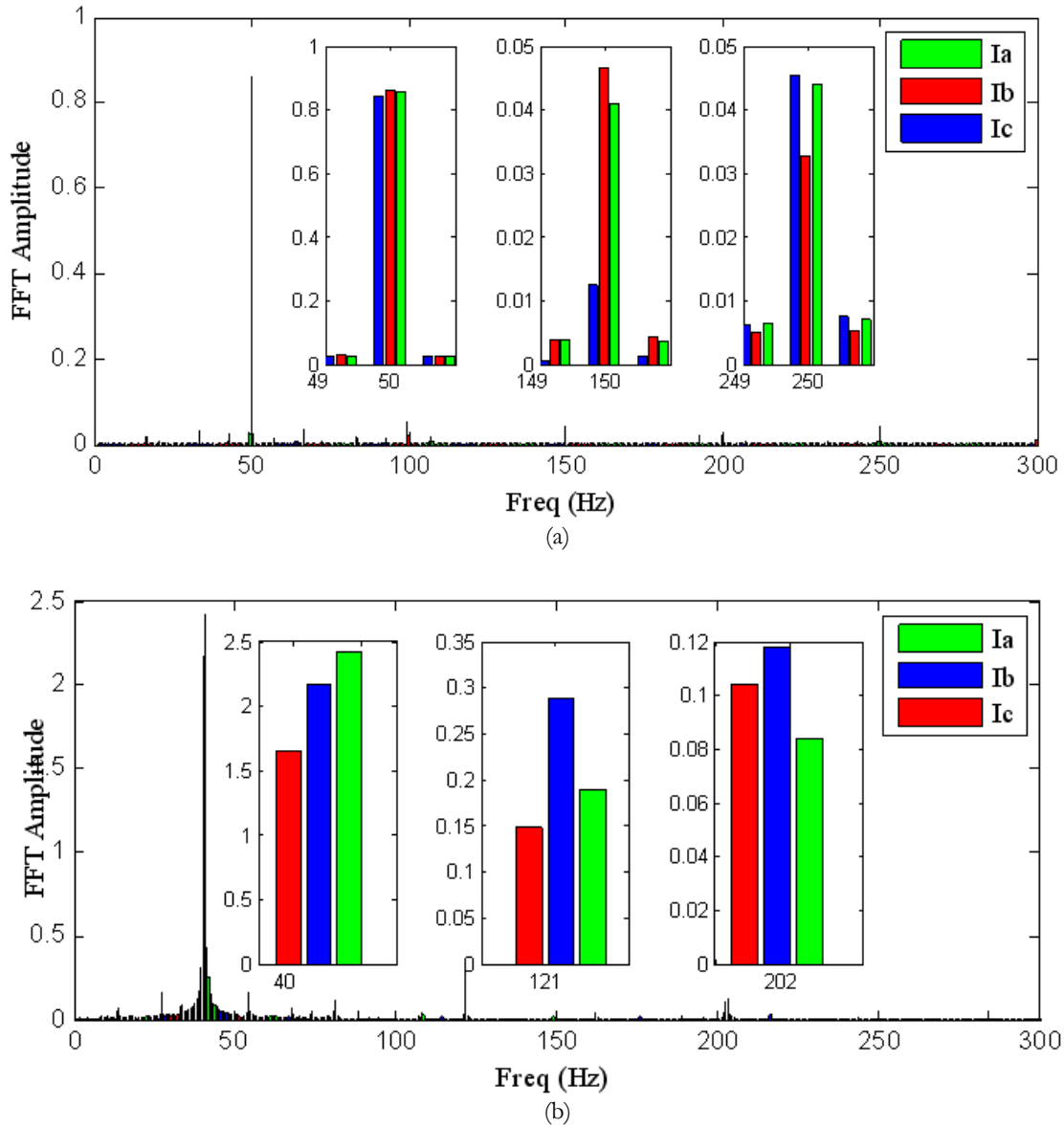


Fig. 3.5 : (a) - FFT analysis of stator current in healthy mode; (b) - Harmonic analysis of stator current in faulty mode

The harmonic analysis of currents (figure (3.5a)) shows that the amplitude of three currents is not same and there also exists a third harmonic which may be due to some dissymmetry in the machine. Thus, several types of short circuit faults were simulated. The Figure (3.5b) shows the stator currents FFT analysis in the case of a single phase inter-turn fault in phase 'a' with 20% turns short circuited at a speed of 1000rpm. It is clear that third harmonic components are stronger than the healthy operating mode.

The above study shows that although third and fifth harmonic component was present in the currents in healthy mode; there is an increase in this component in case of fault. As a first conclusion, this indication can be used for diagnosis purposes. However, it is necessary to find the origin of the 3rd orders in the current harmonic spectra when the machine is in its healthy operating mode. As a first step, the finite element software Flux2D has been used to simulate the real geometry of the studied machine.

In order to investigate the presence of third harmonic component in the stator currents even in healthy mode, the machine was opened and its dimensions were taken to simulate its structure in the Flux2D Finite Element software. A unique feature observed in the structure of studied machine was that one of the teeth has double width compared to others (Figure (3.6)). This dissymmetry may be the cause of third harmonic in the stator currents even in healthy mode.

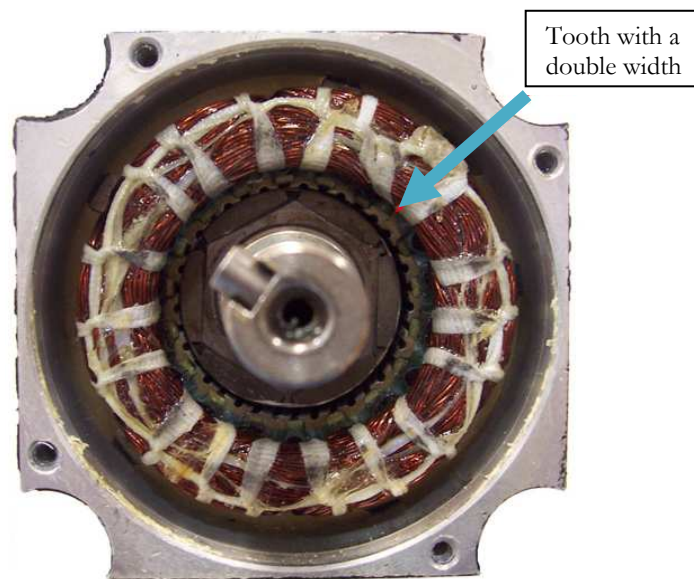


Fig. 3.6 : Cross section of the studied machine with one teeth having double width

The figure (3.7) shows the structure of machine simulated in Flux2D. The stator slots were modified to simulate short circuit fault. The machine was first simulated without fault. Figure (3.8) shows the harmonic analysis of stator currents; clearly there exists a third harmonic component which may be due to the double width tooth.

After analyzing the stator currents in healthy mode, the same short circuit faults were simulated as implemented on the real motor. Figure (3.9) shows FFT analysis of stator currents for the case of single phase inter-turn short circuit in phase 'a' with 20% turns short circuited at a speed of 1000 rpm. It is clear that there is increase in the amplitude of third harmonic component.

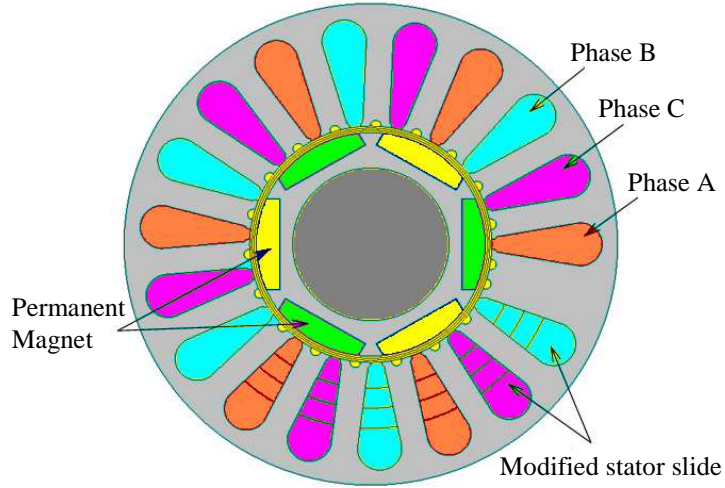


Fig. 3.7 : Geometry of machine drawn in Flux2D

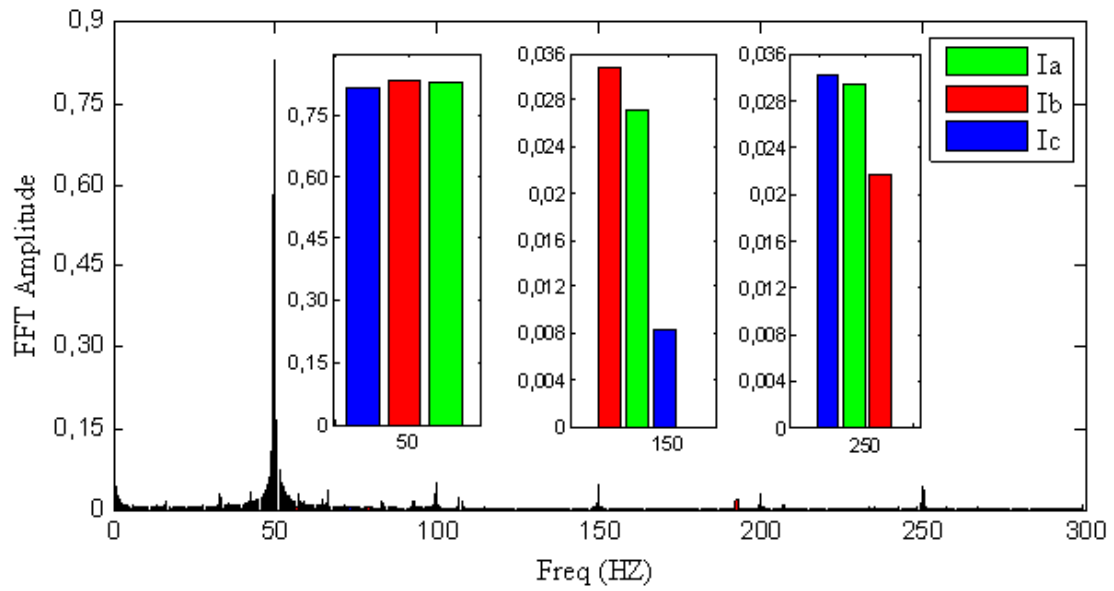


Fig. 3.8 : FFT analysis of stator currents simulated in healthy mode

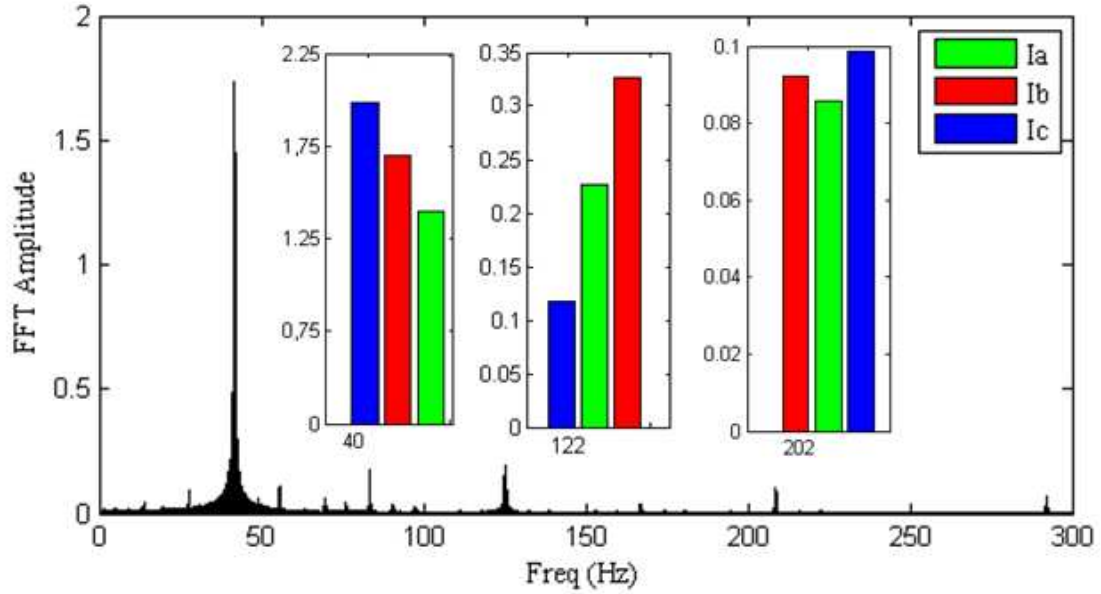


Fig. 3.9 : FFT - analysis of stator currents in case of single phase circuit in phase 'a' with 15% turns short circuited at a speed of 1000 rpm.

Once validated that a short circuit fault (inter-turn or phase to phase) generates a third harmonic component in the stator currents, it was interesting to find the origin of third harmonic component in the stator currents even in the healthy mode. The geometry of the machine was modified with all teeth having equal width as shown in figure (3.10).

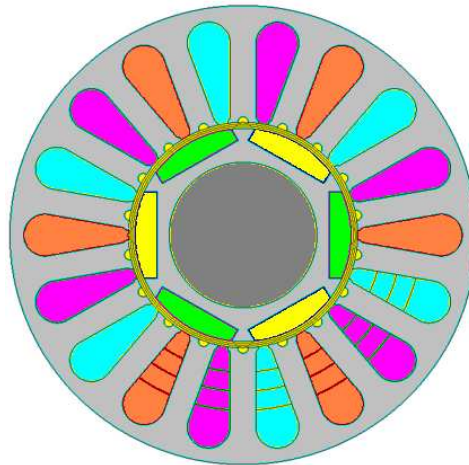


Fig. 3.10 : Modified geometry of the studied PMSM machine “symmetric magnetic circuit”

Simulations of the machine above were carried out in normal mode. Figure (3.11) shows harmonic analysis of stator currents, clearly the third harmonic component vanishes which confirm that its origin was due to the dissymmetry in the stator core.

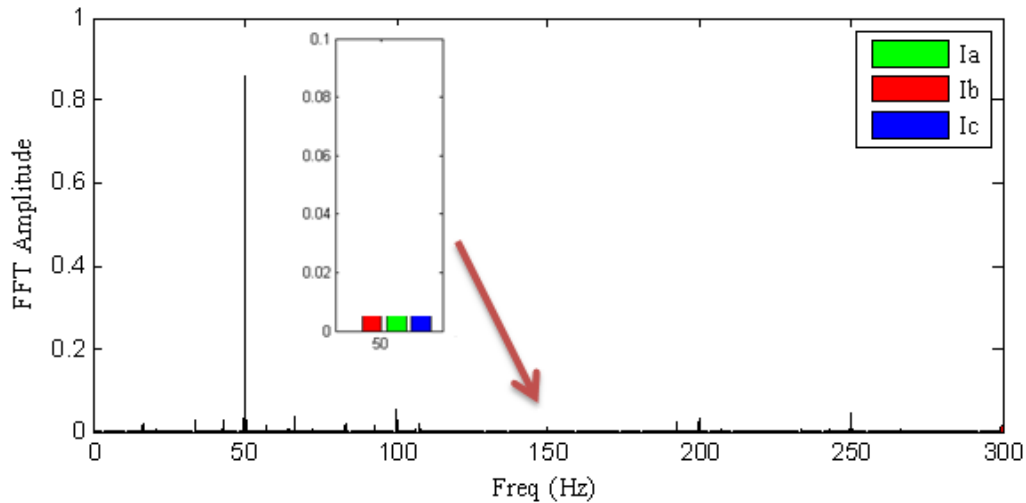


Fig. 3.11 : FFT- analysis of stator currents in healthy mode “symmetric magnetic circuit”

On the basis of these results, it can be concluded that the origin of the presence of a third harmonic in the current spectra, even the machine operates in healthy mode, is due to the presence of a tooth with a double width regarding to the other stator teeth. This geometrical abnormality allows reducing considerably the cogging torque of the machine. However, it should be taken into account in the modeling process of the machine especially when the searched models are dedicated to a diagnosis purposes. This justifies the use of the experimental approach detailed in the next section.

2.2. Experimental approach: faults characterization of PMSM associated to its controller

2.2.1 Set up description

This part presents experimental model that has been established with the objective of model validation. An especially PMSM made to perform these tests and a system of real-time control DSPACE were used. First, a description of the various components of this test bench is presented. The computer program developed to perform this measurement. Finally, the experimental results of several types of short circuits will be added. A focus on the healthy/faulty behaviors is performed.

The figure (3.12) shows the general plan of test bench. The components of this test bench can be classified into two categories: electronic and electromagnetic.



Fig. 3.12 : The general plan of test bench

In electromagnetic part, they consist of the permanent magnets synchronous machine (PMSM), a hysteresis brake and an angular position sensor. The PMSM under study has a conventional structure with an inner rotor and an outer stator. The machine has three pairs of poles placed on the inset surface of the rotor and separated from each other by lamination so, the rotor of the machine is 'magnets inserted'. The magnets are of neodymium-iron-Bor (Nd-Fe-B). In this category the machine along the axis inductance L_q quadrature is slightly larger than that of the direct axis L_d .

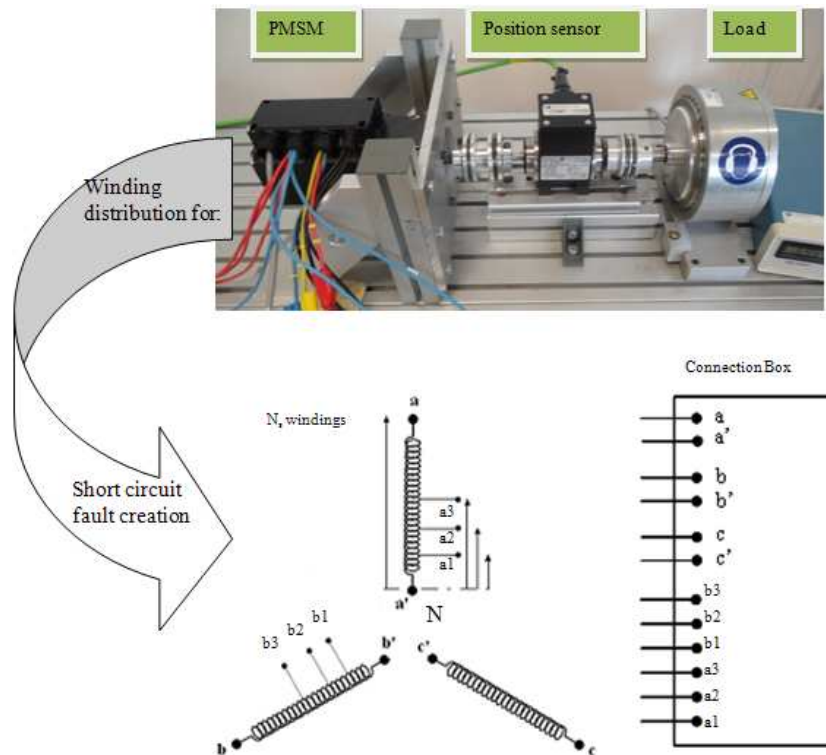


Fig. 3.13 : PMSM motor structure, load situation and stator winding distribution by aiming different short circuit test.

It is close enough to the configuration of the analytical models have been developed that is, MSAP to magnet surface to which the inductors according to the d and q axes are equal ($L_d=L_q$). The stator has 18 slots containing a three-phase winding specially manufactured with access to the coils of phases 'a' and 'b' in order to provide them

achieve partial short circuit. Figure (3.13) shows the motor, its load and the terminal thereof and the equivalent circuit of the magnetic circuit. It is clear that it provides the ability to simulate three types of short-circuit in phase 'a' and 'b'. This allows for the benefit of degrees of freedom for developing an intern-turn short circuit fault diagnosis ANN model.

For angular position and speed measurements the system used an electromagnetic position sensor resolver. It is mounted on the motor shaft and is provided with connections for the supply and the acquisition of the signals issued. In this case a separated cart has been used by helping a 24 V DC power supply to charge it and A/D (analog to digital and position signal acquisition board) as are shown in figure (3.14).

In most training applications based synchronous motors, the rotor position is necessary to achieve precise control. Among the various position sensors, the resolver has very remarkable characteristics in terms of robustness and insensitivity to various disturbances (electromagnetic, mechanical and thermal). Hence it has become very attractive for applications in industrial environments. How the performance of resolver is mentioned in the Appendix 3A completely.

Otherwise the experimental test bench is not yet equipped with an accurate system for measuring the stator currents of the machine. Thus, three current clamps (external Hall Effect current sensors) are used through the analogic inputs of the DSPACE board. The latter is limited in terms of signal acquisition to 1kHz. So this limitation will cause poor current control so poor quality torque and speed control. This aspect is not the aim of the thesis so, we consider the system PMSM and its control device in good health despite the poor quality control.

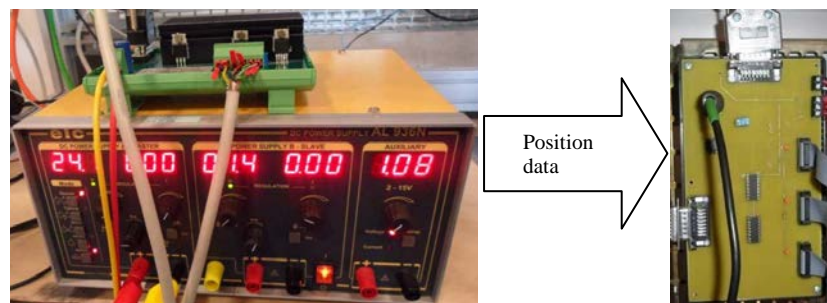


Fig. 3.14 : Angular position measurement

In electronic part, they consist mainly of a three-phase inverter for supplying the PMSM control system and real-time called DSPACE. The system is built around a DSP functioning as Matlab/Simulink ® software and equipped with a driving test called Control-Desk software.

Inverter, as a big and important part of electronic component defines. This is a voltage inverter with the power circuit consists of three power switches arms. There are six IGBT type SEMIKRON SKM-GB123D ordered with drivers SEMIKRON type SKHI22 as shown in figure (3.15).

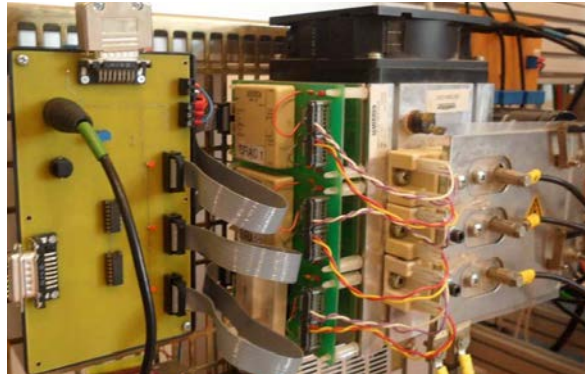


Fig. 3.15 : Inverter and its drivers

Real time Control system: DSPACE is widely used in modern electrical control systems R&D, Indeed, DSPACE hardware and software provide an opportunity to share development much easier and faster and allows the realization of monitoring functions in addition to the conventional control.

DSPACE is a complete real-time control system based on DSP kind of MPC8240. The control card is used types of DS1104 with the inputs/outputs and analog digital as shown in figure (3.16) (see Appendix 3B for more details on its technical characteristics). The main DSP platform can be programmed directly by using the Matlab/Simulink ® software. This program was first built in Simulink using the basic functions of 'drag and drop' and the specific blocks DSPACE system available in the Toolbox Simulink. After simulation features popular program developed, just a simple 'click' for implantation in the DSP. It will use the application control test, developed with ControlDesk software to monitor the experiment. The system also offers the option to access the various measurements, modify different online program parameters such as gains regulators, and save different magnitudes.



Fig. 3.16 : DSPASE 1104

2.2.2 Software program of the PMSM vector control

In order to overcome the inherent coupling effect and the sluggish response of scalar control the vector control is generally employed to drive the PMSM in automotive applications. By using the vector control, the performance of the AC machines can be made similar to that of a DC machine in terms of drivability, robustness and accuracy the figure (3.17) shows the bloc diagram implemented into the DSPACE device to control the PMSM under tests.

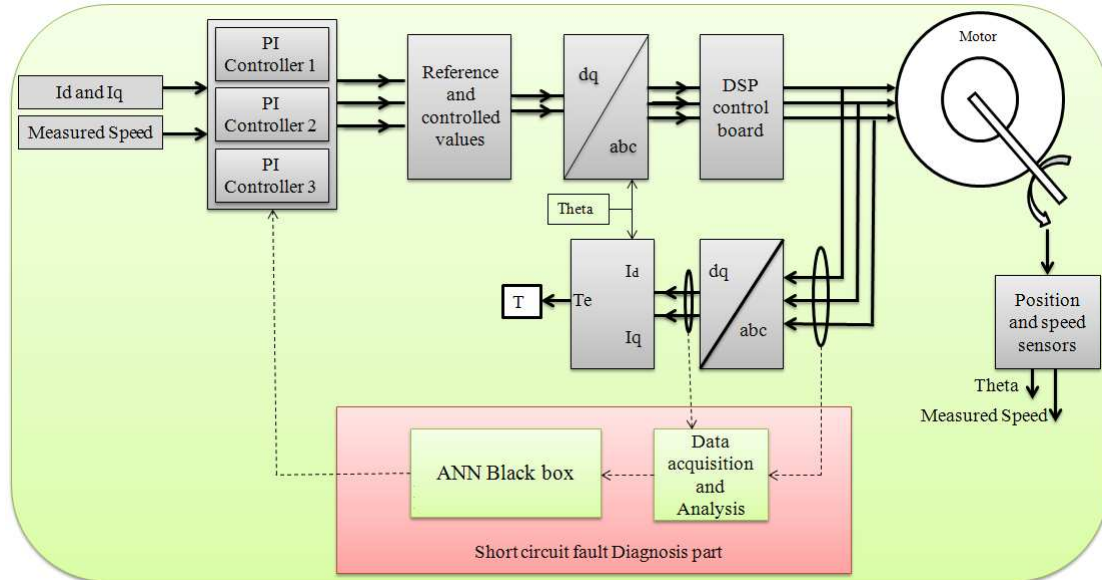


Fig. 3.17 : Model of identification and diagnosis of inter turn fault of the vector controlled PMSM

In this diagram, we used three PI controllers. In this case, even in fault state we will be able to control of system, however with some limitations. Also it lets us to achieve auto tuning of the K_p and K_i coefficients in experimental tests by using DSP board. In this case, the values of K_p and K_i and also “theta” defened variable and with connection of DSP, the system adjusts them according to feedback of position of rotor and motor currents.

This method of control provides us a possibility of doing different expected tests according to HEV application. It means inter turn short circuit fault have been done in different speed, load and severity of short circuited turns. In this case, it will be suited to do required tests to train our ANN.

Figure (3.18) shows the control tests window, it is displayed when the program developed under Control-Desk. It has a display function of variables (speed, position, current, voltage ...), the recording of these parameters and tool setting interface speed references, current.

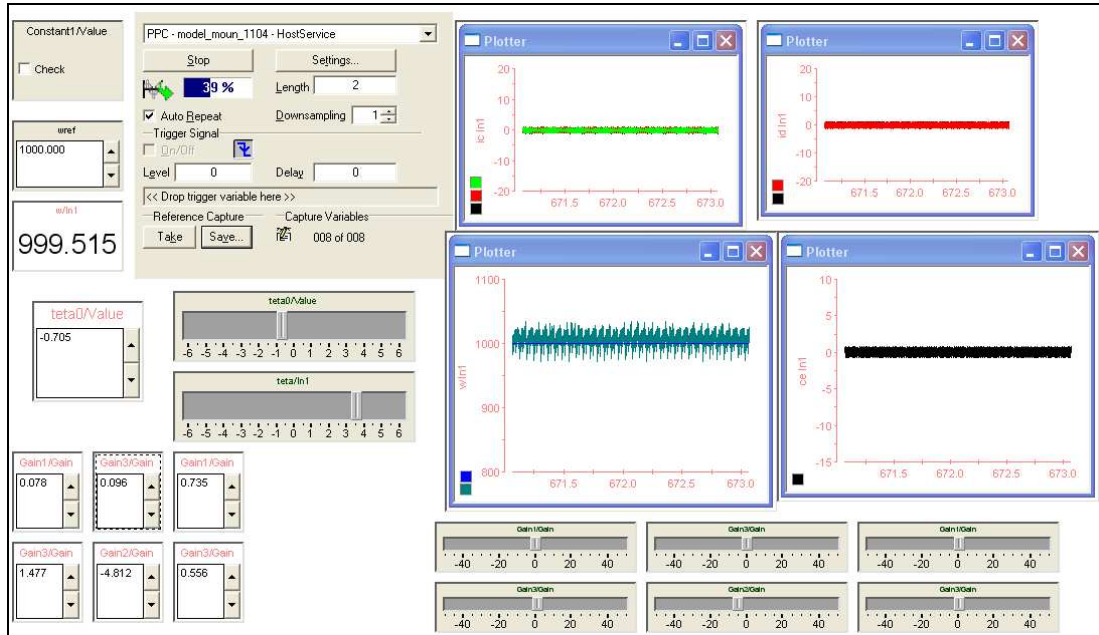


Fig. 3.18 : Computer interface for managing the experimental tests

Firstly motor behaviors (currents, speed and torque) in healthy operation mode in different speeds and load are presented. Then, different types of short circuit have been experimented. In continue the comparison between healthy and faulty mode have been done. Finally, the Fast Fourier Transform (FFT) has been used for fault characterization between healthy and faulty modes of the vector controlled PMSM.

This control diagram is used to ensure the speed control of the PMSM under test notably while doing faulty measurements. To check the setting of PI controllers, several tests were conducted at several speed references. The figure (3.19) and (3.20) show two examples of these tests. The figure (3.19) illustrates the steady state of that speed control at 1000rpm while the figure (3.20) shows the transient characteristic of the speed when a change in the reference seed from 1000rpm to 900rpm. We notice the existence of oscillations on the measured speed of about 4% according to the reference. As mentioned above, this is mainly due to the quite bad measurement of stator currents. So, this operating mode is considered a “healthy one” despite the quite poor quality of control.

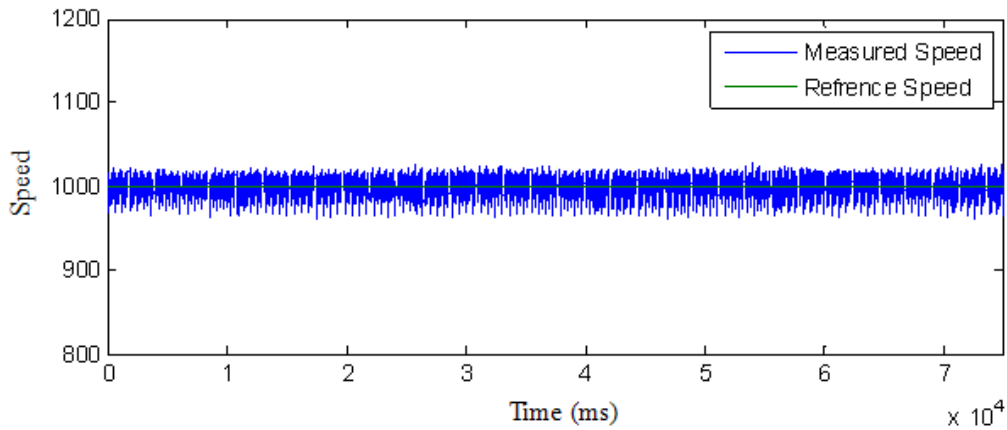


Fig. 3.19 : Motor speed under health operation

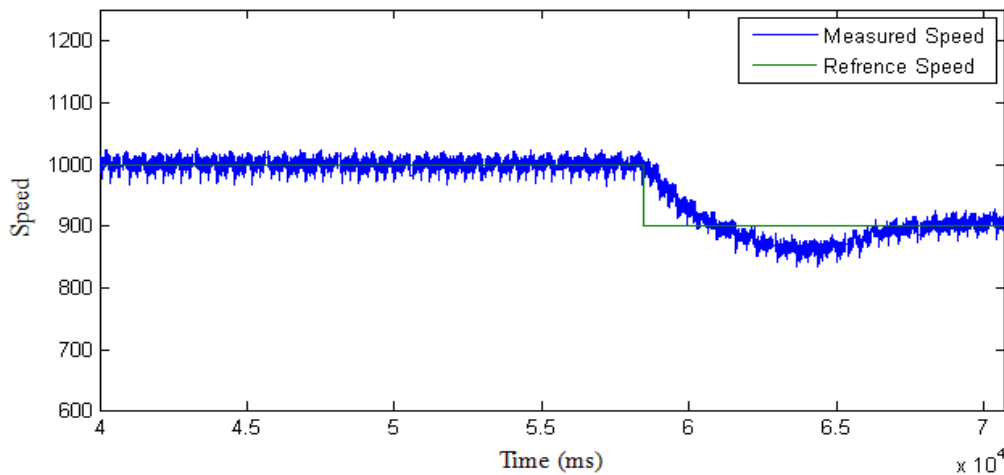


Fig. 3.20 : The measured speed changes based on reference speed changes by helping vector control regulation of 1000 rpm to 900 rpm

2.2.3 Healthy mode: constant speed - unloaded motor

In this section the motor under study is controlled without load; the motor reference and measured angular speed are the same presented in figure (3.19). We notice that the measured speed follows the reference but with a presence of oscillations which are due to the fact that bed quality of speed measurements and not to a fault in the drive system.

Three phase motor currents waveforms and the corresponding FFT spectrum in the case of healthy operating mode at 1000rpm are respectively shown in figures (3.21) and (3.22). Note the presence of high level oscillations on measured currents. This is due to the poor quality of current measurement (lack of precision current sensors and poor performance of the acquisition of these measures). The higher magnitude concerns that of the fundamental having a frequency of 50 Hz. Also, we notice the presence of harmonics at 100Hz, 150Hz and 200Hz. The 3rd harmonic order (150Hz) is due to the natural geometrical abnormality detailed above while the 2nd and 4th harmonics (respectively 100Hz and 200Hz) are due to the bad behaviors of the controller device. No matter, we consider this state as the state of the machine saint. This is the main advantage of the experimental approach does not require a priori knowledge of the system.

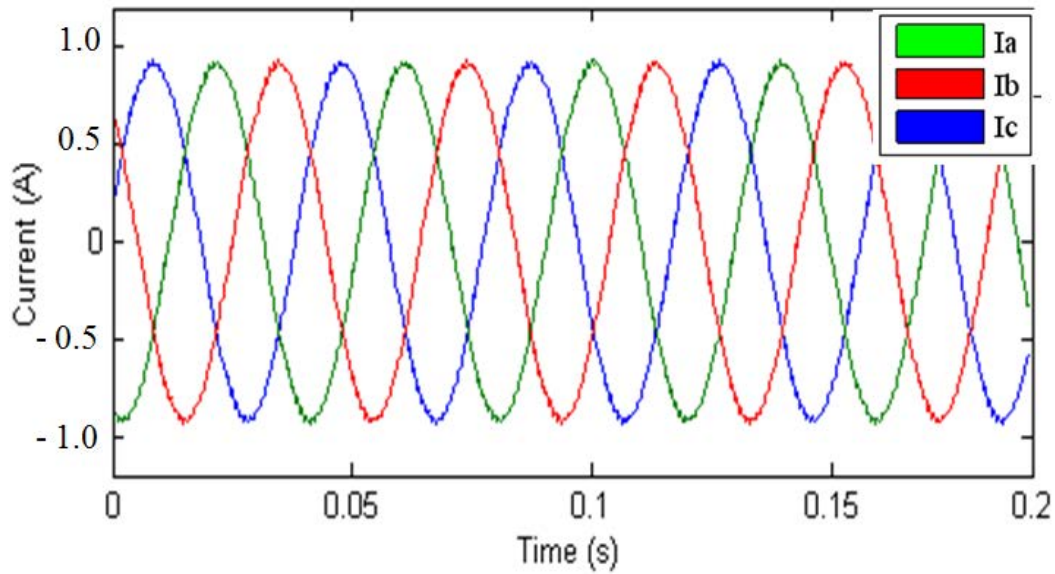


Fig. 3.21 : Motor 3 phase currents under healthy operation

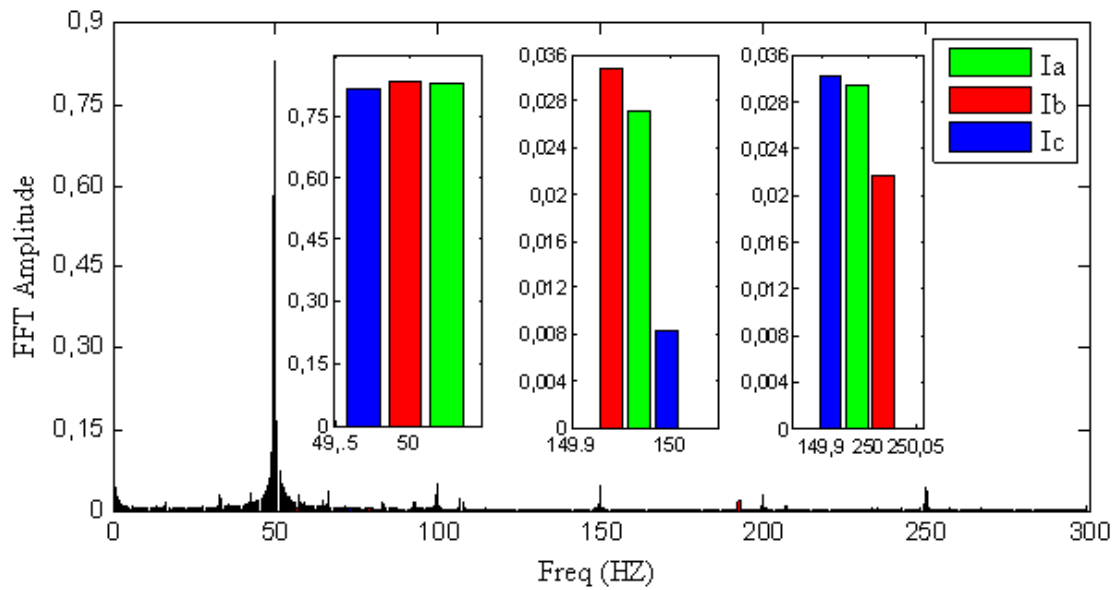


Fig. 3.22 : FFT analysis of motor 3 phases currents under healthy operation.

2.2.4 Healthy mode: constant speed – loaded motor

Now we consider load changes and its influence on motor current features for a half load condition in both healthy and faulty operations. It must pay attention that; short circuit fault in full load condition may have an irreparable result on motor parameters. However the fault diagnosis is more helpful in load conditions because it is the state where the machine operates most of time. In this case, figure (3.23) show motor 3 phase currents FFT analysis. The same remarks as below are observed (i.e. higher magnitude of the fundamental and presence of harmonics fundamental, 3th and 5th). The difference compared to the case without load treated previously is observed at the increasing of

values of these harmonics: 1st harmonics increases from 0.8 to 1.5, 3rd harmonic increases from 0.03 to 0.08; the 5th harmonics from 0.03 to 0.07.

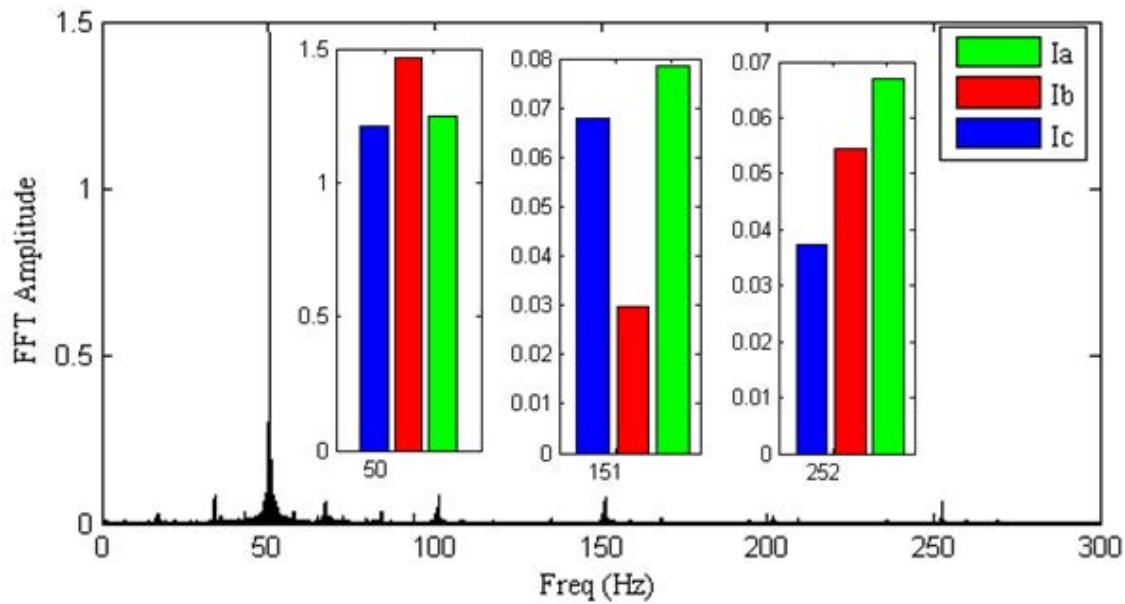


Fig. 3.23 : FFT analysis of motor 3 phases currents under half load health operation

2.2.5 Faulty mode: Influence of the short circuit fault on motor currents

In this section, different levels of short circuit fault tests have been performed. The experimental setup shown in figure (3.12) offers the possibility of 18 different levels of short circuit fault by access to 3 separated connection in each of the phases “A” and “B”. In this section, the PMSM is mechanically loaded at the half of its nominal torque and controlled under a constant speed of 1000rpm. Both the healthy and faulty operating modes are considered in this test.

As it is shown in figure (3.24a), a double phase inter turn short circuit (25% on phase B) is introduced after 5.8s of simulation time. This defect introduced an increase in the amplitude of the current but also a deep change in their angular phase (see figure (3.24b)). This causes an internal unbalance in motor windings and a high amplitude of currents flowing in short circuited turns. Angular phase replacement introduce as a new feature of short circuit fault that help us to fault localization.

Consider that a short circuit fault occurred in phase B as it is shown in figure (3.24a). If θ_{Ia} , θ_{Ib} , θ_{Ic} be angular phase deviation of currents of phase A and phase B and phase C in order to reference values, respectively, because of a short circuit in phase B, in this base the most angular phase changes will be happened in phase C. why? Because as it is shown in figure (3.24b) the first phase that senses this short circuit fault is phase C according to motor magnetic flux rotation. It means $\theta_{Ic} > \theta_{Ia}, \theta_{Ib}$. This feature can be used for fault location detection. The methodology of work has been introduced in the same work titled impedance angle of stator windings changes applied to short circuit fault detection completely [6], [7]. The on line impedance evaluation is a complex process

so we avoid to use directly this parameter to train our ANN. To take into account this feature this feature the currents I_d and I_q has been added to the ANN model training.

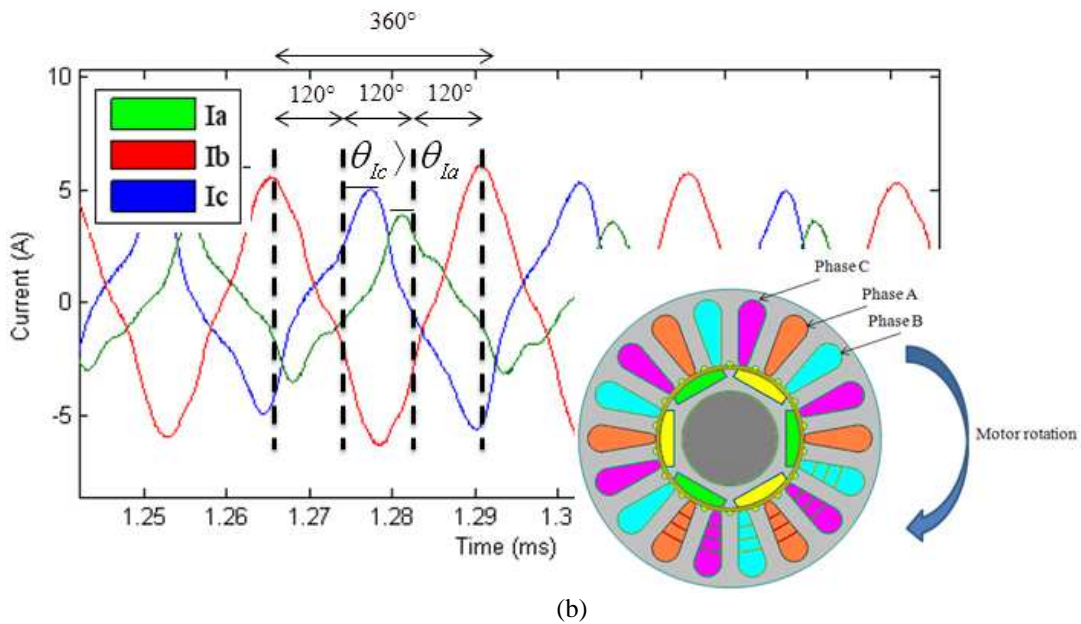
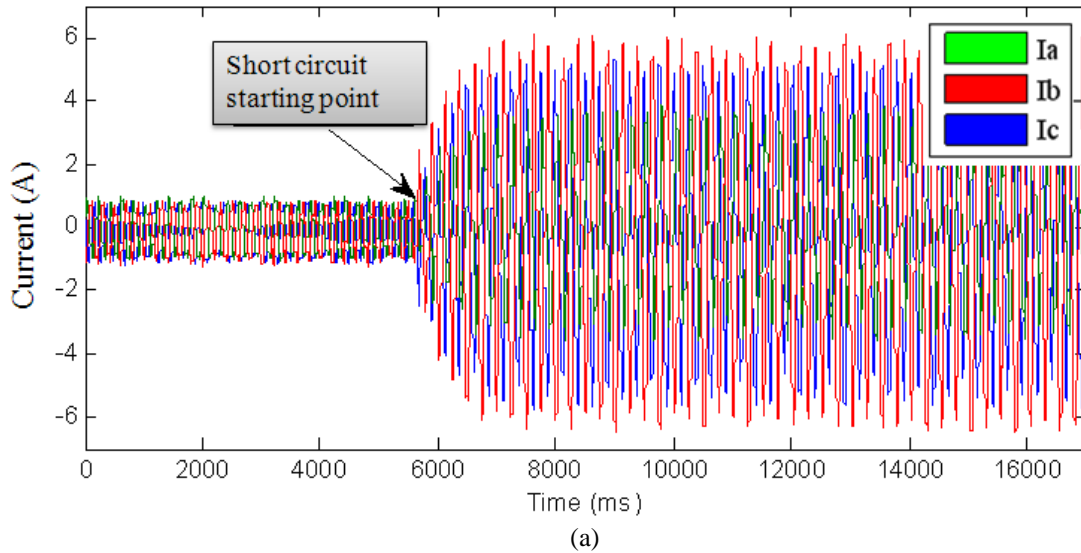


Fig. 3.24 : (a)- Three PMSM stator currents in healthy and short circuit fault conditions (25% short circuit fault on phase A); (b)-Zoom on the same three PMSM stator currents

These shapes of the currents show that there is no current regulation. This means the short circuit disabled the current control loop (inner loop). The speed control loop is also affected so that the rotor angular speed decreased to around 800rpm.

The FFF analysis of these currents under faulty conditions, lead to the results illustrated on the figure (3.25). It is clearly shown a clear increase of the fundamental and harmonics values. The fundamental frequency is changed to around 40Hz which confirm the speed decrease. We still find the presence of the 3rd harmonic at 120Hz. Otherwise; we notice an appearance of one 5th harmonic at 200Hz.

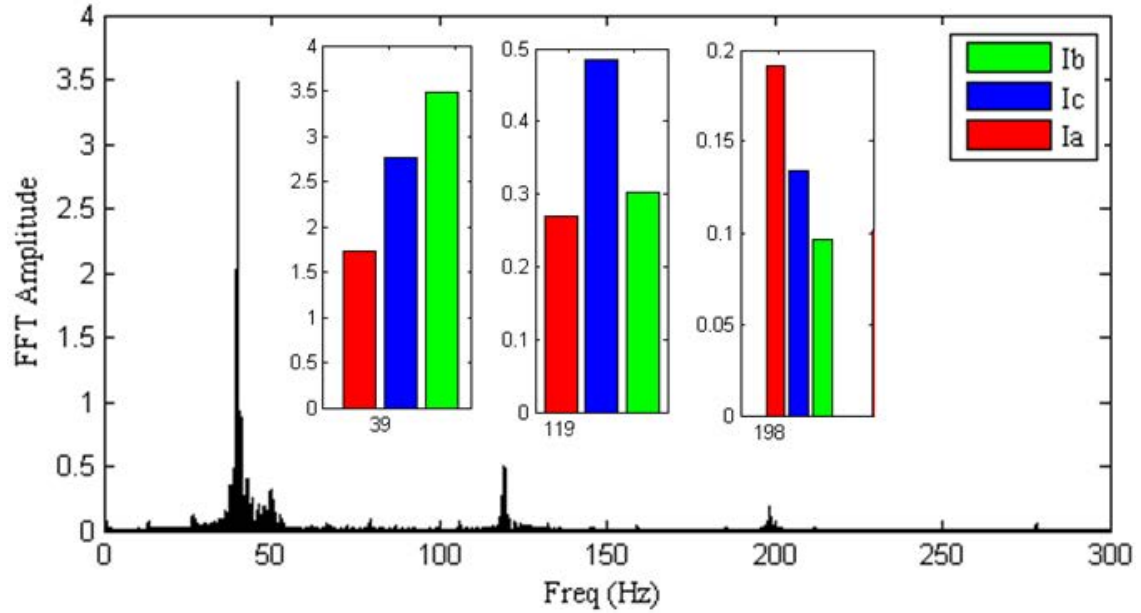
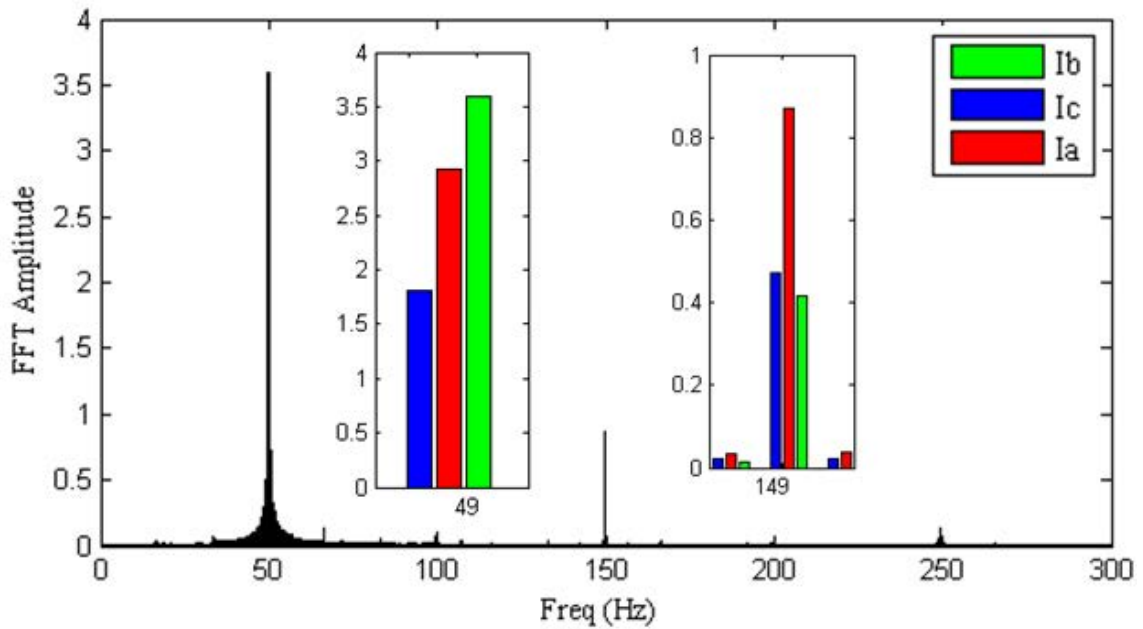


Fig. 3.25 : FFT analysis of motor 3 phases currents under 25% short circuit fault operation in phase B.



(a)

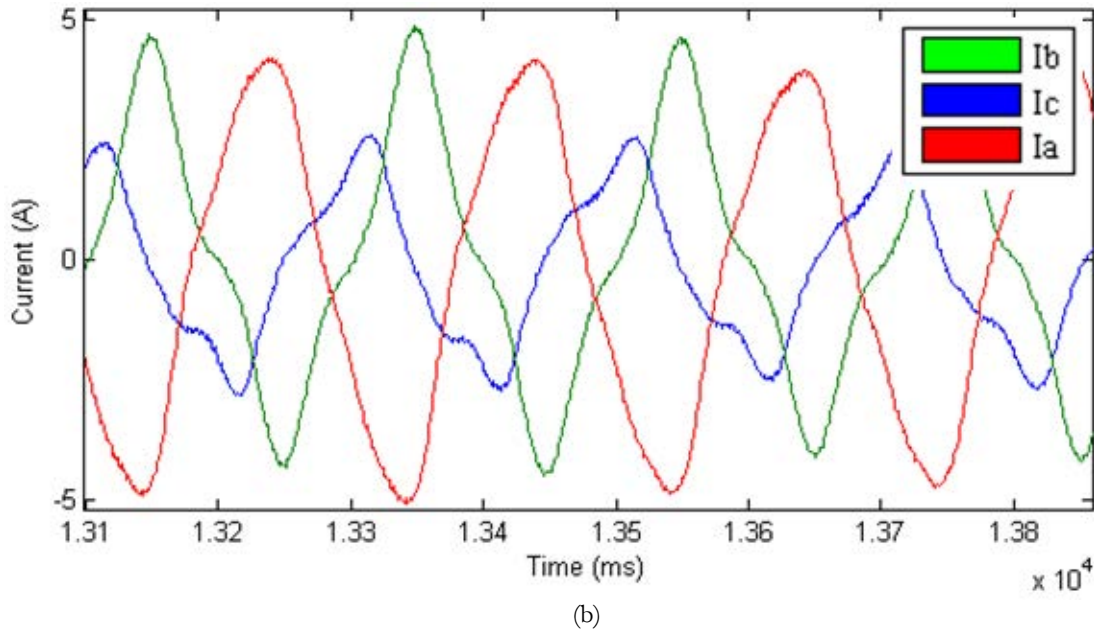


Fig. 3.26 : FFT analysis of motor 3 phases currents under 25% short circuit fault operation in phase B by speed fixed in 1000rpm. (b)-Zoom on the same three PMSM stator currents

The vector control used in this work let us to increase the speed in 1000rpm, even after short circuit. We have done this test to ensure about fault feature under speed decreases by normal vector control application. Figure (3.26a) and (3.26b) show the FFT analysis of the same short circuit severity (25%) presented in figure (3.25), by fixed speed in 1000rpm. Also the angular phase change will have the same feature as figure (3.24.b). The highlight point in this change, increase of 3th harmonic against operation in normal speed (800rpm), that is not our favorite.

The Park currents presented on the figure (3.27) show also a clear impact of the short circuit. The FFT analysis of these two magnitudes allows characterizing quite well the short circuit severity (see figure (3.28)). The latter can be evaluated through two main parameters the value of fundamental (H1) and the harmonic distortion rate (THD). For more diagnosis accuracy, the harmonics amplitudes and phases until the 5th order can be used for characterizing the signatures of the short circuit in terms of type (which windings are concerned?) and severity (which percentage of winding is in defect?).

The experimental results of this work and also ref [6] show a proper feature of short circuit in currents I_d and I_q . As it is shown in figure (3.28a) and (3.28b), the short circuit fault have an effect on 2th harmonic of currents I_d and I_q . This feature helps us to an accurate and enough data for training ANN aiming to short circuit fault diagnosis and classification. The changes of the I_d and I_q currents amplitudes inform us about the phases changes following each fault.

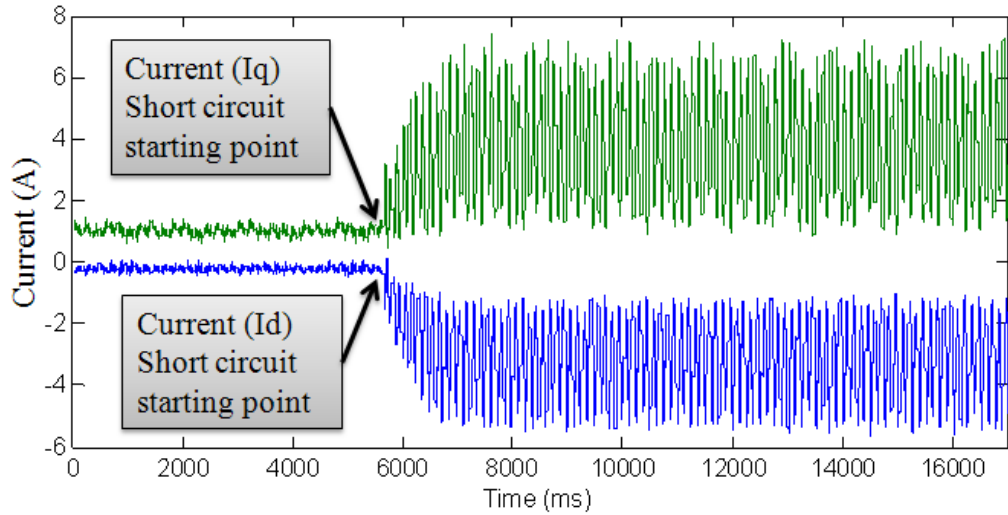


Fig. 3.27 : Currents I_d and I_q under faulty operation.

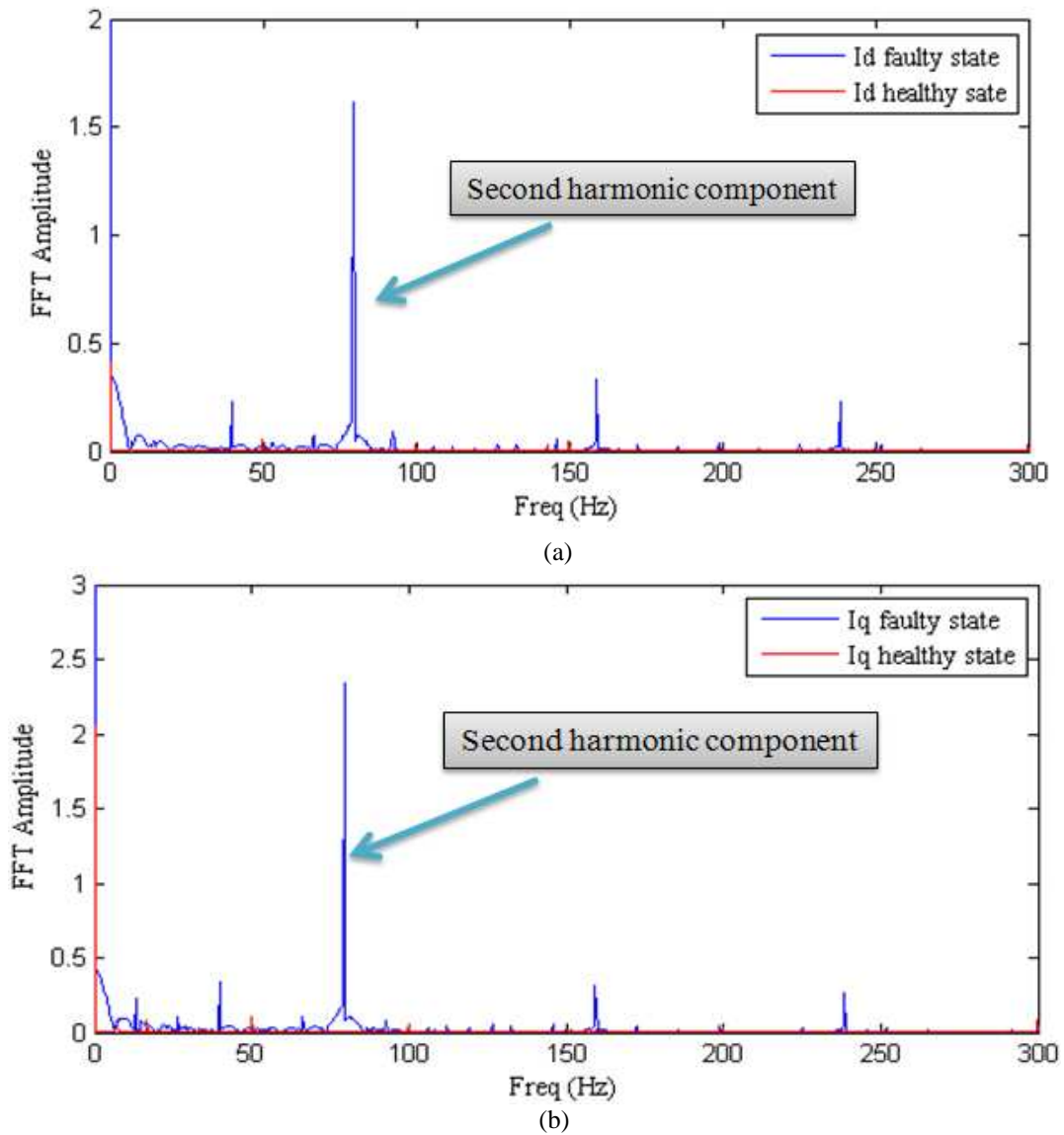


Fig. 3.28 : FFT analysis under healthy and faulty operation (a)- Motor I_d currents; (b)- Motor I_q current

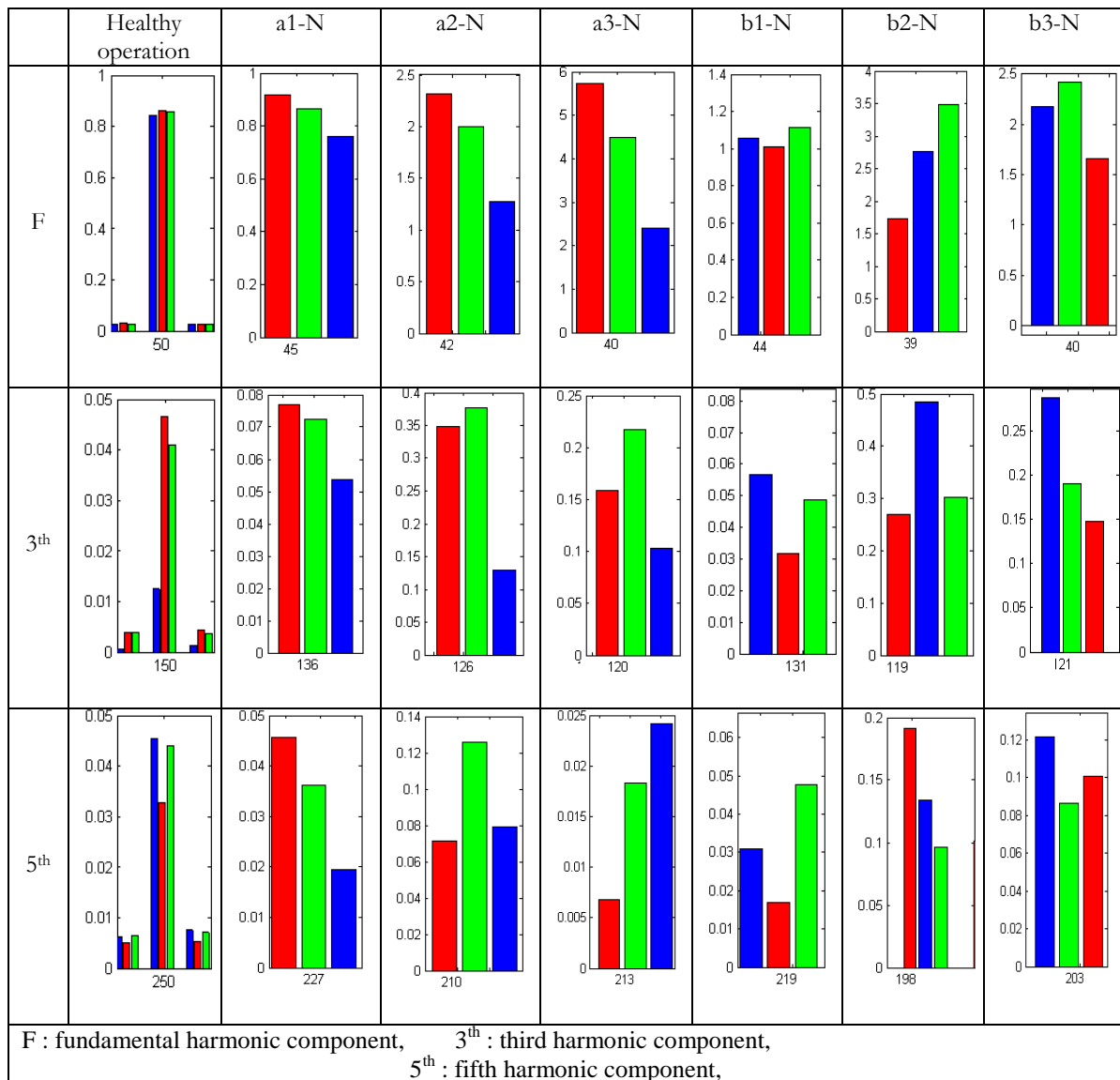
2.2.6 Motor behaviors under different inter-turn short circuits faults: variable speed operating

The experimental set up allows performing different levels of short circuits by the mean of 3 different connectors in the PMSM phases A and B. Table (3.1) shows all the short-circuits done in experimental tests.

Table 3.1 : Possibility of experimental short circuit faults efforts according introduced connection in figure (3.13).

Type of fault	a1-N	a2-N	a3-N	b1-N	b2-N	b3-N	a1a2	a1a3	a2a3	b1b2	b1b3	b2b3
Fault percentage	2%	25%	35%	3%	30%	22%	6%	20%	5%	15%	18%	4%

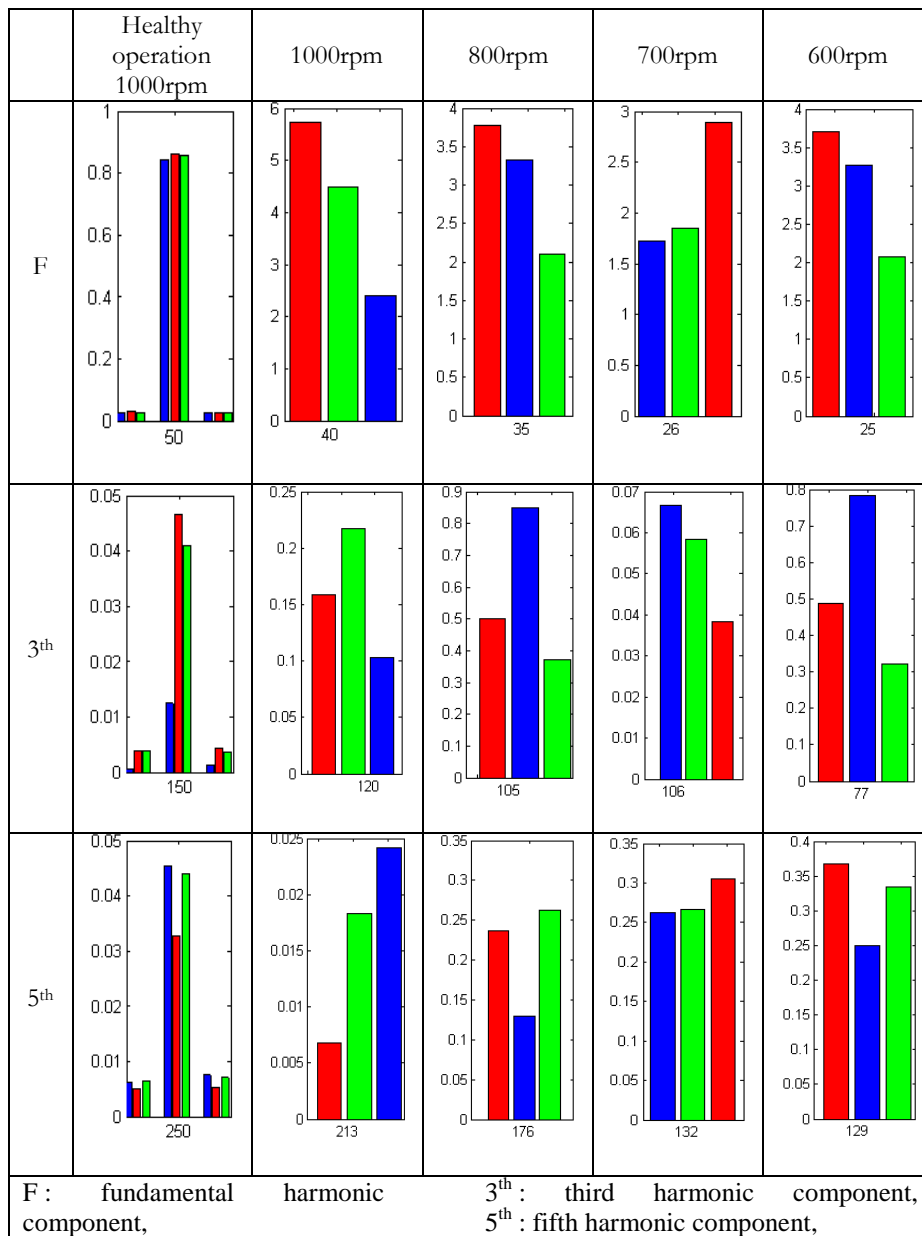
Table 3.2 : 3 phase motor current FFT analysis under different severity of short circuit fault noted in table (3.1).



The table (3.2) shows the changes of FFT analysis (and their effects on motor speed changes) on motor three phase current for fault states of short circuits a1-N (short circuit between connection point a1 and Null), a2-N, a3-N, b1-N, b2-N and b3-N respectively.

According to our objective to diagnosis of short circuit fault in several different cases of faults, the short circuit fault in a3-N case has been considered in 5 different rotor speeds. Table (3.3) shows the FFT analysis of 3 phase motor current under short circuit in a3-N case and speeds 1000 rpm, 800 rpm, 700 rpm and 600 rpm.

Table 3.3: 3 phase motor current FFT analyses in different speeds under short circuit fault a2-N case.



2.3. Diagnosis algorithm of PMSM short circuit faults

Figure (3.29) presents the synoptic scheme of the proposed algorithm for the PMSM diagnosis processing under inter turn short circuit. According to HEV application, the load and speed variations shall to be considered in all the different types and severity of possible faults. This will lead to make complete and accurate diagnosis based ANN model which will be discussed more in details in chapter 5.

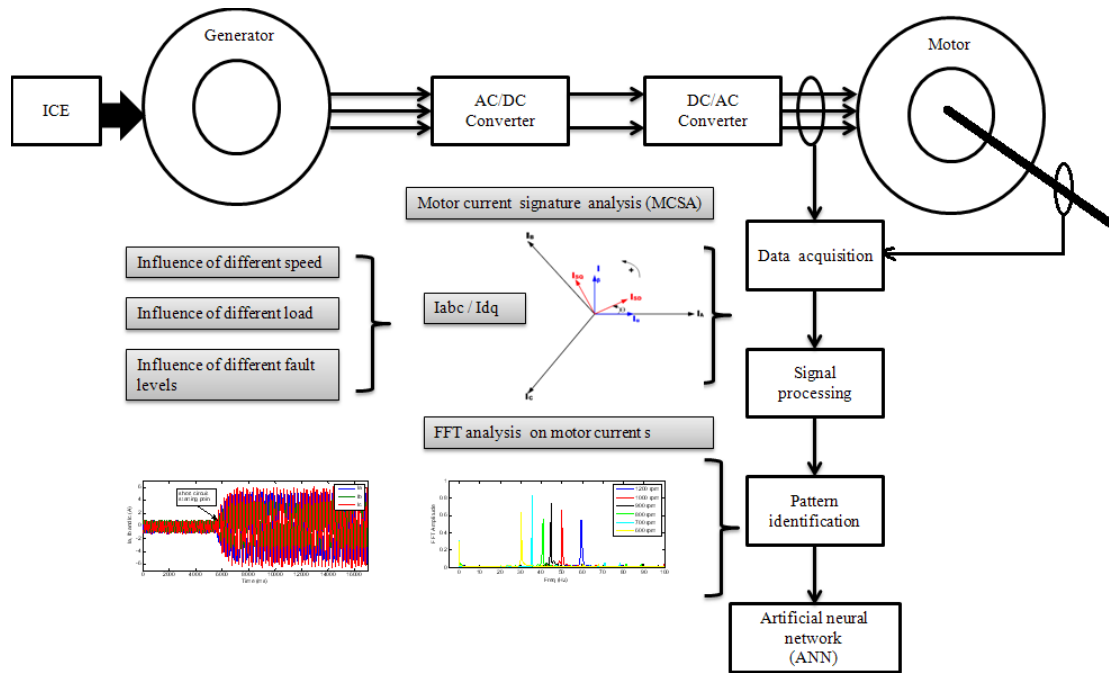


Fig. 3.29 : Fault diagnosis strategy of PMSM inter turn short circuits for SHEV application

3. Demagnetization fault

Irreversible demagnetization of the magnets found among the most important rotor faults in permanent magnet synchronous machines (PMSM) [8], [9-11]. Indeed, once this fault occurred can affect the overall performance of the machine. In addition, existence of a lack in the literature in relation to study of this particular fault is evident. Thus, this part of work is mainly directed towards the development of studies in this area.

3.1. Theoretical approach

Numbers of modeling approaches for permanent magnet machines are reported in the literature to calculate the magnetic field in the gap. Some most famous of these are: the analytical solution of Laplace equation in polar coordinates and the method of network permeability/reluctance [4]. In this chapter we discuss one analytical model of demagnetization in ISPMMSM and its validation thanks to finite element simulations under FLUX 2D software.

A defect of a magnet may occur due to armature reaction or the appearance of a crack. This means that the absence of a magnet can be classified as a type of defect that is uniformly distributed over its entire surface, or located at a specific zone of the pole. To

take into account this non-uniformity in the analytical model, the magnet is considered to be composed of small elements as shown in figure (3.35).

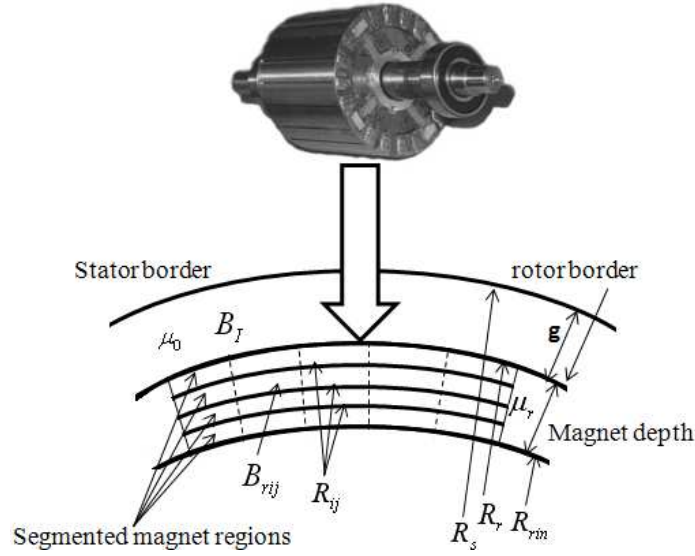


Fig. 3.30 : Geometry of the electromagnetic problem

Where B_f is air-gap flux density, B_{rij} is magnet remnant induction of the magnet element with suffix (i,j) indicating its position in a magnet pole, μ_0 is the air-gap permeability, μ_r is the relative permeability, R_s is length of stator border to center of motor, R_r is length of rotor external border to center of motor, R_{rin} length of rotor internal border to center of motor, R_{ij} is length of each rotor magnet segments border to center of motor and g length of the air gap. In this case, magnet depth = $R_r - R_{rin}$.

This representation has been notably deeply used in [4] where two theoretical models have been developed: an analytical model and a permeance network model which is generally called “semi-analytical” model. In the present thesis the analytical model was used to simulate the effects of different kinds of demagnetization (symmetrical or unsymmetrical ones) on the back EMF of the PMSM. Such model is based on the Maxwell equations resolutions through the vector potential formulation.

The obtained expression is as following:

$$e(t) = -N_s \frac{\partial \phi}{\partial t} = -N_s \frac{\partial \theta}{\partial t} \frac{\partial \phi}{\partial \theta} = -N_s \Omega \frac{\partial \phi}{\partial \theta} \quad (3.18)$$

Where N_s is the turns number one phase coil, Ω is the angular velocity of the rotor of the machine and ϕ is the magnetic flux is given by:

$$\phi(\theta) = \int_{\alpha}^{\alpha+\alpha_{cp}} B_f^r(r, \theta) d\theta \quad (3.19)$$

Where α_{cp} is the coil pitch, $B_j^r(r, \theta)$ is the total flux density in the air-gap produced by the contributions of 25 elements of the magnet. The appendix 3C expose the main steps followed to establish the expression of $B_j^r(r, \theta)$.

3.2. FEM fault simulation with FLUX-2D software

The use of FEM in demagnetization fault modeling offers the following main possibilities considered as advantages regarding to the analytical models:

- Taking into account the slots effects and the non-linearity such as the saturation of the iron steel.
- Simulating the whole 2D structure of the PMSM which allows considering a lot of cases of demagnetization faults symmetrical as well as non-symmetrical.
- High accuracy of computation.

Otherwise the principal drawback of the FEM consists in the high time consuming in the development phase as well as in the exploitation phase (running the simulation program).

In this section we briefly present the developed FEM simulation model and some results for validating the analytical model. The appendix 3D is added at the end of the report to explain the main steps followed to establish this model. The same PMSM presented in the section §3.1 has been considered for this study so that to continue our developments in the focus of a complete diagnosis of this machine. Despite the fact that the developed model has not been used for training an ANN model, the strategy of its future use will be also exposed.

3.2.1 FEM simulation results: health and demagnetized PMSM

In figure (3.31), one see the magnetic field lines distribution across the three pairs of poles (6 magnets), the 18 tooth and the air gape of the developed FEM model.

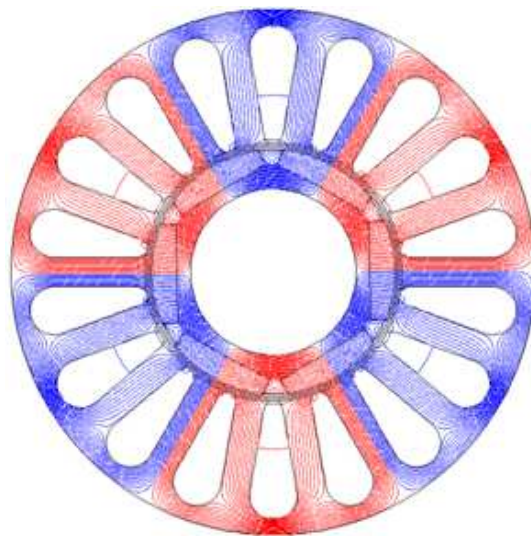


Fig. 3.31 : Cross section of the simulated PMSM geometry and the corresponding field distribution

Electromagnetic phenomena affecting of the behavior of the machine (B, flow ...) prove mainly at the air-gap. Figure (3.32a) and (32.b) shows the magnetic flux density (B) and its FFT analysis under healthy operating mode respectively (without demagnetization faults).

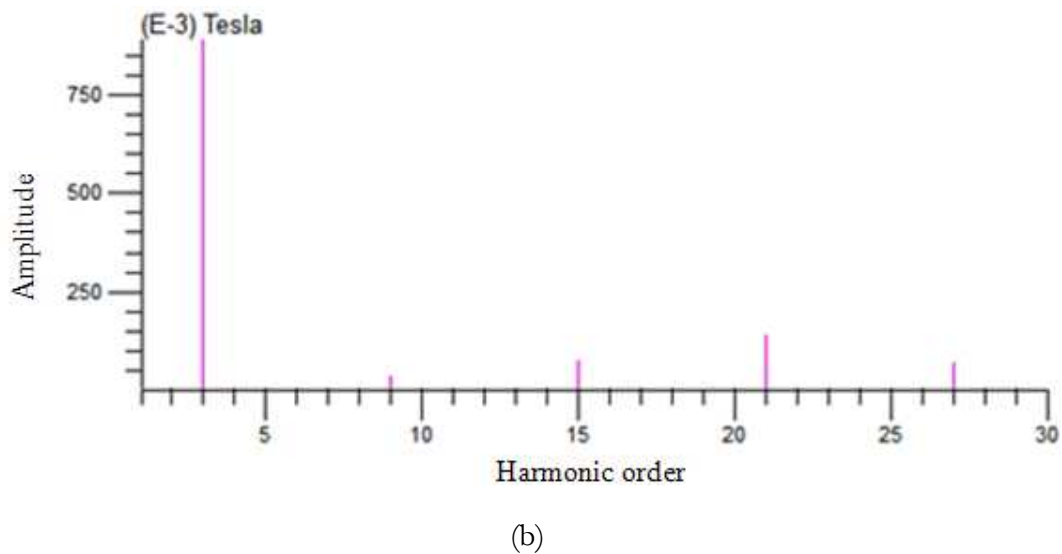
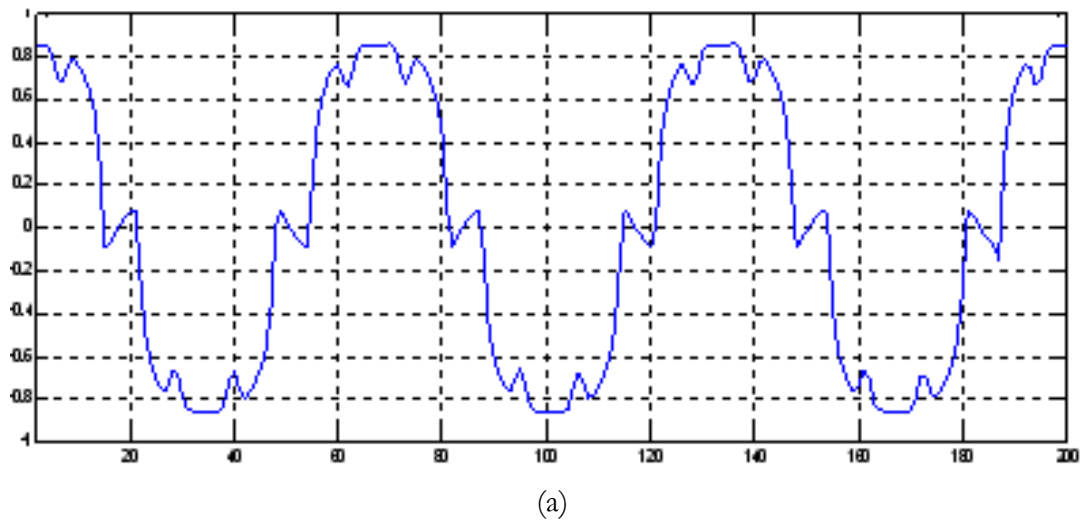


Fig. 3.32 : (a) Magnetic flux density (B) FFT analysis of flux density in health case of PMSM

Now, we show how the developed model can be used to study the demagnetization faults in PMSM. For this purpose, three different demagnetization faults are simulated: symmetric and partial and complete asymmetric magnet demagnetizations. The figures (3.33a), (3.33b) and (3.33.c) show respectively the 6 poles of the PMSM studied under symmetric demagnetization.

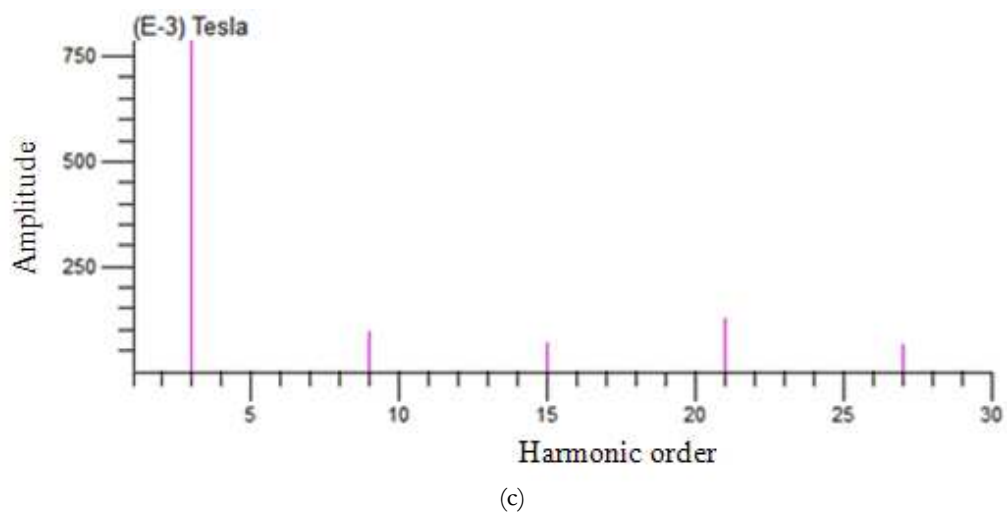
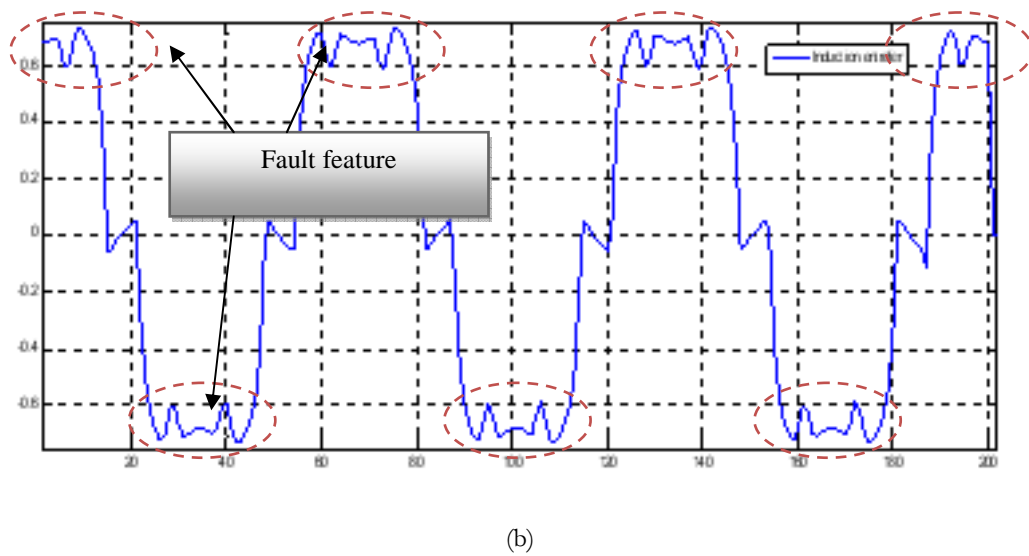
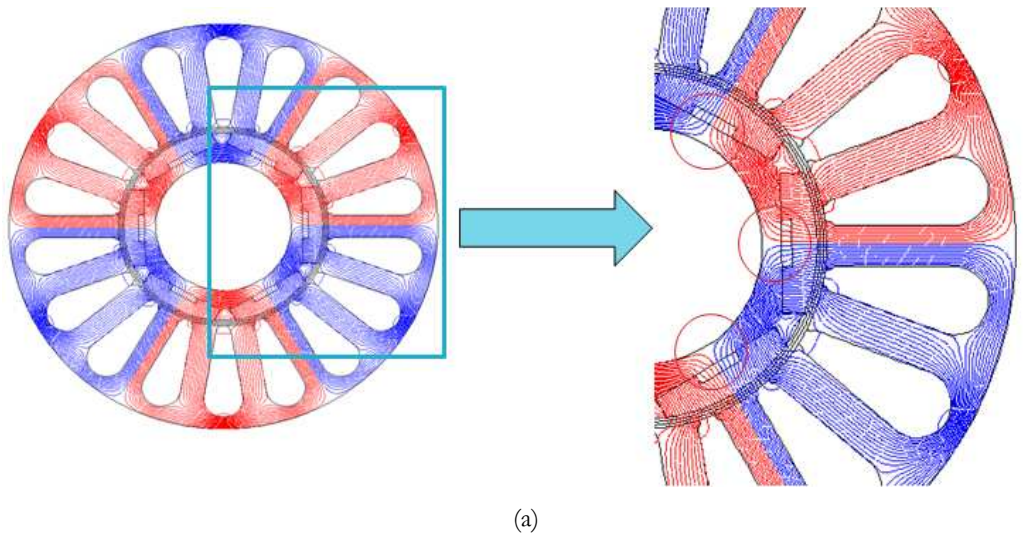
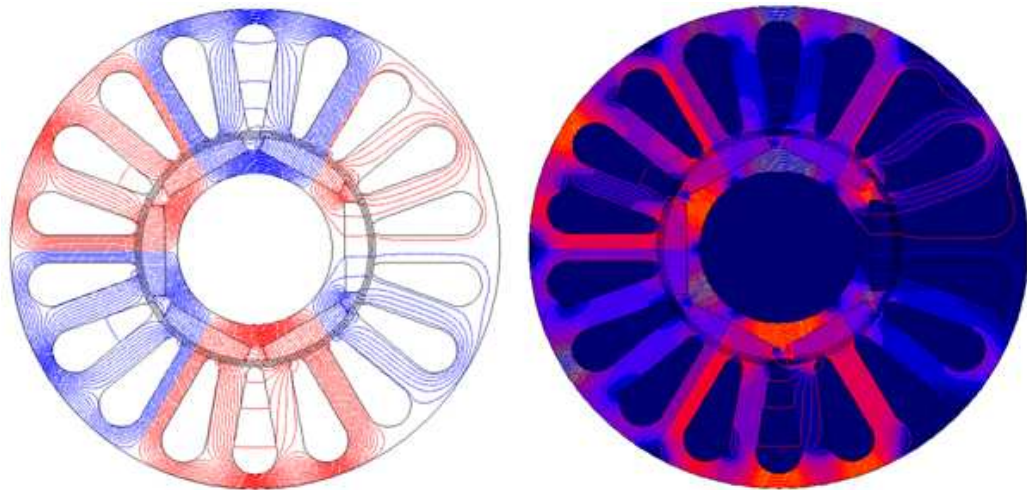
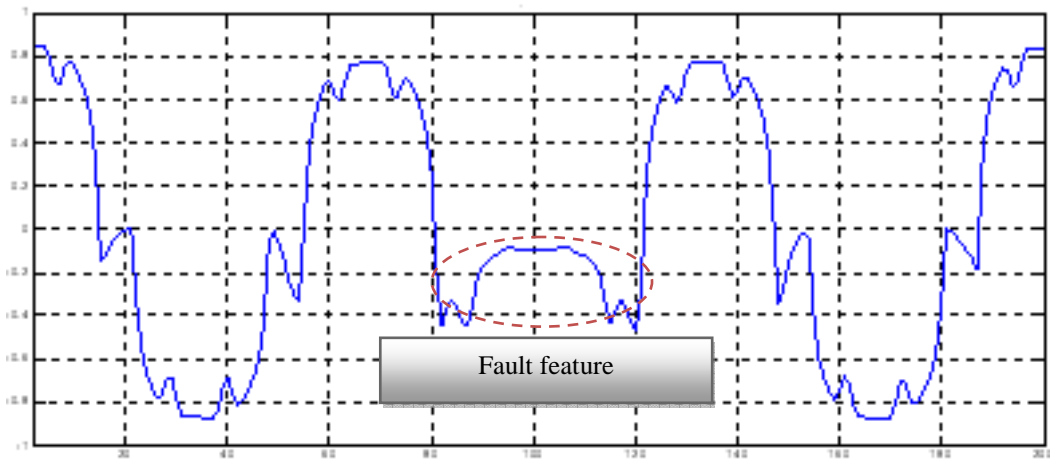


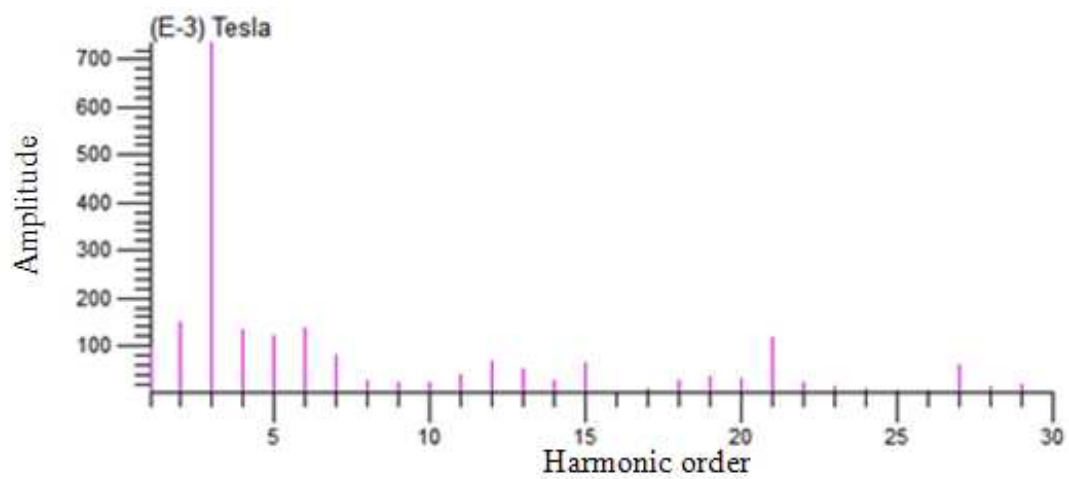
Fig. 3.33 : (a) Symmetric magnet failure and magnetic field distribution; (b) Flux density characteristic; (c) FFT analysis of the flux density



(a)

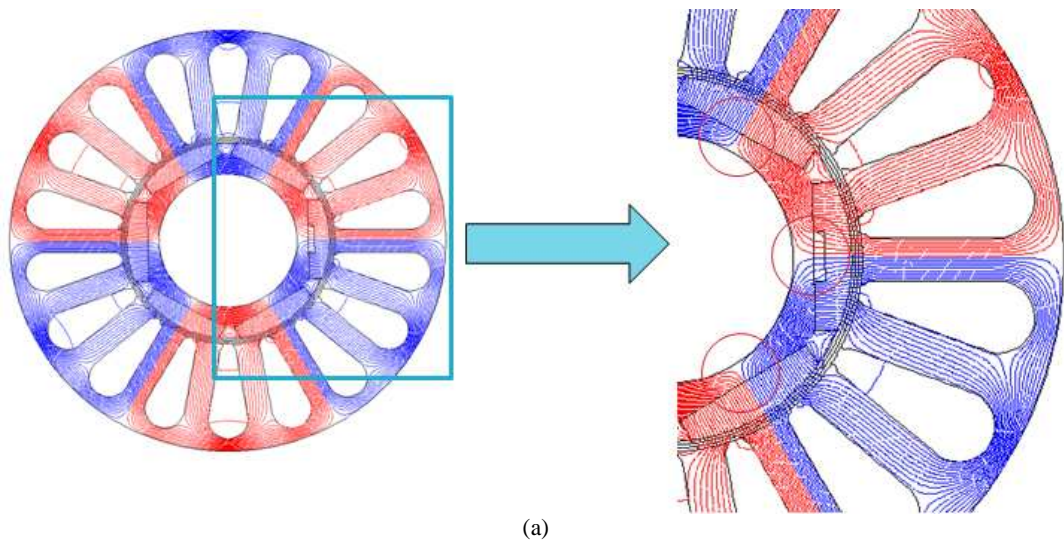


(b)

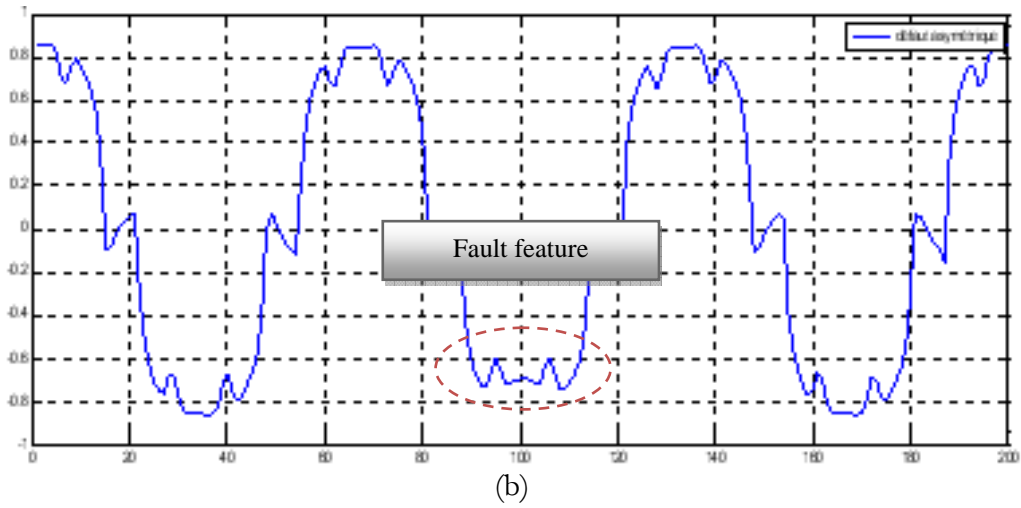


(c)

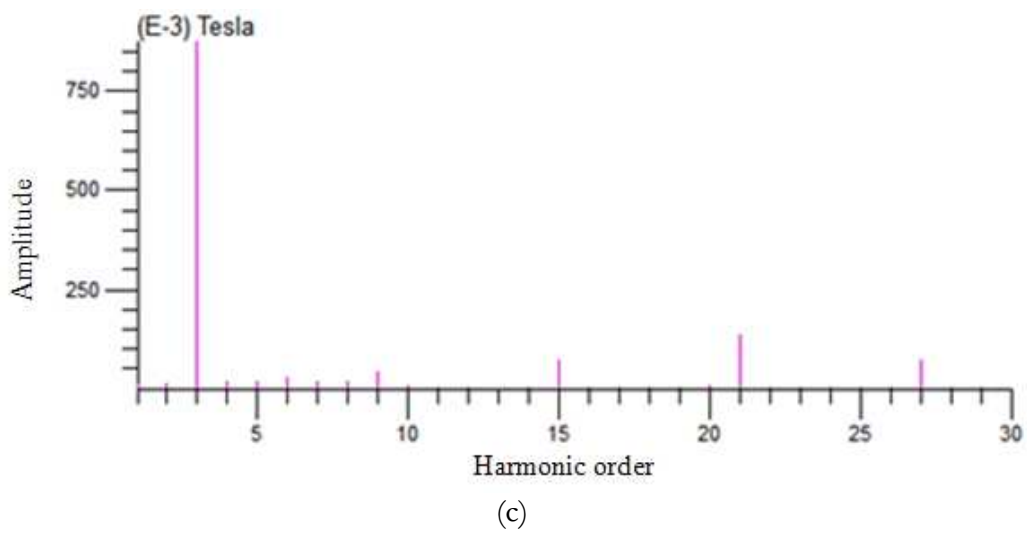
Fig. 3.34 : (a) Complete asymmetric for one magnet failure and magnetic field distribution; (b) Flux distribution; (c) FFT analysis of the flux



(a)



(b)



(c)

Fig. 3.35 : (a) Partial asymmetric for one magnet failure and magnetic field distribution; (b) Flux distribution; (c) FFT analysis of the flux density

This investigation shows the changes in the pick of flux density waveform in each faulty state against to healthy state operation. This change is more highlighted for a complete asymmetric demagnetization in comparison of health operation. Also the changes of harmonic component of amplitude of FFT analysis of the flux density is another feature, that can be used for demagnetization fault detection as shown in figures above.

3.2.2 Comparison study between analytical and FEM models

The analytical model developed with segmented magnet was implemented in MATLAB. One of the interesting uses of the FEM simulation model is to check the validity of the analytical models but also to well parameterize them to obtain satisfactory accuracy. The validation process consists in comparing the back EMF signals of the two models.

The Figure (3.36) and (3.37) show the results of both the models under healthy and faulty states respectively.

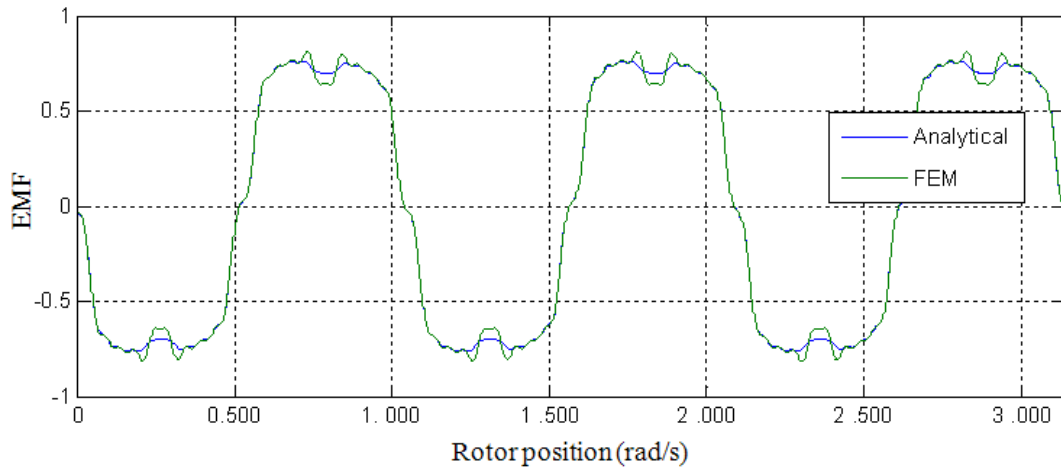


Fig. 3.36 : Back EMF under healthy motor operation

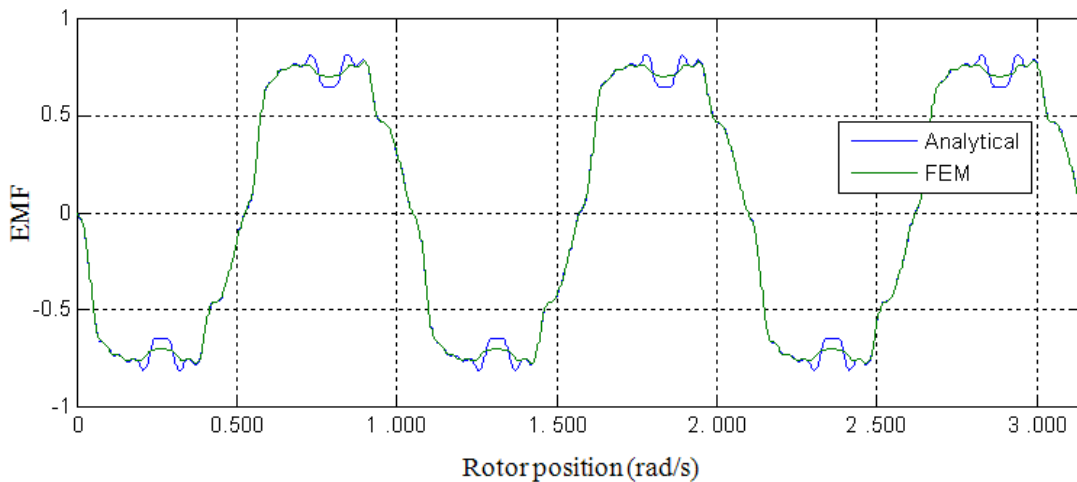


Fig. 3.37 : Back EMF under Faulty motor operation (in this case one segment of 25 segments is demagnetized)

On the basis of these results the proposed analytical model has been validated for modeling the PMSM in both healthy and faulty modes while the conditions of assumptions made for its developments are fulfilled. This means that for a good characterization of the demagnetization phenomenon the use of the FEM simulation model remain very useful.

3.3. Diagnosis algorithm of PMSM demagnetization fault

The figure (3.38) presents the synoptic scheme of the proposed algorithm for the PMSM diagnosis processing for detecting and localizing the demagnetization faults. This algorithm is based on the back EMF estimation because of the non-existence of sensors able to measure this magnetite. That estimation has not been done in the framework of this thesis but we think that the use of estimators based on minimizing errors between the measured and the computed stator currents and mechanical speed. Once the ANN model established it may be easily integrated in the diagnosis algorithm of the drivetrain which will be discussed more in details in chapter 5.

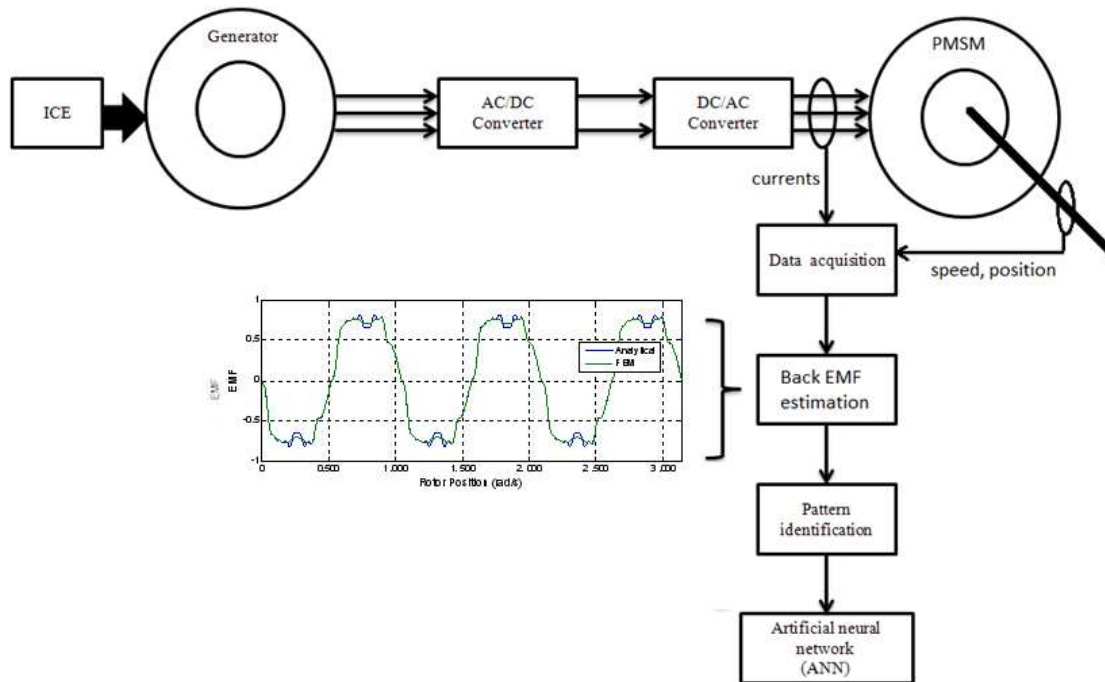


Fig. 3.38 : Fault diagnosis strategy of PMSM demagnetization for SHEV application

4. Eccentricity & bearing fault

In chapter 2 sections 3.6 and 3.7, the main causes of eccentricity and bearing faults in PMSM have been presented. The different types of eccentricity as static, dynamic and mixed eccentricity have been studied and different methods to detection and diagnosis of these types of faults have been investigated.

4.1. Eccentricity & bearing sensitive modeling

Figure (3.39) shows a modeling procedure of eccentricity and bearing fault diagnosis of PMSM respectively (As the same process of eccentricity and bearing fault in order to use of vibration signal and usage of FFT and TF, we shown both of them in one figure). FFT analysis on motor current and vibration is highlighted by literatures as well as mentioned in chapter 2. ANN is used to classify the different percentage of eccentricity and the various types of eccentricity as well as it is able to different percentages of bearing fault detection. Of course in non-stationary states, TF methods will be a useful method against FFT weakness. In this work a FFT and TF method have been used for eccentricity and bearing fault investigation as well as shown in appendix 3E in detail.

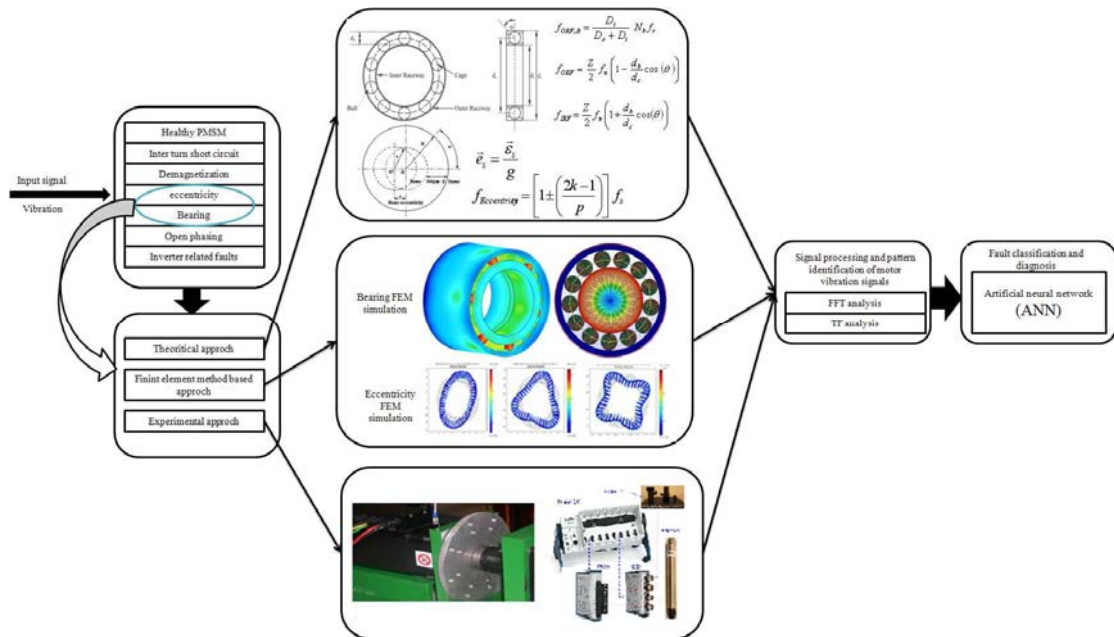


Fig. 3.39 : Model of identification and diagnosis of eccentricity and bearing fault of PMSM for electric vehicles

4.2. Diagnosis algorithm of PMSM eccentricity & bearing

Within the framework of diagnosing the PMSM drivetrain of a SHEV, the figure (3.40) illustrates the synoptic scheme of the proposed algorithm for the PMSM diagnosis processing for detecting the eccentricity and bearing faults. This algorithm is based on the stator vibrations of the PMSM combined to electro-vibratory models. The accelerations measured, back EMF estimation because of the non-existence of sensors able to measure this magnetite. That estimation has not be done in the framework of this thesis but we think that the use of estimators based on minimizing errors between the measured and the computed stator currents and mechanical speed. Once the ANN model established it may be easily integrated in the diagnosis algorithm of the drivetrain which will be discussed more in details in chapter 5.

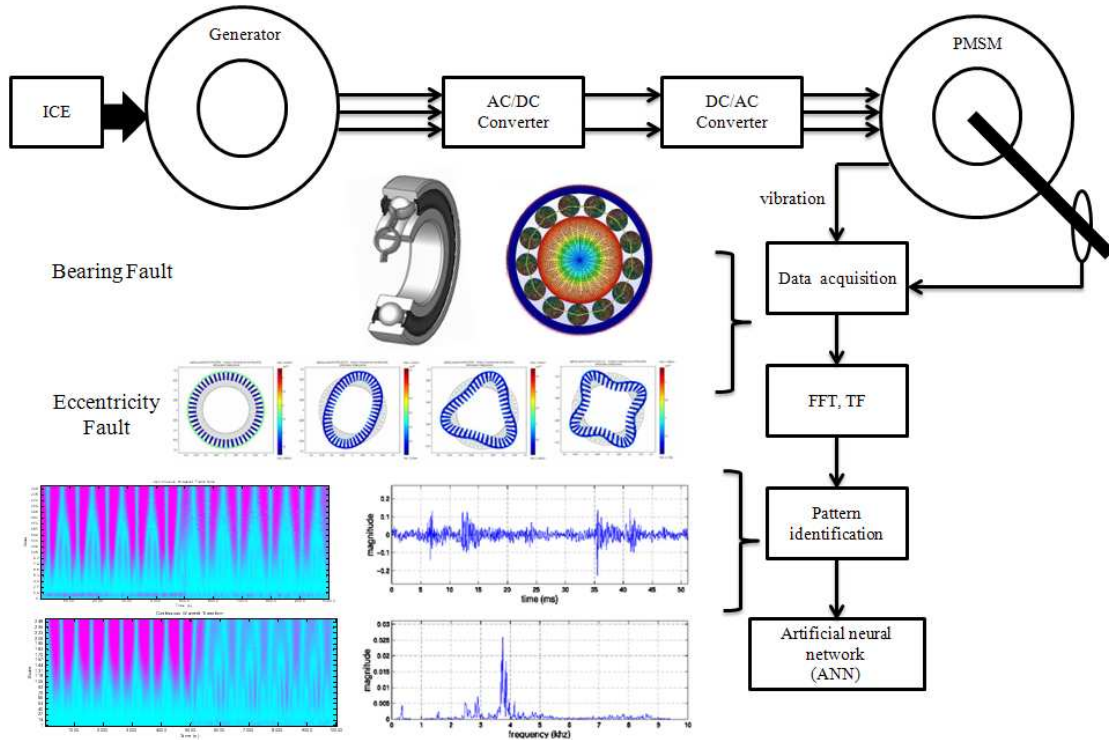


Fig. 3.40 : Fault diagnosis strategy of PMSM eccentricity for SHEV application

5. Conclusion

A deep investigation on fault effects in inter turn short circuit fault state of PMSM has been done in this chapter by experimental results extraction. The effects of this fault in different states of SHEV application as different speed and different load have been considered. For generalization of fault diagnosis, several severity of short circuited turn (several different percentages of short circuits) has been done for a better training of ANN. Experimental results show the variations in FFT amplitudes, FFT phases frequencies of motor currents. To know features of faults help us to choose proper parameters (or samples) to train artificial neural network (ANN) by aim diagnosis and classification of this types of fault.

A classical analytical model has been developed for studying the demagnetization fault of PMSM. The obtained results have been partially validated by a FEM simulation program established especially for this need under the FLUX 2D software. So far a lake in demagnetization fault investigation didn't led to do a deep characterization of this fault type, however this research topic remains in agenda of the laboratory IRTES-SET. Experimental validation of analytical and FEM have been considered as a future work for continue of this issue.

Concerning the eccentricity and bearing fault of PMSM (and also for induction motors), the work done was principally experimental. The theoretical development was focused on the signal processing of the measured stator vibrations notably through the FFT and TF techniques. Finally, the principles of three diagnostic algorithms have been presented to show how the fault sensitive models of short-circuits; demagnetization, bearing and eccentricity can be used to diagnose a PMSM driving a SHEV. More details about these algorithms and about the technique of ANN used in this research work will be explained in the chapter 5.

6. References of Chapter III

- [1] Song Chi, M.S.E.E, “Position-Sensorless Control of Permanent Magnet Synchronous Machines over Wide Speed Range”, Presented in Partial Fulfillment of the Requirements for the Degree Doctor of Philosophy in the Graduate School of The Ohio State University.
- [2] Peter Vas, Sensorless and Direct Torque Control, 1st Edition, Oxford University Press, 1998.
- [3] Paul C. Krause, Oleg Wasynczuk and Scott D. Sudhoff, Analysis of Electric Machinery, IEEE Press, Inc. New York, 1986.
- [4] J. A Farooq, Study and Detection of demagnetization and Short-Circuit in permanent Magnet Synchronous Machines, PhD Thesis, University of Technology Belfort Montbéliard, France, 2008.
- [5] J. A. Farooq, A. Djerdir, and A. Miraoui, “Analytical Modeling Approach to Detect Magnet Defects in Permanent-Magnet Brushless Motors”, IEEE TRANSACTIONS ON MAGNETICS, VOL. 44, NO. 12, DECEMBER 2008.
- [6] S. Saeid. Moosavi, A. Djerdir, Y. Aït-Amirat, D. A. Khaburi, “ Impedance Angle Changes Analysis Applied to Short Circuit Fault Detection ”, IEEE XXth International Conference on Electrical Machines (ICEM'2012), Septembre 2-5-2012, Marseille, France.
- [7] Xu Boqiang; Baoding, China ; Li Heming ; Sun Liling, “Apparent impedance angle based detection of stator winding inter-turn short circuit fault in induction motors”, Conference Record of the Industry Applications, 38th IAS Annual Meeting. (Volume: 2) 12-16 Oct. 2003.
- [8] Satish Rajagopalan, Wiehan le Roux, Thomas G. Habetler, and Ronald G. Harley, “Dynamic Eccentricity and Demagnetized Rotor Magnet Detection in Trapezoidal Flux (Brushless DC) Motors Operating Under Different Load Conditions”, IEEE TRANSACTIONS ON POWER ELECTRONICS, VOL. 22, NO. 5, SEPTEMBER 2007.
- [9] Ruschetti. C, Bossio. G, De Angelo. C, Verucchi. C, “Effects of partial rotor demagnetization on permanent magnet synchronous machines”, IEEE International Conference on Industrial Technology (ICIT), 2010 Publication Year: 2010 , Page(s): 1233 – 1238.
- [10] W. Le Roux, R. Harley, and T. Habetler, “Rotor fault analysis of a permanent magnet synchronous machine”, International Conference on Electrical Machines (ICEM'02), Brugge, Belgium, 2002.
- [11] S. Rajagopalan, W. le Roux, T. G. Habetler, and R. G. Harley, “Diagnosis of potential rotor faults in brushless dc machines,” in Second International Conference on Power Electronics, Machines and Drives (PEMD 2004). (Conf. Publ. No. 498), vol. 2, 2004, pp. 668–673.

Chapter IV

Fault sensitive modeling of the power converters the drivetrains of SHEV

1. Introduction	125
2. Power converters behaviors in healthy and faulty operation mode.....	126
2.1. AC-DC converter fault modeling: theoretical and experimental investigation.....	126
2.2. Experimental setup	127
2.3. Best data identification for acquisition by aim of successful signal processing	128
2.3.1 Simulation result validation of AC-DC converter fault detection of SHEV....	128
2.3.2 Experimental results.....	131
2.4. Pattern identification	134
2.4.1 Fault detection strategy and algorithm for the experimental setup.....	134
2.4.2 Influence of the DC-Bus capacitor on fault signatures	137
2.4.3 Influence of the load changes on fault signatures	137
2.4.4 Influence of the speed changes on fault signatures.....	138
2.5. Fault detection investigation thyristor base AC-DC converter operation.....	139
2.5.1 Pattern identification.....	139
2.6. Fault sensitive modeling DC/AC inverter	141
3. Conclusion.....	145
4. References of chapter IV	146

1. Introduction

Today, industrial electronic has a vast and principal role in electric vehicle applications. In different types of electric vehicle that 3 samples of its most common are mentioned in chapter 1 section 3.1, power converters (as AC/DC converters and DC/AC inverters) play an important roles in transfer of electric power to the main consumer of this energy that called electric motors. In regard of fault diagnosis on electric vehicle, because of presence different electrical elements, each one can be exposed the risk of its special failure. These faults can affect on other relevant parts by defective element. Finally, this will lead to error in fault detection and diagnosis of other adjacent elements. So it is important to investigate all relevant elements in chain of traction and to consider their interactions with each other. Of course it won't be possible in format of one project [1], [2], and [3].

A significant proportion of faults in power converters are caused by failures of power semiconductor devices. Such faults may be classified into open circuit and short circuits faults. Short circuit faults are typically caused by excessive voltage or current. Open circuit faults may be caused by breaking of bond wires due to thermal cycling, short circuit induced rupture, or driver failure in the case of rectifiers implemented using IGBT's. Fuses, breakers, overload relays, and electronic over current protection circuits provide protection when short circuit faults occur and the normal reaction is to shutdown the entire system. Open circuit faults are more challenging to detect because these are not normally recognized by the protection logic so the system will usually continue to operate after a failure occurs but with degraded performance. The degraded performance is not without cost; it usually places increased stress on other system components leading, in time, to further failure [4], [5], and [6].

In this case, this work firstly presents a study on AC/DC power converter as an electric power bridge crossing for supplying PMSM, before investigation on EM fault diagnosis. This helps us to avoidance of error in a proper methods selection of faults diagnosis. However DC/AC inverters can be under the risk of failure more than AC/DC converters, but because of our facility in doing experimental validation on AC/DC converter faults, to study on this issue selected as one of our objective in this work, while research is ongoing over inverter faults too.

According to mentioned aims, a deep theoretical and experimental investigation on fault modeling on drive-train of SHEV has been done in this chapter. In the first, a structure of sample SHEV modeled and open phase fault effects on AC/DC converter have been studied. Two new patterns have been identified for this type of fault and the results validate by experimental test in different states of HEV application.

2. Power converters behaviors in healthy and faulty operation mode

2.1. AC-DC converter fault modeling: theoretical and experimental investigation

The schematic diagram of SHEV studied for experimental test is shown in figure (4.1) The $S_1, S_2, S_3, S_1', S_2', S_3'$ are introduced here in order to create different types of faults. The most common electrical faults in AC-DC converter is single phase open circuit faults. The presence of capacitor between converter and inverter will compensate some of voltage drop and also harmonic changes under some types of faults that lead to fault detection hardly.

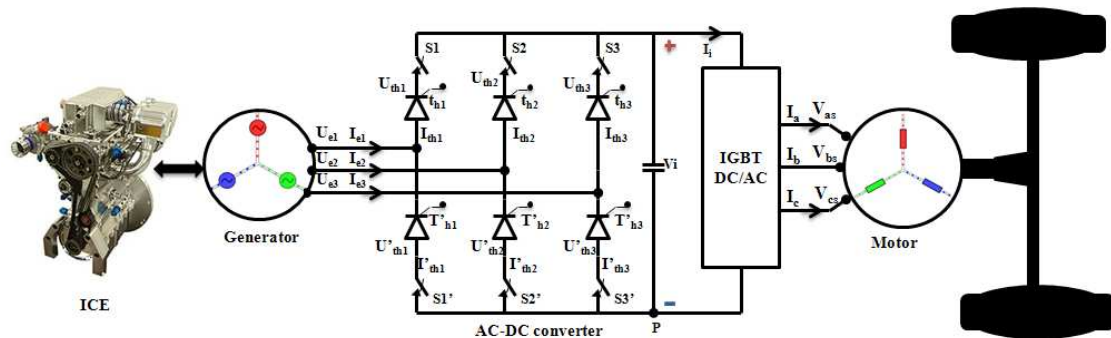


Fig. 4.1 : Schematic diagram of a generator (G), 3-phase full bridge rectifier, 3-phase full bridge inverter and 3-phase induction motor by application in SHEV

This work shows a useful and new method to reach this goal. With 6 bridge of AC-DC converters $2^6 = 64$ different states of switching operation is possible. According to switching operation and objective of fault detection, we considered 51 states of existing different structure including one health mode and 50 fault conditions in 5 groups as shown in table (4.1) (thirteen remain state such as all switches-off or 3 upper/or/downer switches-off and other impossible state are worthless to check because of in this states, any power doesn't transfer for motor operation and system will be shut down).

In group 1, the AC-DC converter in health state of its operation is considered. In groups 2, 3, 4 and 5, respectively, open phase faults assuming failure in 1, 2, 3 and 4 switches has been investigated. However the power transferred on motor in group 5 isn't enough to operation under full load, but motor can continue to work under this situation. According to different state of thyristor fire angle, we consider all 51 states in 3 different condition of thyristor Angle Fire operation in degrees of $0^\circ, 15^\circ, 30^\circ$ and 45° as shown in table (4.2). It is obvious that thyristor operation under $\alpha = 0$ is in diode based function.

Table 4.1 : Different fault structures in 3-phase full bridge ac/dc converter investigated by application in SHEV.

FG		S1	S2	S3	S1'	S2'	S3'
		G1	0	H	H	H	H
G2	1	F	H	H	H	H	H
	2	H	F	H	H	H	H

	6	H	H	H	H	H	F
G3	7	F	F	H	H	H	H
	8	F	H	F	H	H	H

	21	H	H	F	H	H	F
G4	22	F	F	H	F	H	H
	23	F	F	H	H	F	H

	40	H	H	F	H	F	F
G5	41	F	F	H	H	F	F
	42	F	F	H	F	H	F

	51	F	H	F	F	H	F

(H: HEALTHY MODE) (F: FAULTY MODE)
(FG: FAULTY GROUPS) (SS: SWITCH STATE) (FS: FAULTY STATE)

Table 4.2 : Different thyristor angle fire in investigated 3-phase full bridge ac/dc converter

Thyristor Groups	Fire angles (°)			
	0	15	30	45
G1	✓	✓	✓	✓
G2	✓	✓	✓	✓
G3	✓	✓	✓	✓
G4	✓	✓	✓	✓
G5	✓	✓	✓	✓

2.2. Experimental setup

A general plan of the experimental setup is shown in figure (4.2). In this system a 3 phase power supply is used to generate 3 phase sinusoidal voltage and current for the use of AC-DC converter. The 3 phase induction motor windings are Y connected. A variable electromagnetic brake is used for different levels of load on the motor shaft applying. The main parts of this experimental setup are shown in table (4.3). Also the main parameters of motor are presented in table (4.4).

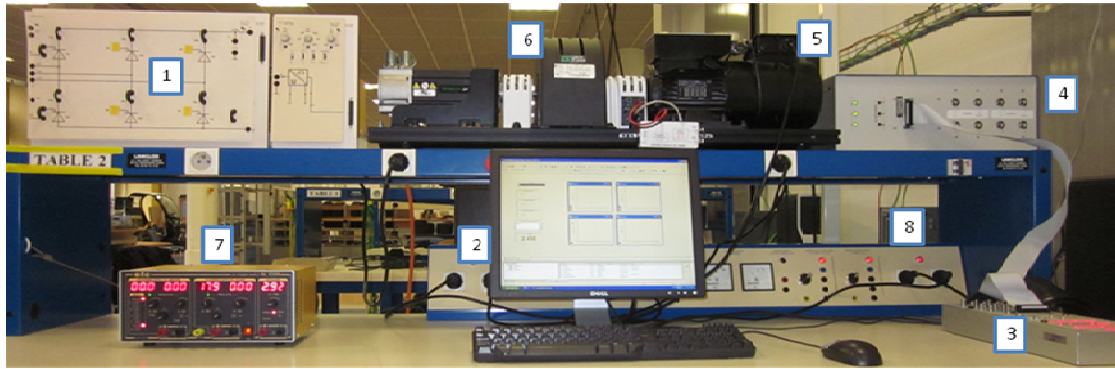


Fig. 4.2 : Experimental setup

Table 4.3 : Main parts of experimental setup presented in figure (4.2).

1) 3 phase full bridge AC-DC converter. This especial type of AC-DC convertor let us to test all of 6 faulty groups as mentioned in table (4.1).	2) PC, for data transfer and data analysis.
3) A system equipped with a data acquisition controller that it is able to connect with DSPACE-DS1104 for sampling the electrical data at adjustable frequency. For advanced uses input / output, the card has a DSP subsystem Slave to ensure the measurement acquisition and generation of PWM signals.	4) The voltage inverter in which the power circuit consists of three arms of power switches. There are six SEMIKRON IGBTs ordered with drivers. This inverter include 6* (EPCOS-B43303-A0158-M90) parallel capacitor, 1500 μ F, 200V, 25 A, between inverter input and DC-BUS output.
5) The 3 phase induction motor. For which the parameters of used IM are shown in table (4.4)	6) Electromagnetic brake,
7) DC power supply for electromagnetic brake,	8) Power network

Table 4.4 : Rated characteristic of the used three-phase motor

power	0.75 KW
frequency	50 Hz
voltage	220 V
Speed(rpm)	1440 min ⁻¹
Cos Φ	0.72
Number of poles	4
Full load current	2 A

2.3. Best data identification for acquisition by aim of successful signal processing

2.3.1 Simulation result validation of AC-DC converter fault detection of SHEV

To present an original and accurate results and also because of importance of fault detection in AC-DC converters by application of EV, all results used in this work are based on experimental data analysis, however a simulation program has been developed under MATLAB/SIMULINK software as shown in figure (4.3) and validated by a

comparison study between simulation and experimental results. The results will be shown in both diode base and thyristor base operation states. We start by $\alpha = 0$ as a diode operation state in this part.

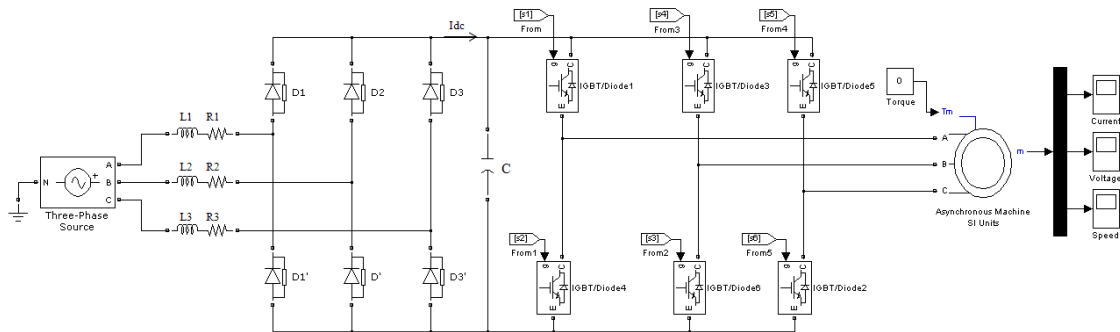
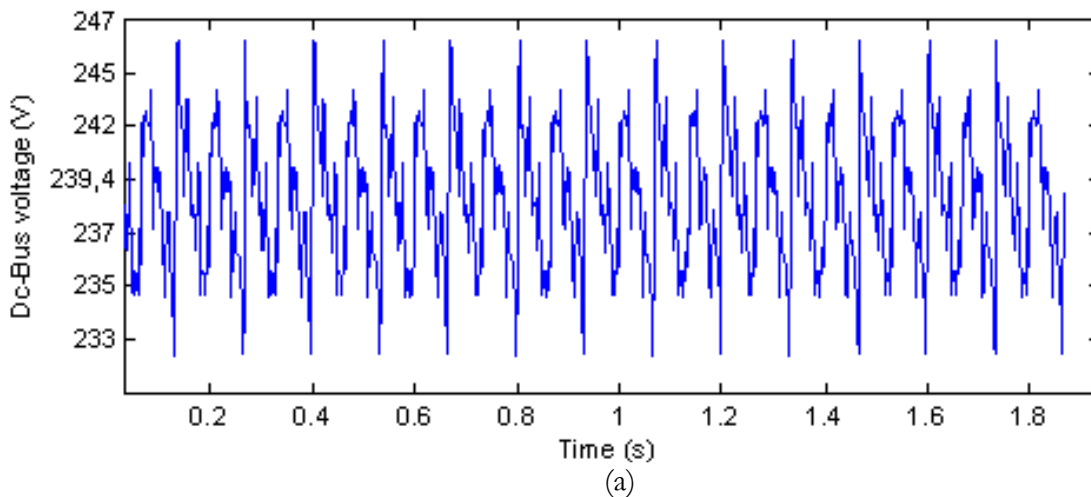


Fig. 4.3 : MATLAB/SIMULINK Simulation of a sample of SHEV

In this base, DC-BUS voltage and DC-BUS current in simulation and Experimental state are shown in figure (4.4) and figure (4.5) respectively. Also, FFT analysis on DC-BUS current under healthy and faulty mode operation of AC-DC converter presented in figure (4.6) and figure (4.7) respectively. It may be clearly seen that the wave forms and FFT analysis of both the simulation and experimental results are quite the same. Thus, one can conclude that the developed simulation program of the power supply of the SHEV is valid in both faulty and healthy modes. So, this software tool can be used in total security to simulate more faulty conditions especially those difficult to perform experimentally.



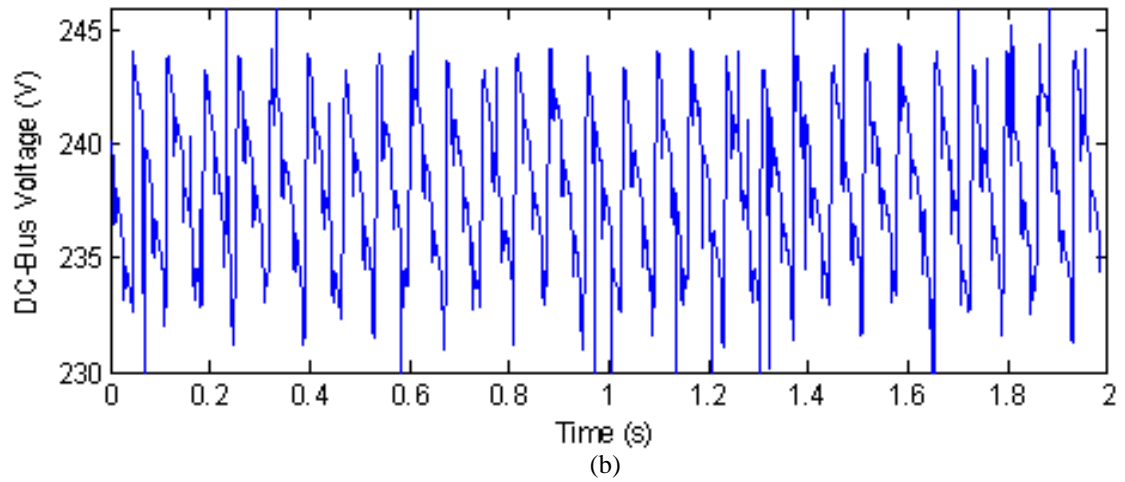


Fig. 4.4: DC-BUS voltage under healthy mode operation (a- Simulation result; b- Experimental result)

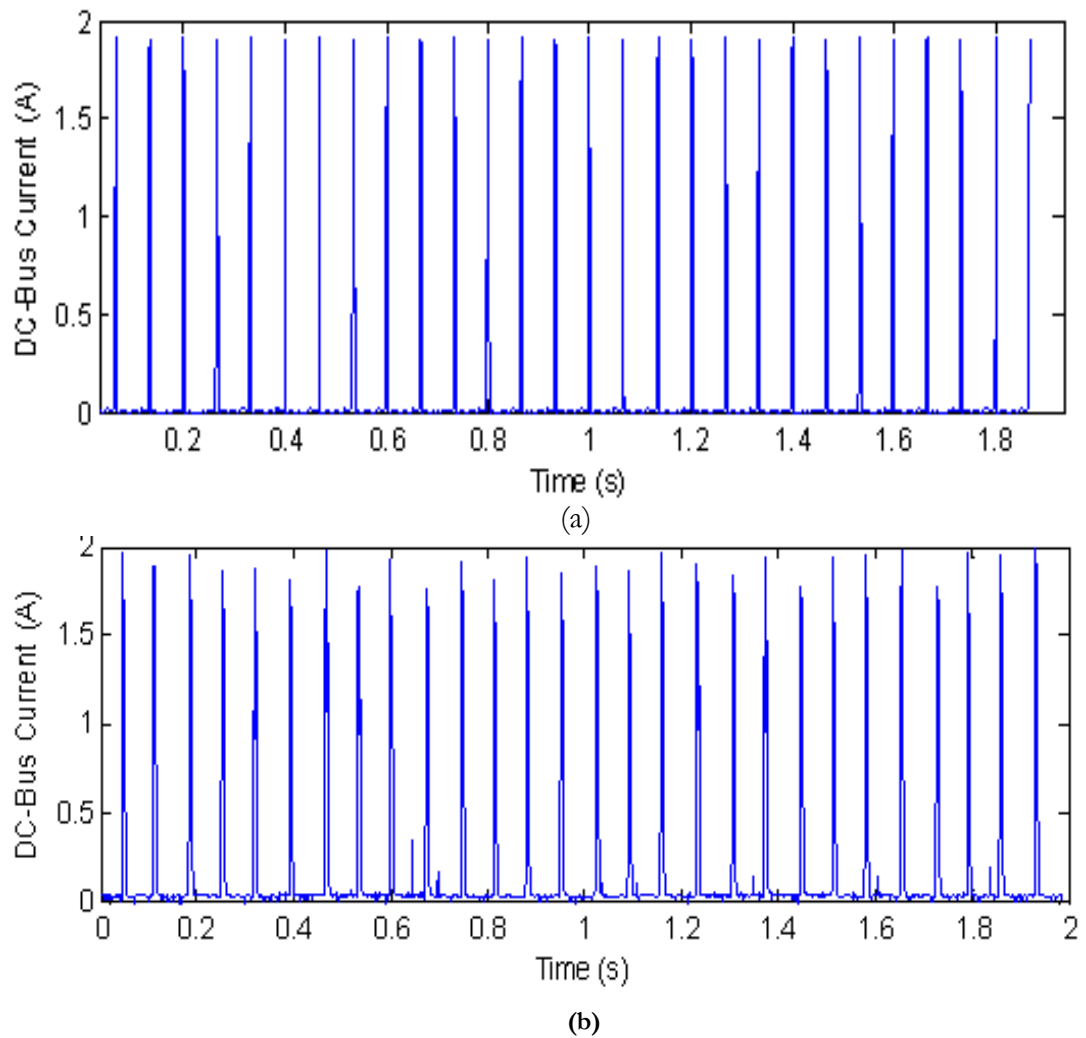


Fig. 4.5 : DC-BUS current under healthy mode operation (a- Simulation results; b-Experimental result)

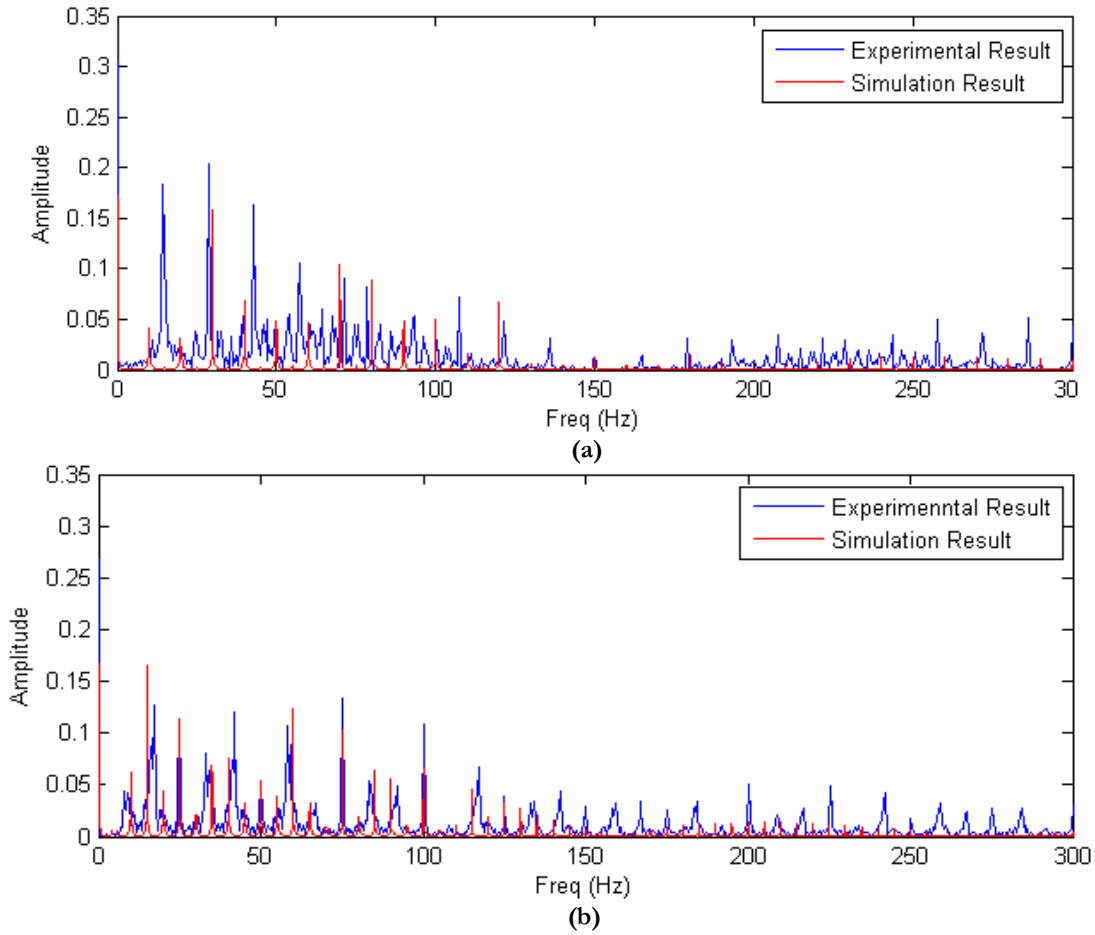


Fig. 4.6 : FFT analysis on DC-Bus current, a- healthy mode simulation and experimental result; b- Faulty mode simulation and experimental result (switch S2 is opened)

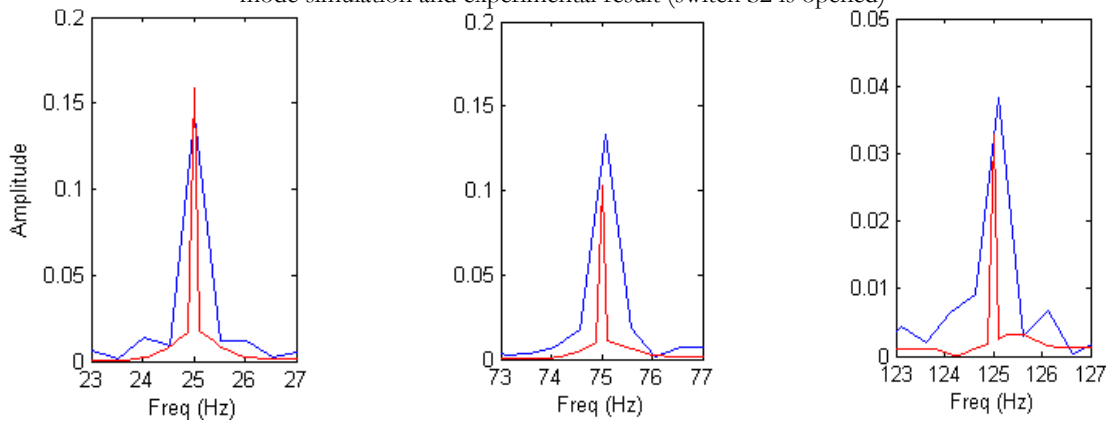


Fig. 4.7 : Zoom view of experimental and simulation FFT analysis results under faulty mode operation of motor (switch S2 is opened)

2.3.2 Experimental results

Electric vehicle fault detection need to a deep knowledge of system operation and fault detection techniques together. Different parts of EV likes generator, AC-DC converter, capacitor, inverter and motor, dependence together and fault detection dedicated for one especial fault will require a high precision to avoid errors in fault detection. However the existence of capacitor between AC-DC converter and inverter

may filter several possible faults, especially when they are minor ones: (little reduced of input current, small voltage ripples and etc) in this case the fault detection will to become hard.

Generally, in case of especial operation of electrical motors by application of HEV, because of moving of HEV, it is under an inherence vibration in addition inherence asymmetries during manufacturing. Therefore waveforms of motor and other instruments are with some distortion that unreliable to refer the fault detection only the amplitude changes. Today, usage of Fast Fourier Transform (FFT) still very responded for fault detection in steady state [4], [35], [3], [51], [53], [115], [126], [127-129]. Even though, sometimes, it is non-efficiency for fault detection in transient condition.

For usage of FFT analysis, it must choose a proper signal. Otherwise, FFT will be ineffective, even in steady state. To identify proper data by aim of successful FFT analysis, in fault state operation, two types of faults are considered:

- Open phase fault by considering group 2 condition as mentioned in table (4.1) and, because the signal variations are very small.
- Open phase fault under operation by considering condition of group 5.

This is confirmed by figure (4.8) and figure (4.9) where it can be seen that there isn't any discriminant information via FFT analysis of the induction motor current and Dc-bus voltage where compare harmonic spectrum of the health mode and fault state of AC-DC converter operation.

The use of Dc-bus current "Idc" can help us to find discrimination between health and fault states as shown in figure (4.10). The advantage of this method is reproducibility and high resolution in separation of different faults states at specific periods of FFT analysis compared to fundamental harmonic.

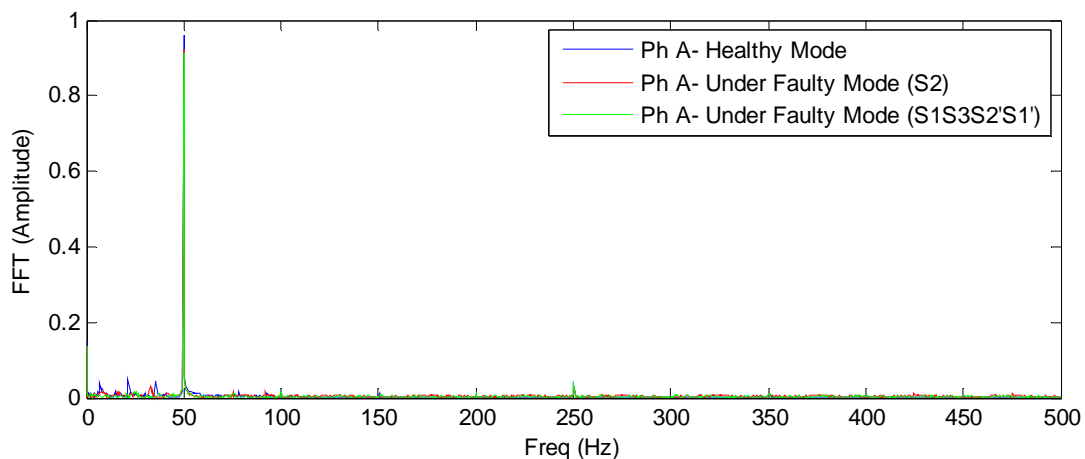


Fig. 4.8 : FFT analysis Comparison between motor current phase A under healthy mode operation, faulty mode by open phasing in switch S2 and also under open phasing fault by opening S1S3S2'S1' of Fig. (4.1).

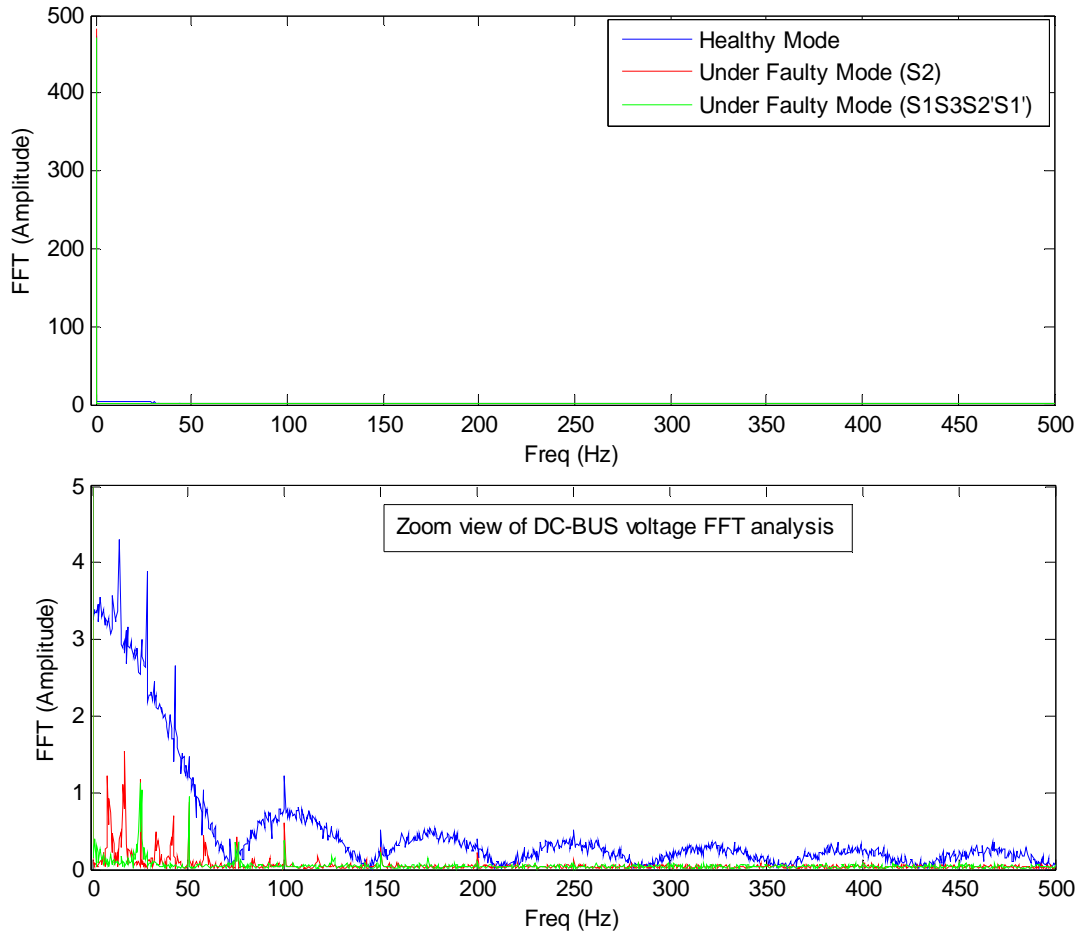
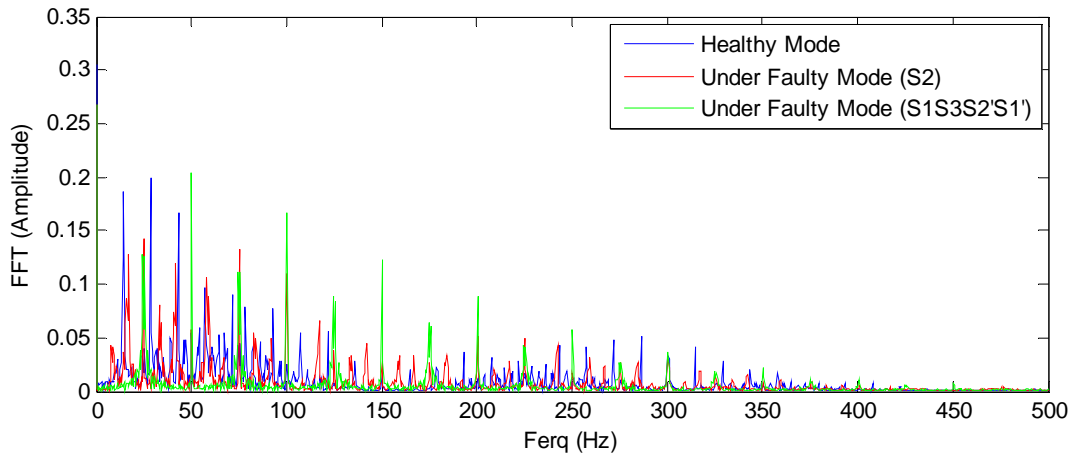


Fig. 4.9 : FFT analysis comparison between DC-BUS voltage under normal mode operation, under open phase fault by opening S2 and under open phase fault by opening S132'1' of Fig. (1.4).



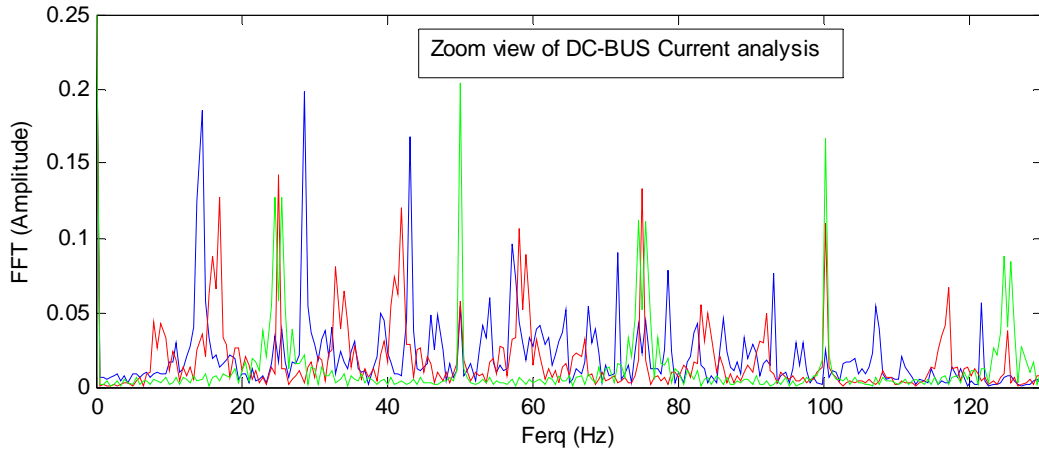


Fig. 4.10 : FFT analysis Comparison between DC-BUS current under normal mode operation, under open phase fault by opening S2 and under open phase fault by opening S132'1' of Fig (1.4).

2.4. Pattern identification

2.4.1 Fault detection strategy and algorithm for the experimental setup

Figure (4.11) presents a pattern identification and fault detection strategy in an AC-DC converter of SHEV. Also fault detection and implementation algorithm is shown in figure (4.12) subsequently.

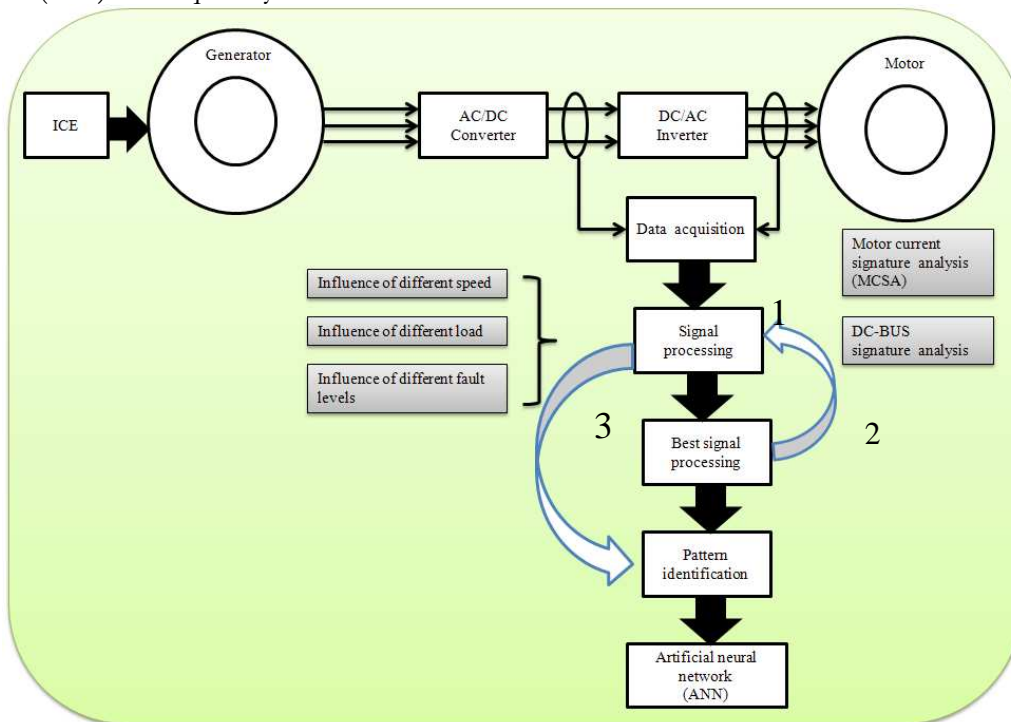


Fig. 4.11 : Pattern identification and fault detection strategy

As it was mentioned in previous part, I_{DC-BUS} can help us in reach to goal easier and accurate than other introduced methods. By helping Fast Fourier Transform (FFT) on I_{DC-BUS} , we can have a targeted comparison between healthy and faulty mode operation for fault detection.

Each one of faulty groups will lead to presence of frequently harmonics in $f_f/2$, $(f_f+(f_f/2))$, $(2f_f+(f_f/2))$ and etc, in I_{DC-BUS} , in compare to health state.

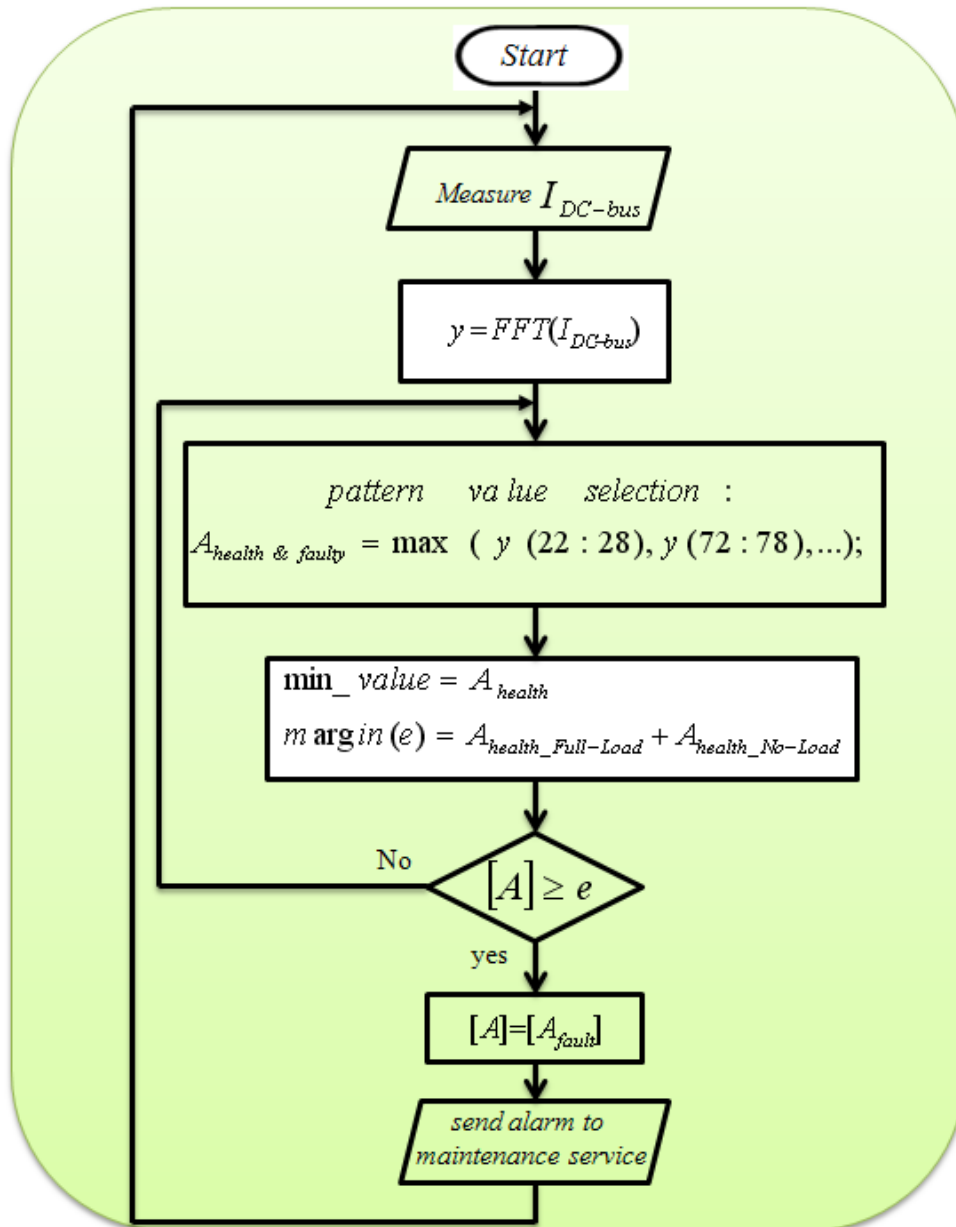


Fig. 4.12 : Fault Detection and implementation algorithm

In figure (4.13), the comparison between I_{DC-BUS} under healthy state operation and under open phase fault by opening switches in conditions of group 2, 3, 4 and 5 is presented. The amplitude of harmonic will be decrease with increase of severity of fault in group 2, 3, 4, 5 respectively. It is because of power transferred to AC-DC converter output in each one of faults levels.

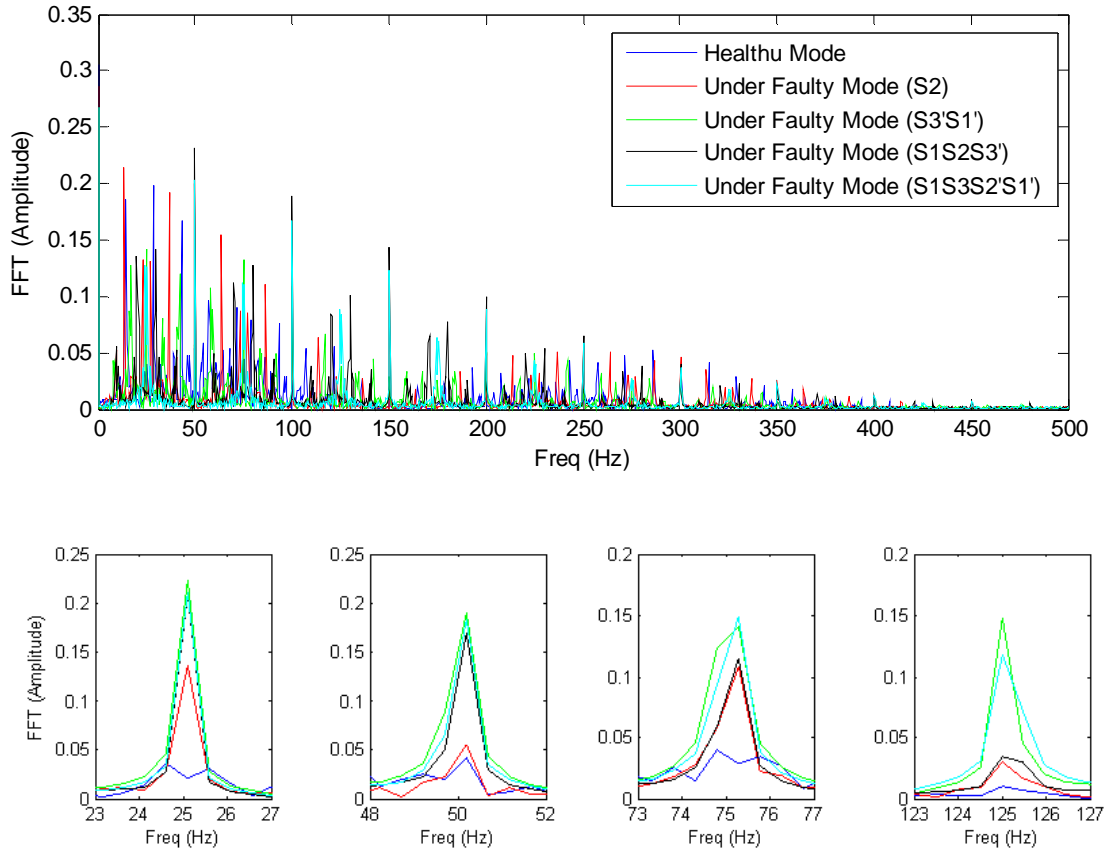


Fig. 4.13 : Comparison between DC-BUS current under health state operation and under open phase fault by opening S2 of group 2 in table (4.1)

As final result, it can be considered for fault detection in these types of faults and in all groups presented in table (4.1) as (4.1):

$$f_{open_phase\ fault} = \frac{(2k+1)f_f}{2} \quad (4.1)$$

Where $k = 0, 1, 2, 3 \dots$ and f_f is index of fundamental frequency.

The important advantage of this pattern is the detection ability under group 2 fault state. Because it is expected in this case, the fault should be detect and void if its progress to other groups.

To make generalization the algorithm presented in all states, a margin is considered as $A_{health} + e$. A_{health} is the matrix of pattern in healthy state and e is maximum value of the difference of $[A_{health}]$ values under different conditions include no load, full load, different speeds and different capacitors used in this operation.

2.4.2 Influence of the DC-Bus capacitor on fault signatures

In this work, the influence of capacitor size changes because of validation of our pattern has been considered. In this base, four different level of capacitor have been compared together under healthy and faulty operation of AC-DC converter. Also because of experimental facility used the nominal value of capacitor $C_n=9000 \mu\text{F}$. $C_n/2$, $C_n/10$ and $C_n/100$ are other different size for validate of pattern identified under faulty operation in compression with healthy mode operation. The results presented in figure (4.14), show the pattern identified in (1.4) is independent of the size of capacitor.

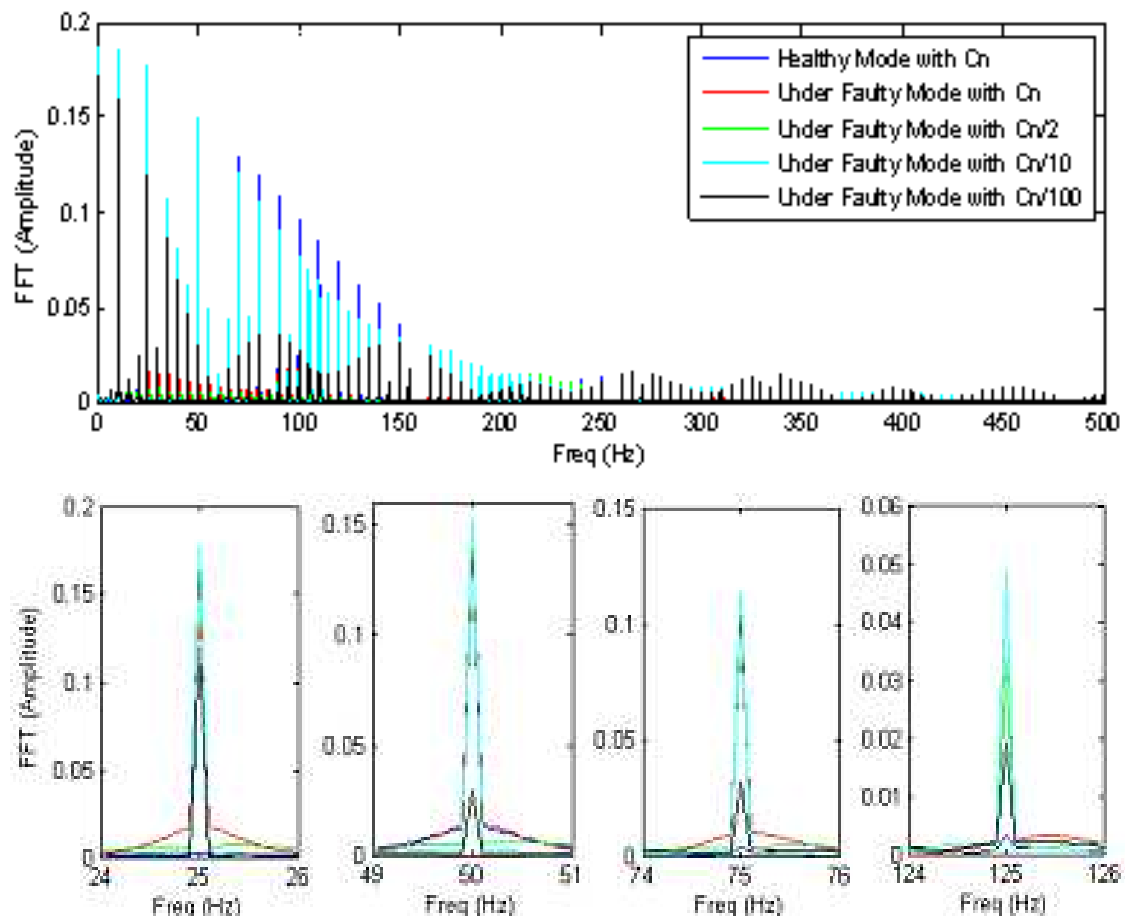


Fig. 4.14 : Consideration of capacitor influence on pattern identified under healthy and faulty operation of AC-DC converter (switch S2 is opened)

2.4.3 Influence of the load changes on fault signatures

One of the most important problems in any fault detection method is the investigation of load variation on the proposed indices. Accurate fault detection is not possible without consideration of relations between indices, load variations, and types of faults. In this paper, the effects of load variation on fault detection under five different state as no-load, $\frac{1}{4}$ load, $\frac{1}{2}$ load, $\frac{3}{4}$ load and full-load have been presented and results

are shown in figure (4.15) The results show that the load variations do not have noticeable impacts on pattern identified too.

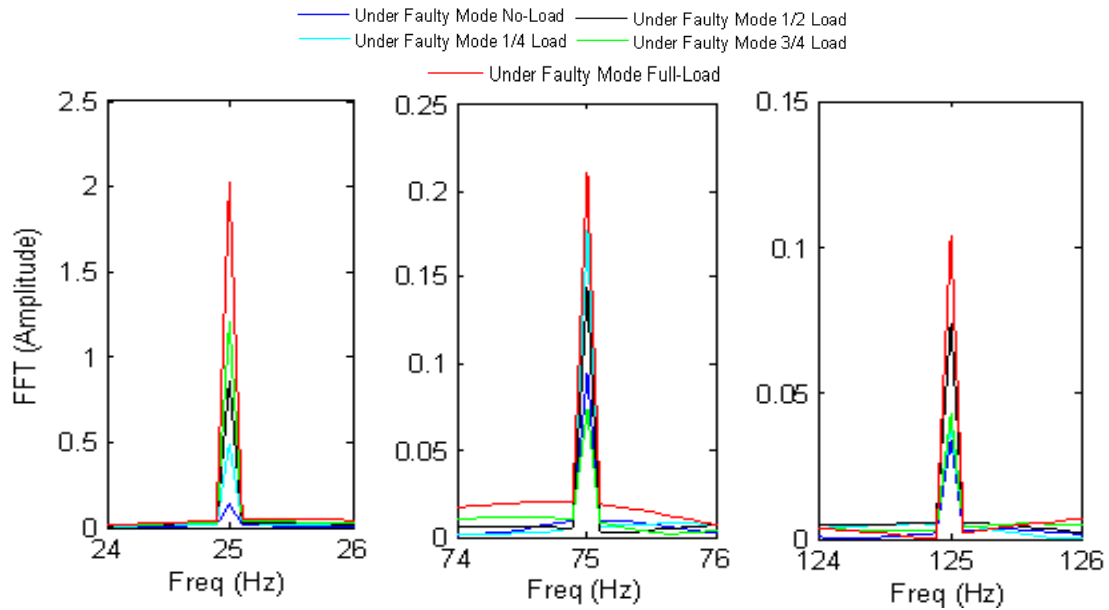


Fig. 4.15 : Consideration of load variations influence on pattern identified under faulty operation of AC-DC converter (switch S2 is opened)

2.4.4 Influence of the speed changes on fault signatures

Speed variation operation in EV is one of important items to separate EV application compared to other industrial applications. According to this application, in different speed, this part considers the pattern identified for 5 different speed 1000 rpm, 800 rpm, 600 rpm, 400 rpm and 200 rpm under healthy and faulty operation mode, as the results shown in figure (4.16).

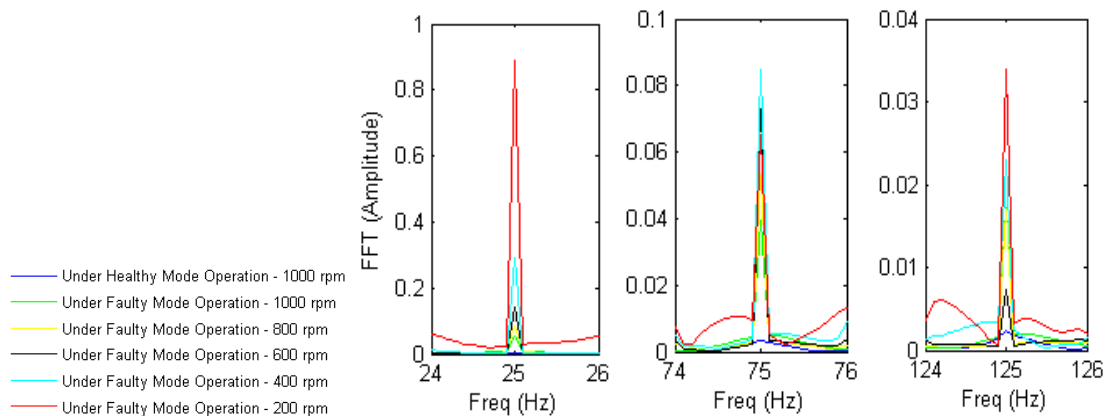


Fig. 4.16 : Consideration of speed variations influence on pattern identified under faulty operation of AC-DC converter (switch S2 is opened)

2.5. Fault detection investigation thyristor base AC-DC converter operation

In all previous part a deep study on AC-DC fault detection have been presented under thyristor operation by fire angle $\alpha = 0$. This part presents new pattern identification by change of fire angles.

2.5.1 Pattern identification

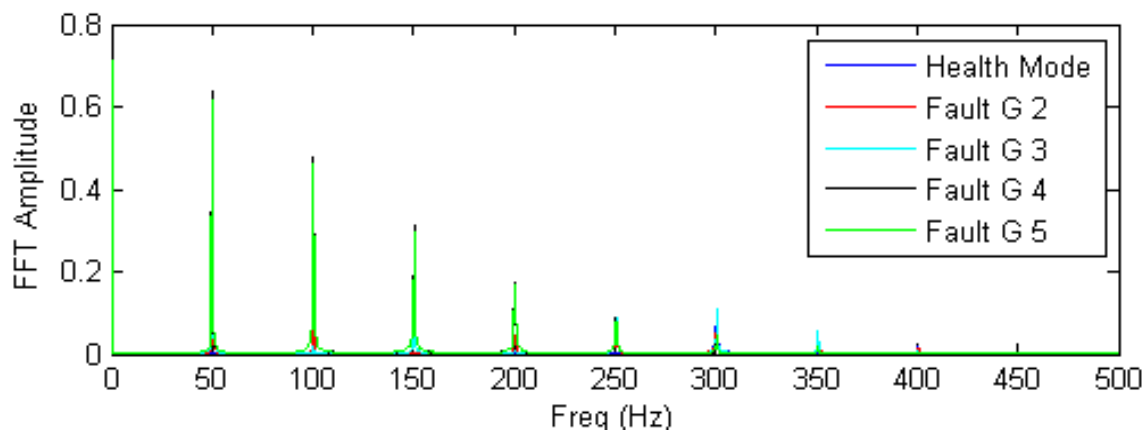
The process of open phase fault detection on thyristor based AC/DC converter switches repeated same as section 2.5, with the difference that we used of fire angle regulator for access to several different degrees (in this work, for $\alpha = 0$, $\alpha = 15^\circ$, $\alpha = 30^\circ$, and $\alpha = 45^\circ$). In this case we can be sure about effects of fire angle variation on pattern. Each group of mentioned faults in table (4.1) will lead to production especial frequently harmonics that not observed in Dc-bus current FFT analysis under health state operation. Figure (4.17), (4.18) and (4.19) show the FFT analysis on DC-Bus current under said fire angles.

In figure (4.17), the comparison between Dc-bus current under health state operation and under open phase fault by opening switches in conditions of group 2/3/4/ and 5 with fire angle of $\alpha = 15^\circ$ is presented. This test repeated for fire angles variations under $\alpha = 30^\circ$ and $\alpha = 45^\circ$ frequently in figure (4.18) and (4.19). The amplitude of harmonics in no load will increase with increase in the severity of fault in group 2, 3, 4 and 5 respectively. All mentioned fault groups in table (4.1) and under all thyristor fire angles change harmonic component in f_f , $3f_f$ and $5f_f$ and so on. As final result, it can be considered as a new pattern for AC-DC converter open phase fault detection in all groups presented in table (4.1) as (4.2):

$$f_{open_phase\ fault} = (2k + 1)f_f \quad (4.2)$$

Where $k = 0, 1, 2, 3 \dots$ and f_f is index of fundamental frequency.

However in group 2, the severity of fault is very low and because of presence of capacitor, even in full load, EV is able to continue its work. But it will lead to increase of temperature and decrease of efficiency and life time of motor and finally increase of cost.



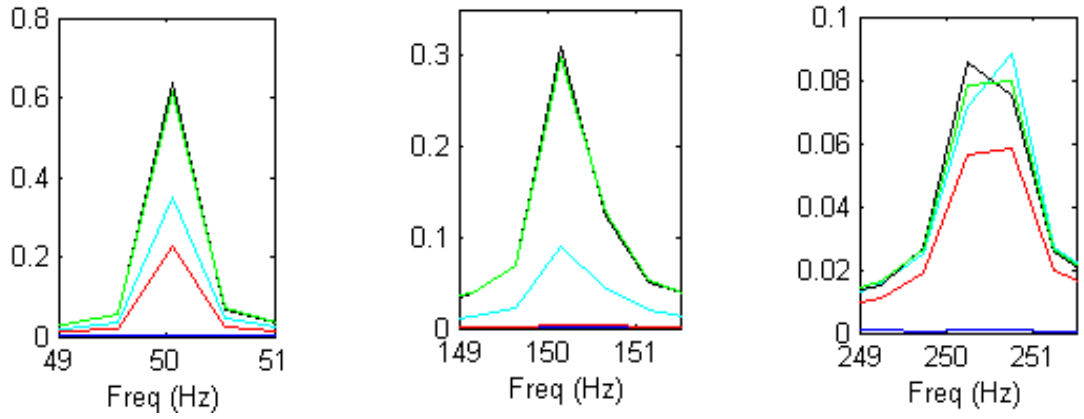


Fig. 4.17 : FFT analysis under health and all faulty states operation (G2 – G5) with thyristor fire angle of ($\alpha=15^\circ$)

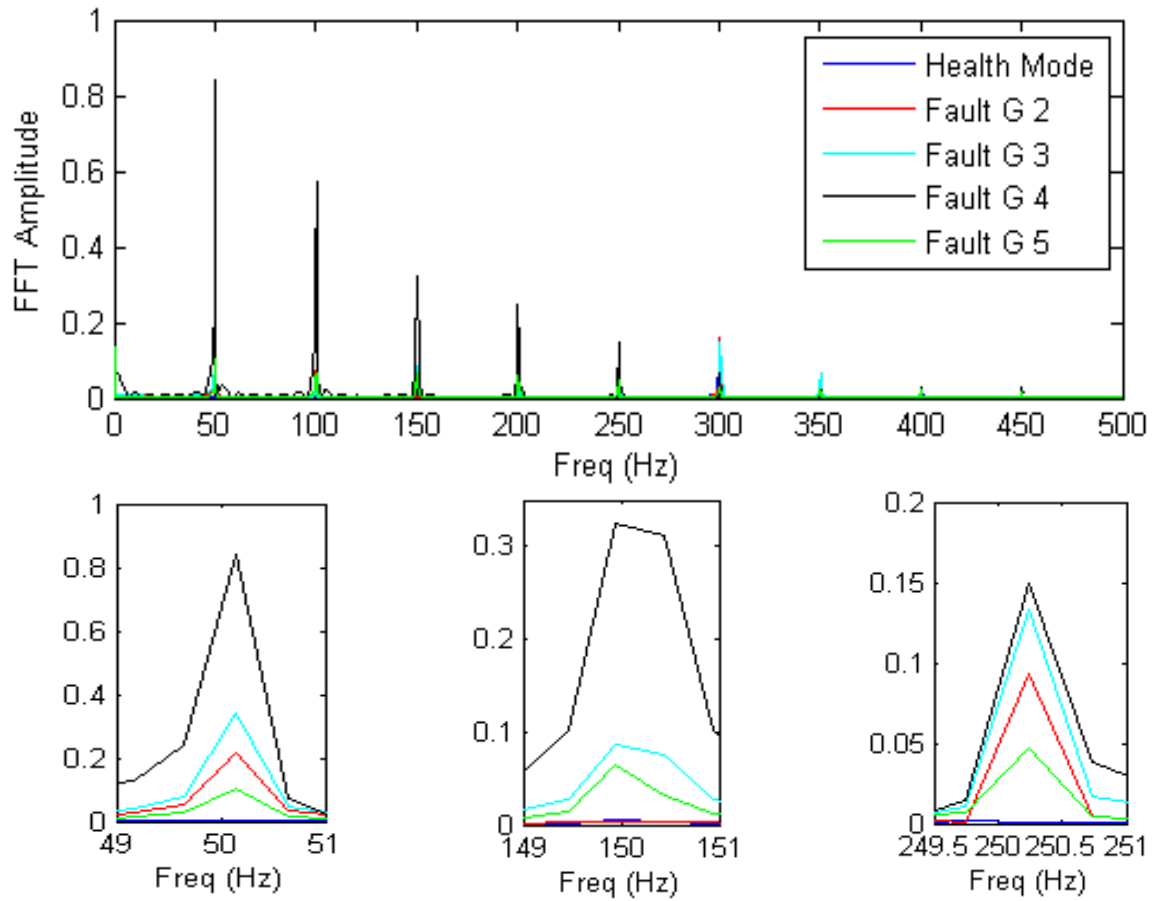


Fig. 4.18 : FFT analysis under health and all faulty states operation (G2 – G5) with thyristor fire angle of ($\alpha=30^\circ$)

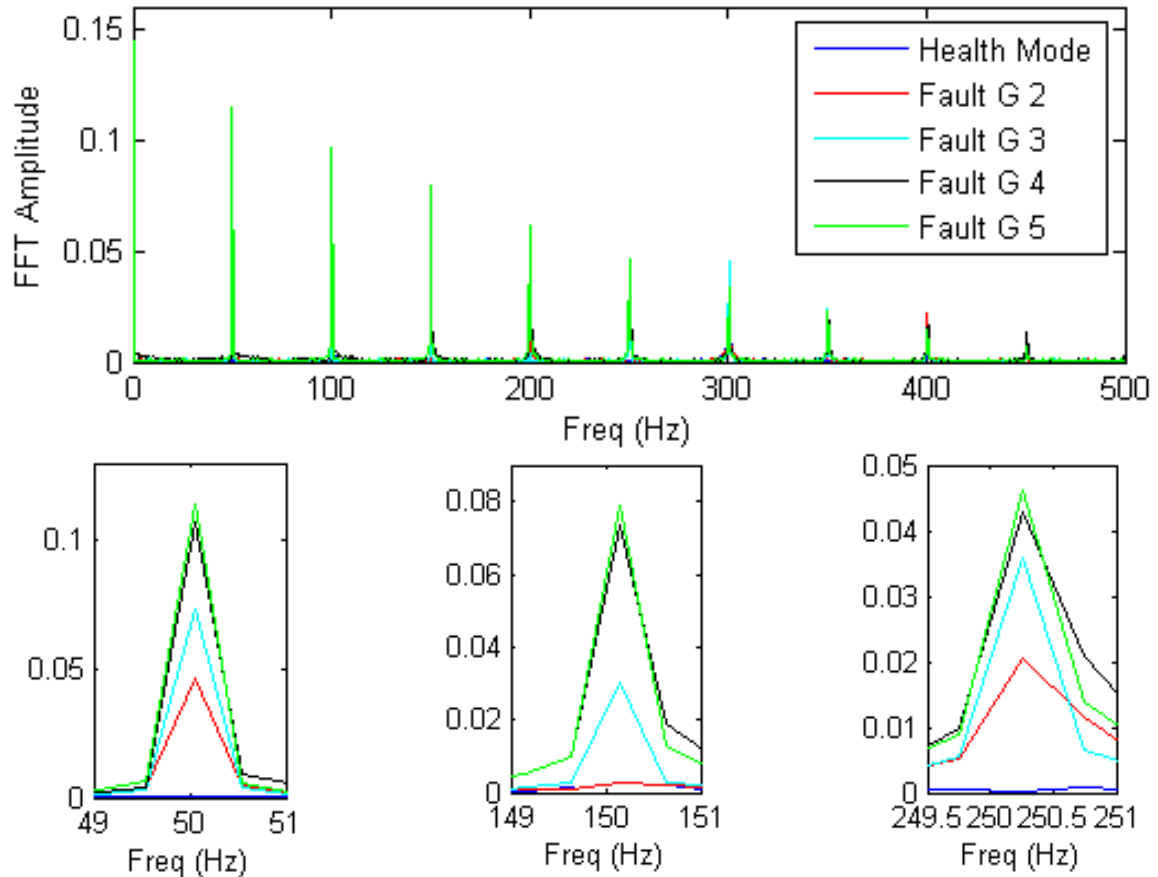


Fig. 4.19 : FFT analysis under health and all faulty states operation (G2 – G5) with thyristor fire angle of ($\alpha = 45^\circ$)

2.6. Fault sensitive modeling DC/AC inverter

As it is mentioned in introduction of present chapter, DC/AC inverter is the electric power crossing bridge to electric machine as well as AC/DC converters.

In chapter 1, section 5.3, the main perspectives of power converter requirements, power converter control methods, performance specification and challenges have been presented. Also chapter 2 sections 3.8 presented a quick state of the art on DC/AC inverters and different condition monitoring technique for power converter fault detection.

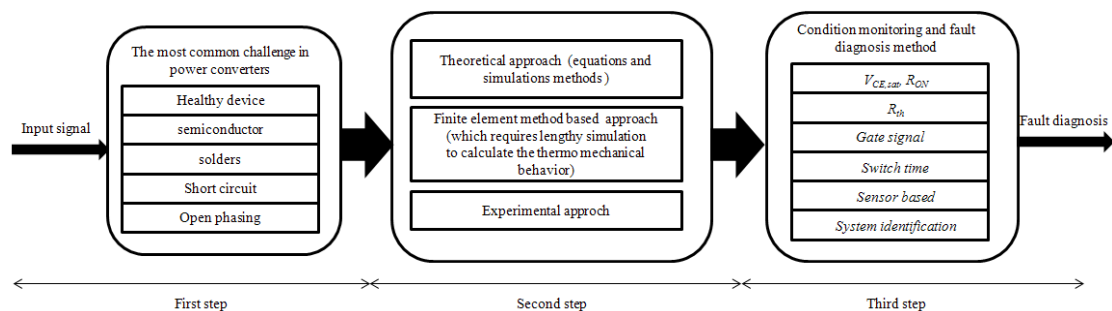


Fig. 4.20 : Model of identification and diagnosis of power converter fault in electric vehicles

Modeling procedure of abnormal sources of power converter in order of fault diagnosis is shown in figure (4.20). In the first step, the most common challenge of power electronics devices have been presented. The main abnormal noise sources of power converter for electric vehicles are taken into account in this model. The second step has been proposed different methods of fault investigation and in the end, the third step discusses about different signal processing method to reach to power converter fault diagnosis.

Figure (4.21) shows a modeling procedure of unbalanced voltage fault diagnosis caused by open phasing in DC/AC converter of PMSM drivetrain. Motor voltage and current amplitude changes (and also FFT analysis on motor current) are highlighted by literatures as well as mentioned in chapter 2 as a proper feature to detection of these types of faults. ANN is used to classify the different percentage of unbalanced voltage.

Figure (4.22), shows 3 phase motor voltage in healthy operation of motor and DC/AC converter. The voltage wave form seems near sinusoidal and symmetric. The distortion can be cause of used filter in input of data acquisition block in Matlab Simulink. In case of outbreak of one switch of DC/AC power converter, a open phasing fault occur that lead to unbalance voltage in input of motor as shown in figure (4.23). The current of open circuited phase will be zero and the current of two other phases will be asymmetric as shown in figure (4.24).

According to mentioned equation in chapter 2 section 3.4, by knowing V_{max} , V_{min} , and $V_{average}$, the percent of unbalanced voltage (UV%) can be calculate easily. According to speed and voltage changes under open phase fault, different percentage of unbalanced voltage can be resulted. Figure (4.25) and (4.26) show an example of change of speed (800rpm) and its effect on voltage and current amplitude. This change lead to new UV% (in this example 15%) in comparison by figure (3.23) that introduced 13% unbalanced voltage in rated speed (1000rpm) and no load operation. As the same of unbalanced voltage, this feature can be defined for unbalanced current (UC%) too.

Electric vehicle application force us to diagnosis all possible states in order of this fault. However it seems by loss of current of one phase, the continue of operation will experience a dangerous situation, but also by knowing the severity of fault, it would be possible to operation under degraded mode.

In this base, different test under various speeds and load, as we explained it in previous part for AC/DC converter, aiming to find suitable feature have been done to train ANN that will explain in chapter 5.

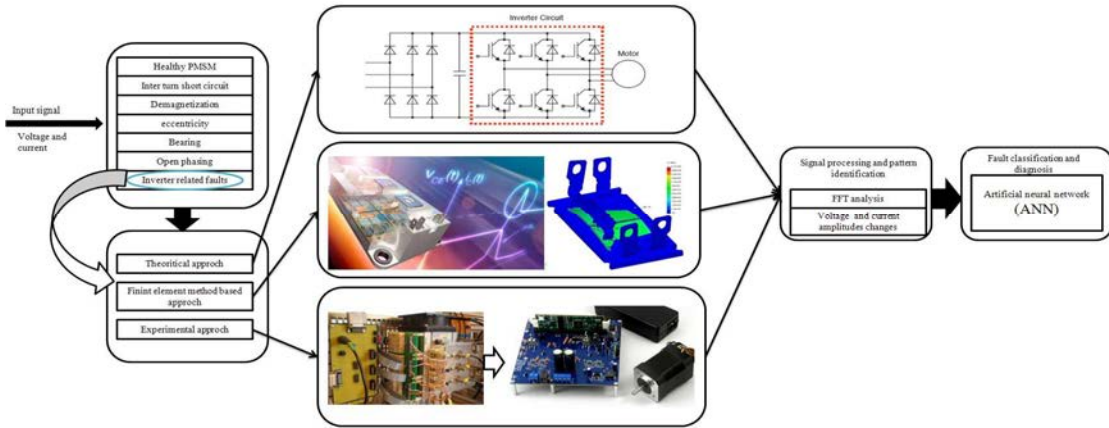


Fig. 4.21 : Model of identification and diagnosis of open phasing fault of DC/AC power converter for electric vehicles

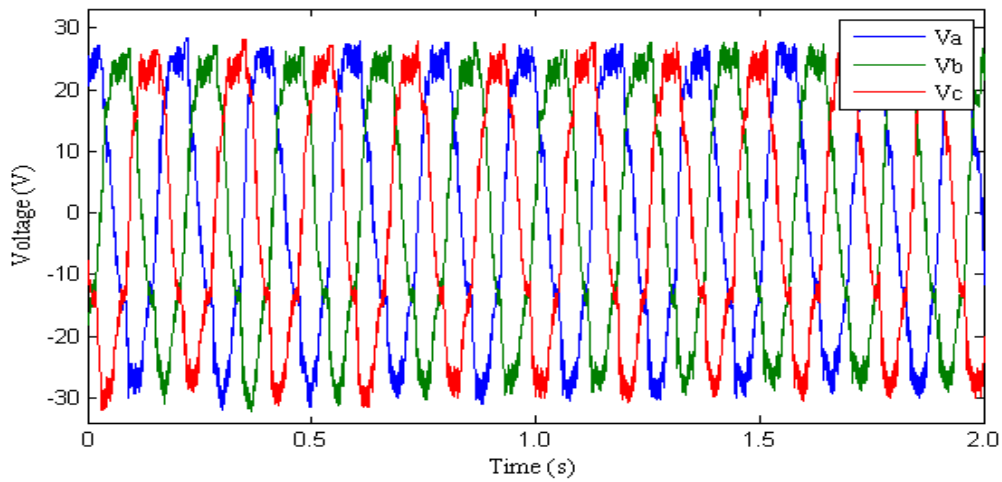


Fig. 4.22 : 3 phase motor voltage in healthy operation in 1000 rpm

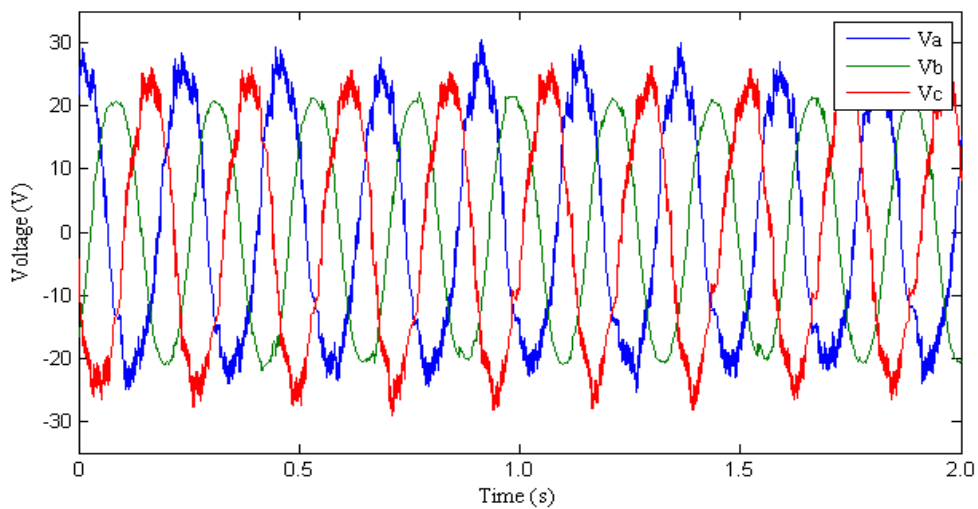


Fig. 4.23 : 3 phase motor voltage in faulty operation in 1000 rpm and no load (13% UV)

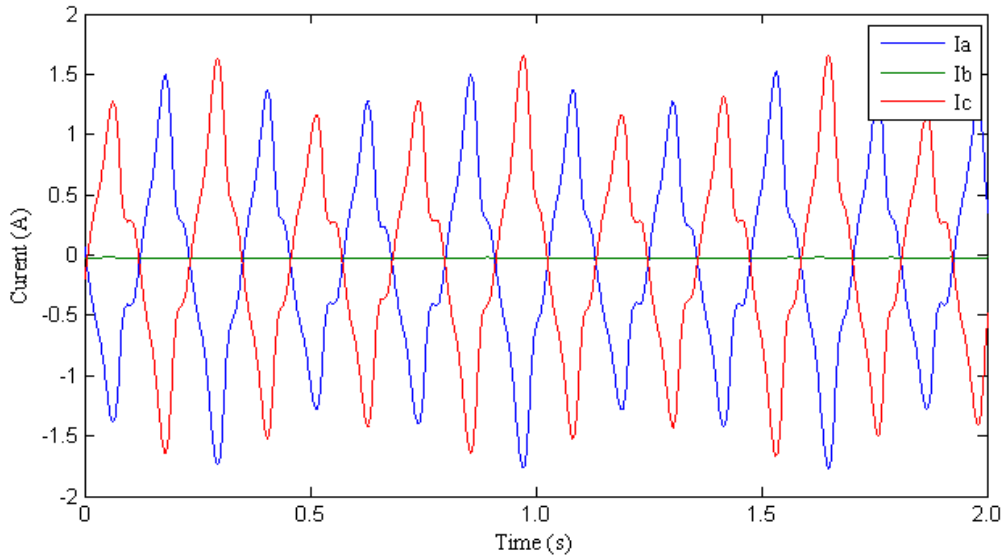


Fig. 4.24 : 3 phase motor current in faulty operation in 1000 rpm and no load (22% UC)

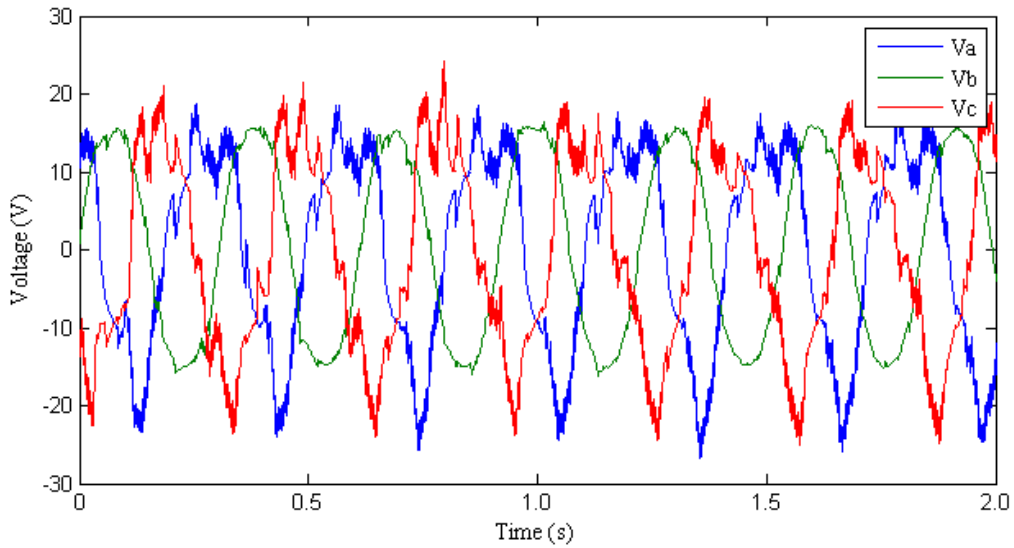


Fig. 4.25 : 3 phase motor voltage in faulty operation in 800 rpm and no load (15% UV)

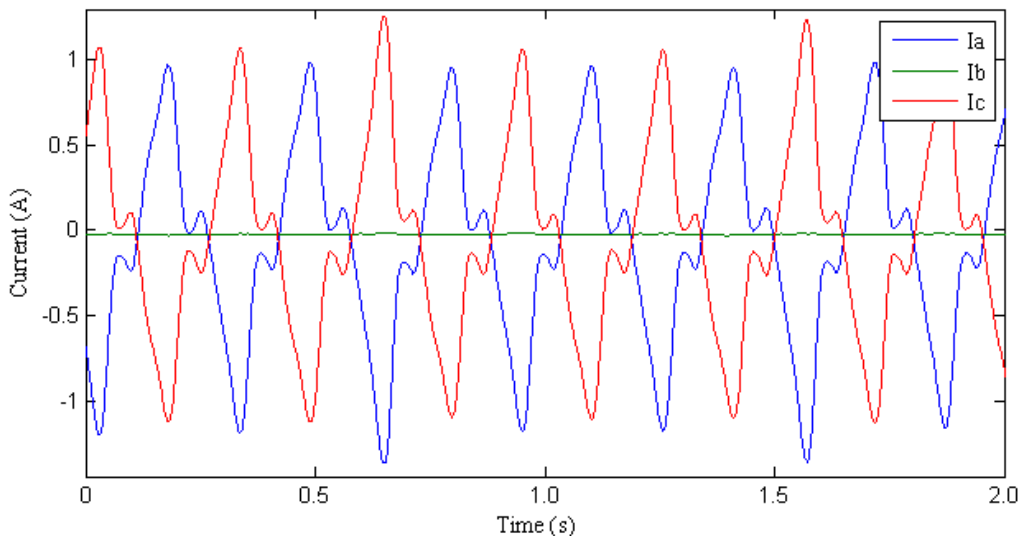


Fig. 4.26 : 3 phase motor current in faulty operation in 800 rpm

The effect of speed and load changes lead to have different percentages of unbalanced voltage. It will be interesting to classify them. It will provide the possibility of fault tolerant control and degraded mode design methodology.

3. Conclusion

In this chapter, a fault sensitive modeling of power converter has been purposed. Fault detection in thyristor based AC-DC converter with fire angle $\alpha = 0$ has been firstly studied. A new pattern identified such that:

$$f_{open_phase\ fault} = \frac{(2k+1)f_f}{2}$$

As a frequency pattern was introduced to aim AC-DC converter switches fault recognition for application as SHEV. The experimental results are used to verification of simulation results. On this basis, 5 groups of different states of AC-DC converter switches failures have been considered and difference of analysis results are compared with group 1 (healthy state of operation) by aim of finding feature those lead to a new pattern in fault condition.

This result has been validated through theoretical simulations but also experimental measurements. This allowed us to use the developed software tool to study the influence of capacitor size changes, and load and speed variations on the identified pattern. The obtained results show successfulness of this pattern.

To make this study widely applicable the case of the full thyristor-bridge has been also treated. In this case 3 fires angles such as $\alpha = 15^\circ$, $\alpha = 30^\circ$ and $\alpha = 45^\circ$ have been considered. A new pattern in these conditions was introduced as:

$$f_{open_phase\ fault} = (2k+1)f_f$$

Finally, an ANN based fault detection and diagnosis strategy and the related algorithm have been developed to show the way of using the identified patterns in the supervision and the diagnosis of the AC-DC converter in the drive train of SHEVs.

4. References of chapter IV

- [1] Harvey J. Schwartz, "A Summary of HEV Propulsion Technology", IEEE Transactions On Vehicular Technology. Vol. Vt-32. No. 1, February 1983.
- [2] Alcalá, A. Claudio, G. V. Guerrero, "Analysis of Propulsion Systems in Electric Vehicles", 2nd International Conference on Electrical and Electronics Engineering (ICEEE) and XI Conference on Electrical Engineering (CIE 2005) Mexico City, Mexico. September 7-9, 2005.
- [3] Ali Emadi, Young Joo Lee, and K. Rajashekara, "Power Electronics and Motor Drives in Electric, Hybrid Electric, and Plug-In Hybrid Electric Vehicles"; IEEE Transactions On Industrial Electronics, Vol. 55, No. 6, June 2008.
- [4] Mehdi Rahiminejad, Chris Diduch, Maryhelen Stevenson, and Liuchen Chang, "Open-Circuit Fault Diagnosis in 3-Phase Uncontrolled Rectifiers", 3rd IEEE International Symposium on Power Electronics for Distributed Generation Systems (PEDG) 2012.
- [5] Fabien Meinguet, Paul Sandulescu, Xavier Kestelyn, and Eric Semail, "A Method for Fault Detection and Isolation Based on the Processing of Multiple Diagnostic Indices: Application to Inverter Faults in AC Drives", IEEE Transactions On Vehicular Technology, Vol. 62, No. 3, March 2013.
- [6] M. Abul Masrur, ZhiHang Chen and Yi Lu Murphey, "Intelligent diagnosis of open and short circuit faults in electric drive inverters for real-time applications", Power Electronics, IET (Volume:3 , Issue: 2 , Date of Publication: March 2010 , Page(s): 279 - 291 , ISSN : 1755-4535.

Chapter V

Supervision and diagnosis of the PMSM drivetrains for SHEV application

1. Introduction	149
2. Global strategy of supervision and diagnosis of drive-trains of SHEVs	149
2.1. Level 0	150
2.2. Level 1	150
2.3. Level 2	151
2.4. Level 3	151
3. Global algorithm of drive-trains fault diagnosis and classification.....	152
4. ANN Based Fault Diagnosis of Stator Winding Inter-Turn short circuit ...	154
4.1. Justification of ANN for Using Inter-Turn Fault Diagnosis.....	154
4.2. ANN training.....	156
4.3. Implementation of short circuit fault diagnosis by using ANN	158
5. ANN Based Fault Diagnosis of switch open circuit of AC-DC Power Converter.....	160
5.1. Justification of ANN for using AC-DC fault diagnosis.....	160
5.2. ANN training.....	161
5.3. Implementation of open phase fault diagnosis in AC/DC converter by Using ANN	163
6. ANN based fault diagnosis of switch open circuit of DC-AC power converter	165
7. Conclusion.....	167
8. References of chapter V	169

1. Introduction

Recently neural network fault detection based methods have been used in fault detection and diagnosis. Neural networks offer a number of advantages, including requiring less formal statistical training, ability to implicitly detect complex nonlinear relationships between dependent and independent variables, ability to detect all possible interactions between predictor variables, and the availability of multiple training algorithms. Disadvantages include its "black box" nature, its greater computational burden, proneness to over fitting, and its empirical nature of model development [1] and [2].

In this chapter, a Multilayer Perception (MLP) feed-forward neural network has been employed to classify the PMSM drivetrains faults. Different kinds of inter turn short circuit fault in stator winding of PMSM, different groups of switch breakout of AC/DC power converter and open circuit in DC/AC inverter faults have been detected by three dedicated ANN: 13 different classes of inter turn short circuit, 6 different classes of open phase fault in AC/DC converter and 13 different classes of unbalanced voltage caused by open circuit in DC/AC inverter have been detected, classified, and introduced as contribution of this ANN diagnosis model. In this regard, the sensitive models developed in chapters 3 and 4 are employed to train ANN to reach the said goal.

This chapter firstly presents a global strategy of SHEV diagnosis, and then explains the used ANN structure to reach the goals of that diagnosis strategy. Also, the ANN modeling process for each component of the PMSM drivetrains is exposed.

2. Global strategy of supervision and diagnosis of drive-trains of SHEVs

The diagnosis process developed within this thesis concerns the drivetrains of the SHEV (see chapter 1, figures (1.5) and (1.6)). The part of the drivetrain which we focused through this study consists in the AC/DC converter, the PMSM and DC/AC converter with its vector control.

Regarding to whole the vehicle, the drivetrain becomes just one subsystem among a lot of other subsystems as for example the ICE, the harness including the power grid, the measurements and the control, the navigation system, etc. Thus the faults can be divided in different levels according to the depth of their location within the vehicle (see figure (5.1)). In this section we explain this scheme around our thesis work whose topics are pointed out by a green frame.

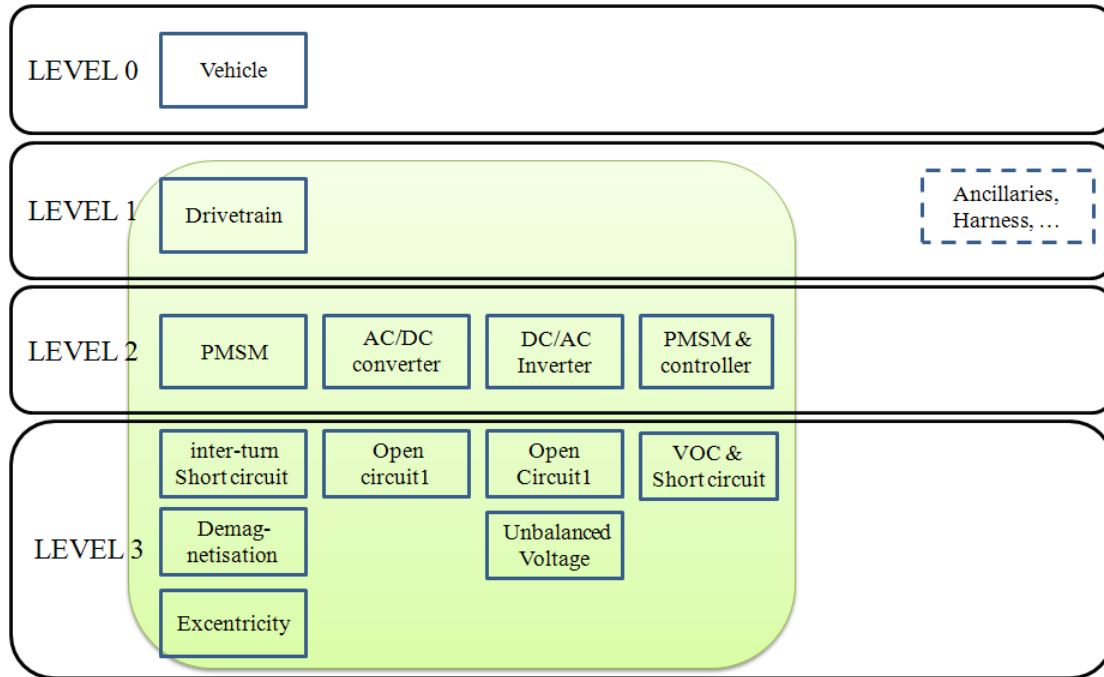


Fig. 5.1: Global strategy of supervision and diagnosis on drive trains of SHEV

2.1. Level 0

This level of diagnosis represents the vehicle itself and it includes all the external systems without which the vehicle may be immobilized. However the simplicity of these systems from a technical point of view makes those defects easily detectable by a simple user of the vehicle. This kind of defects consists for example a in broken windshield, bad windshield glasses, lack of administrative documents (technical control certificate, license, ..) and so on. In this level 0 of diagnosis no automatic supervision is necessary so it can be done by a visual inspection only (see figure (5.2)).

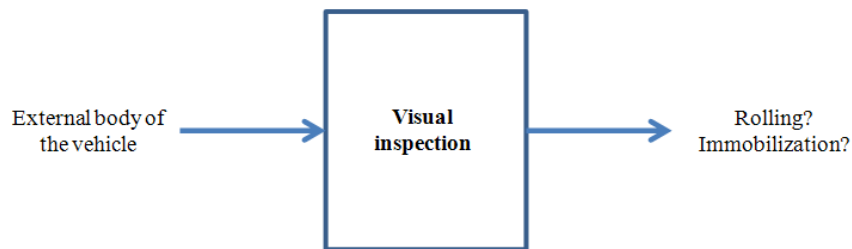


Fig. 5.2 : Illustration of the "Level 0" of the vehicle diagnosis

2.2. Level 1

This diagnosis level takes care about the functionalities of main systems inside the vehicle. These devices generally called subsystems or main components include the powertrain, the embedded grids (or the electrical harness), the ICE, the steering column, wheels, etc. In this level 1, a defect is detected through a basic supervision algorithm in which sensors send to the main Electronic Control Unit (ECU) the State of Operating of

each Subsystem (SOS). Thus a Boolean supervision algorithm (true/false) sends a fault signal and indicates the subsystem in which the false input is detected (see figure (5.3)).

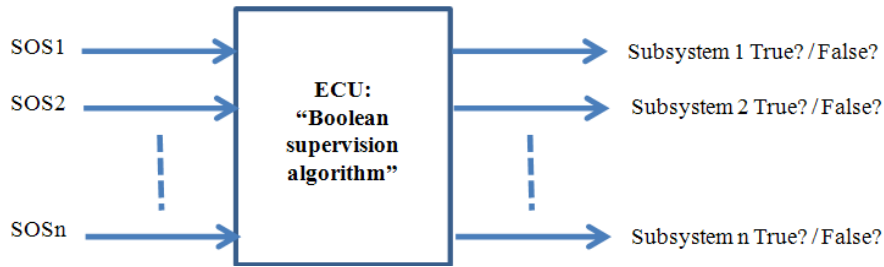


Fig. 5.3 : Illustration of the “Level 1” of the vehicle diagnosis

2.3. Level 2

The level 2 of the diagnosis deals with the faulty main components of the vehicle indicated in the level 1. The subsystem considered in our work is the PMSM drivetrain. The aim of the level 2 is to indicate accurately which component of the drivetrain is in fault i.e. the PMSM, the AC/DC power converter, the DC/AC power converter or the PMSM automatic control. This supposes that a classification of faults has been done so that starting from the measurements of currents, voltages, angular speed, angular position and stator vibrations to define which of these four components manifest abnormal behavior? The response on this question gives the component operating in faulty mode (see figure (5.4)). This diagnosis level 2 will have an interest once it is done on line in order to offer the possibility for the vehicle to run in degraded modes. Indeed, this kind of running is very important in transport application where the availability is a first necessity.

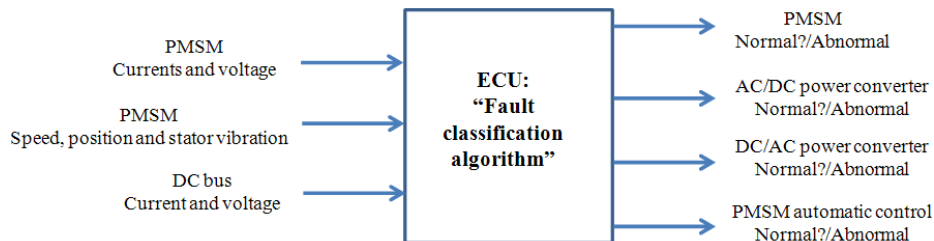


Fig. 5.4 : Illustration of the “Level 0” of the vehicle diagnosis

2.4. Level 3

When an abnormal behavior is identified in on subsystem our diagnosis strategy is to evaluate the fault severity and its impact on the subsystem performance. The loss of performance can be expressed through a function between 0 and 1 traducing the actual State Of Health (SOH) of the subsystem. That parameter can be used in a control algorithm in degraded mode of the drivetrain. To evaluate efficiently the parameter SOH it is necessary to have a deep knowledge on the corresponding system. In the frame work of this thesis, this study has been developed on the drive train. This was achieved through the sensitive modeling of defects presented in Chapters 3 and 4, but also through the proportion of models based on ANN. These models, subject of the next

section of the present chapter, allow evaluating the SOH parameter of each component. Thus a subsystem SOH algorithm will be used to evaluate the SOH of the PMSM drivetrain (see figure (5.5)).

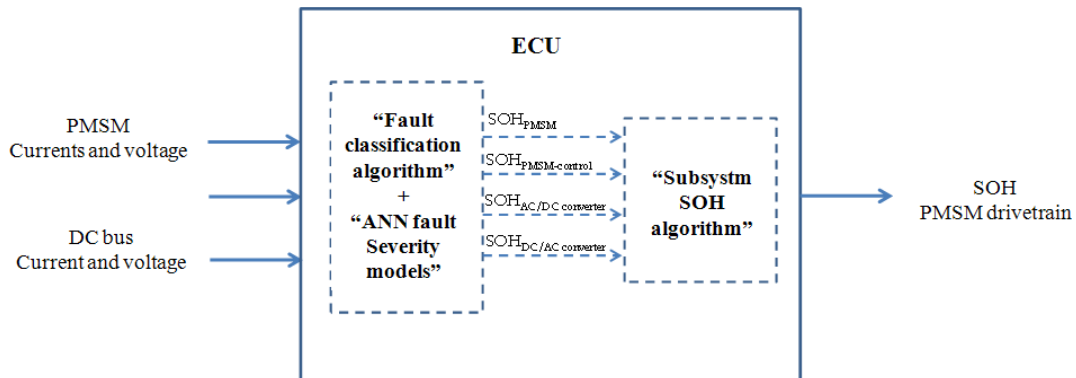


Fig. 5.5: Illustration of the “Level 3” of the vehicle diagnosis

3. Global algorithm of drive-trains fault diagnosis and classification

The most important part of diagnosis strategy by using ANN is proper pattern identification, usable to training ANN. Because of electromotive application in this work, the ANN must be able to detect the fault but also to evaluate its severity so that to be able to evaluate if the subsystem is in trip or can continue its mission.

But how ANN can help us to achieve these goals? Figure (5.6) show the synopsis representation of the proposed algorithm of drive-trains fault diagnosis and classification for SHEV application, where “Imbalance $\delta^* = 1$ ” introduce a consideration of symmetric 3 phase voltage of motor. It is obvious there is an inherent asymmetric in currents and voltages of most of motors because of their manufacturing process. In this base we consider that $V_{amax} = V_{bmax} = V_{cmax}$. During the three year of thesis, the developed ANN black box model can be used to diagnosis only inter turn short circuit, open phase and unbalanced voltage faults. So, three phase motor currents and voltages has been employed for inter turn short circuit and unbalanced faults while the DC-bus current has been used for AC/DC power converter fault. As it explained in chapter 2, FFT analysis is a suitable method in stationary state fault detection. Thus the FFT has been used to reach proper pattern identification by aim training ANN. It called ANN black box because of its complex function in classification of different existence states. In next section, a comprehensive explanation about structure of ANN has been presented as well as a detail statement of how fault diagnosis in each mentioned fault.

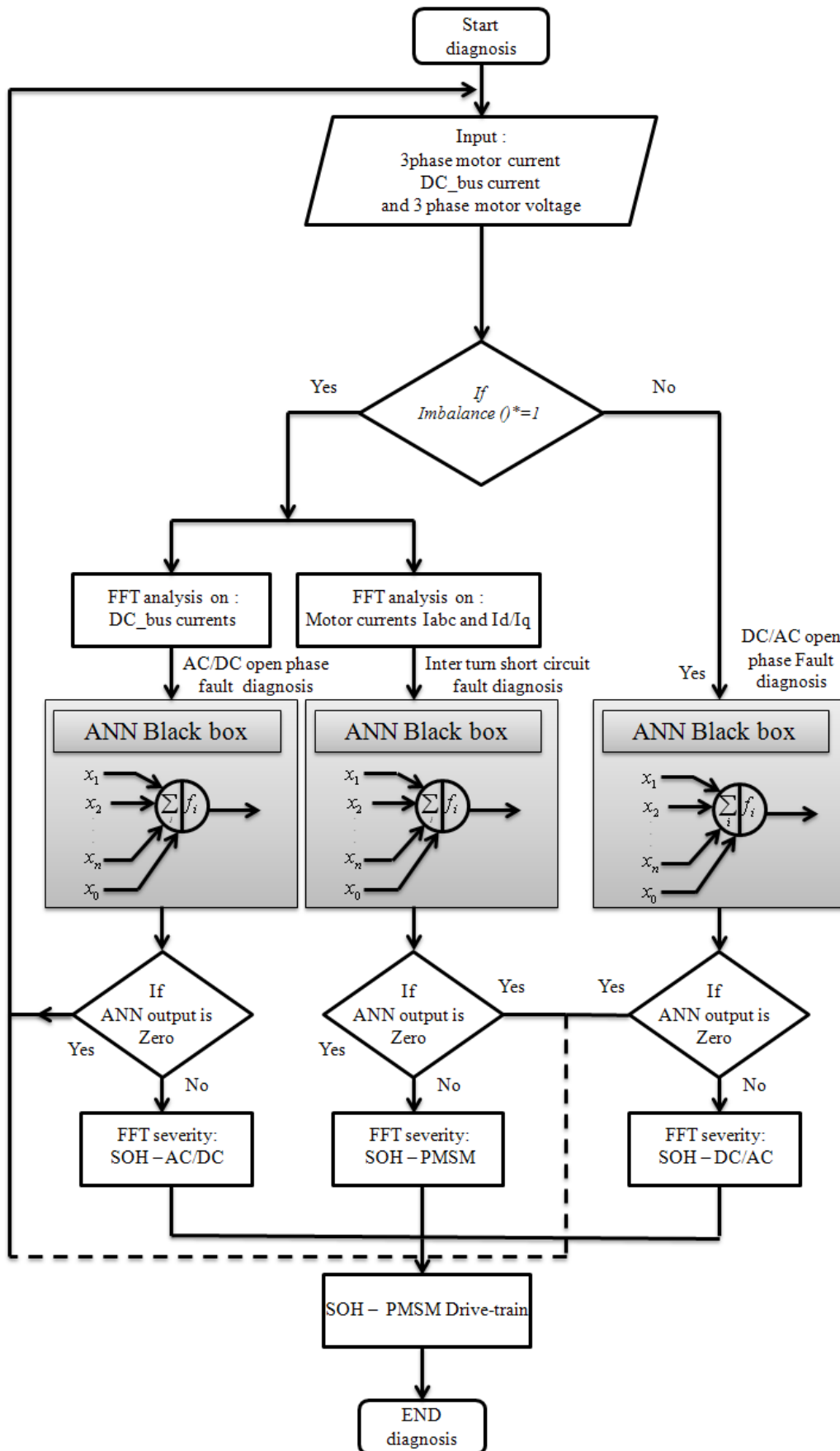


Fig. 5.6 : Implementation algorithm of drive-train fault diagnosis of SHEV

4. ANN Based Fault Diagnosis of Stator Winding Inter-Turn short circuit

In this work, a 3 layer feed-forward ANN has been used in order to fault diagnosis and classification. The structure of ANN is different according to raised issue.

There are no general rules to determine the number of hidden layers and hidden nodes; this also depends on the complexity of the mapping to be achieved. The number of input (input nodes) and output (output nodes) is of course determined by the specific problem. The number of neurons and connections limit the number of patterns a neural network can store reliably [3]. A comprehensive investigation about ANN structure and application has been presented in appendix 5A.

4.1. Justification of ANN for Using Inter-Turn Fault Diagnosis

A non linear ANN has been trained aiming to inter turn short circuit fault diagnosis of PMSM stator winding. The different groups defined in table (5.1) have a non-linear relation together (or maybe it is better to say, these groups have overlap together). So usage of some linear method (even linear ANN) will not be a good way to reach the goal.

Table 5.1 : Possibility of experimental short circuit faults efforts according introduced connection in chapter 3-figure (3.13).

Types Of faults	a1-N	a2-N	a3-N	b1-N	b2-N	b3-N	a1a2	a1a3	a2a3	b1b2	b1b3	b2b3	H
	C1	C2	C3	C4	C5	C6	C7	C8	C9	C10	C11	C12	C13
Fault percentage	2%	25%	35%	3%	30%	22%	6%	20%	5%	15%	18%	4%	0%
H: Healthy mode operation													

According to ability to implicitly detect complex nonlinear relationships between dependent and independent variables, ability to detect all possible interactions between predictor variables, and the availability of multiple training algorithms by ANN, and also according to complexity, nonlinearity relationship between dependant feature identified to detect different severity of inter turn short circuit, as these are shown in figure (5.7a, 5.7b, 5.7c, and 5.7d), the usage of ANN can be justified.

The training data include motor 3 phase currents amplitude, currents Id and Iq amplitude and also their FFT analysis components.

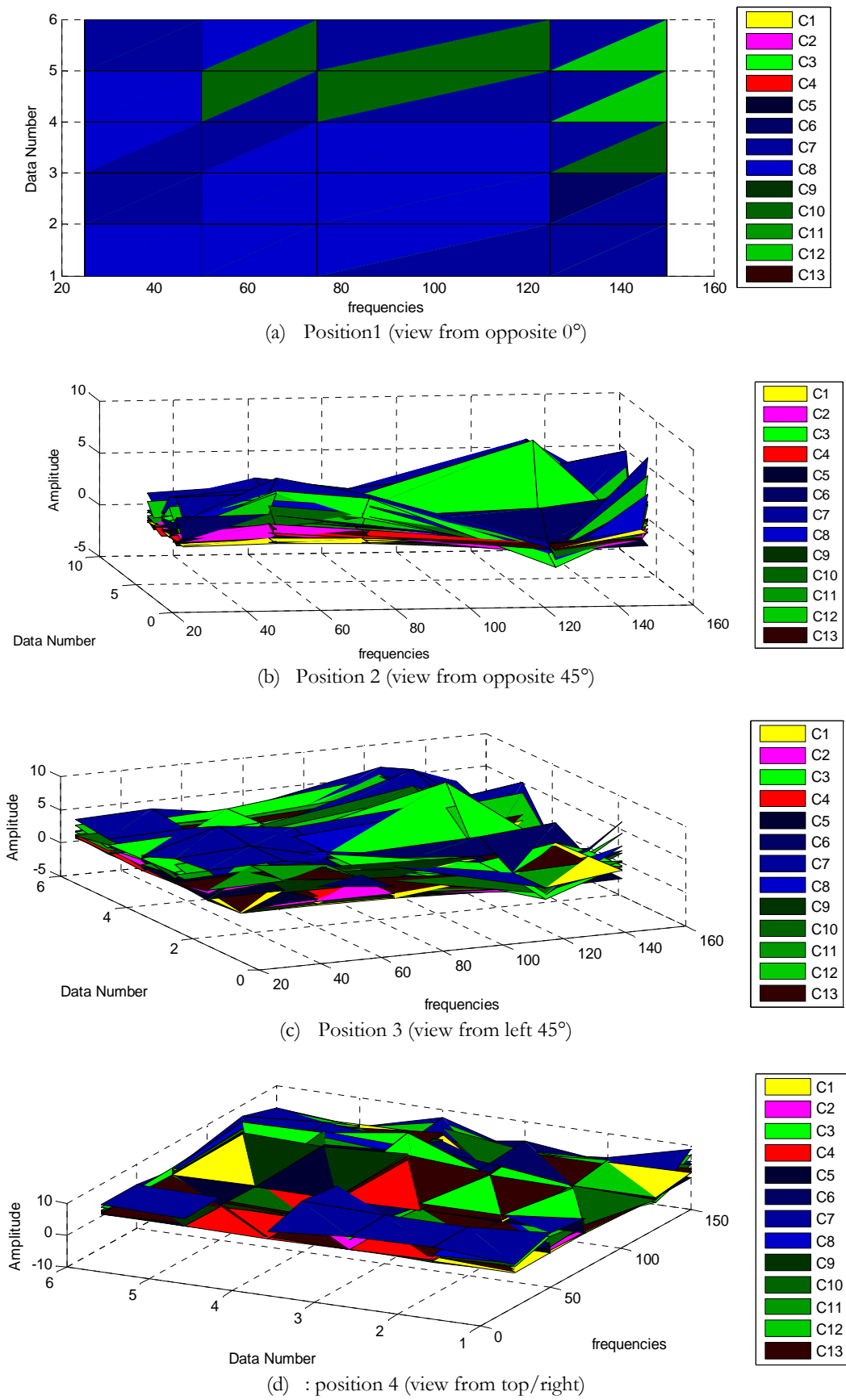


Fig. 5.7 : Different position of overlap between ANN training data,

4.2. ANN training

Before implementation of ANN by experimental test, we must train and test the ANN function. After finding proper feature (pattern) identification that was explained before (in this case: motor current amplitude and their FFT frequency component amplitude -- see chapter 3 section 4.1), these components have employed to train ANN. After training ANN, the last step will be test of ANN. If ANN gives a suitable response to these test, so it can be used for intended purpose otherwise, implement of a weakness trained ANN will lead to an error in processing. Figure (5.8) shows the ANN training efforts for 6 iterations. The results indicate the success of training ANN. All 13 different levels of short circuit mentioned in table (5.1) are trained and are detectable by ANN.

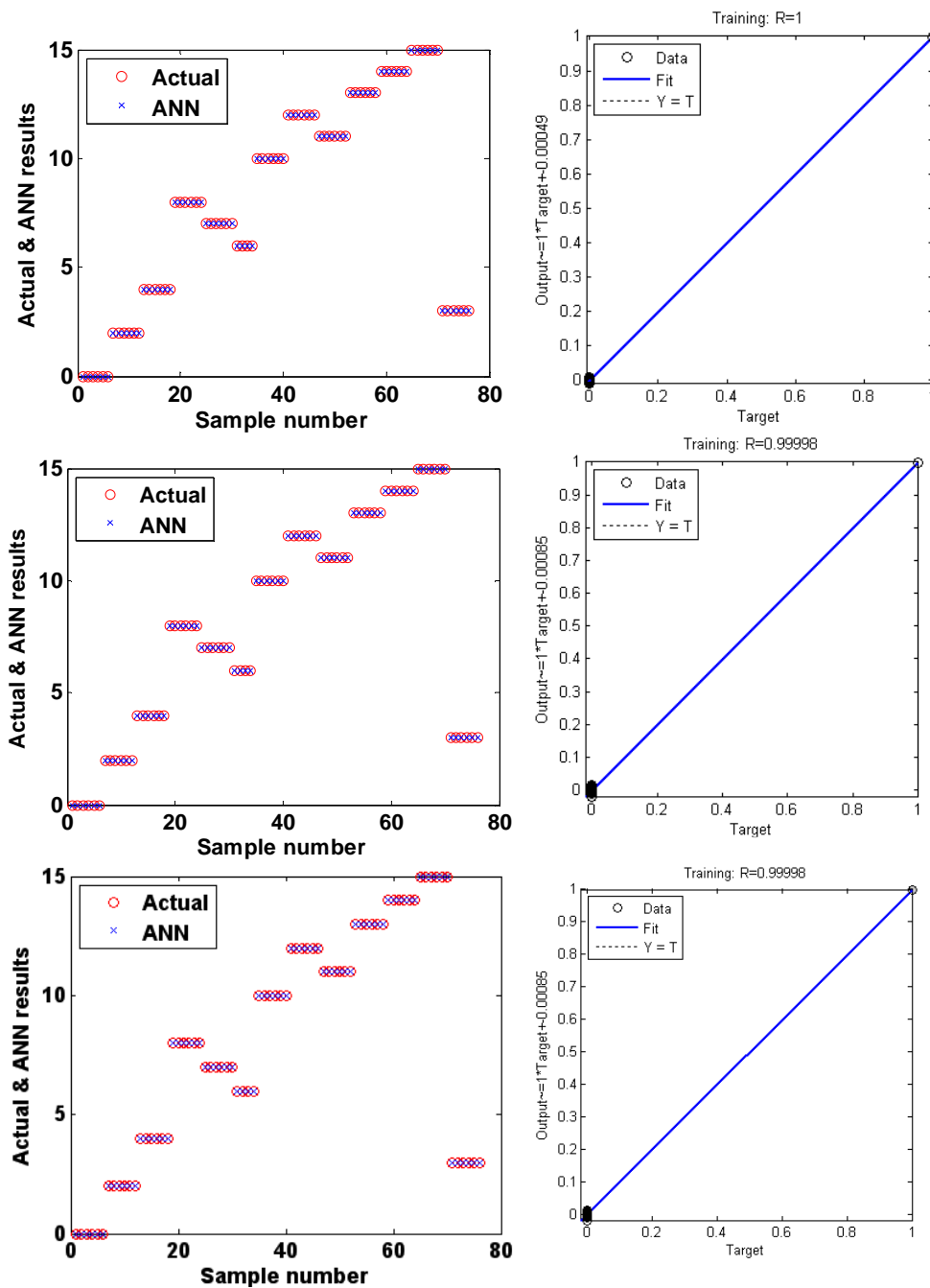


Fig. 5.8 : ANN training results for 6 iterations

After training ANN, and before implementing it, we test it by real experimental data to insure its performance correctness. Figure (5.9) shows the response of trained ANN to new faulty data. The response is acceptable to implement of trained ANN in experimental test.

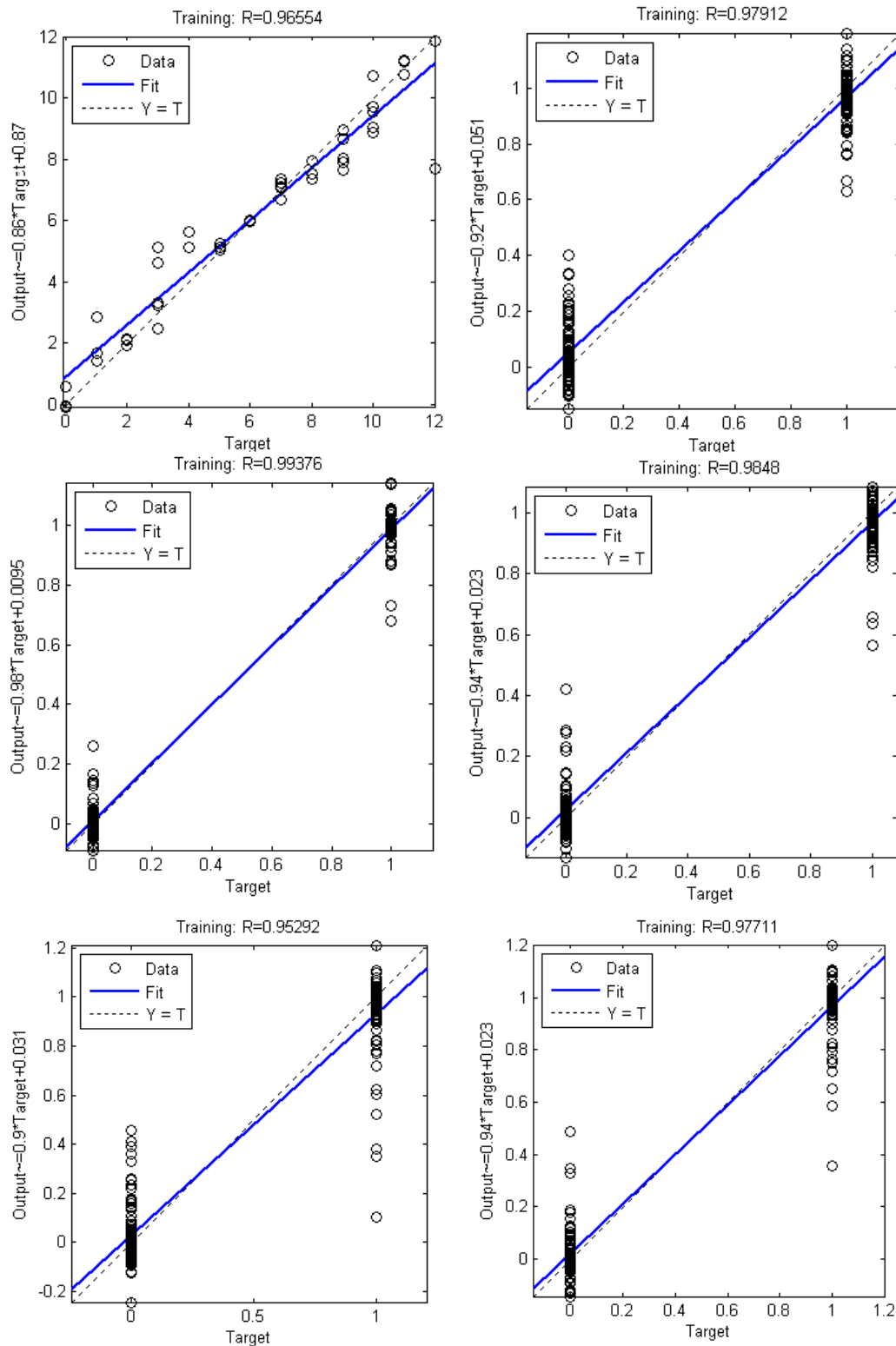


Fig. 5.9 : ANN based inter turn short circuit fault diagnosis test results for 6 iterations

4.3. Implementation of short circuit fault diagnosis by using ANN

The aim of this part of chapter is inter-turn short circuit fault diagnosis by possibility of different percentages of short circuited turns of stator windings of PMSM and in different speed and load, as it is expected in SHEV application by this fact that ANN is able to diagnosis all faults mentioned in table (5.1). The 4 steps of the implementation method of the ANN to fault diagnosis model developed for the short circuit diagnosis of the PMSM associated to its control device is shown in figure (5.10).

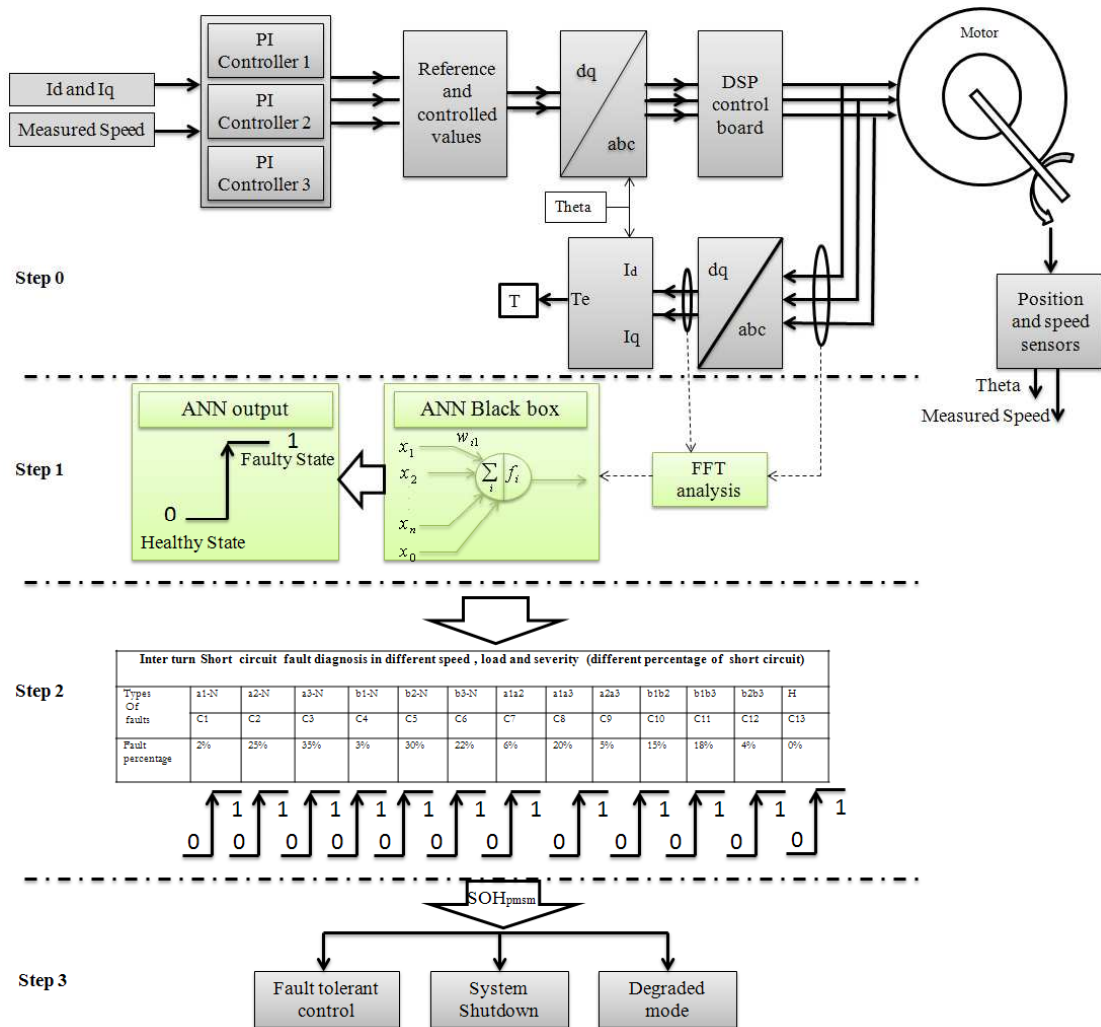


Fig. 5.10 : ANN based inter turn short circuit fault diagnosis implementation

The contribution of this work indicates three steps shown in figure (5.10): step 0, step 1 and step 2. The result of ANN can be used by one of mentioned objective in step 3. The step 3 will be considered as a future plan of this work. Table (5.2) shows the output of the implemented of ANN under different conditions of short circuit fault with various speeds and load. So, it can be used by designed strategy in step 3.

According to figure (5.10):

Step 0: In this step, a vector controlled PMSM has been employed for operation under different inter turn short circuit. The parameters of motor and description of test bench

have been explained in chapter 3. Three LEM 55 Hall Effect current sensors have been employed to data acquisition as needed for ANN usage.

Step 1: In this step an ANN black box is used to fault diagnosis. The contents and structure of ANN have been explained in present chapter section 4 thoroughly. In this base, after FFT of targeted data, the trained ANN analyses the data and produces results. The ANN output can be Zero (0): that means a healthy operation without fault and one (1): that means there is inter turn short circuit fault as it is shown in table (5.2).

Step 2: According to the diagnosis strategy, 13 outputs have been considered for the used ANN in this work. One output for healthy operation and remaining for different levels of short circuit. It was tested for 10 different data under faulty state as results are visible in table (5.2). These data can be used to evaluate the loss of performances of the PMSM i.e. the value of SOH_{PMSM} .

Step 3: in this step three perspectives of ANN output usage have been drawn. Fault tolerant control and degraded mode in order to ensure a continuity of service of the drivetrain. In fact, shutdown the system is easiest way but not a proper solution in electromotive application.

Table 5.2 : ANN output results under different level of short circuit in SHEV application

	Fault value	Load condition	Speed condition	Output 1 C1	Output 2 C2	Output 3 C3	Output 4 C4	Output 5 C5	Output 6 C6
1	Health	Half-load	600rpm	0.0009	0	-0.0002	0.0009	0	0
2	2%	Half-load	1000rpm	0.9975	0.0013	-0.0009	0.0013	0	0
3	3%	0.25-load	700rpm	0	-0.0008	0.0002	0.987	0.0006	0.0002
4	4%	No-load	800rpm	0.0016	-0.0023	0.001	-0.0023	0.0026	-0.0011
5	5%	Half-load	900rpm	0	-0.0023	0.0009	-0.0023	0.0024	-0.0001
6	6%	No-load	600rpm	-0.0013	0.0114	0.001	0.0014	0	0
7	15%	No-load	1000rpm	0.0013	0	0	0.0003	0.0043	0
8	18%	Half-load	700rpm	-0.0003	0.0014	0.0041	0.0104	0.0028	0
9	22%	0.25-load	900rpm	0.0079	0.0015	-0.001	0.0115	0.0017	0.9817
10	25%	No-load	800rpm	-0.005	1.00	-0.0006	0.0012	0	0.0036

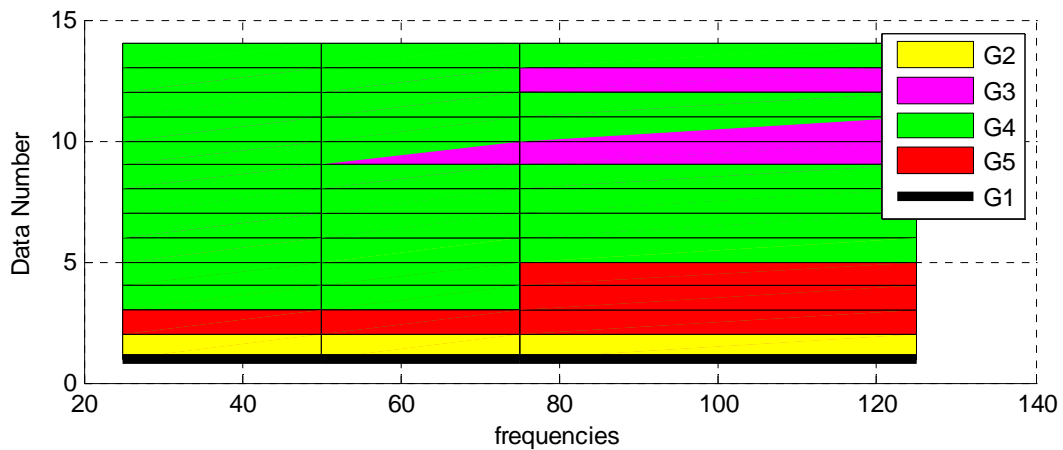
	Output 7 C7	Output 8 C8	Output 9 C9	Output 10 C10	Output 11 C11	Output 12 C12	Output 13 C13	Detection
1	0.0001	0.0001	0.0011	0.0004	0	-0.0052	0.981	T
2	-0.0007	0	0	-0.0007	0	-0.0009	-0.0011	T
3	0.0008	0	0.0018	0.0008	0.0002	0.0002	0	T
4	0.0044	0	0.0003	0.0044	0.975	0.0008	0	T
5	0.0044	0.0006	0.992	0.0044	-0.0001	0.0003	0	T
6	0.9909	0.003	0.0004	0.0007	0	-0.001	-0.0013	T
7	0.0004	-0.0004	0	0.977	0	0.0004	-0.0213	T
8	0.0001	0	0.0004	0.0031	0	0.96	-0.0013	T
9	0	0.0068	0	0	0.005	0.0001	0.0079	T
10	-0.0613	0.0008	0.0071	0.0013	0.0045	0.006	-0.0035	T

As it is explained in step 1, the value “1” in output of ANN show a fault in terms of each level and severity of short circuit in PMSM stator winding. This results can be used as mentioned in step 3.

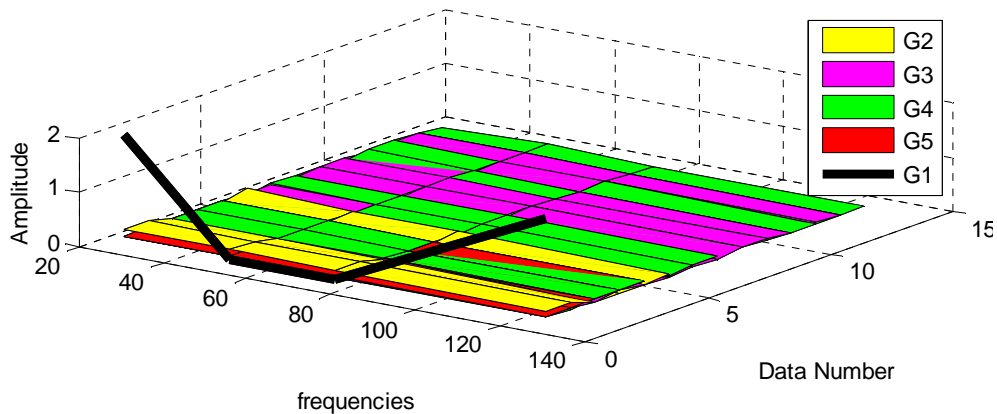
5. ANN Based Fault Diagnosis of switch open circuit of AC-DC Power Converter

5.1. Justification of ANN for using AC-DC fault diagnosis

The different groups defined in table (4.1) (chapter 4, section 2.1) have been considered to validate their non-linear relation together. According to this objective, firstly, all trained data to ANN draw in a 3D mapping to clarify their non-linearity as shown in figure (5.11a, 5.11b, 5.11c and 5.11d). According to complexity and nonlinearity relationship between training data and according to the power of ANN function to solve this types of problems (see section 4.1 of this chapter too) , we can justify using of ANN for these nonlinear structure. The training data include identified pattern in chapter 4 section 2.4.1 and 2.5.1.



(a) position 1 (view from opposite 0°)



(b) position 2 (view from left 45°)

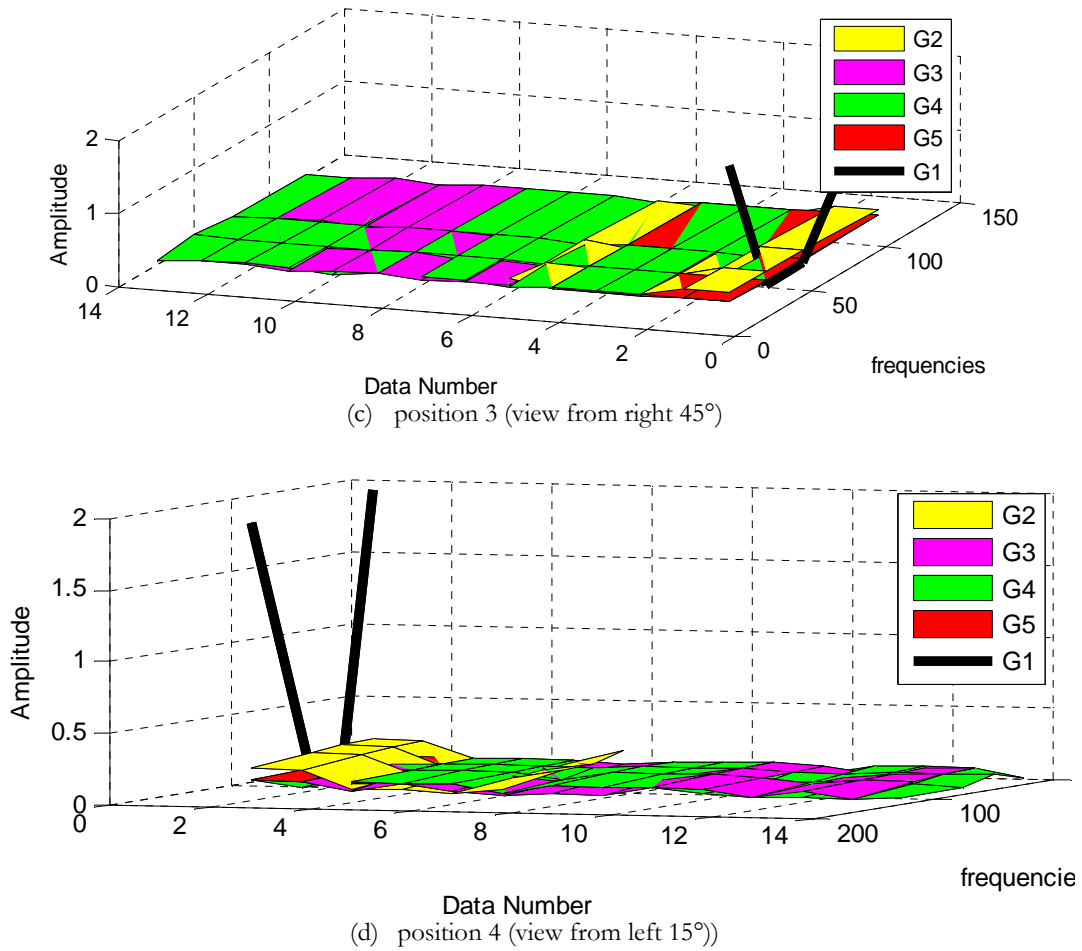
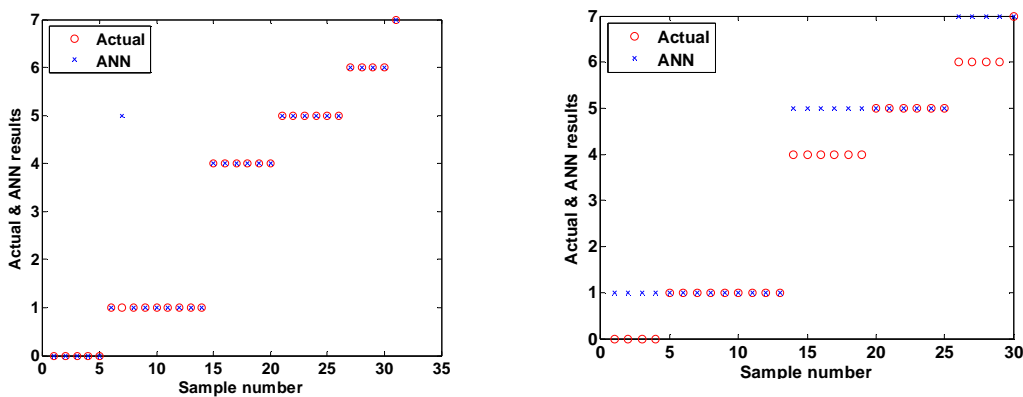


Fig. 5.11 : Different position of overlap between training data to ANN

5.2. ANN training

As in section 4.2 of this chapter, aiming to justify ANN, figure (5.12) show the ANN training efforts for 6 time repetition. The results indicate the success of training ANN. All 6 different levels of open circuit fault mentioned in table (4.1) of chapter 4, section 2.1 is trained and is detectable by ANN.



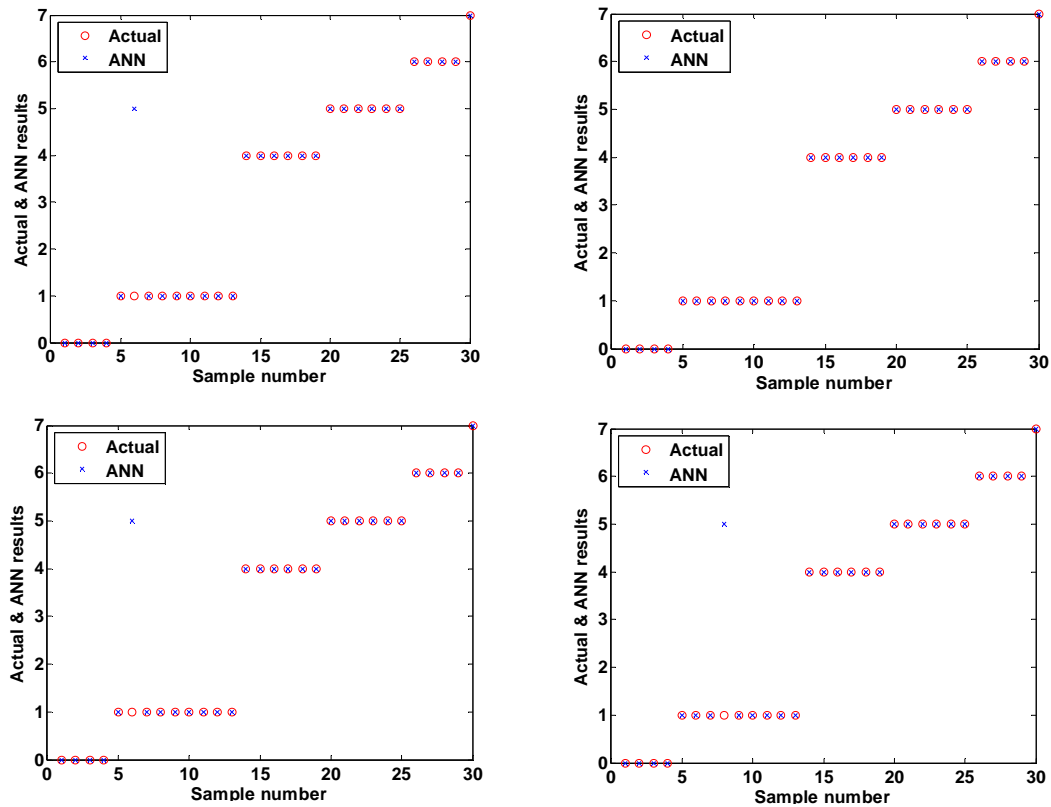
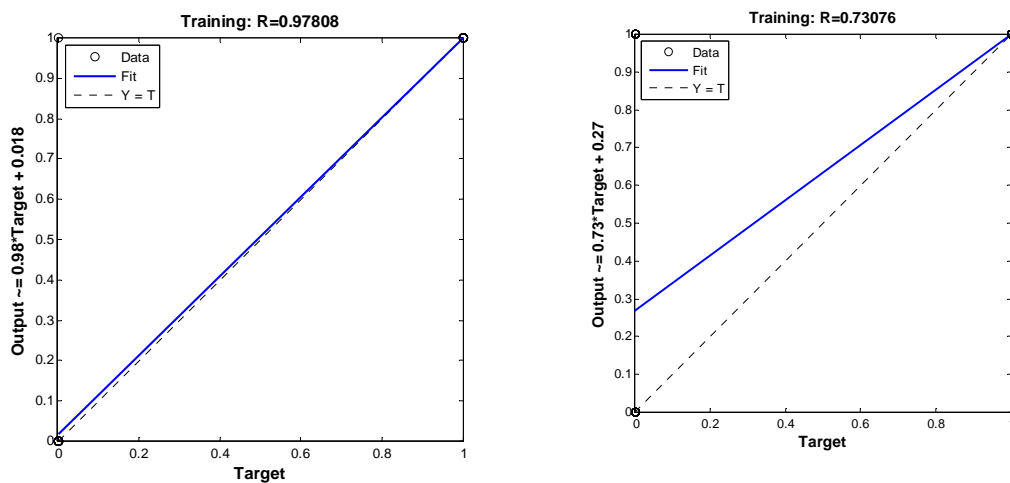


Fig. 5.12 : ANN training results for 6 iterations

Also same as in section 4.2 of this chapter, to ensure about ANN performance correctness, figure (5.13) show the response of trained ANN to new faulty data. The response is acceptable to implement of trained ANN in experimental test.



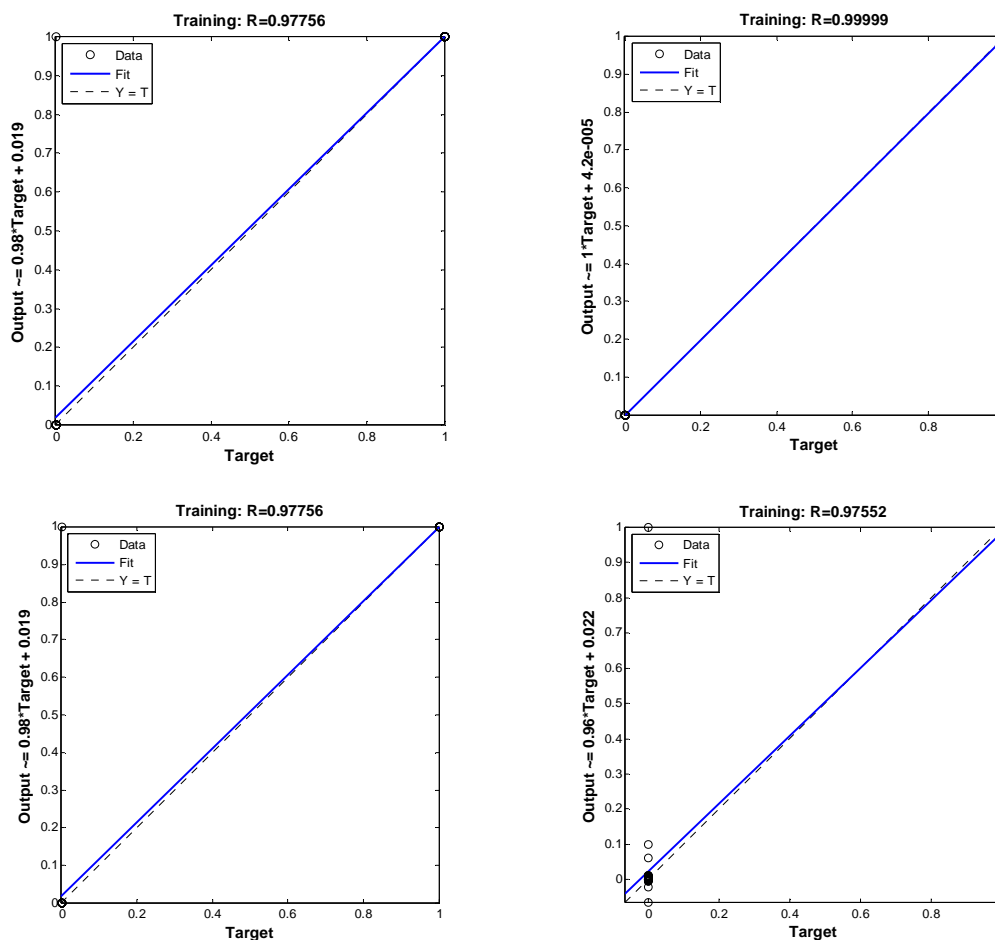


Fig. 5.13 : ANN result for fault diagnosis of AC-DC converter for 6 time repetition

5.3. Implementation of open phase fault diagnosis in AC/DC converter by Using ANN

The aim of this part is open phase fault diagnosis of AC-DC power converter switches. In this base, ANN will be able to detect each one of groups defined in Table (4.1) of chapter 4, section 2.1. Implementation strategy of fault diagnosis is shown in figure (5.14). The amplitude of frequencies of pattern has been used for training NN. The results after 20 times repetitions show 97.26% accuracy in trained ANN.

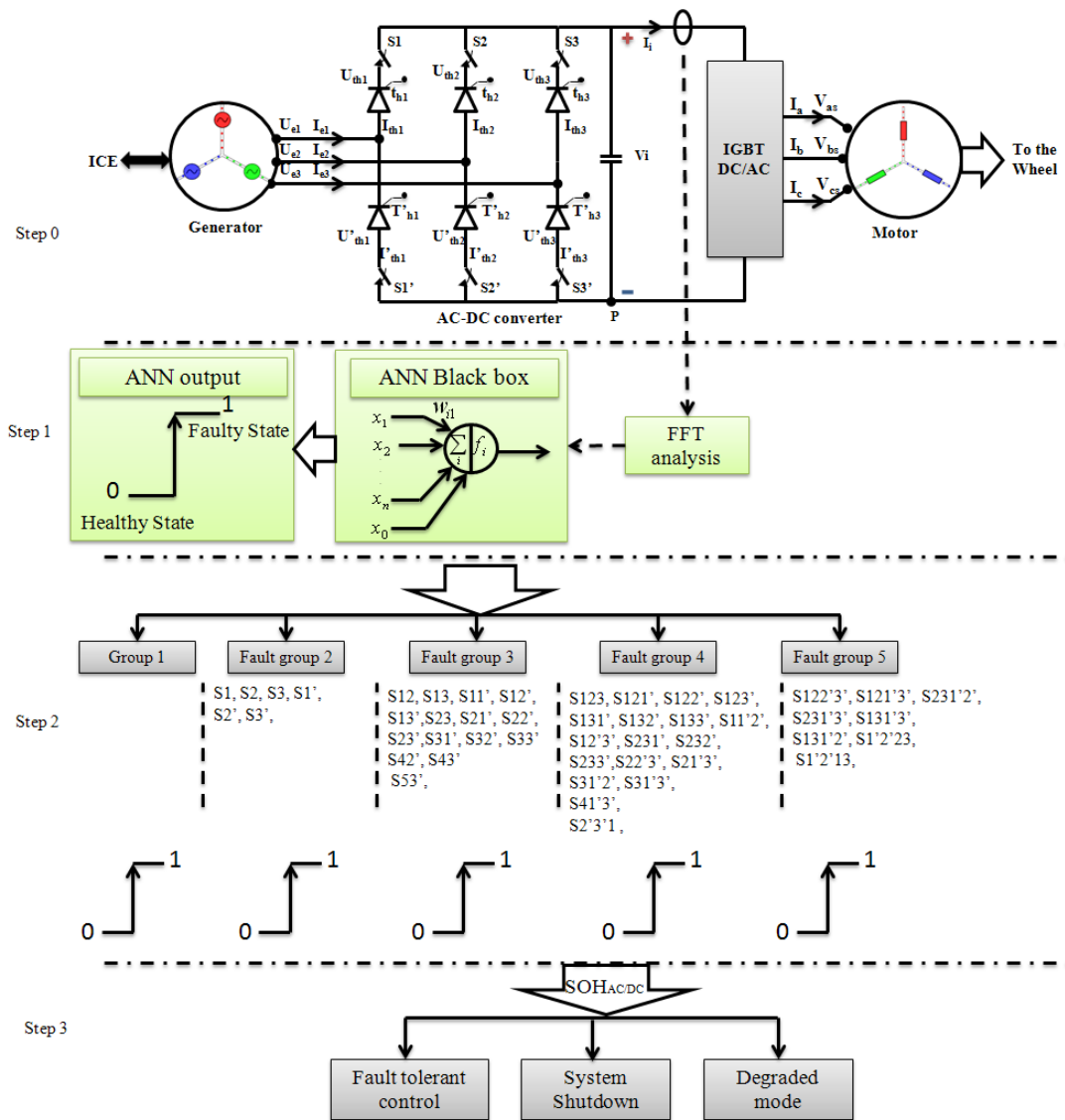


Fig. 5.14 : AC/DC power converter fault diagnosis implementation

The contribution of this work indicates three levels shown in figure (5.14) including step 0, step 1 and step 2. The result of ANN can be used by one of mentioned objective in step 3 too. The step 3 will be considered as a future plan of this work. Table (5.2) show the output of ANN implementation under different conditions of open circuit fault with various speeds and load that can be used by the designed strategy in step 3.

According to figure (5.14):

Step 0: In this step schematic of studied SHEV structure has employed for operation under different possibility of open phasing in AC/DC power converter switches. The performance of this work and how apply of test bench have been explained in chapter 4 section 2.1 and 2.2.

Step 1: In this step an ANN black box have been used to fault diagnosis. The contents and structure of ANN have been explained in present chapter section 5 thoroughly. In this base, after FFT of targeted data, the trained ANN tries to analysis of data and

produce of results. The ANN output can be Zero (0): that means a healthy operation without fault and one (1): that means there is an open circuit fault.

Step 2: According to diagnosis strategy, 5 outputs have been considered for used ANN in this work. One output for healthy operation and remaining for different levels of open phase fault, it was tested for 10 different data under faulty state as results are visible in Table (5.3). These data can be used to evaluate the loss of performances of the AC/DC converter i.e. the value of $SOH_{AC/DC}$.

Step 3: in this step three perspective of ANN output usage have been drawn. Fault tolerant control and degraded mode in order to ensure a continuity of service of the drivetrain. In fact, shutdown the system that is easiest way but not a proper solution in electromotive application.

Table 5.3 : ANN output results under different level of AC/DC switches open circuit in SHEV application (for 10 sample test)

	Fault value	Load condition	Speed condition	Output 1	Output 2	Output 3	Output 4	Output 5	Detection
1	Healthy mode	Full-load	200rpm	0.981	0.0001	0	0	-0.0042	T
2	Healthy mode	Full-load	1000rpm	1.001	0.0012	-0.0006	-0.0006	0	T
3	Group2 S1	Half -load	400rpm	0	0.9841	-0.0008	0.0002	0.0002	T
4	Group2 S3	No-load	600rpm	0	0.964	-0.0023	0.0008	0.005	T
5	Group3 S23	Full-load	800rpm	0.0007	0.0034	0.95	0.003	0.0005	T
6	Group3 S11'	0.75-load	1000rpm	-0.0013	0	0.964	-0.001	0.0009	T
7	Group4 S122'	Half-load	600rpm	-0.0213	0.0004	0	0.97	0.0058	T
8	Group4 S233'	0.25-load	800rpm	-0.0013	0.0001	0.0014	0.967	0.0087	T
9	Group5 S122'3'	No-load	1000rpm	0.0079	0	0.0015	0.0001	0.985	T
10	Group5 S122'3'	No-load	800rpm	0	-0.0019	0	0.0069	0.9945	T

6. ANN based fault diagnosis of switch open circuit of DC-AC power converter

Similar of 2 previous sections with the same way as previously, the open phase fault of DC-AC inverter is implemented under an ANN model for classification and diagnosis of this type of fault as it is shown in figure (5.15).

According to open phase fault in one switch of DC/AC inverter or one phase of motor, the 3 phase motor voltage will be unbalanced. In base of different speed and load levels, there are different levels of unbalanced voltage as well as it considered of 1% until 20%. How calculate unbalanced voltage and the effect of this fault has been explained in chapter 2 section 3.4. This type of fault according to our practical experiment can be very dangerous to ensure a continuity of service of SHEV. But this classification can help us to know about severity of fault and take a proper decision in order to stop of motor or select of a suitable degraded mode.

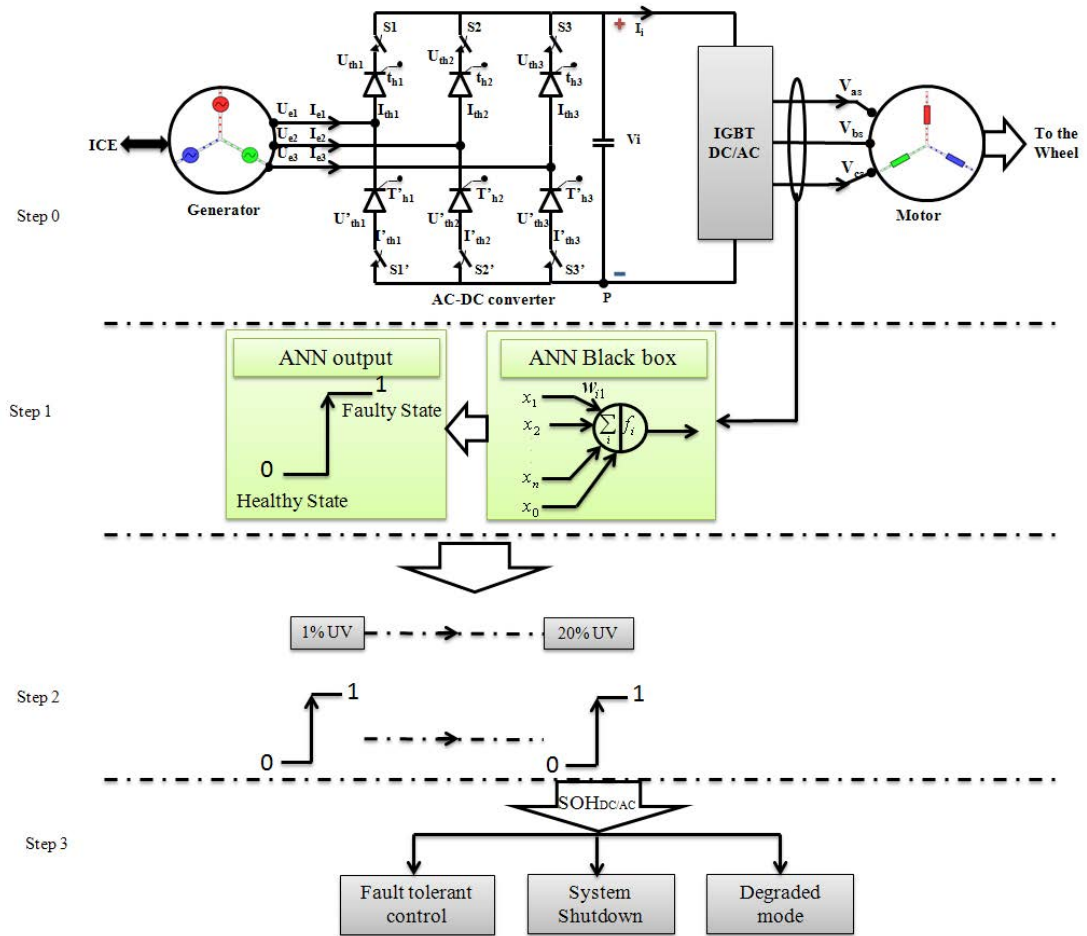


Fig. 5.15 : DC/AC power converter fault diagnosis implementation

The contribution of this work indicates three levels shown in figure (5.15) including step 0, step 1 and step 2. The result of ANN can be used by one of mentioned objective in step 3 too. Table (5.5) show the output of ANN implementation under different conditions of open circuit fault with various speeds and load that can be used by designed strategy in step 3.

According to figure (5.15):

Step 0: In this step schematic of studied SHEV structure has employed for operation under different possibility of open phasing in DC/AC power converter switches. The performance of this work and how apply of test bench have been explained in chapter 4 section 2.6.

Step 1: In this step an ANN black box have been used to fault diagnosis. The contents and structure of ANN have been explained in present chapter section 5 thoroughly. In this base, 3 phase voltage and current of motor have been employed to train ANN which analyses data and produces results. The ANN output can be Zero (0): that means a healthy operation without fault and one (1): that means there is an open circuit fault and also its severity.

Step 2: According to diagnosis strategy, 14 outputs have been considered for used ANN in this work as shown in table (5.4). One output dedicated to healthy operation and

remaining for different levels of unbalanced voltage (UV) caused by open phase fault. It was tested for 5 different data under faulty state as results are visible in table (5.5). These data can be used to evaluate the loss of performances of the DC/AC power converter i.e. the value of $SOH_{DC/AC}$.

Step 3: in this level three perspective of ANN output usage have been drawn. Fault tolerant control and degraded mode in order to ensure a continuity of service of the drivetrain. In fact, shutdown the system that is easiest way but not a proper solution in electromotive application.

Table 5.4 : Possibility of experimental unbalanced voltage faults efforts in terms of open phasing fault

Types Of faults	G1	G2	G3	G4	G5	G6	G7	G8	G9	G10	G11	G12	G3	G14
Fault percentage	2%	3%	5%	7%	8%	10%	11%	13%	14%	15%	17%	18%	20%	H
H : Healthy operation G: fault group 1														

Table 5.5 : ANN output results under different level of DC/AC switches open circuit in SHEV application (for 5 sample test)

	Fault value	Load condition	Speed condition	Group 1	Group 2	Group 3	Group 4	Group 5	Group 6
1	0	0.75-load	1000rpm	0.0005	0.0141	0.006	-0.0052	0	0.0009
2	2%	0.25-load	600rpm	0.9911	-0.007	-0.0008	-0.0009	0	-0.0011
3	5%	Half-load	800rpm	0	0.0008	0.9613	0.0072	0.0002	0
4	11%	No-load	1000rpm	0	0.0044	-0.0023	0.008	-0.0001	0
5	14%	Half- load	800rpm	0	0.0044	-0.0023	0.0018	-0.0001	0

	Group 7	Group 8	Group 9	Group 10	Group 11	Group 12	Group 13	Health operation	Detection
1	0	0.0041	0.0061	-0.0042	0	0.0009	0.0005	0.9951	T
2	-0.0011	-0.007	0.0013	-0.0009	0	-0.0011	-0.0011	-0.0011	T
3	0	0.0008	-0.0008	0.0072	0.0002	0	0	0	T
4	0.9945	-0.0023	0.004	0.0099	-0.0001	0	0	0.0004	T
5	0	0.0044	0.9723	0.008	-0.0001	0	0	0	T

7. Conclusion

In this chapter the ANN method have been used to develop three diagnosis based models for : the vector controlled PMSM under inter turn short circuit, the AC/DC power converter under an open phase fault and also the PMSM under unbalanced voltage caused by open phase DC/AC inverter. 13 different classes of inter turn short circuit, 6 different classes of open phase fault in AC/DC converter and 13 different classes of unbalanced voltage caused by open circuit in DC/AC inverter have been detected, classified, and introduced as contribution of this ANN diagnosis model.

These models allow supervising the main components of the PMSM drivetrains used to propel the SHEV. The ANN advantages of ability to include a lot of data made possibility to classify the faults in terms of their type and severity. This allows estimating

the performance degree of that drivetrains during faulty conditions through the parameter SOH. The latter may be integrated into a fault tolerant control algorithm which is an interesting perspective of this part of thesis.

8. References of chapter V

- [1] S. Saeid. Moosavi, A. Djerdir, Y. Ait-Amirat, D. A. Khaburi, “Fault Detection In 3-Phase Traction Motor Using Artificial Neural Networks”, 2012 IEEE Transportation Electrification Conference and Expo (ITEC 2012)- Michigan, USA.
- [2] S. Saeid. Moosavi, A. Djerdir, Y. Ait-Amirat, D. A. Khaburi, “Artificial Neural Networks Based Fault Detection In 3-Phase PMSM Traction Motor ”, IEEE XXth International Conference on Electrical Machines (ICEM'2012), Septembre 2-5-2012, Marseille, France.
- [3] Peter Vas, “Artificial intelligence based electrical machines and drives”, Oxford university press.

General Conclusion

According to upcoming challenge on pollution the use of EV/HEV is in increase. Normally the electrical parts of vehicle as the other mechanical, chemical parts will expose the risks that require the faults diagnosis and prevention of fault propagation. In base of the objective of this work, two major part of drivetrain of SHEV have been considered as permanent magnet synchronous motor (PMSM) and power converter.

Hence, there is a need to develop an intelligent diagnostic and monitoring system based on fast and efficient methods for drivetrain health monitoring. The system should have the ability to predict the machine and power converter condition in the same sense as that of a professional expert engineer. The monitoring system should have the ability to distinguish between the different parts under its supervision. This can be achieved by the use of advanced instrumentation, processing and intelligent diagnostic methods.

It proposes, considering the appropriate diagnosis of this method and other similar methods when facing different faults, the existence of a supplementary mean like neural network for classification of faults that seems to be a necessary factor. Employing expert system for fault diagnosis of PMSM drivetrain using rules obtained from the connection weight of a supervised neural network and rules extracted from heuristic knowledge, this combination of ANN knowledge and expert knowledge may enhance the monitoring system for diagnosis too.

This thesis confirmed that although a short circuit fault, in an early stage when a small number of turns are shorted, cannot lead to demagnetization, no timely diagnosis will lead to additional flux from turn to turn and demagnetization in PMs Motors. It mentions the relation between different faults and their effect on one another. This would be true about open phasing fault and two phase short circuit fault too. So a complete diagnosis system must be able to detect all major faults and their discrimination.

It must attention that in mechanical faults as eccentricity and bearing, FFT analysis on vibration signal gave us proper information in stationary states, but usage of FFT analysis in non stationary state will lead to same situation that it is discussed in previous parts. However the work presented in this report, investigated the on line detection of bearing fault by using wavelet analysis under non-stationary operation but a deeper investigation in this issue is expected because of breadth of this subject. Presented method is able to load changes, identification under different regimes of motor operation as no-load and full load, healthy or faulty conditions. It can propose as a good method in faults detection under non stationary operation too. It must pay attention that vibration signal processing is more interesting than motor current signature analysis (MCSA) in order to mechanical fault detection and diagnosis.

In the SHEV application, we needed to a classification method for all changeable state. It is obvious operation of SHEV in different speed and different load. So the selected method must be able to support this specification.

Fault sensitive modeling of PMSM stator winding short circuit, demagnetization, eccentricity and bearing has been proposed. The most important step of ANN based fault diagnosis called feature (pattern) identification has been done. The FFT amplitudes

of the three phase motor current and also park currents I_d and I_q have been considered as a suitable feature to use for ANN training aiming short circuit fault. Also the changes of back EMF FFT harmonics can be used as a proper feature to demagnetization fault detection. However, a fast and accurate estimation of this magnitude (back EMF) has to be performed on line. This is one of interesting perspective of our work. For eccentricity and bearing fault investigation, the vibration signal has been introduced as the best solution. During operation the machine is always associated to its control device and it is very difficult to find an analytical model able to take into account all phenomena so an experimental approach has been preferred to ANN developments.

Fault sensitive modeling of power converter has been also purposed. Two new frequency patterns were introduced to aim AC-DC converter switches fault recognition for application as SHEV. The cases of diodes and full thyristor bridges have been treated. The experimental results are used to verification of simulation results. On this basis, 5 groups of different states of AC-DC converter switches failures have been considered and difference of analysis results are compared with healthy state of operation, by aim of finding feature those lead to a new pattern in fault condition. This result has been validated through theoretical simulations but also experimental measurements. This allowed us to use the developed software tool to study the influence of capacitor size changes, and load and speed variations on the identified pattern. The obtained results show successfulness of this pattern.

On the basis of the developed fault sensitive models above, an ANN based fault detection, diagnosis strategy and the related algorithm have been developed to show the way of using the identified patterns in the supervision and the diagnosis of the PMSM drivetrain of SHEVs. ANN method have been used to develop three diagnosis based models for : the vector controlled PMSM under inter turn short circuit, the AC/DC power converter under an open phase fault and also the PMSM under unbalanced voltage caused by open phase DC/AC inverter. These models allow supervising the main components of the PMSM drivetrains used to propel the SHEV.

The ANN advantages of ability to include a lot of data mad possible to classify the faults in terms of their type and severity. This allows estimating the performance degree of that drivetrains during faulty conditions through the parameter state of health (SOH). The latter can be used in a global control strategy of PMSM control in degraded mode in which the control is auto-adjusted when a defect occurs on the system. The goal is to ensure a continuity of service of the SHEV in faulty conditions to improve its reliability.

Appendix 3A

Application of resolver

1. Principle of operation of the resolver	175
2. Analog / digital converter (ADC).....	176
3. ADC integrated circuit (IC)	176
4. ADC software	177

1. Principle of operation of the resolver

The resolver is used to measure the absolute angular position of the motor shaft, whose operation is that of a rotary transformer. It has three windings, a primary and two secondary. Also called the primary excitation winding is wound on the rotor. The other two coils 'secondary' are identical and the wound stator where they are arranged at 90° to one another. The primary is energized with a sinusoidal voltage through a coupling transformer in turn supplied to the stator by a function generator 'GBF'. The output signals measured at the terminals of the two secondary consist of two sinusoidal voltages whose amplitudes are modulated by sine and cosine of the absolute position of the rotor. A simplified circuit diagram of the said resolver is shown in figure (3A.1).

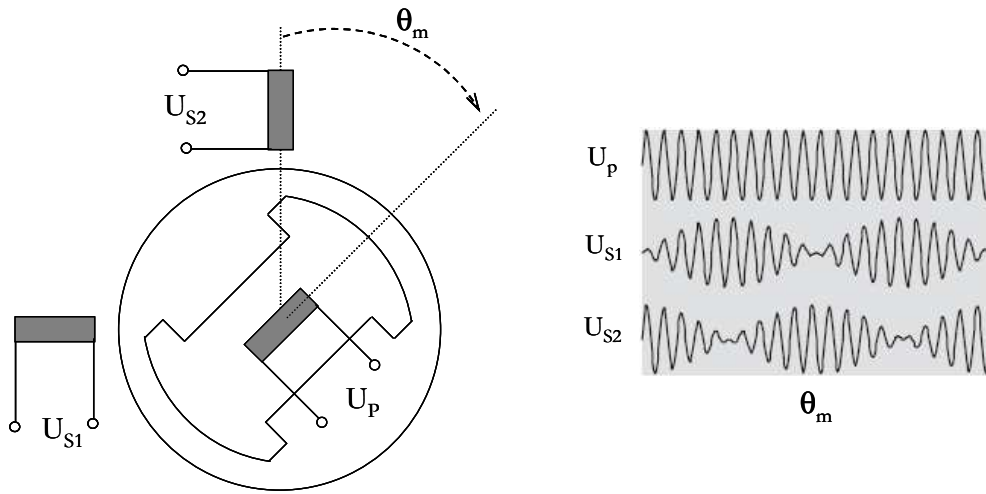


Fig. 3A.1: Simplified diagram of the resolver (left) signals to the primary and secondary (right)

The two voltages across the secondary (output) can be expressed in the temporary domain:

$$U_{\sin} = U_0 k \left[\sin \theta_m \cos(\omega_e t) + \frac{1}{\omega_e} \frac{d\theta_m}{dt} \cos \theta_m \sin(\omega_e t) \right]$$

$$U_{\cos} = U_0 k \left[\cos \theta_m \cos(\omega_e t) + \frac{1}{\omega_e} \frac{d\theta_m}{dt} \sin \theta_m \sin(\omega_e t) \right]$$

Where,

k is the ratio of rotor / stator transformation;

t is the time variable;

U_0 is the amplitude of the excitation signal;

θ_m is the absolute angular position of the rotor;

ω_e is the angular frequency of the excitation signal.

If the angle of the excitation pulse signal is sufficiently large compared to the speed of rotation, the above equations can be simplified as follows:

$$U_{\sin} = U_0 k [\sin \theta_m \cos(\omega_e t)]$$

$$U_{\cos} = U_0 k [\cos \theta_m \cos(\omega_e t)]$$

Altering the excitation signal component in the equations above, can be extracted the value of the angular position of the rotor easily.

2. Analog / digital converter (ADC)

In order to use the captured analog signals in output of the resolver, the numerical control program of the DSP must be converted into digital format. This conversion can be performed by using specific integrated circuits or by using software routines in the DSP.

3. ADC integrated circuit (IC)

In the integrated circuit, each of the two signals from the resolver is first conditioned through a differential amplifier in order to reference relative to a ground signal and to amplify them to reject the common mode noise. The signals are conditioned and sent to the ADC inputs, which demodulates and provides the angular position of the resolver rotor and that after a phase of digital processing. Figure (3A.2) shows the block diagram of the conventional estimation of the angular position system using an integrated ADC.

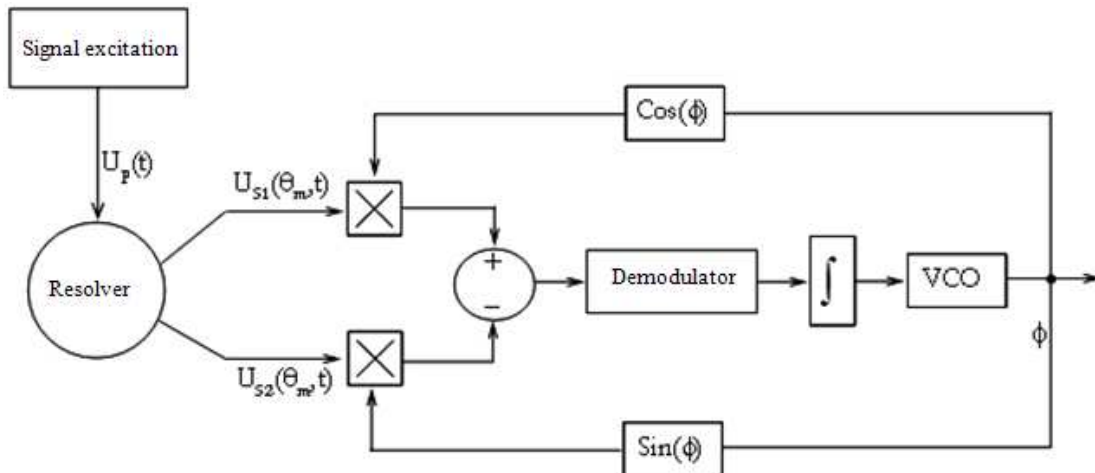


Fig. 3A.2: Block diagram of an estimator of the angular position based on an ADC integrated

In summary, the traditional system of ADC-based integrated circuit assumes that the output of the current position is ' ϕ ' (Figure (3A.2)). Input signals 'US1' and 'US2' are multiplied by ' $\cos\phi$ ' and ' $\sin\phi$ ', the result is compared and demodulated. The signal obtained is proportional to $\sin \Delta\theta_m = \sin(\theta_m - \phi)$, ie of the error of position. The latter is supplied to an integrator, providing the speed of the analog signal, which is supplied in turn to the voltage controlled oscillator (VCO). It gives to its output the numeric value estimated of the position ' ϕ ' closing the tracking loop position.

The traditional solution presents the problem of the cost of the integrated circuit close to the resolver. Dynamic and static performance of such integrated circuits are fixed or can be made by using external passive components such as resistors and capacitors.

Therefore the stability of the performance of the tracking loop of position depends on stability and the lifetime of these components.

4. ADC software

ADC software is the alternative solution for the angular position of the rotor. This option has the advantage of eliminating the additional cost of external integrated circuit. Considering a modern training system that is normally equipped with DSPs, the software technique is very interesting and easy to implement.

Once established, this technique offers the possibility of controlling static and dynamic tracking of the position loop performance. This helps to improve the flexibility of the whole system and control system. For these reasons, mentioned software technique has been adopted in this work.

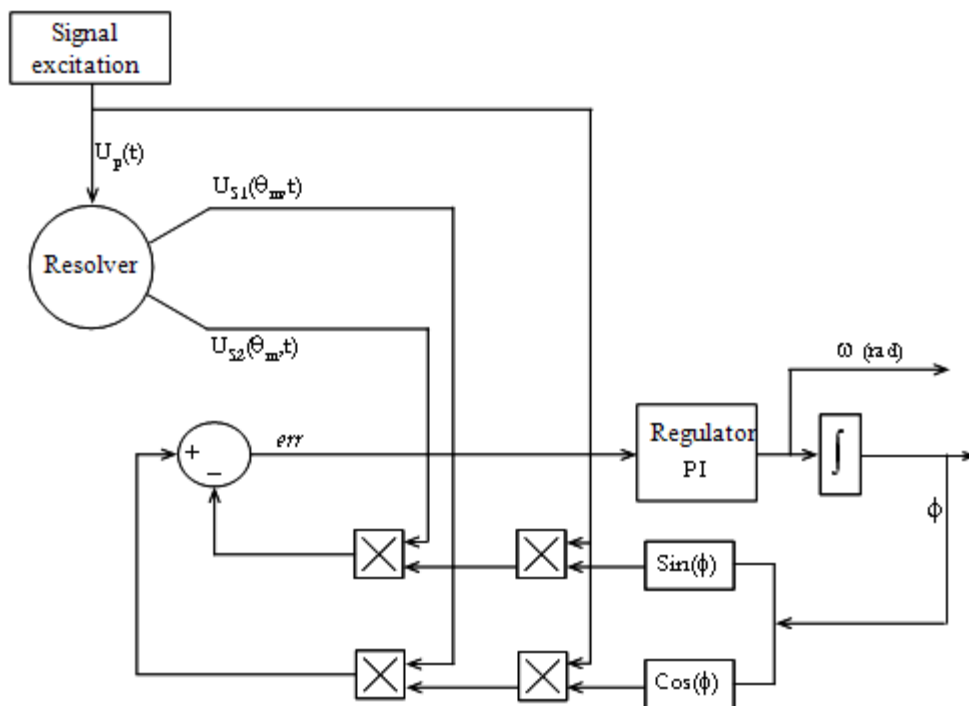


Fig. 3A.3: Block diagram of the tracking system of the angular position of the rotor

Figure (3A.3) shows the power of the closed loop system tracking the position that has been developed and implemented in DSPACE card (DS1104) scheme.

The algorithm is based on the technique of over-sampling (over sampling technology). The excitation signal and the sine and cosine resolver signals were sampled 10 times per period of the excitation signal which the frequency is 2 kHz (ie of 20 kHz sampling). Moreover, the sampling of analog input (ADC) of the card DSPACE for the resolver signals has been synchronized with the PWM block using an interrupt signal.

This algorithm is designed to minimize the error between the angular position of the rotor ' θ_m ' and the calculated angle ' ϕ ' using a feedback loop. The error calculation is based on the following trigonometric equations:

$$err = (U_0 \sin(\omega_e t) \cos \phi) \cdot (U_0 \cdot k \sin \theta_m \sin(\omega_e t)) - (U_0 \sin(\omega_e t) \sin \phi) \cdot (U_0 \cdot k \cos \theta_m \sin(\omega_e t))$$

$$err = U_0(t) \cdot (U_0 \cdot k \sin(\omega_e t)) \cdot [\sin \theta_m \cos \phi - \cos \theta_m \sin \phi]$$

$$err = A[\sin(\theta_m - \phi)]$$

Where

$$A = U_0(t) \cdot (U_0 \cdot k \sin(\omega_e t))$$

And

$$U_0(t) = U_0 \sin(\omega_e t),$$

is excitation signal.

This error is reduced to a value close to zero using a PI regulator. The gains of the latter are adjusted online during operation of the model so as to minimize the best possible error. The integrator increases the resolution of the calculated angle. Once the control loop is completed (ie $err \cong 0$), then the calculated angle ' ϕ ', that is in the interval $[0, \square]$, is equal to the actual position of the rotor ' θ_m '. Figures (3A.4) to (3A.7), present the results of algorithm implemented for motor speed equal 1000 rpm.

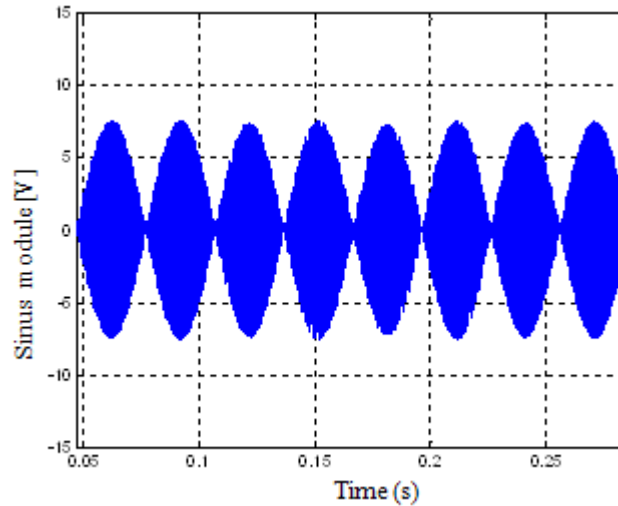


Fig. 3A.4 : Resolver output signal modulated sine

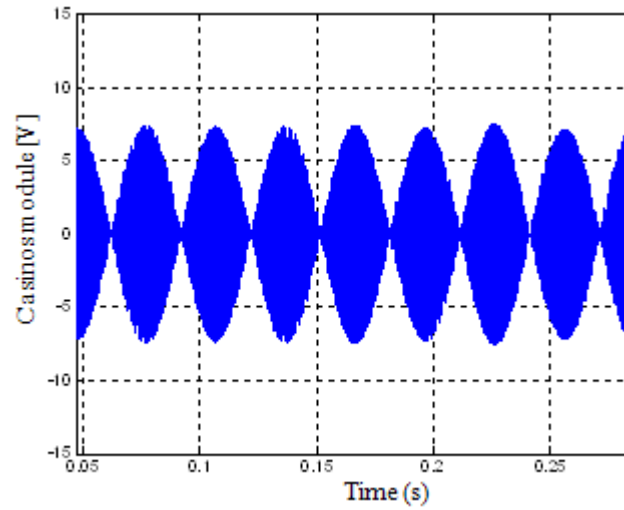


Fig. 1A.5 : Resolver output signal modulated in cosine

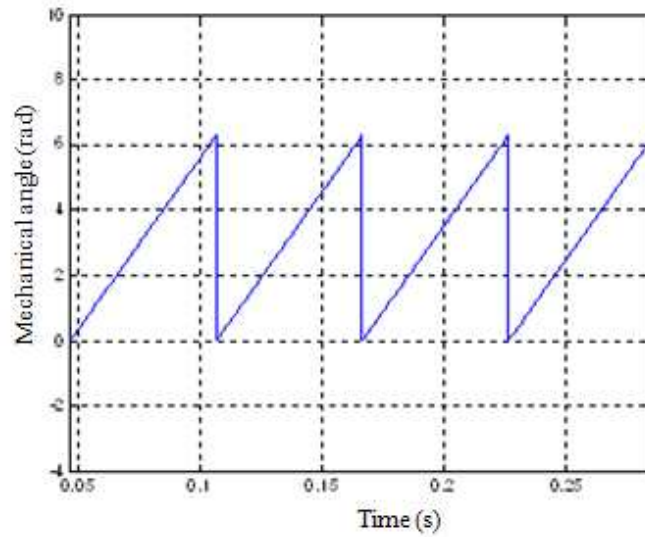


Fig. 3A.6 : Mechanical angle

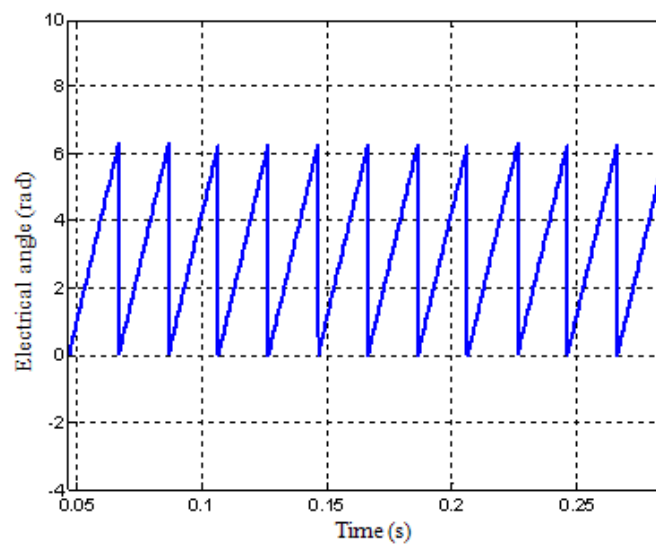


Fig. 3A.7: Electrical angle

Appendix 3B

DSPACE card (DS1104)

1. Characteristics of the DSPACE card (DS1104)183

1. Characteristics of the DSPACE card (DS1104)

The DS1104 control card is specially designed to development of a controller multi-level high-speed for various fields of applications. It is a control system in real time with a complete processor type '6 O3 PowerPC floating point processor, 250MHz '. For advanced uses of I/O the card has a sub DSP (Slave DSP) to ensure of acquisition of measurements and generation of PWM signals. The heart of this subsystem is a DSP TMS320F240 from Texas Instruments.

The DS1104 card control can be programmed directly by using MATLAB / Simulink or C language. A connection box (Figure (3B.1)) gives easy access to all signals input / output through BNC access cable. External systems can be connected or disconnected without welding said connectors. This simplifies the implementation of the system and the tests. The DS1104 card is normally inserted into a PCI slot of a PC. A description of the characteristics provided by the DS1104 card is shown in Table (3B.1):

Table 3B.1: Technical specifications of the DS1104 card

<i>manufacturer</i>	<i>dSpace GmbH Technologiapark 25, 33100 Paderborn Germany</i>
<i>processor</i>	<ul style="list-style-type: none"> ▪ <i>MPC 8240 with PPC630e core and on chip peripherals</i> ▪ <i>64-bit floating point processor</i> ▪ <i>250 MHz CPU</i>
<i>Memory</i>	<ul style="list-style-type: none"> ▪ <i>Global memory : 32MB SDRAM</i> ▪ <i>Flash memory : 8MB</i>
<i>ADC (Analog Input)</i>	<ul style="list-style-type: none"> ▪ <i>4 multiplexed channels, 16-bit resolution, 2 μs conversion time</i> ▪ <i>4 A/D channels, 12-bit resolution, 800 ns conversion time</i>
<i>DAC (Analog output)</i>	<ul style="list-style-type: none"> ▪ <i>8 D/A channels, 16-bit resolution, 10 μs max. settling time</i>
<i>Input / Output Digital I / O</i>	<ul style="list-style-type: none"> ▪ <i>20-bit digital I/O (bit selectable direction)</i>
<i>interface incremental encoder</i>	<ul style="list-style-type: none"> ▪ <i>2 channels</i> ▪ <i>Single ended TTL or differential RS422 input</i> ▪ <i>Max. 1.65 MHz input frequency</i> ▪ <i>24-bit loadable position counter</i>
<i>serial port</i>	<ul style="list-style-type: none"> ▪ <i>Serial UART (RS232, RS485 and RS422)</i>
<i>DSP slave</i>	<ul style="list-style-type: none"> ▪ <i>Texas Instruments TMS320F240 DSP</i> ▪ <i>20 MHz clock frequency</i> ▪ <i>1 x 3-phase PWM output</i> ▪ <i>4 x 1-phase PWM output</i>



Fig. 3B.1 : Connection box of the DS1104 card

The DS1104 card consists of a main processor (PPC) 'Power PC 603e', an interrupt controller, a synchronous DRAM controller, a series of clock registers and a place of PCI slot. The main processor controls the analog inputs / outputs, digital inputs / outputs and pulse encoder interface.

The analog inputs convert the analog signals to digital and the analog outputs transform the discrete data into analog. The encoder interface operates at a frequency of 1.65 MHz (ie it can measure to 1.65 million lines per second). The serial interface of the DS1104 card contains a receiver and a transmitter for asynchronous connections with external systems. PPC processor also has a feature to synchronize the analogue / digital outputs as well as the encoder interface. The various clock and interrupt registers can be used to control of a complex system.

The block (1 x 3 Phase PWM) of the slave DSP generates the PWM signals. These are the signals with a frequency and fixed amplitude and a variable width. The width of the PWM signal depends on the modulating. As the frequency of the PWM and very high compared to the modulating; transferred energy is largely dependent on the modulating signal. The PWM block also provides an opportunity to enter a dead time to control the switches.

Figure (3B.2) shows the block diagram of the DS1104 card, with the characteristics of controllers, main and slave.

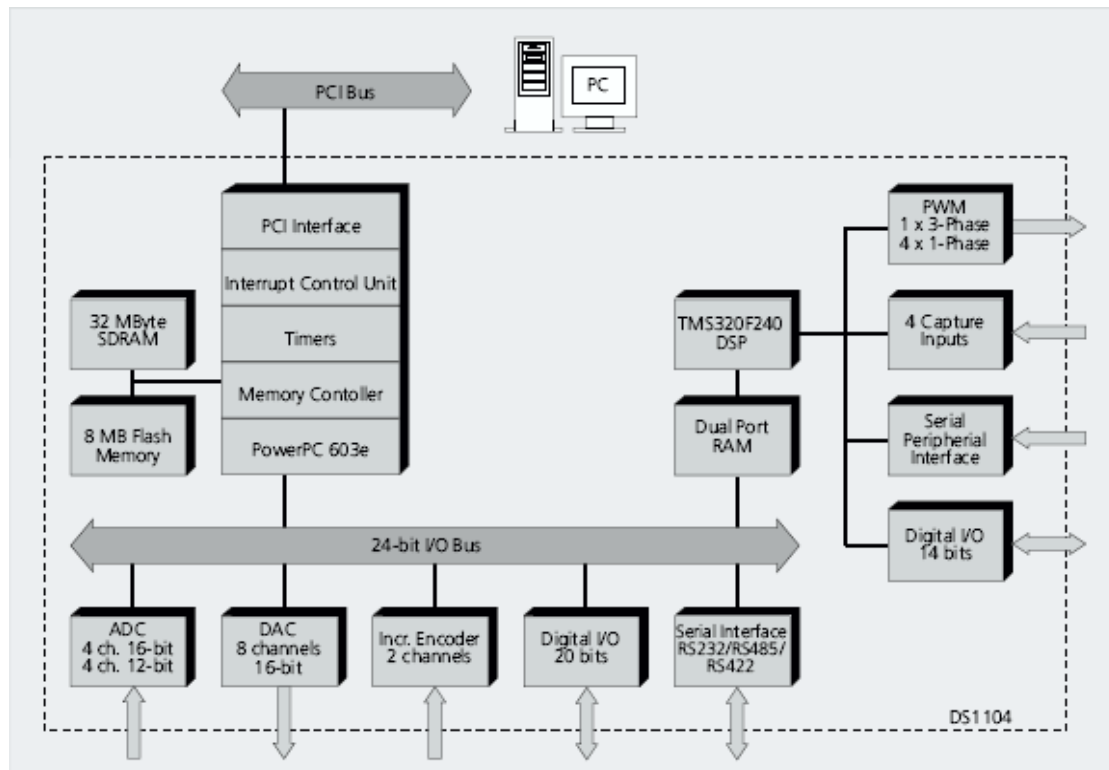


Fig. 3B.2 : Block diagram of the module DSPACE

Appendix 3C

**Analytical equation aiming
to demagnetization fault
description in PMSM**

1. Introduction.....	189
2. Maxwell's equations aiming to demagnetization fault description	190

1. Introduction

As it mentioned in chapter 2 section 3.5, a defect of a magnet may occur due to armature reaction or the appearance of a crack. This means that the absence of a magnet can be classified as a type of defect that is uniformly distributed over its entire surface, or located at a specific location of the pole. To account for this non-uniformity of the defect in the analytical model, the magnet is considered to be composed of small elements as shown in figure (3C.1).

Where B_I is air-gap flux density, B_{rij} is magnet remanent induction of the magnet element with suffix (i, j) indicating its position in a magnet pole, μ_0 is the air-gap permeability, μ_r is the relative permeability, R_s is length of stator border to center of motor, R_r is length of rotor external border to center of motor, R_{rim} length of rotor internal border to center of motor, R_{ij} is length of each rotor magnet segments border to center of motor and g length of the air gap. In this case, magnet depth = $R_r - R_{rim}$.

For formulate of analytical model used of Maxwell's equation that are applied with the following assumptions:

- Small magnet elements are magnetized radially and uniformly.
- The effects of edges are ignored.
- The permeability of the rotor and stator yoke is considered infinite.
- The effect of teeth is neglected.

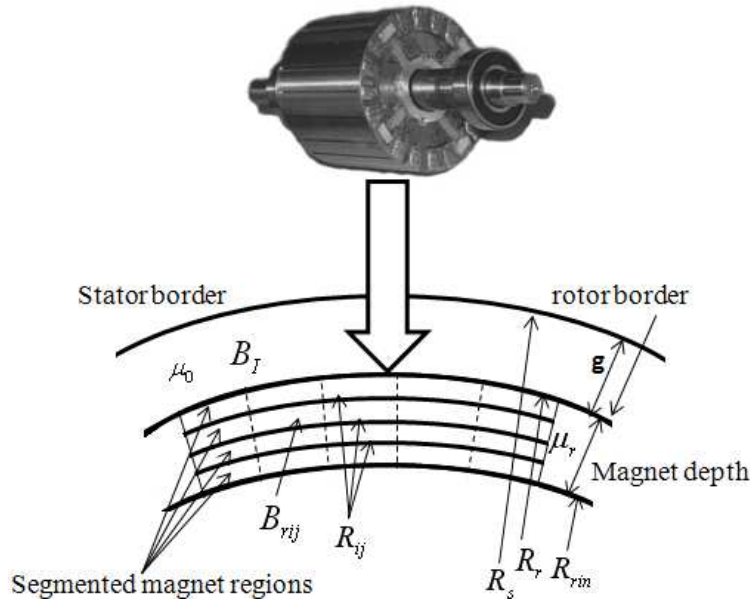


Fig. 3C.1 : Geometry of the electromagnetic problem

By neglecting the effect of teeth, the distribution of magnetic field generated by the magnets can be calculated by solving the partial differential equations in the gap and in each element of the magnet.

2. Maxwell's equations aiming to demagnetization fault description

From Maxwell's equations (for static filed), we can write:

$$\text{rot} \vec{H} = J \quad (3C.1)$$

$$\text{div} \vec{B} = 0 \quad (3C.2)$$

In the air gap region I:

$$\vec{B}_{I,i,j} = \mu_0 \vec{H}_{I,i,j} \quad (3C.3)$$

And the magnets (elements), region II:

$$\vec{B}_{II,i,j} = \mu_0 \mu_r \vec{H}_{II,i,j} + B_{ri,j} \quad (3C.4)$$

Where \vec{H} is the field intensity. We assume that each magnet is divided into 25 parts. The position of each element can be defined according to figure (3C.2).

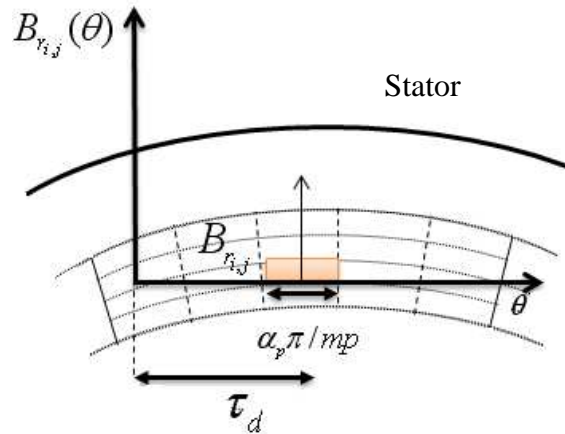


Fig. 3C.2 : Position definition of an element of the magnet in the transverse plane of the machine

The remanent flux density of a magnet radially magnetized is expressed using a Fourier series as follows:

$$B_{r_{i,j}}(\theta) = \frac{\alpha_p B_{r_{i,j}}}{2m} + \sum_{n=\text{odd}}^{N_h} \frac{2B_{r_{i,j}}}{n\pi} \sin\left(n \frac{\alpha_p \pi}{2m}\right) \cdot \cos(n.p(\theta - \tau_d)) \quad (3C.5)$$

where ‘i,j’ defines the position of an element, α_p is the magnetic pole arc angle, m is the number of vertical divisions of a pole, τ_d is the distance between center of magnet element and that of a pole, p is the poles pairs number, τ_d is the distance between the element and the center of the north pole and N_h is the number of harmonics.

Equation (3C.5) hold for a magnetic pole (North Pole here), similar equation can be written for another pole. For the reason of simplicity we consider a case of a machine with two poles. The field equations are written in the two regions (that is to say region I: the air gap and region II: the magnet).

The vector potential equations in the region I of the air-gap are written as:

$$\Delta A_{I_{i,j}} = 0 \quad (3C.6)$$

$$\frac{\partial^2 A_{I_{i,j}}}{\partial r^2} + \frac{1}{r} \frac{\partial A_{I_{i,j}}}{\partial r} + \frac{1}{r^2} \frac{\partial^2 A_{I_{i,j}}}{\partial \theta^2} = 0 \quad (3C.7)$$

In Region II, of the magnet, the vector potential equations are expressed by:

$$\Delta A_{II_{i,j}} = \frac{1}{r} \frac{\partial B_{ri,j}(\theta)}{\partial \theta} \quad (3C.8)$$

$$\frac{\partial^2 A_{II_{i,j}}}{\partial r^2} + \frac{1}{r} \frac{\partial A_{II_{i,j}}}{\partial r} + \frac{1}{r^2} \frac{\partial^2 A_{II_{i,j}}}{\partial \theta^2} = \frac{1}{r} \cdot \frac{\partial B_{ri,j}(\theta)}{\partial \theta} \quad (3C.9)$$

The partial differential equations for the two regions are solved taking into account all the small pieces of the magnet. In the case of a magnet with 25 elements, there will be three sets of equations to solve. Under these conditions the general form of the vector potential in both regions I and II is given by:

$$A_{I_{i,j}}(r, \theta) = \sum_{n \neq 0} (\alpha_{i,j} \cdot r^{np} + \beta_{i,j} \cdot r^{-np}) \sin(np(\theta - \tau_d)) \quad (3C.10)$$

$$A_{II_{i,j}}(r, \theta) = \sum_{n \neq 0} (\chi_{i,j} \cdot r^{np} + \gamma_{i,j} \cdot r^{-np}) \sin(np(\theta - \tau_d)) + A_{II_{i,j}}^p \quad (3C.11)$$

Where $A_{II_{i,j}}^p$ is the particular solution and is from the same form as the second term of the equation (3C.6):

$$A_{II_{i,j}}^p(r, \theta) = \sum_{n=\text{impair}} \lambda_{i,j} \cdot r \sin(np(\theta - \tau_d)) \quad (3C.12)$$

Value of $\lambda_{i,j}$ is determined after substitution of equation (3C.12) in (3C.9), we obtain:

$$\lambda_{i,j} = -\frac{2pB_{i,j}}{(1-(np)^2)\pi} \sin\left(\frac{n\alpha_p\pi}{2m}\right) \quad (3C.13)$$

Equation (3C.11) becomes:

$$A_{II_{i,j}}(r, \theta) = \sum_{n \neq 0} \left[(\chi_{i,j} r^{np} + \gamma_{i,j} r^{-np}) - \frac{2pB_{i,j} r}{(1-(np)^2)\pi} \sin\left(\frac{n\alpha_p\pi}{2m}\right) \right] \sin(np(\theta - \tau_d)) \quad (3C.14)$$

Using the equations of the vector potential, the radial components and tangential of the induction in the two regions are obtained as follows:

$$B_{I_{i,j}}^r(r, \theta) = \sum_{n \neq 0} np \cdot (\alpha_{i,j} \cdot r^{np-1} + \beta_{i,j} \cdot r^{-np-1}) \cos(np(\theta - \tau_d)) \quad (3C.15)$$

$$B_{I_{i,j}}^\theta(r, \theta) = \sum_{n \neq 0} -np \cdot (\alpha_{i,j} \cdot r^{np-1} - \beta_{i,j} \cdot r^{-np-1}) \sin(np(\theta - \tau_d)) \quad (3C.16)$$

$$B_{II_{i,j}}^r(r, \theta) = \sum_{n \neq 0} \left(np \cdot (\chi_{i,j} \cdot r^{np-1} + \gamma_{i,j} \cdot r^{-np-1}) - np^2 M_{ni,j} \right) \cos(np(\theta - \tau_d)) \quad (3C.17)$$

$$B_{II_{i,j}}^\theta(r, \theta) = \sum_{n \neq 0} \left(-np \cdot (\chi_{i,j} \cdot r^{np-1} - \gamma_{i,j} \cdot r^{-np-1}) + pM_{ni,j} \right) \sin(np(\theta - \tau_d)) \quad (3C.18)$$

$$M_{ni,j} = \frac{2B_{i,j}}{(1-(np)^2)\pi} \sin\left(\frac{n\alpha_p\pi}{2m}\right) \quad (3C.19)$$

In equations (3C.15) - (3C.19), ' α ', ' β ', ' χ ' and ' γ ' are constants of integration. Their values can be found by applying the boundary conditions that exist at the boundaries of different regions, namely:

$$\left\{ \begin{array}{ll}
H_{I_{i,j}}^\theta (R_s, \theta) = 0 & 0 \forall \theta \\
H_{V_{i,j}}^\theta (R_{rin}, \theta) = 0 & 0 \forall \theta \\
B_{I_{i,j}}^r (R_r, \theta) = B_{II_{i,j}}^r (R_r, \theta) & (R_r, \theta) \forall \theta \\
H_{I_{i,j}}^\theta (R_r, \theta) = H_{II_{i,j}}^\theta (R_r, \theta) & (R_r, \theta) \forall \theta \\
B_{II_{i,j}}^r (R_1, \theta) = B_{III_{i,j}}^r (R_1, \theta) & (R_1, \theta) \forall \theta \\
H_{II_{i,j}}^\theta (R_1, \theta) = H_{III_{i,j}}^\theta (R_1, \theta) & (R_1, \theta) \forall \theta \\
B_{III_{i,j}}^r (R_2, \theta) = B_{IV_{i,j}}^r (R_2, \theta) & (R_2, \theta) \forall \theta \\
H_{III_{i,j}}^\theta (R_2, \theta) = H_{IV_{i,j}}^\theta (R_2, \theta) & (R_2, \theta) \forall \theta \\
B_{IV_{i,j}}^r (R_3, \theta) = B_{V_{i,j}}^r (R_3, \theta) & (R_3, \theta) \forall \theta \\
H_{IV_{i,j}}^\theta (R_3, \theta) = H_{V_{i,j}}^\theta (R_3, \theta) & (R_3, \theta) \forall \theta \\
B_{V_{i,j}}^r (R_4, \theta) = B_{V_{i,j}}^r (R_4, \theta) & (R_4, \theta) \forall \theta \\
H_{V_{i,j}}^\theta (R_4, \theta) = H_{V_{i,j}}^\theta (R_4, \theta) & (R_4, \theta) \forall \theta
\end{array} \right. \quad (3C.20)$$

Once the coefficients ' α ', ' β ', ' χ ' and ' γ ' are obtained, the terms of the vector potential in the air-gap and in the elementary magnets can be easily calculated. The vector potential total gap or a magnet is the sum of contributions from all elements. Thus the new equations, the vector potential of the air-gap and the magnet have been developed. These are a function of the residual induction of all elements of the magnet. Thus, equation (3C.21) expresses the potential at the air gap and produces a column of elementary magnet. Equation (3C.23) then gives the vector potential total of the gap produced by a full pole magnet. This equation is also valid for the other magnetic pole.

$$A_{I_{i,j}}(R_s, 0) = \sum_{n=odd}^{Nh} \frac{1}{n} \frac{R_s^{np}}{(R_s^{2np} + R_{rin}^{2np})} \quad (3C.21)$$

$$\left[\begin{array}{l}
\left(R_r^{np+1} (M_{11})(1-np) + R_r^{-np+1} R_{rin}^{2np} (M_{11})(1+np) + R_1^{np+1} ((M_{21})(1-np) - (M_{11})(1-np)) + \right. \\
R_1^{-np+1} R_{rin}^{2np} ((M_{21})(1+np) - (M_{21})(1+np)) + R_2^{np+1} ((M_{31})(1-np) - (M_{21})(1-np)) + \\
R_2^{-np+1} R_{rin}^{2np} ((M_{31})(1+np) - (M_{21})(1+np)) + R_3^{np+1} ((M_{41})(1-np) - (M_{31})(1-np)) + \\
R_3^{-np+1} R_{rin}^{2np} ((M_{41})(1+np) - (M_{31})(1+np)) + R_4^{np+1} ((M_{51})(1-np) - (M_{41})(1-np)) + \\
\left. R_4^{-np+1} R_{rin}^{2np} ((M_{51})(1+np) - (M_{41})(1+np)) - 2(M_{31}) R_{rin}^{np+1} \right) \sin(np(\theta - \tau_d))
\end{array} \right]$$

$$A_I(R_s, 0) = (A_{I_{11}} + A_{I_{12}} + A_{I_{13}} + A_{I_{14}} + A_{I_{15}}) \quad (3C.22)$$

$A_{I_{11}}$, $A_{I_{12}}$ And $A_{I_{13}}$ is obtained by replacing τ_d renewed both to the equation (3C.23)

respectively with: $\frac{\alpha_p \pi}{3p}$, 0 and $-\frac{\alpha_p \pi}{3p}$.

$$A_l(R_s, 0) = \sum_{n=odd} \frac{1}{n} \frac{R_s^{np}}{(R_s^{2np} - R_{rin}^{2np})}. \quad (3C.23)$$

$$\left[\begin{array}{l} R_r^{np+1} (M_{11} + M_{12} + M_{13} + M_{14} + M_{15})(1 - np) + R_r^{-np+1} R_{rin}^{2np} (M_{11} + M_{12} + M_{13} + M_{14} + M_{15})(1 + np) + \\ R_1^{np+1} (M_{21} + M_{22} + M_{23} + M_{24} + M_{25} - M_{11} - M_{12} - M_{13} - M_{14} - M_{15})(1 - np) + \\ R_1^{-np+1} R_{rin}^{2np} (M_{21} + M_{22} + M_{23} + M_{24} + M_{25} - M_{11} - M_{12} - M_{13} - M_{14} - M_{15})(1 + np) + \\ R_2^{np+1} (M_{31} + M_{32} + M_{33} + M_{34} + M_{35} - M_{21} - M_{22} - M_{23} - M_{24} - M_{25})(1 - np) + \\ R_2^{-np+1} R_{rin}^{2np} (M_{31} + M_{32} + M_{33} + M_{34} + M_{35} - M_{21} - M_{22} - M_{23} - M_{24} - M_{25})(1 + np) + \\ R_3^{np+1} (M_{41} + M_{42} + M_{43} + M_{44} + M_{45} - M_{31} - M_{32} - M_{33} - M_{34} - M_{35})(1 - np) + \\ R_3^{-np+1} R_{rin}^{2np} (M_{41} + M_{42} + M_{43} + M_{44} + M_{45} - M_{31} - M_{32} - M_{33} - M_{34} - M_{35})(1 + np) + \\ R_4^{np+1} (M_{51} + M_{52} + M_{53} + M_{54} + M_{55} - M_{41} - M_{42} - M_{43} - M_{44} - M_{45})(1 - np) + \\ R_4^{-np+1} R_{rin}^{2np} (M_{51} + M_{52} + M_{53} + M_{54} + M_{55} - M_{41} - M_{42} - M_{43} - M_{44} - M_{45})(1 + np) - \\ 2(M_{31} + M_{32} + M_{33} + M_{34} + M_{35})R_{rin}^{np+1} \end{array} \right] \sin(np(\theta - \tau_d))$$

The vector potential total of the air-gap which is a function of all the elements of the magnet is then used to find the different electromagnetic quantities of the machine. Some of them are, such as, the induction in the air-gap, electromotive force, etc. The electromotive force will be assessed by:

$$e(t) = -N_s \frac{\partial \phi}{\partial t} = -N_s \frac{\partial \theta}{\partial t} \frac{\partial \phi}{\partial \theta} = -N_s \Omega \frac{\partial \phi}{\partial \theta} \quad (3C.24)$$

Where N_s is the number of turns of the coil, Ω is the angular velocity of the rotor of the machine and ϕ is the magnetic flux is given by:

$$\phi(\theta) = \int_{\alpha}^{\alpha + \alpha_{cp}} B_l^r(r, \theta) d\theta \quad (3C.25)$$

Where $B_l^r(r, \theta)$ is the total induction in the air-gap after contributions of the 25 elements of the magnet. Also α_{cp} is the coil pitch.

Appendix 3D

**Modeling of
demagnetization fault by
help of FLUX-2D
simulator**

1. Introduction.....	197
2. FLUX-2D simulator application aiming to modeling of demagnetization fault.....	197

1. Introduction

In this section, we explain the method used to break the magnet to smaller parts and create the demagnetization fault in summary. This part can give some idea about demagnetization fault investigation. After finishing a complete geometric model in healthy state and verify the model by EMF and B characteristics, the first step is dividing the magnets to some small pieces. By remove the mesh to be able to manipulate the model and make changes as shown in the figure (3C.1) and figure (3C.2).

2. FLUX-2D simulator application aiming to modeling of demagnetization fault

To facilitate the manipulation of the model we need to create a new local landmark that will facilitate the creation of new items that will be useful to decompose the geometry. We must follow the steps described in figures (3D.1) and (3D.2).

We can process the decomposition geometry. The choice of these points is not arbitrary. It must choose in relation to the geometry of the magnet for decomposing. In order to facilitate this objective, we have created new geometry parameters reusable.

- The creation of a new geometry parameter named “long_aim” representing the length of the magnet millimeter.

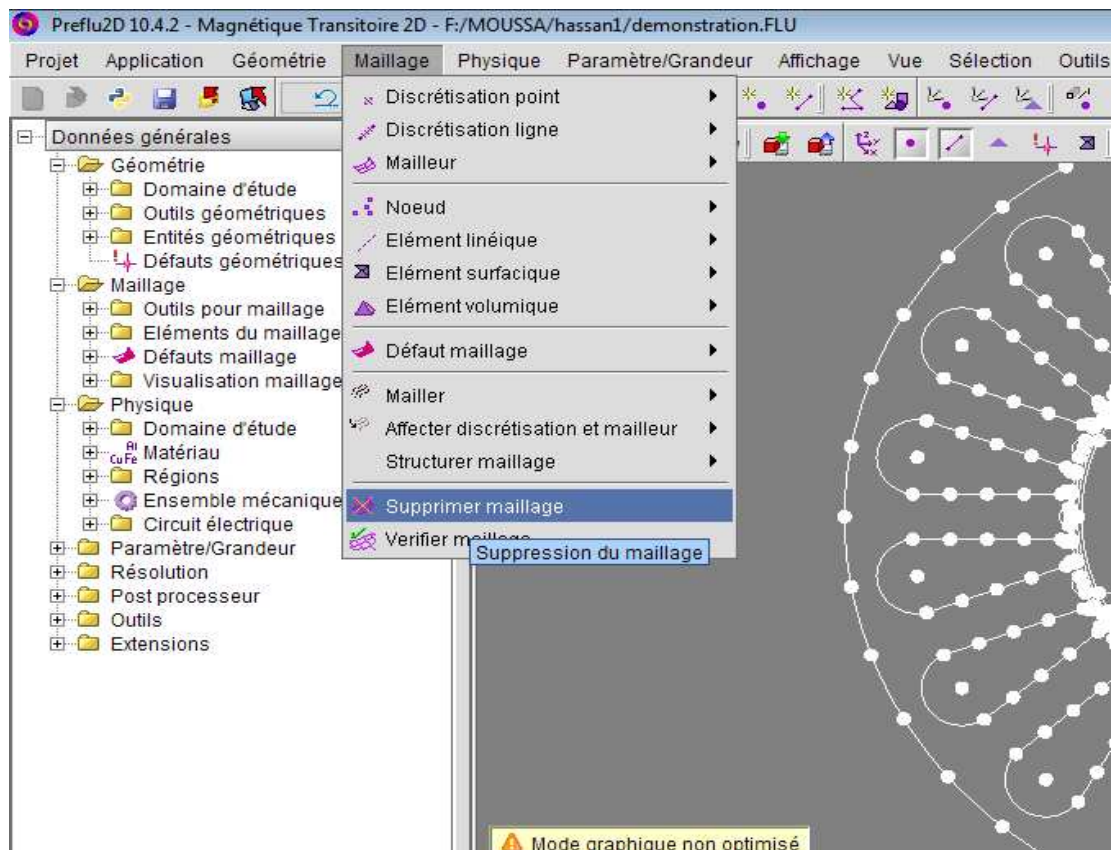


Fig. 3C.1 : meshing development part

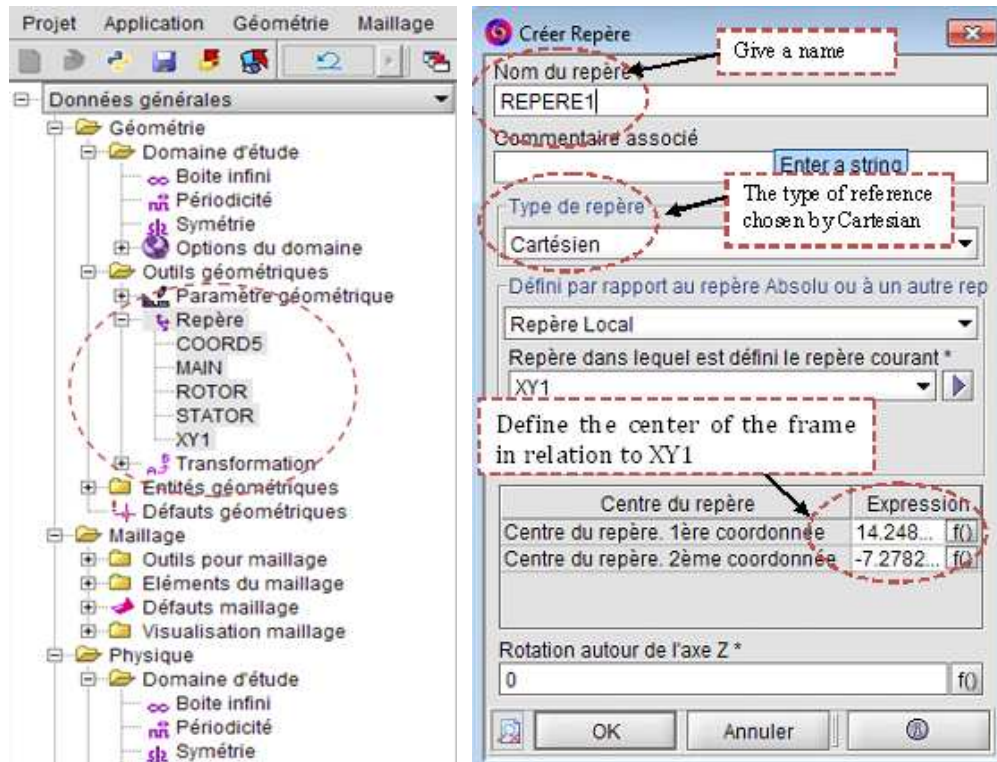


Fig. 3C.2 : new dimension definition of magnet geometry

We have been broken our magnet as described previously for the reason:

- Ability of investigate on partial or complete demagnetization.
- Possibility of investigate on symmetric or asymmetric demagnetization.

These possibilities to demagnetization simulation will be processed subsequently in this work. After adding the necessary points on a magnet, It was discovered a proposed method by FLUX2D to simplify the task. This is the point spread function. This command is simple to use and is valid both for the points, lines and surfaces as shown in the figure (3D.3).

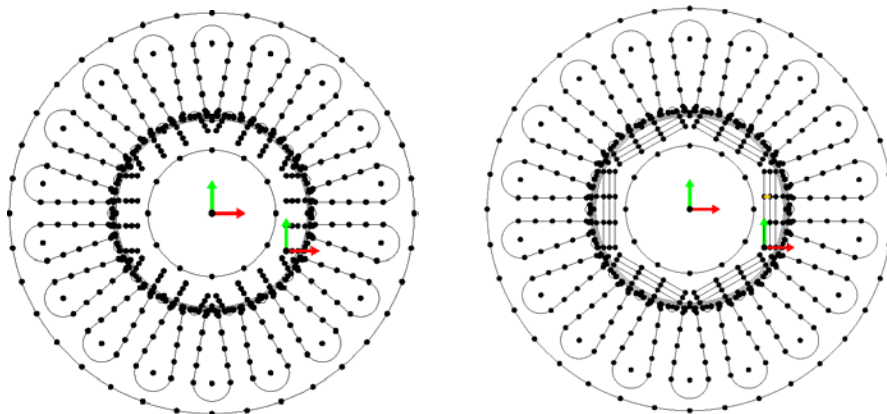

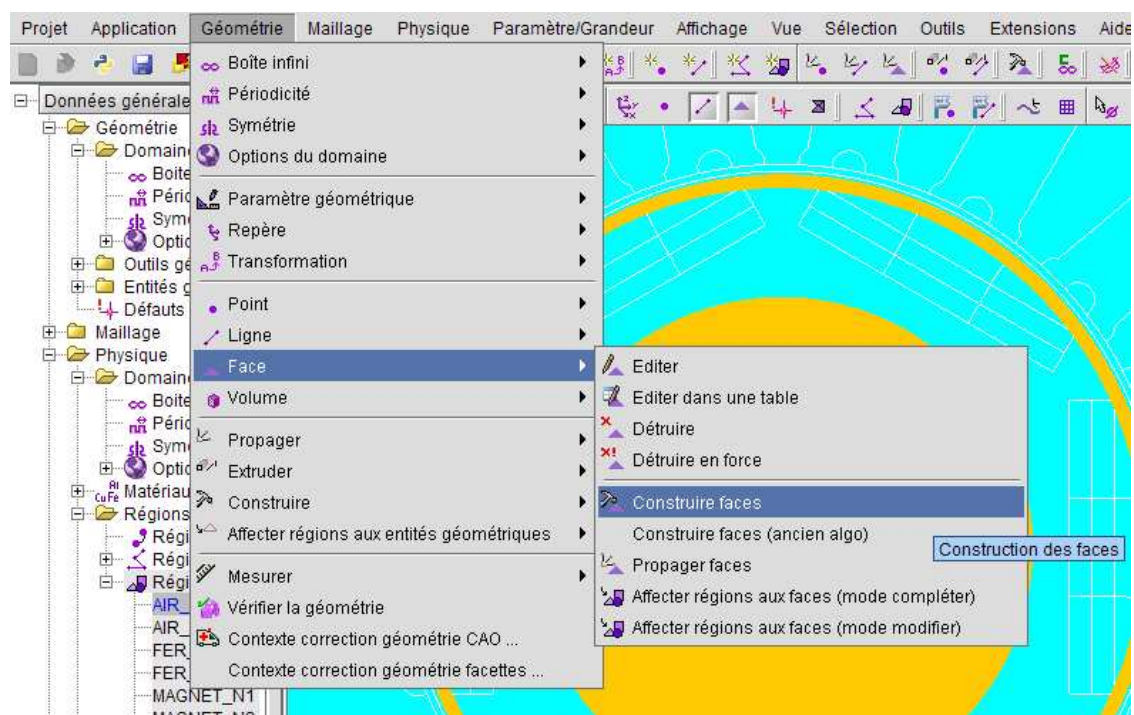
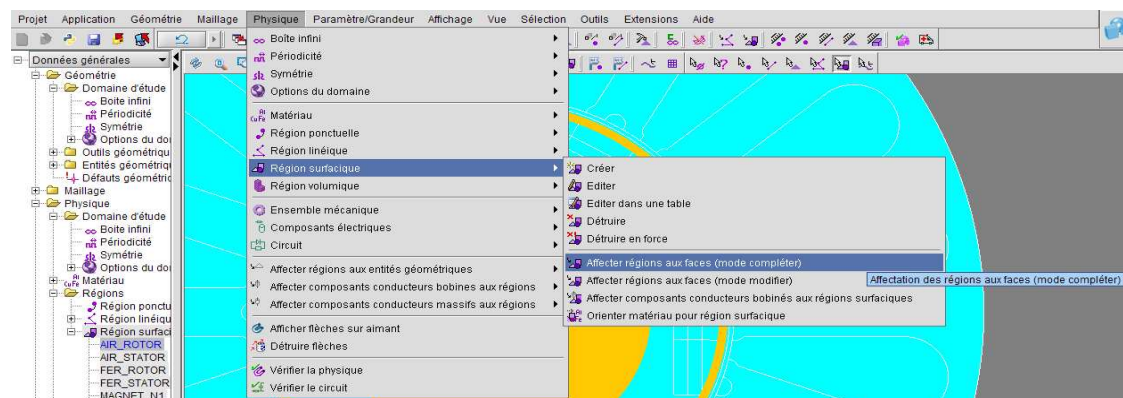


Fig. 3C.3 : New PMSM geometry pointing and lining

Once the creation of the points is made, it must now connect the dots to build new faces in our geometry. Creating line is performed using the "create line"  command is carried out and thereafter a propagation lines on the remaining points wholes. Next step is completing and modification of the geometry. We know that Flux2D is software that calculates each element ends that is to say they work by breaking down the model studied in small elementary surface this functionality is through the mesh. At this stage it must meshing the geometry again, and discrete the new points created based on the old model. This change is made at the "edit point" command to change the mesh point after configuring the mesh and to finally have the file. TRA (simulation file) must recreate already added new surfaces. The figure (3D.4a), (3D.4b) and (3D.4c) below show the procedure for recreating the faces. Finally, the new geometry meshing will be as figure (3D.5).



(a)



(b)



(c)

Fig. 3C.4 : procedure for recreating the faces in new geometry, (a): Geometry →Face → constructs faces (b): Physics→ Surface region→Assign regions to the surfaces (Complement Mode) (c): Mesh →Meshing faces

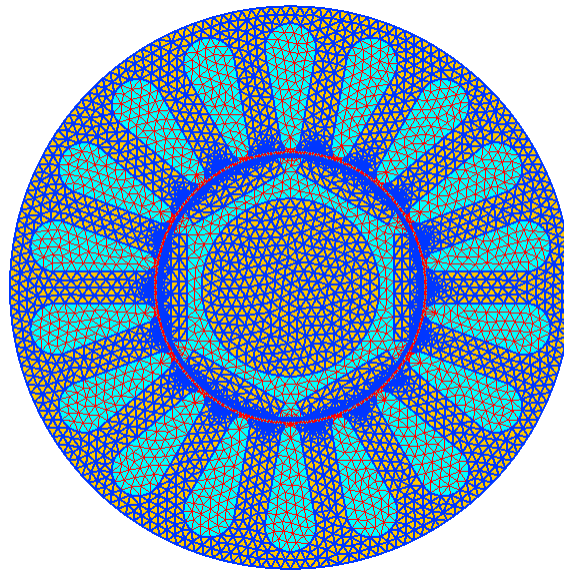


Fig. 3C.5 : Modified geometry and meshing

Appendix 3E

Bearing fault investigation

1. Setup description.....	203
2. Bearing fault investigation	204

1. Setup description

The experimental setup is shown in figure (3F.1). The rated data of the motor under tests is presented in Table (3F.1). The bearing is used single-row, deep groove ball bearing, type 6206 Z where the geometric parameters are given in Table (3F.2). To introduce failure, bearing are drilled on its outer ring. A piezoelectric accelerometer is installed on the frame of the motor to measure the vibration in healthy and faulty cases. For the acquisition of vibration and their treatment, we used the National Instrument card NI 9234 and LabView software.

Table (3F.1): Motor parameter value

<i>Motor parameters</i>	<i>Rated value</i>
<i>power</i>	<i>5 kW</i>
<i>Nominal voltage</i>	<i>85V</i>
<i>Nominal current</i>	<i>25 A</i>
<i>speed</i>	<i>1500 rpm</i>

Table (3F.2): Bearing (6206 Z) parameter value

<i>Parameter</i>	<i>Value</i>
<i>Nominal diameter</i>	<i>30 mm</i>
<i>Outside diameter</i>	<i>62 mm</i>
<i>Contact angle</i>	<i>0 deg</i>
<i>Number of balls</i>	<i>09</i>
<i>Ball diameter</i>	<i>9.52 mm</i>
<i>Inner raceway diameter</i>	<i>36.47 mm</i>
<i>Outer raceway diameter</i>	<i>55.52 mm</i>

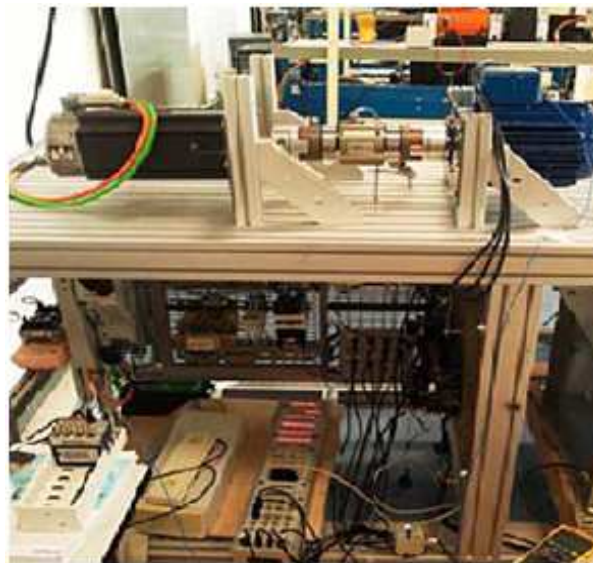


Fig. 3F.1: Experimental setup to test bearing faults,

To introduce failure, bearing are drilled on its outer ring. A piezoelectric accelerometer is installed on the frame of the motor to measure the vibration in healthy and faulty cases. For the acquisition of vibration and their treatment, we used the National Instrument card NI 9234 and LABVIEW software.

2. Bearing fault investigation

The vibration signals under bearing fault in stationary state of motor operation (no load and full load) have been presented in figure (3F.2) and figure (3F.3) subsequently. The figure (3F.4) presents vibration signals under no-load and full-load condition together. At, $t=0.1953$, the motor operate under full-load function.

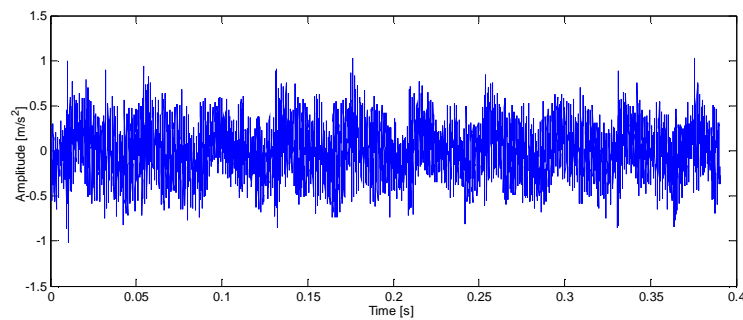


Fig. 3F.2: Vibration signal in no-load operation under bearing fault

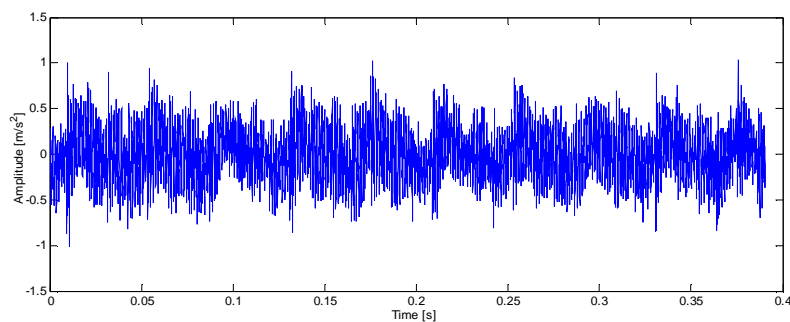


Fig. 3F.3: Vibration signal in full-load operation under bearing fault

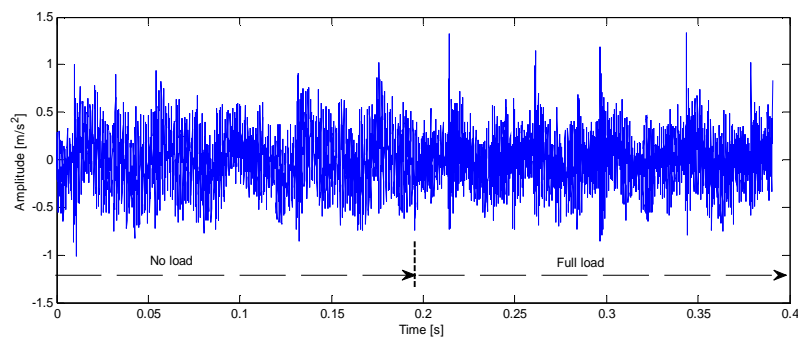


Fig. 3F.4 : Vibration signal in no-load then in full-load operation under bearing fault

A comparison between FFT decomposition of vibration signals in healthy and faulty state and in no-load operation presented in figure (3F.5). We remark that the multiples of the frequency characterizing the bearing defects dominate the vibration spectrum. FFT analysis on vibration spectrum under healthy and faulty full-load operation of motor is shown in figure (3F.6). Also FFT analysis on vibration spectrum for non stationary state and with bearing fault is shown in figure (3F.7).

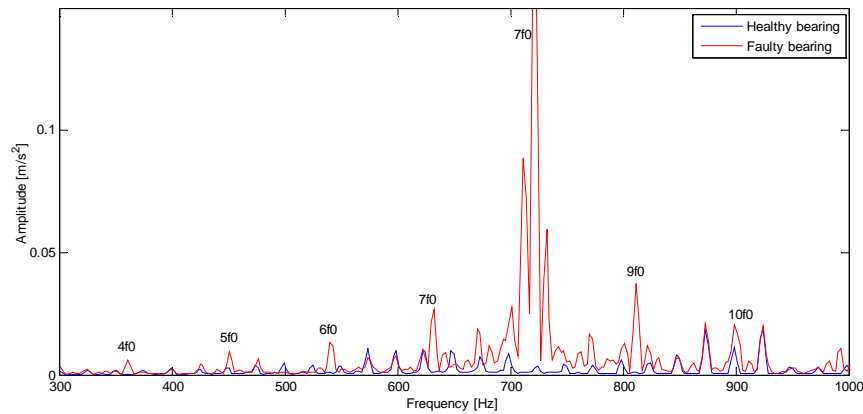


Fig. 3F.5 : FFT analysis on vibration spectrum under healthy and faulty no load operation of motor

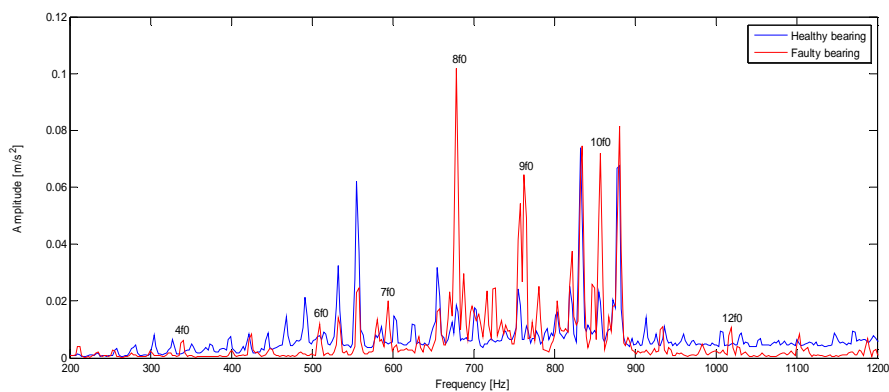


Fig. 3F.6: FFT analysis on vibration spectrum under healthy and faulty full-load operation of motor

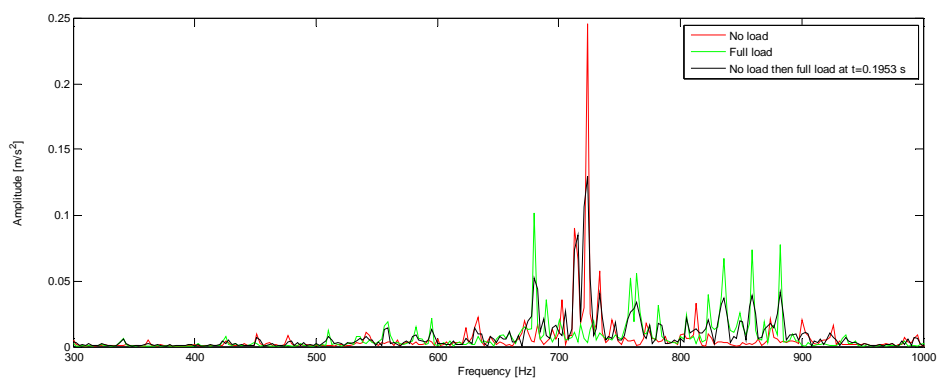


Fig. 3F.7: FFT analysis on vibration spectrum for non stationary state and with bearing fault

From FFT decomposition of vibration signal in healthy and faulty state, we show that the multiples of characteristic frequencies of bearing dominate the vibration spectrum. Note that the frequencies corresponding to fault on bearing outer ring are: 89.76 Hz for no load condition and 85.25 Hz for full load condition state. These frequencies are calculated using the bearing dimensions.

As it is clear in figure (3F.7), by help of FFT analysis on non-stationary signal, when the motor passes from no-load operation to full load operation at $t=0.1953$ s, it does not show this change situation and frequencies dominate the spectrum are closer to the no-load operation. So for non stationary signal, FFT cannot detect the frequencies corresponding to bearing failure or time to transition to full load. For this reason the usage of Continuous Wavelet Transform (CWT) is justified. For the wavelet analysis, we show how operation state changing from no load to full load is clear on the maps in figure (3F.8), this instant correspond to $t=0.1953$ s. In figure (3F.8), the changes of load correspondence to time is clearly spelled out. Figure (3F.9) shows ability of wavelet transform for fault detection too. Also the comparison of wavelet transform analysis on vibration signal under non stationary state is shown in figure (3F.10).

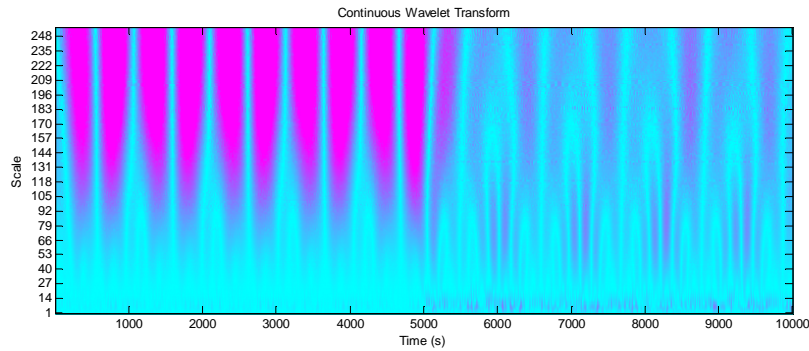


Fig. 3F.8: Continuous Wavelet Transform on vibration signal under healthy mode No-load/full-load operation

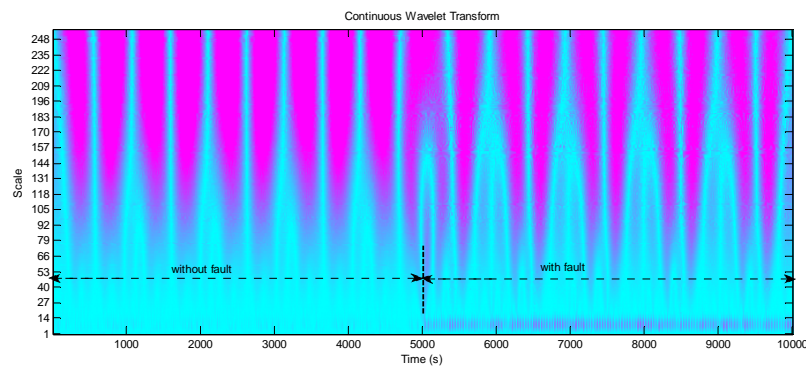


Fig. 3F.9: Continuous Wavelet Transform on vibration signal under healthy mode No-load and faulty mode no-load operation

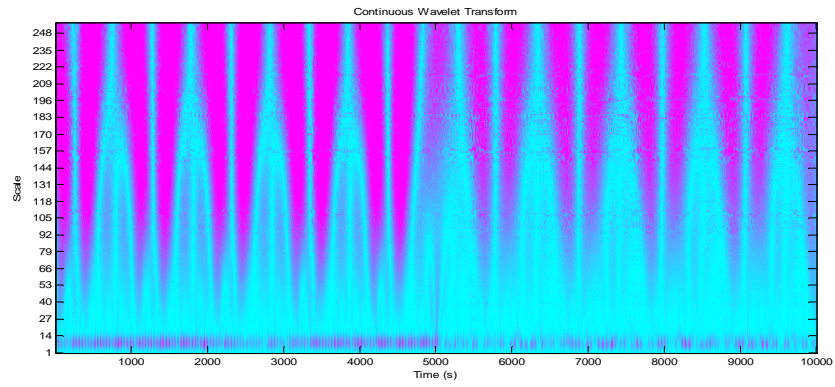


Fig. 3F.10: Continuous Wavelet Transform on vibration signal under faulty mode No-load and full-load at $t=0.1953s$ (5000)

Appendix 5A

Application of artificial neural network

1. Static and Dynamic Artificial Neuron Models: Adaptive Function Estimators.....	211
2. Weights.....	212
3. Inputs	212
4. Activation Function	213
5. Differentiable and Non-Differentiable Function.....	214
6. ANNs, single layer and multilayer feed-forward ANNs.....	214
7. Single Layer ANN	215
8. Multilayer ANN.....	216

1. Static and Dynamic Artificial Neuron Models: Adaptive Function Estimators

General: a very detailed description of the artificial neuron is given below, since this is absolutely necessary for a good mathematical and physical understanding and for all those who also wish to develop other types of ANM (e.g. a fuzzy-neural model, minimum architecture neuron model, etc.). ANNs are based on crude models of the human brain and contain many artificial neurons (computational units) linked via adaptive interconnections (weights) arranged in a massively parallel structure. They are artificial ‘entities’ that can actually learn from given datasets (they estimate functions from datasets) in other words they are adaptive function estimators which are coarse simulators of a biological neural networks in a human brain.

It is very important feature that a suitable ANN is capable of learning the desired mapping between the input signals and output signals of the system under consideration, without knowing the exact mathematical model of the system in this sense, the ANN is a numerical, trainable, model-free adaptive estimator (similarly to a fuzzy system). Since the ANN does not use a mathematical model of the system under consideration, the same ANN configuration and dynamics can be applied to many problems.

A human brain can perform an extremely large number of different operations and there are a number of different ANNs that try to mimic many of these features. Similarly to the human brain, the basic element of an ANN is a single computational neuron, which is basically a multi-input usually non-linear processing element with weighted interconnection of the neuro-biological process of a human brain neuron, it is possible to obtain a relatively simple artificial neuron model which gives a good representation. A simple model of the so-called ‘static’ artificial neuron has four main parts:

- Input(s);
- A weighted summer;
- A non dynamic function (so-called ‘activation function’, which is also sometimes referred to as a transfer function) and in most of the applications is non-linear (there are also ANN models with use linear functions)
- Output(s)

It must be noted that this neuron model is also referred to in the literature as the perceptron neuron, but strictly speaking, by considering its original definition. It should only be called the perceptron if a spatial form of activation function is used (e.g. where the activation function is the hard-limit function). It can be seem that the static artificial neuron model does not contain dynamics. However in a so-called ‘dynamic’ artificial neuron model, in addition to the four main parts described above, the activation function block is followed by a dynamic block. This dynamic block can be represented by a simple delay element (first-order low-pass dynamic block). Figure (5A.1) shows the basic model of a single static artificial neuron (AN), which is the i th neuron in an artificial neuron network containing many neurons.

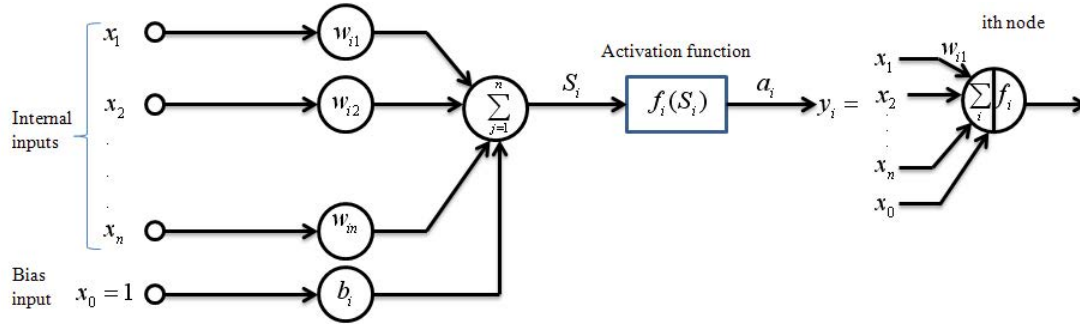


Fig. 5A.1 : Basic static artificial neuron (ith neuron)

Although in the simplest neuron model there is only one neuron, in general there are n inputs to a general i th neuron as shown in figure (5A.1), these are $x_1(t), x_2(t), x_3(t), \dots, x_n(t)$. These can be considered to be the elements of the n -dimensional input vector $x(t) = [x_1(t), x_2(t), x_3(t), \dots, x_n(t)]^T$. The neuron output is the scalar quantity $y_i(t)$. The neuron contains an aggregation operator which e.g. can be a weighted summer and is denoted by \sum_j in figure (5A.1), on the output of which the net value equation 5A.1 is presented,

$$S_i(t) = \sum_{j=1}^n w_{ij} x_j(t) + b_i \quad (5A.1)$$

Where w_{ij} are the connection weights (interconnection strengths) between the i th neuron and the j th inputs and b_i is a constant (which is often called a bias or threshold of the activation function). It follows that the inputs are transmitted through the connection weighted, whereby the weights are multiplied by the inputs and the weighted sum is added, and the net value (S_i) is obtained by adding to this the bias (b_i). Finally the output of the neuron (y_i) is obtained by using the neuron activation function (f_i), thus $y_i = f_i(S_i)$ as shown in figure (5A.1).

2. Weights

The weights are unidirectional communication channels which carry numeric (and not symbolic) data. In many types of artificial neural networks a training (learning) stage is used to obtain the values of the weights and during the training stage the weights are changed on the basis of presented input training data until the output of the system becomes close to the correct output. In figure (5A.1) the weights are variable coefficients indicated only during the learning stage, and once the training stage is over, the weights are constants (of course in general all of them can have different constant values). Usually the initial values of the weights are randomly selected and they can be both positive and negative values.

3. Inputs

Bias the input to a neuron has two sources: external inputs and internal inputs, the latter are inputs from other neurons. It should be noted that by also considering the bias

input in figure (5A.1), there are in total $n + 1$ inputs and the threshold has been incorporated by employing input $x_0 = 1$ and using a corresponding weight of b_i . Thus the bias is simply added to $\sum_{j=1}^n w_{ij}x_j(t)$ and it causes the shifting of the neuron activation function $f_i = f_i(\sum_{j=1}^n w_{ij}x_j(t) + b_i)$ to the left by b_i if function f_i is plotted versus the so-called ‘net’ input to the weight, which is mathematically the argument of the activation function, $S_i = net_i = \sum_{j=1}^n w_{ij}x_j(t) + b_i$ and physically it is the same of the weighted inputs and the bias.

However, it is also possible to use a model with n inputs together with the bias. In this case $S_i = \sum_{j=0}^n w_{ij}x_j(t)$ (not that now the starting value for j is 0 and not 1 as before) where $x_0 = 1$ and $w_{0j} = b_i$. In this case the bias is like a weight, but it has a constant input of “1”. This is the main reason why one of these two very similar static neuron models can be found in various publications. A neuron fires if the weighted sum of its inputs exceeds the (threshold) bias value. In ANN, b_i can be set to be a constant or a variable (which can change like the weights), since in the later case there is added flexibility for the network.

An ANN with biases can represent input-to-output mapping more easily than one without biases, e.g. if all the inputs to a neuron are zero ($x_j = 0, j = 1, 2, \dots, n$), a neuron without a bias will have a net input:

$$S_i = \sum_{j=1}^n w_{ij}x_j(t) + b_i = \sum_{j=1}^n w_{ij}x_j = 0 \quad (5A.2)$$

Thus the activation function becomes a single value $f(S_i) = f(0)$, (which depends only on the activation function employed). However the same neuron has a bias, the input is $S_i = b_i$ and thus the activation function becomes $f(S_i) = f(b_i)$, which (for a specific activation function) can have any value, depending on the bias. This results in greater flexibility.

4. Activation Function

In figure (5A.1) the neuron also contains a non-dynamic activation function, $f(S_i)$. The reason for the use of a non-linear activation function is to deliberately introduce non-linearity in the neuron model, since this makes the network capable of storing strong non-linear activation function were not incorporated into this model then the artificial neuron would represent a linear system which couldn’t be used for the mapping of a non-linear system and cannot suppress noise, so the linear network wouldn’t be robust. However, it should be noted that there exist neuron models, with linear activation function, but these can only be used for the modeling of linear systems.

On the output of the activation block shown in figure (5A.1) the general i th activation value $a_i = f_i(S_i)$ is present, thus:

$$a_i = y_i = f_i(S_i) = f_i\left(\sum_{j=1}^n w_{ij}x_j(t) + b_i\right) \quad (5A.3)$$

There are various type of f_i activation function (mathematical function), which can be used in ANNs. However non-linearity and simplicity are the two key factors for the selection of a specific activation function. Furthermore, since some training techniques (e.g. the back propagation technique) require the first derivative of the activation function (f), when they are used in an ANN using such a learning technique, then the activation function must be differentiable.

5. Differentiable and Non-Differentiable Function

This classification distinguishes the soft-limiting and hard-limiting activation functions. The soft-limiting functions are required in some weight adaptation algorithms and hard-limiting functions are required in discrete algorithm, where they yield a true binary output for illustration purposes two soft-limiting functions, the unipolar sigmoid function (USF) and the radial basis activation function (RBF) are also shown in figure (5A.2). They are mainly used in identification, control and diagnosis applications [3]. The word “unipolar” is used to point out that only positive responses of neurons are produced for this definition of the activation function.

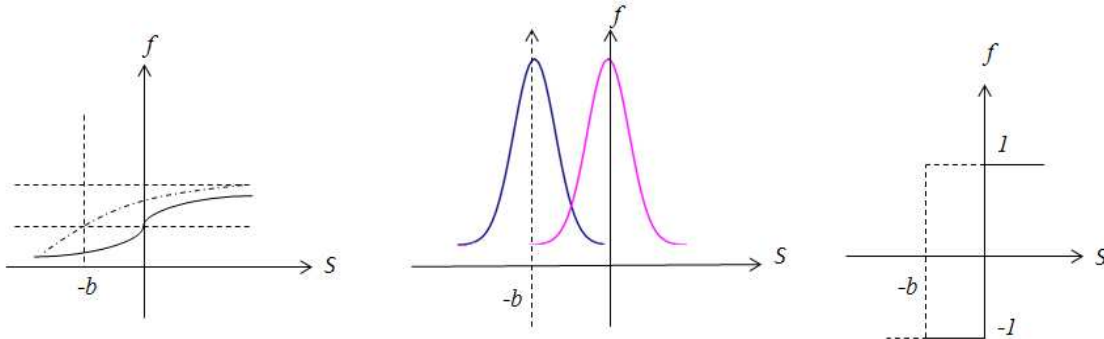


Fig. 5A.2: Unipolar sigmoid, radial basis and signum activation functions with and without bias

6. ANNs, single layer and multilayer feed-forward ANNs

Neural network systems consist of parallel distributed information processing units with different connecting structures and processing mechanism. They have large variety of applications in engineering such as function approximation, pattern recognition and etc. The architecture of a neural network specifies the arrangement of the neural connection as well as the type of units characterized by an activation function. The processing algorithm specifies how the neurons calculate the output vector for any input vector and for a given set of weights. The training algorithm specifies how the NN adapts its weights w with all given input vectors, called training vectors. Thus, the neural network can acquire knowledge through the training algorithm and store the knowledge

in synaptic weights. There are many types of ANNs but the most commonly used ones are the multi-layer feed-forward networks, as, a three-layer network (input, one hidden and output layers) as shown in figure (5A.3).

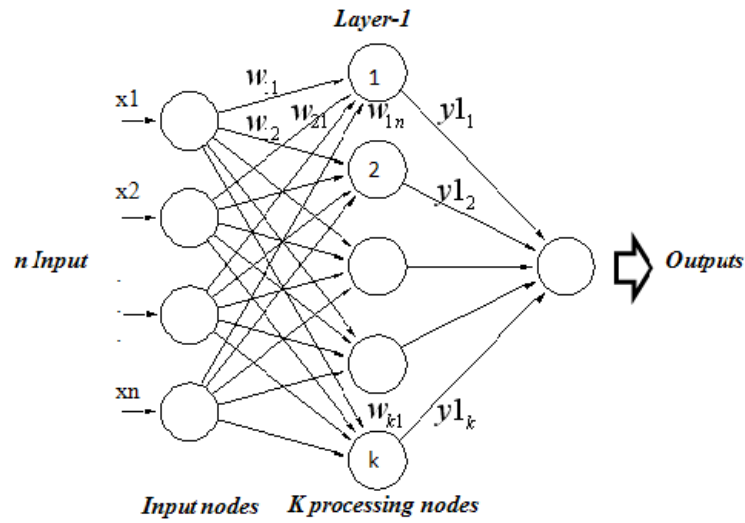


Fig. 5A.3: Single layer feed-forward ANN

7. Single Layer ANN

The neurons are the building blocks of an artificial neural network. In a so-called single-layer feed-forward ANN there is at least a single artificial neuron of the type discussed in previous section. As shown in figure (5A.3) , in general , there can be n inputs $X = [x1, x2, \dots, xn]T$ and k neurons in the single layer of the ANN, where in general $k \neq n$, and an input is connected to each neurons (input) through the appropriate weights. Each neuron performs the weighted sum of its inputs plus the bias and applies this to its activation function. It follows that there is k outputs $y1 = [y11, y12... y1k] T$ to the ANN described by a single layer (where the index 1 in y1 outputs on the first layer are y11, y12... y1k) and:

$$y1 = F1 (W1X + B1) \tag{5A.4}$$

In this expression $F1$ is the activation matrix of this single layer, which is a diagonal matrix with k elements, and which depends on the net inputs to this layer:

$$F1 (S1) = \text{diag}[f1(S1), f1(S2), \dots, f1(Sk)] \tag{5A.5}$$

Where the elements are the activation functions of each of the k nodes, which have been assumed to be equal, $f11 = f12 = \dots = f1k = f1$, $S1$ is the net vector , $S1 = [S1, S2, \dots, Sk]T$ which contains the net inputs $S1, S2, \dots, Sk$ to neurons 1, 2, ..., K,

$S_i = \sum_{j=1}^n w_{ij}x_j(t) + b_i$. Furthermore, $W1$ is the weight matrix of the output layer, which due to the specified architecture must contain k rows and n columns:

$$W1 = \begin{bmatrix} w_{1,1} & w_{1,2} & \dots & w_{1,n} \\ w_{2,1} & w_{2,2} & \dots & w_{2,n} \\ \cdot & \cdot & \cdot & \cdot \\ \cdot & \cdot & \cdot & \cdot \\ w_{k,1} & w_{k,2} & \dots & w_{k,n} \end{bmatrix} \quad (5A.6)$$

A general w_{ij} is the weight from destination (recipient) node j to source node i , where $i = 1, 2, \dots, k; j = 1, 2, \dots, n$ and $B1$ is the bias vector of the single layer, $B1 = [b11, b12, \dots, b1k]T$, where $b11, b12, \dots, b1k$ are the biases of nodes $1, 2, \dots, k$ of the output layer respectively. An ANN with a single layer can be used with only a very limited number of systems and it cannot represent all nonlinear functions. When the activation functions in a single layer ANN are hard-limit functions, the so-called single layer perceptron model arises. Although this can be used for certain types of classification problems, since the hard limit function divides the input space (the space defined by the input vector) into two regions, and the output will be 1 or 0 depending on the input vectors.

However in fact, there can be only two different outputs values is a great limitation. Furthermore, the single layer perceptron cannot learn the mapping of such systems, whose input space is defined by linearly un-separable vectors. It is sometimes convenient to have a geometrical interpretation of this: if the input space contains linearly inseparable vectors, then a straight line or plan which separates the input vectors in the input plane cannot be drawn on the input plane between the input vectors. When a single layer network uses linear activation functions, where the single layer perceptron cannot train the network, so that it has linear neurons and called Widrow-Hoff neurons or ADALINE neurons (Adaptive Linear Neurons), then the resulting network using adaptive learning is called the ADALINE network or MADALINE network for many ADALINES.

8. Multilayer ANN

The neurons are the building blokes of an artificial neural network containing many layers. In a multilayer feed forwards ANN, the neurons are arranged into several parallel layers. The connection of several layers results in a network which has the possibility of more complex non-linear mapping between the inputs and outputs this can be used to implement classifiers and associators to represent complex non-linear relations among variables. In a multilayer artificial neural network the neurons of layer 0 (input layer) don't perform computation (processing), but only feed inputs to the neurons of layer 1 with is called the first hidden layer. There are no interconnections between the nodes of the same layer. Layer 1 can be followed by a second hidden layer (layer 2). In theory there could be any number of hidden layers, but this would significantly increase the complexity of the training of the network and also network with one or two hidden layers appear to provide adequate accuracy, robustness and generalization in many cases. If there is only a single hidden layer satisfactory performance can be obtained by using non-linear activation function only in the hidden layer, and linear activation functions in the output layer when contrasted to the network with a single hidden layer, the network

with two hidden layers may provide higher accuracy at a low cost (fewer processing units).

In the ANN with two hidden layers, the last layer (layer 3) is the output layer. In general, layers between the input and output layers are the hidden layers. Each neuron is connected to all neurons of the adjacent layers and to no other neurons. Connections within a layer are not permitted. Generally there are different numbers of neurons and different weights for different hidden layers. There are no general rules to determine the number of hidden layers and hidden nodes; this also depends on the complexity of the mapping to be achieved. The number of input (input nodes) and output (output nodes) is of course determined by the specific problem. The number of neurons and connections limit the number of patterns a neural network can store reliably. In a multilayer ANN the activation functions in the output layer can be linear functions, since the network is able to represent a non-linear system by using non-linear activation functions in the hidden layer(s).

For illustration purposes figure (5A.4) shows the schematic of three-layer feed-forward ANN. The term 'feed-forward' refers to the fact that the arcs joining the nodes are unidirectional. Such a network is also referred to as a multilayer perceptron also strictly speaking this should only be the terminology used for the same network, when the activation functions are hard-limit functions (see the definition of the perceptron above). It should be noted that in the literature sometimes such a network called a four-layer network, corresponding to the fact that there are four layers of nodes (for the input, hidden 1, hidden 2 and output layers). However the network has only three layers of processing neurons and therefore such a network is also sometimes referred to in the literature as a three layer network. If the latter definition is applied, the term 'layer' refers to the actual number of existing and processing layers. This convention is more logical, since the input nodes (in the input layer 0) don't perform computation. As a result, this is equivalent to saying that the ambiguity could be totally removed by considering such a definition where there is no terminology of an input layer and the layer and the layer to which the inputs are directly connected to is the first layer (first hidden layer). It is then very clear that the number of layers in such a network is equal to the number of hidden layers plus 1. It should also be noted that when this definition is used, an N-layer network has N-1 layers of hidden neurons, whose outputs are not directly accessible. As a consequence, the errors (difference between desired value and actual value) at these outputs are not known directly. They can be obtained by first determining the errors at the output layer, and then by back-propagation these. In general, multilayer artificial neural networks can be considered as versatile non-linear maps with the elements of the weight matrices (weights) and bias vectors as parameters.

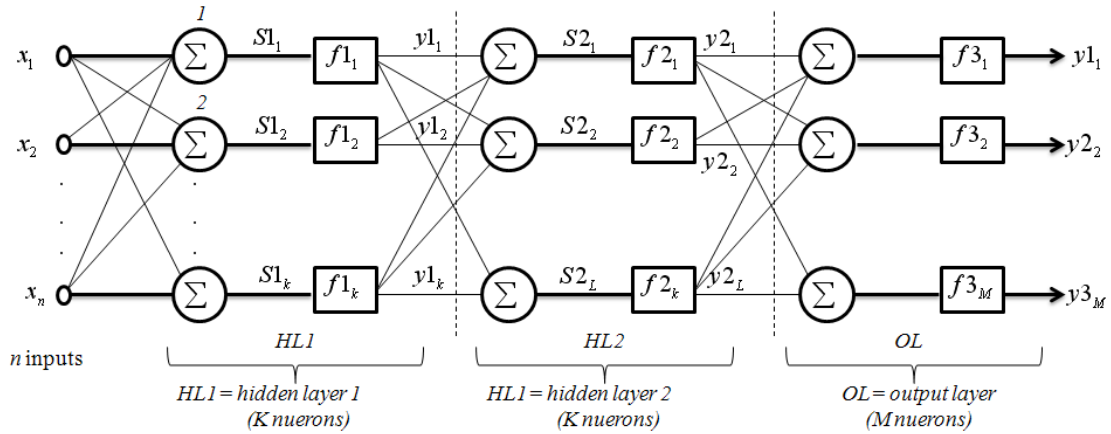


Fig. 5A.4: Schematic of a three-layer feed-forward ANN

In the ANN shown in figure (5A.4) there are n inputs, there is one output layer (OL) with M output nodes and there are two hidden layers (HL1, HL2). In general in each of the layers there can be different number of nodes and all nodes in a given layer are connected to all nodes in the next layer, but there are no inter connections between the nodes of the same layer. The number of input correspond to the number of physical characteristics that are considered to be important for the neural network and the number of output nodes is equal to the number of output quantities to be determined. As discussed above, in general there can be several hidden layers, but often due to the computation burden, this is limited to one or two hidden layer. According to the universal approximation theorem one hidden layer is sufficient to perform any non-linear input-to-output mapping but the theorem doesn't give the number of hidden neurons and doesn't say if a single hidden layer would be optimal in the sense of ease of learning. These can make the training of the network sometimes difficult and in supervised ANNs may necessitate trial-and-error-based computations aimed at obtaining an ANN with optimum of hidden layers and hidden nodes.

It is possible to immediately establish an equation for the outputs of the network shown in figure (5A.4). The output vectors of the three layers (two hidden layer and output layer) can be obtained as follows:

$$\begin{aligned}
 y_1 &= F_1(W_1 x + B_1) = F_1(S_1) \\
 y_2 &= F_2(W_2 y_1 + B_2) = F_2(S_2) \\
 y_3 &= F_3(W_3 y_2 + B_3) = F_3(S_3)
 \end{aligned} \tag{5A.7}$$

Where F_1, F_2, F_3 and W_1, W_2, W_3 are matrices of activation functions and weights respectively of the appropriate layer. The activation matrices ($F_1, F_2, \text{ and } F_3$) are diagonal and the weight matrices ($W_1, W_2, \text{ and } W_3$) can be non-quadratic (if they correspond to a layer whose number of nodes is different to that in the previous layer). For clarity the other quantities present in Eq. (5A.7) are now listed:

x is the input vector, (with n inputs), $x = [x_1, x_2, \dots, x_n]^T$, y_1 is the output vector of the first layer (hidden layer with k nodes), $y_1 = [y_{1_1}, y_{1_2}, \dots, y_{1_k}]^T$, y_2 is the output vector of the second layer (hidden layer with L nodes), $y_2 = [y_{2_1}, y_{2_2}, \dots, y_{2_L}]^T$, y_3 is the output vector of the third layer (output layer with M nodes),

$y_3 = [y_{3_1}, y_{3_2}, \dots, y_{3_M}]^T$, and the input net vectors to the appropriate activations (activation matrices are):

$$\begin{aligned} S_1 &= [S_{1_1}, S_{1_2}, \dots, S_{1_k}]^T, \\ S_2 &= [S_{2_1}, S_{2_2}, \dots, S_{2_L}]^T, \\ S_3 &= [S_{3_1}, S_{3_2}, \dots, S_{3_M}]^T, \end{aligned} \quad (5A.8)$$

And the activation matrices are:

$$\begin{aligned} F_1 &= \text{diag} [F_{1_1}(S_{1_1}), F_{1_2}(S_{1_2}), \dots, F_{1_k}(S_{1_k})], \\ F_2 &= \text{diag} [F_{2_1}(S_{2_1}), F_{2_2}(S_{2_2}), \dots, F_{2_L}(S_{2_L})], \\ F_3 &= \text{diag} [F_{3_1}(S_{3_1}), F_{3_2}(S_{3_2}), \dots, F_{3_M}(S_{3_M})], \end{aligned} \quad (5A.9)$$

It follows from Eq. (5A.8) that the ANN shown in figure (5A.4) implements a non-linear mapping relating the inputs to the output(s) by:

$$y_3 = F_3(W_3 F_2(W_2 F_1(W_1 x + B_1) + B_2) + B_3) \quad (5A.10)$$

Thus for given inputs, activation functions and weights, the output(s) can be determined by using Eq. (5A.8). Based on Eq. (5A.10) the block diagram representation of the feed-forward three-layer ANN is shown in figure (5A.5). It can be seen that this takes a very simple form from which can be easily interpreted physically, since it shows that the appropriate activation functions operate on the appropriate weighted inputs.

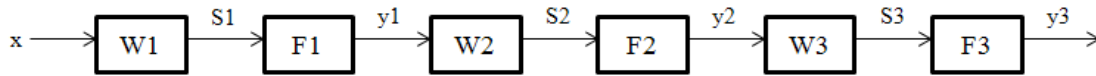


Fig. 5A.5 : Block diagram of a feed-forward three layer ANN using weight and activation matrices

It is very important to note that a feed-forward static ANN responds instantaneously to the inputs since it doesn't contain any dynamic elements. This is in contrast to dynamic neural networks, which contain dynamic elements. It should be noted that in addition to static and dynamic neural networks, there exist also fuzzy-neural networks, which combine the principle of fuzzy logics and neural networks.

Some ANNs are good at pattern recognition, others are reasonably good at prediction and there are ANNs which can quickly discern trends in data. The learning process of ANN is based on training process. In general ANNs can be grouped as those which require supervision while they learn (error based ANN, unsupervised ANN). Supervised training involves training of a network to recognize a new pattern as one of a known set, or a classification of patterns. When the neural network is appropriately trained, it will contain the non-linearity of the desired mapping within the interconnection (weights) between the layers of the ANN.

One of the most widely used training techniques for an unsupervised feed-forward multilayer static ANN (which contains the inputs, one or several hidden layers and an output layer) is the so-called error back propagation technique. When this technique is employed, the ANN is provided with input and output training data and the ANN configures its weights and the weight adjustments force the learning rules to propagate the input layer exactly forward. In other words, when the error back propagation

technique is used, the main task is to configure the weights in such a way that the (least-mean-square) error (between the desired and actual output) of the ANN should be minimum. When the input patterns are applied sequentially (during training) and if its association (corresponding output) is determined to be erroneous, the least-means-square error (E):

$$E = 0.5 \sum_{k=1}^{npat} (d_k - y)^T (d_k - y) \quad (5A.11)$$

Is reduced, where d_k is the desired output vector corresponding to the input vector x_k , $npat$ is the number of training patterns, $y(x_k, W)$ is the output vector for inputs x_k and weight W . during the association phase, the trained ANN operates in a feed-forward manner. However, the weight adjustments force the learning rules to propagate the input layer exactly forward. The back-propagation algorithm is an elegant and effective computational tool for adjusting the weight of the multilayer static ANN.

To summarize a successful back propagation learning process of a multi-layer feed-forward ANN: after a large number of exposures to the data (epochs) the network is able to arrive at a relationship between the input and output datasets and configures the strength of its connections (its weights). This training process is then followed by supplying the ANN (Which now has constant weight) with the real input data, and the ANN then outputs the required data. Thus there is a separate training and a recall (application) mode of operation of the ANN and the two modes should not be confused.

The interest in the electric vehicles rose recently due both to environmental questions and to energetic dependence of the contemporary society. Accordingly, it is necessary to study and implement in these vehicle fault diagnosis systems which enable them to be more reliable and safe enhancing its sustainability. In this work after a review on problem of faults in the drivetrain of series hybrid electric vehicles (SHEV), a deep investigation on fault diagnosis of AC-DC power converter and permanent magnet synchronous motor (PMSM) have been done as two important parts of traction chains in SHEVs. In other major part of this work, four types of faults (stator winding inter turn short circuit, demagnetization, eccentricity and bearing faults) of a PMSM have been studied. Inter turn short circuit of stator winding of PMSM in different speeds and loads has been considered to identify fault feature in all operation aspects, as it is expected by electric vehicle application. Experimental results aiming short circuits, bearing and eccentricity fault detection has been presented. Analytical and finite element method (FEM) aiming demagnetization fault investigation has been developed. The AC-DC converter switches are generally exposed to the possibility of outbreak open phase faults because of troubles of the switching devices. This work proposes a robust and efficient identification method for data acquisition selection aiming fault analysis and detection. Two new patterns under AC-DC converter failure are identified and presented. To achieve this goal, four different level of switches fault are considered on the basis of both simulation and experimental results. For accuracy needs of the identified pattern for SHEV application, several parameters have been considered namely: capacitor size changes, load and speed variations.

On the basis of the developed fault sensitive models above, an ANN based fault detection, diagnosis strategy and the related algorithm have been developed to show the way of using the identified patterns in the supervision and the diagnosis of the PMSM drivetrain of SHEVs. ANN method have been used to develop three diagnosis based models for : the vector controlled PMSM under inter turn short circuit, the AC/DC power converter under an open phase fault and also the PMSM under unbalanced voltage caused by open phase DC/AC inverter. These models allow supervising the main components of the PMSM drivetrains used to propel the SHEV. The ANN advantages of ability to include a lot of data made possible to classify the faults in terms of their type and severity. This allows estimating the performance degree of that drivetrains during faulty conditions through the parameter state of health (SOH). The latter can be used in a global control strategy of PMSM control in degraded mode in which the control is auto-adjusted when a defect occurs on the system. The goal is to ensure a continuity of service of the SHEV in faulty conditions to improve its reliability.

Résumé

L'intérêt pour les véhicules électriques ne cesse de croître au sein de la société contemporaine compte tenu de ses nombreuses interrogations sur l'environnement et la dépendance énergétique.

Dans ce travail de thèse, nous essayons d'améliorer l'acceptabilité sociétale du véhicule électrique en essayant de faire avancer la recherche sur le diagnostic des défauts d'une chaîne de traction électrique. Les résultats escomptés devraient permettre à terme d'améliorer la fiabilité et la durabilité de ces systèmes.

Nous commençons par une revue des problèmes des défauts déjà apparus dans les véhicules hybrides séries qui disposent de l'architecture la plus proche du véhicule électrique. Une étude approfondie sur le diagnostic des défauts d'un convertisseur de puissance statique (AC-DC) ainsi que celle du moteur synchrone à aimants permanents est menée. Quatre types de défauts majeurs ont été répertoriés concernant le moteur (court-circuit au stator, démagnétisation, excentricité du rotor et défaut des roulements). Au niveau du convertisseur, nous avons considéré le défaut d'ouverture des interrupteurs. Afin d'être dans les mêmes conditions d'utilisation réelle, nous avons effectué des tests expérimentaux à vitesse et charge variables. Ce travail est basé aussi bien sur l'expérimentation que sur la modélisation. Comme par exemple, la méthode des éléments finis pour l'étude de la démagnétisation de la machine. De même, l'essai en court-circuit du stator du moteur en présence d'un contrôle vectoriel.

Afin de réaliser un diagnostic en ligne des défauts, nous avons développé un modèle basé sur les réseaux de neurones. L'apprentissage de ce réseau de neurone a été effectué sur la base des résultats expérimentaux et de simulations, que nous avons réalisées.

Le réseau de neurones est capable d'assimiler beaucoup de données. Ceci nous permet de classifier les défauts en termes de sévérité et de les localiser. Il permet ainsi d'évaluer le degré de performance de la chaîne de traction électrique en ligne en présence des défauts et nous renseigner ainsi sur l'état de santé du système. Ces résultats devraient aboutir à l'élaboration d'une stratégie de contrôle tolérant aux défauts auto-reconfigurable pour prendre en compte les modes dégradés permettant une continuité de service du véhicule ce qui améliorera sa disponibilité.

